NASA CR-72458
Allison EDR 5996

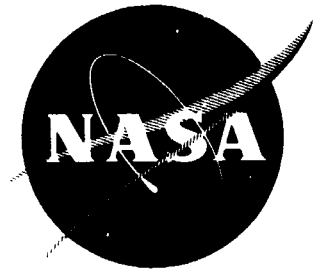

Quiet Engine Definition Program

Prepared for

NATIONAL AERONAUTICS AND SPACE ADMINISTRATION

CONTRACT NAS3-10496

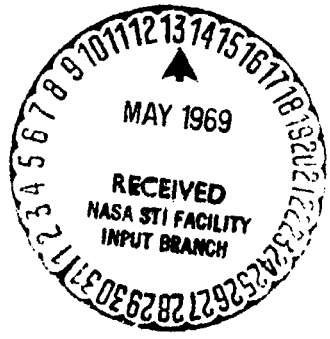

Allison Division • General Motors

Indianapolis, Indiana

NASA CR-72458
Allison EDR 5996

Final Report
Quiet Engine Definition Program

Prepared for

NATIONAL AERONAUTICS AND SPACE ADMINISTRATION

September 19, 1968

CONTRACT NAS3-10496

Technical Management
NASA-Lewis Research Center
Cleveland, Ohio
Propulsion Systems Acoustics Branch
J. J. Kramer
J. F. McBride

Allison Division • General Motors

Indianapolis, Indiana

QUIET ENGINE DEFINITION PROGRAM FINAL REPORT

ABSTRACT

The Quiet Engine Definition Program consisted of a study of the design characteristics and noise production of engines in the bypass ratio range of 3 to 8. A preliminary design was made for an engine having a bypass ratio of 5.5. This engine is rated at 4900-lb (21.8-kN) cruise thrust at 35,000 ft (10.7 km) at Mach 0.82. The specific fuel consumption is 0.627 lb_f/hr/lb_t (0.0177 g/N-sec). The engine weight is 4780 lb (2168 kg), the fan tip diameter is 74 in. (1.88 m), and the length is 153 in. (3.89 m). The predicted four-engine aircraft noise levels during takeoff and approach are 105.6 and 104.1 PNdB, respectively.

TABLE OF CONTENTS

LIST OF ILLUSTRATIONS

LIST OF TABLES

I. SUMMARY

The objective of the Quiet Engine Definition Program is to advance engine acoustic technology to a level which will provide the basis for demonstration of a complete engine system incorporating quieting features. It is desired to obtain maximum engine noise reduction consistent with acceptable performance. The results of the engine preliminary design are reported herein.

Engines having bypass ratios of 3:1, 5:1, and 8:1 were studied for their effect on overall engine noise production in a preliminary optimization study. The effects of tip speed, fan aerodynamics, and row spacing were investigated. As a result, the following three engines were selected for a preliminary design effort:

- 3:1 bypass ratio engine with a two-stage fan
- 5:1 bypass ratio engine with a single-stage fan
- 5:1 bypass ratio engine with a two-stage fan

Preliminary designs were made of each of the three engines in a three-spool engine arrangement to determine overall and detailed source noise levels, weight, and performance. The engines having two-stage fans were predicted to be much noisier than the engine having a single-stage fan even though their fan tip speeds were much less. The 5:1 bypass ratio single-stage fan engine was considerably lighter than an engine having two fan stages. Therefore, a more detailed preliminary design was made of an engine having a single-stage fan. This engine is designated PD218-Q.

By fixing the bypass ratio of the PD218-Q engine at 5.5:1 instead of 5.0:1 with the same cycle design pressure ratio, the primary exhaust velocity and the noise associated with the exhaust velocity were reduced. The aerodynamics of the fan and the intermediate compressor were revised to further reduce the noise emanating from these sources. A preliminary design was made of the PD218-Q engine and performance, weight, and noise level determinations were completed. Significant engine features are as follows:*

Bypass ratio (BPR)	5.5
Cruise thrust at Mach 0.82 and 35,000 ft (10.7 km)	4900 lb (21.8 kN)
Cruise thrust sfc at Mach 0.82 and 35,000 ft (10.7 km)	0.627 $lb_f/hr/lb_t$ (0.0177 g/N-sec)
Rated takeoff thrust	21,964 lb (97.7 kN)
Weight	4780 lb (2168 kg)
Length	153 in. (3.886 m)
Fan tip diameter	74 in. (1.88 m)

*The symbols and units used in this report are defined in Section IV.

Four-engine flyover noise levels	
Takeoff thrust at 1000 ft (304.8 m) at Mach 0.25	105.6 PNdB
Approach thrust, 5000 lb (22.4 kN), at 325 ft (99.06 m) at Mach 0.25	104.1 PNdB
Exit velocity at takeoff	
Primary jet	1261 ft/sec (384.4 m/sec)
Secondary jet	821 ft/sec (250.2 m/sec)

II. INTRODUCTION

Large turbojet engines produce high-intensity jet exhaust noise which is unacceptable in civilian aircraft operations. In recent years the turbojet engines have been replaced by low bypass ratio turbofan engines because the turbofan engines perform better and are significantly quieter than their turbojet counterparts. The current low bypass ratio turbofan engines still produce too much noise in commercial service. Major reductions in the level of turbofan engine exhaust noise are possible by designing engines having high bypass ratios with significantly reduced primary stream exhaust velocity.

The fan of high bypass ratio turbofan engines is the predominant source of noise. Techniques for fan noise reduction must be developed and incorporated in order to achieve further improvements. Work under way on the engines for very large transports (Boeing 747, Lockheed CL-1011, and McDonnell-Douglas DC-10) has eliminated inlet guide vanes, resulting in an anticipated reduction in fan noise. Further advances in noise reduction can be made by aerodynamic and mechanical design changes and by the use of noise suppressors in the inlet and exhaust portions of the engine.

The objective of the Quiet Engine Definition Program is to determine the engine characteristics which will result in the maximum engine noise reduction consistent with acceptable performance. The basis for comparison is current four-engine aircraft. These aircraft, for the most part, are powered by JT3D-3B engines. Therefore, the JT3D-3B engine has been used as a standard of noise comparison in this study. The noise levels for the JT3D-3B have been determined from an Allison-generated synthesis of the cycle and mechanical configuration. The noise levels predicted for the JT3D-3B compare favorably with published data and are intended for comparative purposes only.

This report includes the results of optimization studies completed to determine the exact design cycle to be incorporated in the preliminary engine design. Further optimization studies were made to investigate the effect of aerodynamic and mechanical design choices on noise production.

The noise evaluation method used by Allison included an evaluation of each noise source and finally a summation of the individual source outputs to derive overall levels. The relationships of fan and compressor noise sources have been determined by the method of Smith and House of Rolls-Royce.[1]* The turbine noise sources have been estimated using a similar approach. The jet exhaust noise levels have been based on the method provided by SAE AIR 876A with additional correlations at low velocities. Directivity is based on Allison correlations. The individual elements have been combined in an IBM computer program for overall evaluation.

---

*Superscripts indicate references in Section V.

The PD218-Q engine derived during the preliminary design study is predicted to be significantly quieter than current low bypass ratio engines. The estimated noise reduction is 13 PNdB at takeoff power and 14.5 PNdB at approach conditions below current operating levels for the bare engine. Further noise reductions are possible by incorporating sound attenuation treatment in the inlet and fan discharge portions of the engine.

III. TECHNICAL APPROACH

The technical approach used in the Quiet Engine Definition Program involved:

- Selection of an engine configuration
- Design of engine components
- Engine installation studies

Initially, parametric studies were made in which a broad spectrum of turbofan engine configurations were compared on the basis of performance, weight, noise production, and development risk. From this comparison, three engine configurations were selected for further cycle optimization, preliminary aerodynamic and mechanical design analysis of components, and installation studies. The results of this effort showed that a 5:1 bypass ratio, single-stage fan engine was the quietest and lightest of the three engine configurations studied. However, further study indicated that increasing the bypass ratio to 5.5:1 could reduce noise and specific fuel consumption. A detailed design of a 5.5:1 bypass engine was completed.

This section is divided into four major subsections:

3a. Cycle Performance Characteristics
3b. Summary of Engine Configurations Studied
3c. Noise Evaluation
3d. PD218-Q Engine Description

3a. Cycle Performance Characteristics

The objective of Task II of the Quiet Engine Definition Program was a continuation of noise reduction studies and the completion of a preliminary design for a 5.5:1 bypass ratio, three-spool, single-stage fan engine. The design point for this engine cycle was Mach 0.82 at 35,000 ft (10.7 km).

During the Task I phase of the program the two-spool arrangement was eliminated from consideration and the effort was directed toward the three-spool engines. The two-spool arrangement required a higher pressure ratio for the HP rotor system, resulting in a reduction in efficiency. Thus, the specific fuel consumption (sfc) penalty coupled with the development risk associated with high pressure components detracted from the two-spool arrangement.

A series of engine cycles having bypass ratios of 3:1, 5:1, and 8:1 were studied to determine their effect on overall engine noise production. The effects of tip speed, fan aerodynamics, and row spacing were investigated and from this initial optimization study, three engines were selected for the preliminary design effort of Task I:

- 3:1 bypass ratio engine having a two-stage fan
- 5:1 bypass ratio engine having a two-stage fan
- 5:1 bypass ratio engine having a single-stage fan

As a result of the preliminary design effort, the engine cycle recommended as having the lowest noise production level, lightest weight, and yet having an acceptable performance level was the 5:1 bypass ratio, three-spool, single-stage fan configuration.

PARAMETRIC ANALYSIS

The initial phase of Task I was concerned with a parametric analysis of engine cycles at each of three bypass ratios. The three-spool cycles were optimized for turbine inlet temperature, fan pressure ratio, and overall pressure ratio at bypass ratios of 3:1, 5:1, and 8:1. In this parametric study, single line characteristics were used to define the components; the design point was 4600 lb (20 kN) of thrust at 35,000 ft (10.7 km) and Mach 0.8. Performance at a mid-cruise power requirement of 75% of design thrust was considered of equal importance in selection of the engine cycle. Figures 3a-1 through 3a-8 show some of the criteria considered for the selection of the initial cycles. The cycle trade-off studies indicated that small variations in parameters within the ranges studied could be made without affecting engine performance capabilities appreciably.

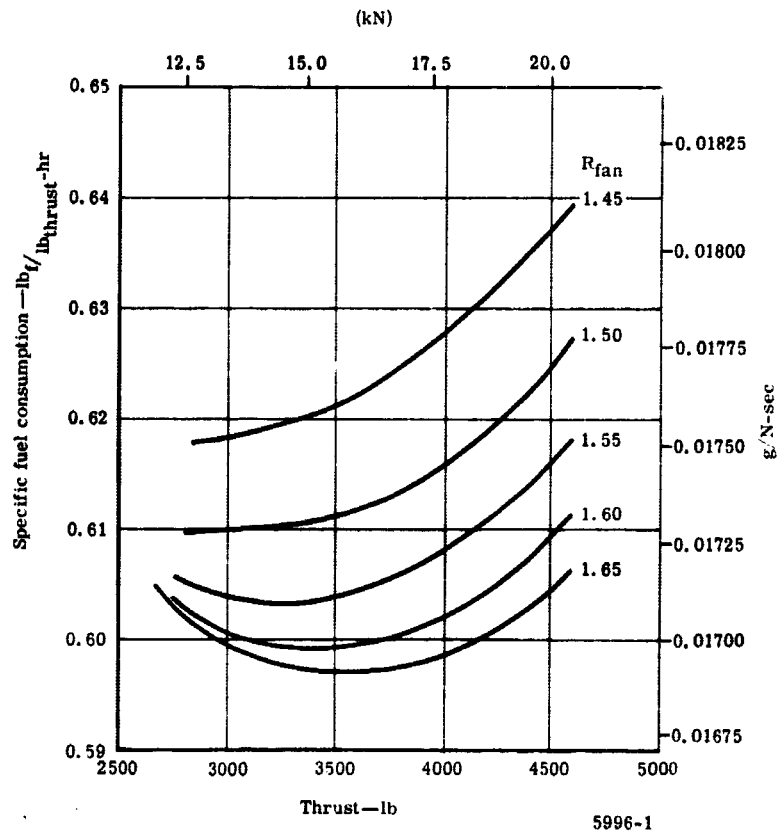

Figure 3a-1. Effects of fan pressure on throttled performance—5:1 bypass ratio.

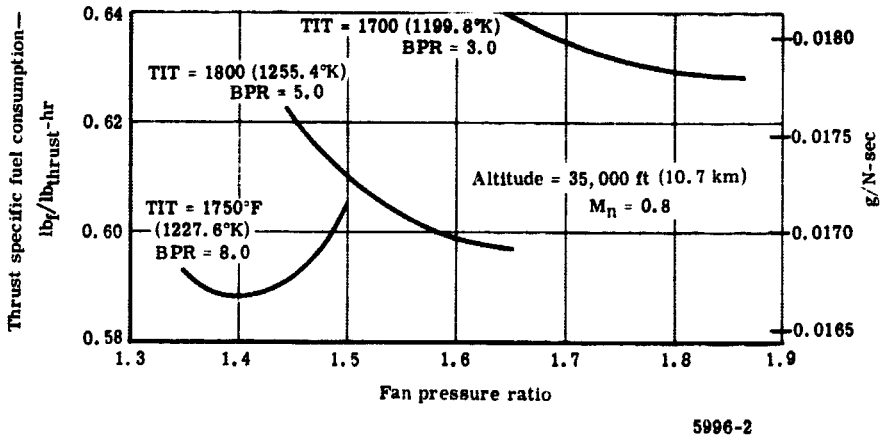

Figure 3a-2. Effects of fan performance on sfc at mid-cruise thrust.

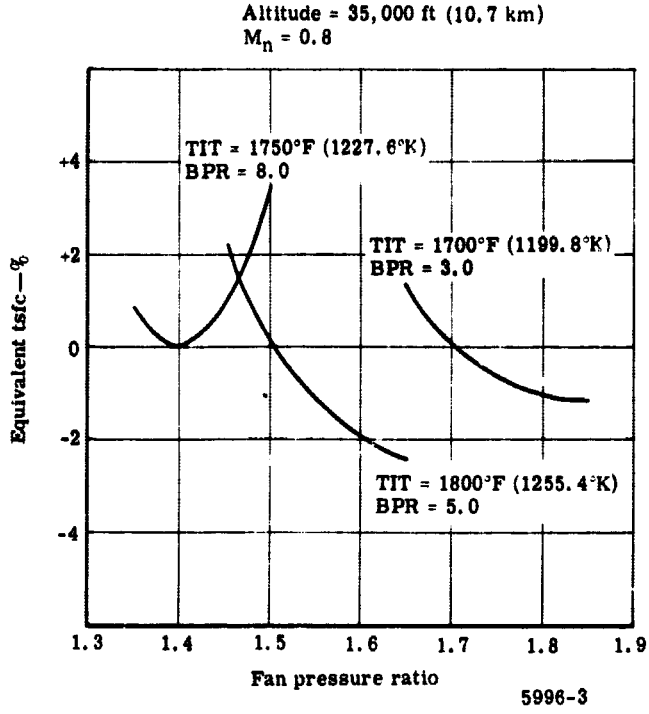

Figure 3a-3. Effects of fan performance on weight-traded tsfc at mid-cruise.

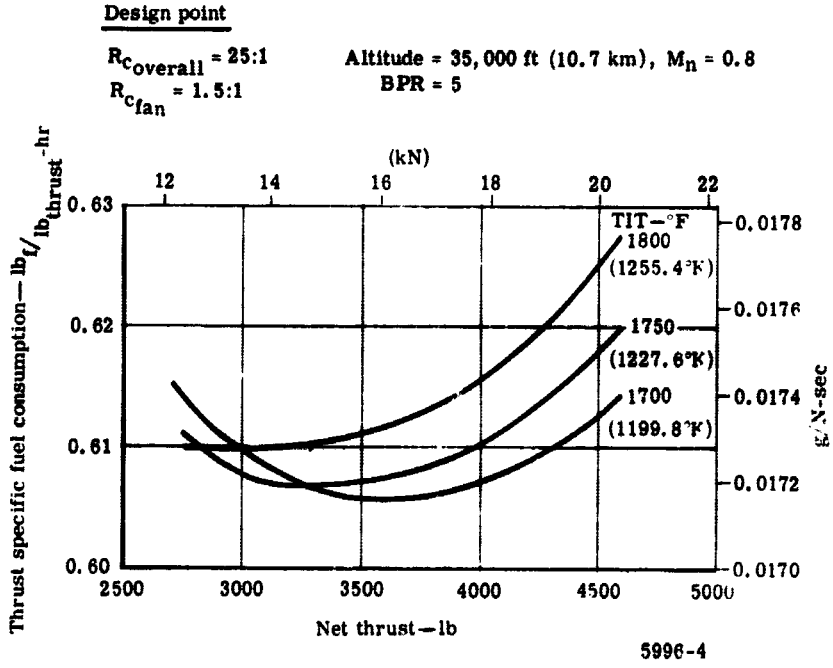

Figure 3a-4. Effects of TIT on total net thrust and tsfc.

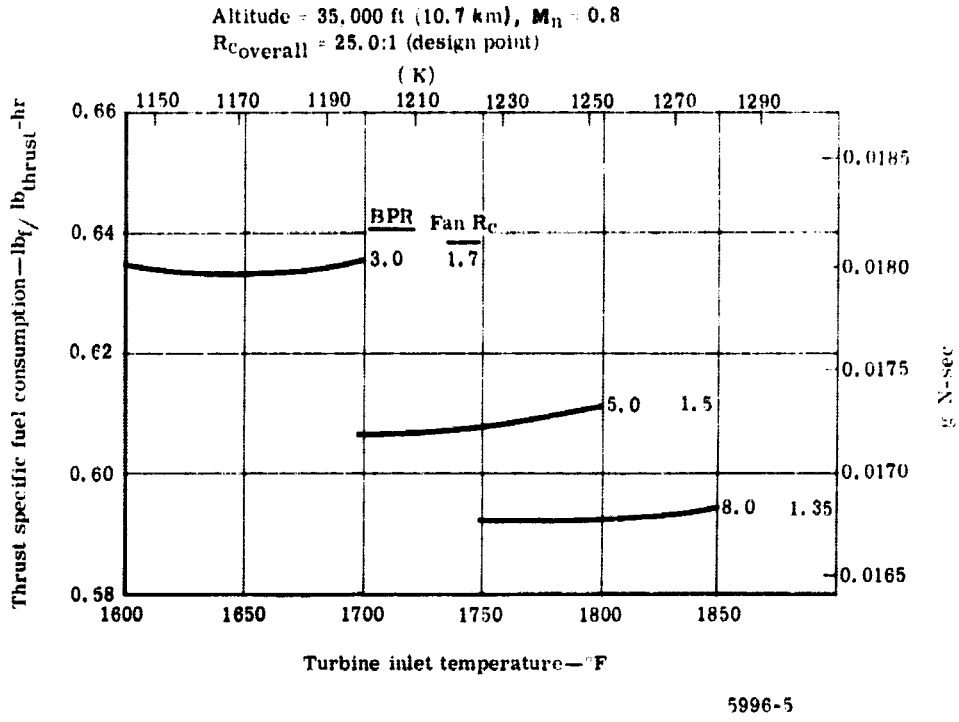

Figure 3a-5. Effects of TIT on tsfc at 75% thrust, mid-point cruise.

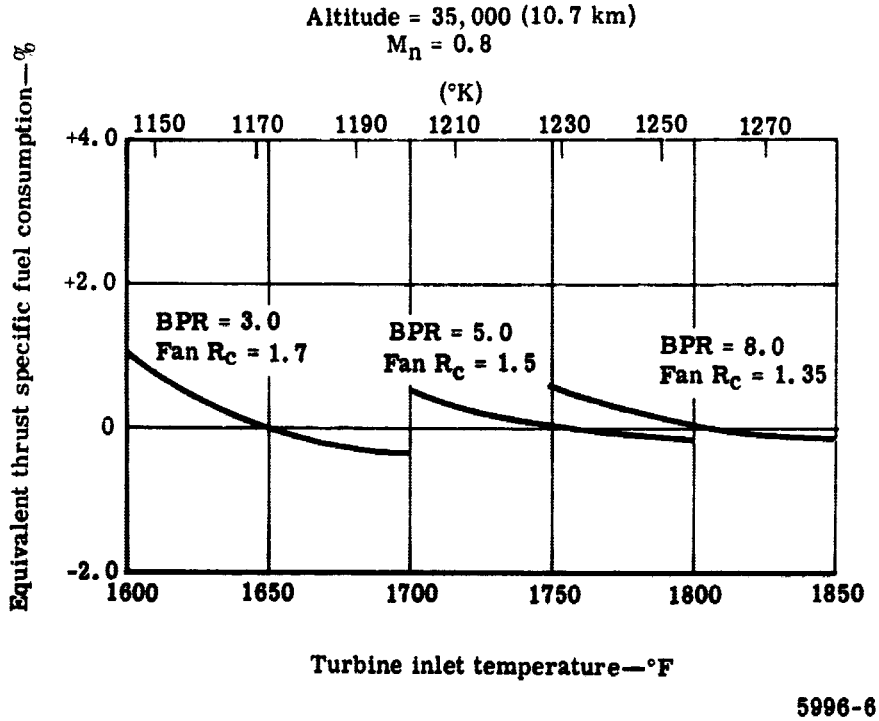

Figure 3a-6. Effects of TIT on weight-traded tsfc at mid-point cruise.

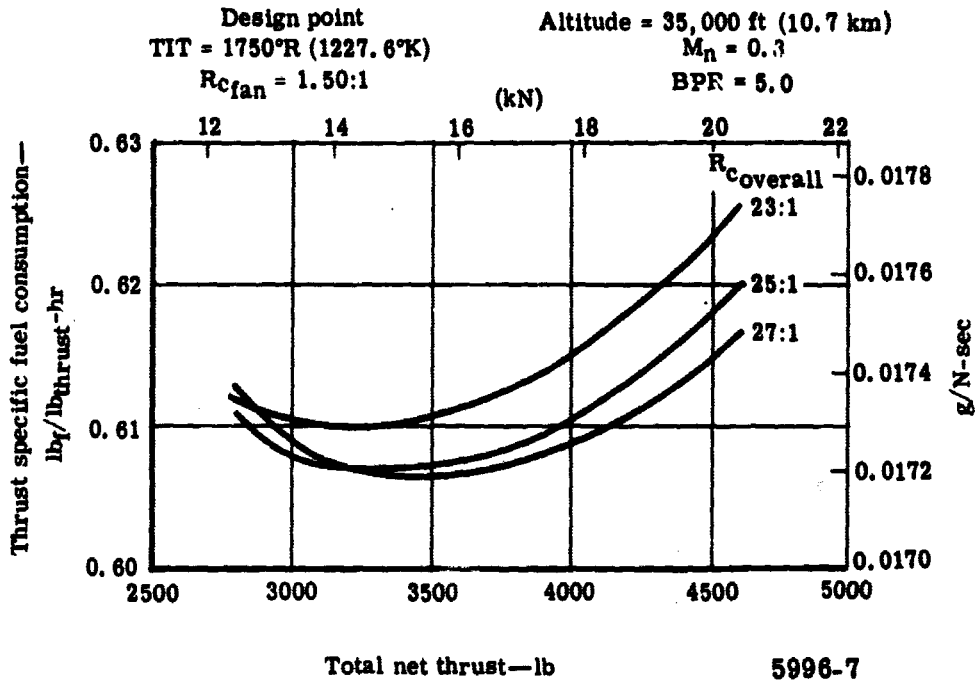

Figure 3a-7. Effects of overall pressure on total net thrust and tsfc.

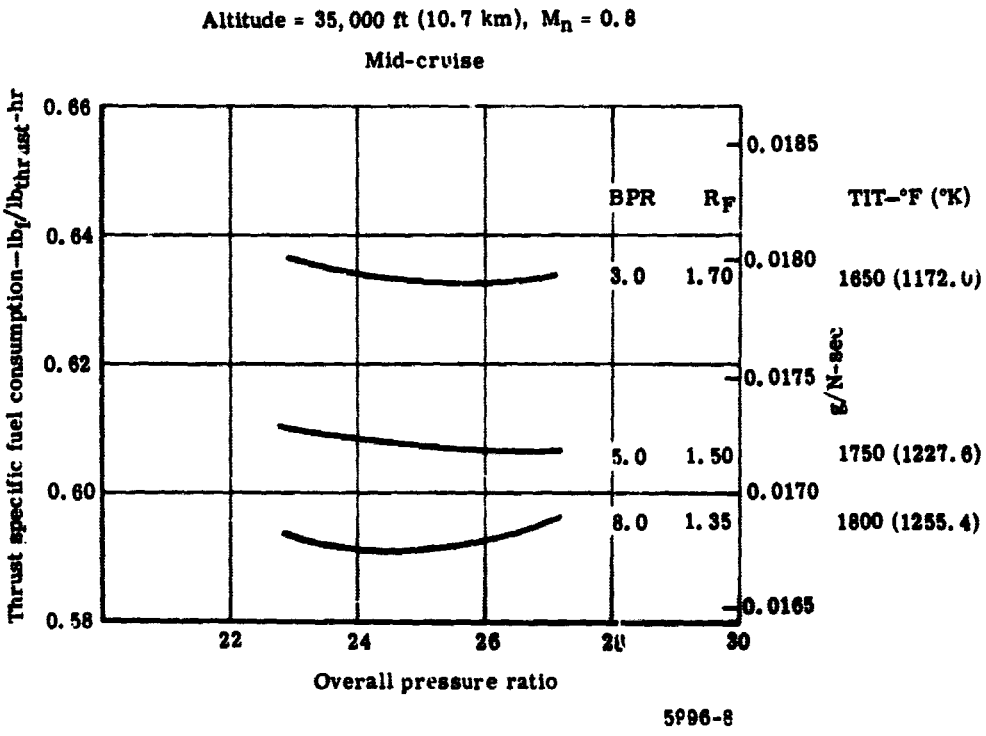

Figure 3a-8. Effects of overall pressure ratio on tsfc.

From the parametric analysis, three engine configurations were selected and a mission analysis and noise characteristics investigation was made. Component maps were developed for each of the engine components and were integrated into an IBM performance program.

The overriding criterion for the final engine selection in Task I was noise reduction; performance and weight, while important, were secondary. Based on noise, cycle trade-offs, and light weight, the Task I recommended cycle was the 5:1 bypass ratio, single-stage fan designated as PD218-5A1.

An additional noise reduction trade-off study was made to compare the 5.5:1 and 5:1 bypass ratio engines. This comparison showed that with the 5.5:1 bypass ratio engine, an improvement of 1 PNdB rearward noise level with a better specific fuel consumption could be obtained at the expense of engine diameter and weight. This cycle, designated PD218-5.5A2, is compared with the PD218-5A1 engine cycle in Table 3a-I.

Table 3a-I.
PD218-5A1 and PD218-5.5A2 cycle comparison.

Design point: 35,000 ft (10.7 km) at Mach 0.8.

	PD218-5A1	PD218-5.5A2
Bypass ratio, BPR	5:1	5.5:1
Net thrust, lb (kN)	5175 (23.02)	5175 (23.02)
sfc at design, $lb_f/hr/lb_t$ (g/N-sec)	0.623 (0.01765)	0.612 (0.01733)
sfc at mid-cruise, $lb_f/hr/lb_t$ (g/N-sec)	0.610 (0.01728)	0.603 (0.01708)
TIT, °F (°K)	1750 (1227.6)	1750 (1227.6)
Fan tip R_c	1.5	1.5
Hub R_c	1.45	1.45
IP compressor R_c	4.08	4.08
HP compressor R_c	4.08	4.08
Corrected airflow, lb/sec (kg/sec)	935 (424.1)	994 (450.9)
Fan tip diameter, in.(m)	74.4 (1.8898)	76.2 (1.9355)
Engine weight, lb (kg)	4544 (2061)	4698 (2131)

TASK II CYCLE

During the Task II phase of the program, noise reduction studies and a detailed preliminary design of a 5.5:1 bypass ratio engine were completed. The engine was designated the PD218-Q and cycle calculations were refined by using typical thrust nozzles having state-of-the-art characteristics. A change in thrust level and Mach number requirements at the

design point resulted in the design point data listed in Table 3a-II and the engine performance ratings given in Table 3a-III. The minimum sfc level was 0.619 $lb_f/hr/lb_t$ (0.01753 g/N-sec) at the altitude cruise condition.

All performance data generated and presented in this report were calculated using the following assumptions:

- ICAO model atmosphere
- 100% inlet recovery
- Real gas properties for turbine expansion process
- No bleed or power extraction

A flat rating was established for the engine such that at takeoff, the engine is flat rated up to standard temperature plus 25°F (14°K) and at the lesser power settings up to standard temperature plus 31°F (17°K).

Table 3a-II.
PD218-Q design point data.

35,000 ft (10.7 km) and Mach 0.82

Bypass ratio, BPR	5.5:1
Net thrust, lb (kN)	4900 (21.8)
sfc, design, $lb_f/hr/lb_t$ (g/N-sec)	0.627 (0.01776)
sfc, mid-cruise, $lb_f/hr/lb_t$ (g/N-sec)	0.619 (0.01753)
TIT, °F (°K)	1763 (1234)
Fan tip R_c	1.5
Hub R_c	1.45
IP compressor R_c	4.08
HP compressor R_c	4.08
Corrected airflow, lb/sec (kg/sec)	941 (426)
LHV, BTU/lb (joule/kg)	18,400 (42.77×10^6)

Table 3a-III.
PD218-Q rating table.

	Altitude			TIT		Thrust		sfc	
Power setting	ft	km	Mach No.	°F	°K	lb	kN	$lb_f/hr/lb_t$	g/N-sec
Takeoff	0		0	1900	1311	21,964	97.7	0.335	0.00948
Max continuous	0		0	1815	1264	19,871	88.39	0.327	0.00926
Max cruise	0		0	1763	1235	18,585	82.67	0.323	0.00915
Max continuous	35,000	10.7	0.82	1815	1264	5,145	22.89	0.634	0.01796
Max cruise	35,000	10.7	0.82	1763	1235	4,900	21.8	0.627	0.01776

Table 3a-IV gives sea level and 35,000-ft (10.7-km) altitude standard and hot day performance data. Engine component inlet and outlet pressures and temperatures, component rotational speeds, and corrected airflows are tabulated for each of the points. Also, data are given for two critical noise situations—takeoff and approach; noise studies have been made at these two conditions. Figure 3a-9 shows the flight operational limits envelope.

Basic uninstalled engine performance data have been calculated at selected conditions and are presented in Tables 3a-V, 3a-VI, and 3a-VII. Figure 3a-10 shows the cycle station numbers consistent with these data.

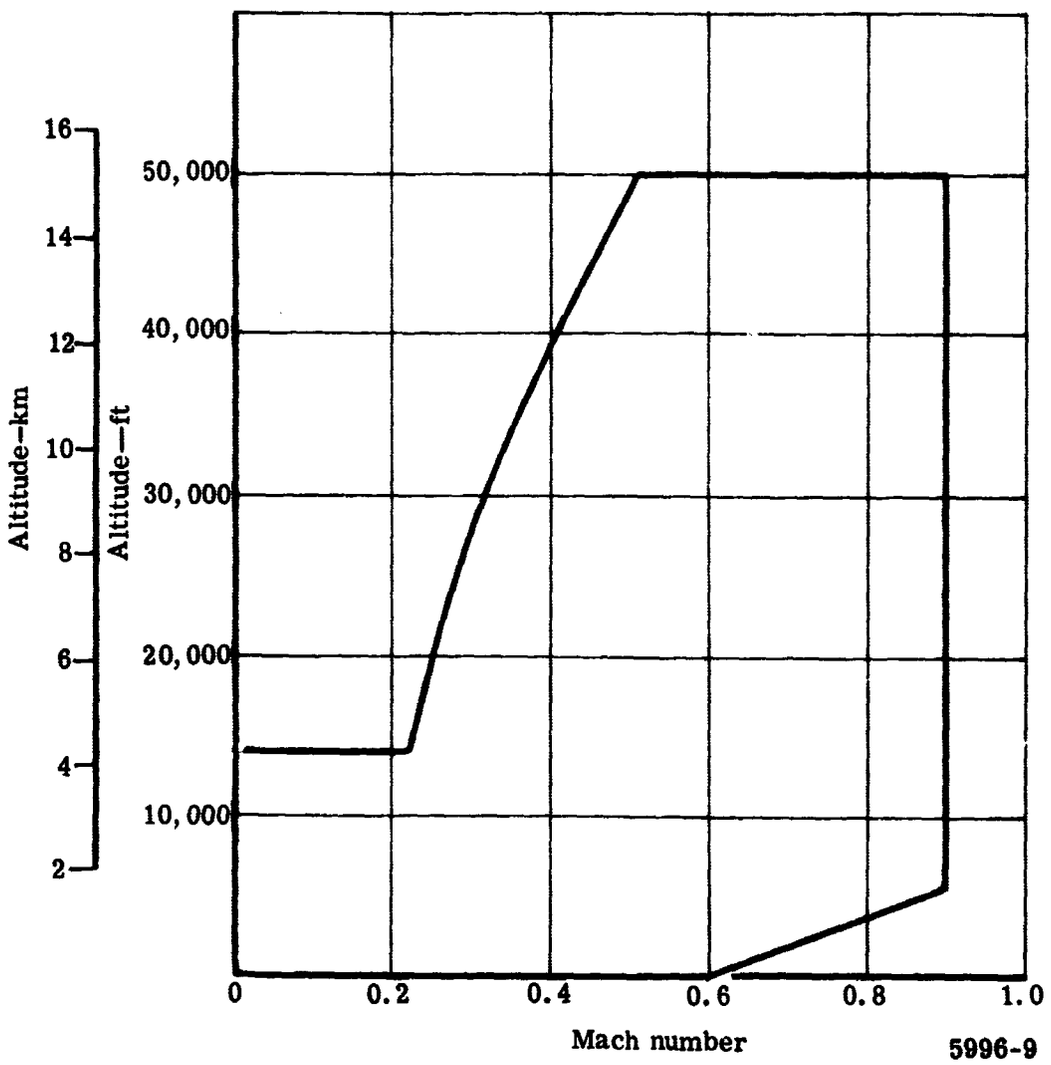

Figure 3a-9. Engine operating envelope.

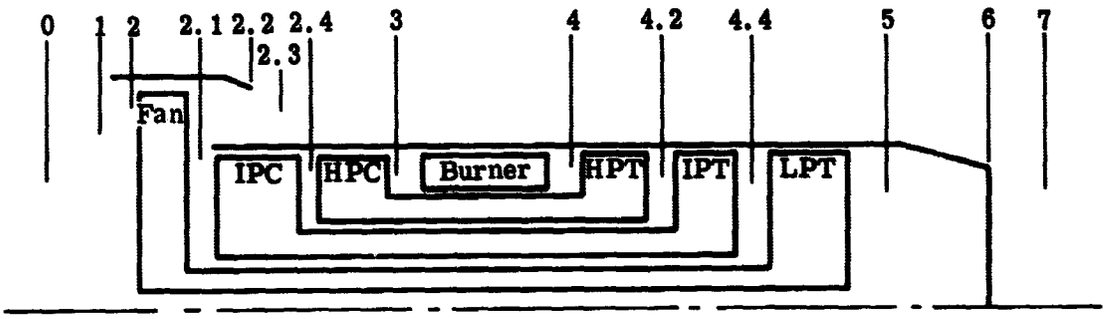

Engine Data Stations

0	Free stream
1	Engine inlet
2	Fan inlet
2.1	Intermediate compressor inlet
2.2	Fan exhaust nozzle
2.3	Fan exhaust region
2.4	High pressure compressor inlet
3	High pressure compressor discharge
4	High pressure turbine inlet
4.2	Intermediate turbine inlet
4.4	Fan turbine inlet
5	Fan turbine discharge
6	Engine outlet
7	Engine exhaust region

Engine Data Parameters

T_2	Fan inlet temperature	°R (°K)
P_2	Fan inlet pressure	psia (kpa)
F_n	Net thrust	lb (kN)
sfc	Specific fuel consumption	lb/hr/lb (g/N-sec)
W_f	Fuel flow	lb/hr (kg/sec)
FNTAM	Corrected net thrust	F_n/δ_{amb}, lb (kN)
RPM L	Fan shaft speed	rpm (rps)
RPM I	Intermediate shaft speed	rpm (rps)
RPM H	High pressure shaft speed	rpm (rps)
WACOR	Total corrected airflow	$W_a\sqrt{\theta_2}/\delta_2$, lb/sec (kg/sec)
BPR	Bypass Ratio	$W_{aBP}/W_{a_{pri}}$
P24P2	Intermediate pressure compressor discharge pressure ratio	
T24T2	Intermediate pressure compressor discharge temperature ratio	
P3P2	High pressure compressor discharge pressure ratio	
T3T2	High pressure compressor discharge temperature ratio	
P22P2	Fan duct exhaust pressure ratio	
T22T2	Fan duct exhaust temperature ratio	
P5P2	Primary exhaust pressure ratio	
T5T2	Primary exhaust temperature ratio	

5996-10

Figure 3a-10. Cycle station number nomenclature.

Table 3a-IV.
PD218-Q engine performance summary.

Flight Condition	Design point standard day	Design point hot day	Sea level takeoff standard day	Sea level takeoff hot day	Takeoff standard day	5000-lb, standard day
Altitude, ft (km)	35,000 (10,688)	35,000 (10,688)	0	0	1000 (0,305)	325 (0,099)
Mach number	0.82	0.82	0	0	0.25	0.25
Ambient temp, °R (°K)	393.9 (218.8)	424.5 (235.8)	518.7 (288.17)	543.7 (302.1)	515 (286.1)	517.5 (287.51)
Total net thrust, lb (kN)	4900 (21.80)	4983 (22.17)	21,964 (97.70)	22,212 (98.80)	16,720 (74.37)	5000 (22.24)
sfc, $lb_f/hr/lb_t$ (g/N-sec)	0.627 (0.0177)	0.658 (0.0186)	0.335 (0.0095)	0.346 (0.0098)	0.436 (0.0123)	0.499 (0.0141)
Bypass ratio	5.5	5.49	5.39	5.37	5.52	6.55
Shaft Speed						
Low pressure rotor						
N corrected, %	100	100.6	88.6	89	88.9	52.3
N physical, rpm (rps)	3286 (54.77)	3430 (57.17)	3137 (52.28)	3227 (57.83)	3155 (52.83)	1861 (31.01)
Intermediate pressure rotor						
N corrected, %	100	100.2	95.1	95.4	95.0	73.7
N physical, rpm (rps)	8382 (139.7)	8721 (145.3)	8508 (141.8)	8736 (145.6)	8508 (141.8)	6400 (106.7)
High pressure rotor						
N corrected, %	100	100.1	98.5	98.6	98.4	92.5
N physical, rpm (rps)	12,555 (209.2)	13,053 (217.5)	12,994 (216.6)	13,317 (221.9)	13,000 (216.7)	11,224 (187.1)
Fan Inlet						
Temperature, °R (°K)	446.8 (248.2)	481.6 (267.6)	518.7 (288.2)	543.7 (302.1)	521.6 (289.8)	524 (291.1)
Pressure, psia (kpa)	5.4 (37.2)	5.4 (37.2)	14.7 (101.4)	14.7 (101.4)	14.8 (102.0)	15.2 (104.8)
$W\sqrt{\theta}/\delta$, lb/sec (kg/sec)	941 (426.8)	943.8 (428.1)	824.8 (374.1)	828.9 (376.0)	836.2 (379.2)	533.8 (242.1)
W_a, lb/sec (kg/sec)	371 (168.3)	358.3 (162.5)	824.8 (374.1)	809.7 (367.3)	840.0 (381.0)	548.2 (248.7)
IP Compressor Inlet						
Temperature, °R (°K)	505 (280.6)	544.8 (302.7)	574.7 (319.3)	603 (335.0)	577 (320.6)	542 (301.1)
Pressure, psia (kpa)	7.8 (53.8)	7.8 (53.8)	20.3 (14.0)	20.3 (14.0)	20.3 (14.0)	16.8 (11.6)
$W\sqrt{\theta}/\delta$, lb/sec (kg/sec)	106.1 (48.13)	106.3 (48.22)	98.5 (44.68)	99.0 (44.90)	98.2 (44.54)	64.9 (29.12)
W_a, lb/sec (kg/sec)	57.1 (25.9)	55.2 (25.0)	129.2 (58.6)	127.0 (57.6)	128.9 (58.47)	72.6 (32.93)
HP Compressor Inlet						
Temperature, °R (°K)	792 (440)	854 (474)	874 (486)	917 (509)	876 (487)	740 (411)
Pressure, psia (kpa)	31.8 (219.2)	31.9 (385.4)	77.0 (530.9)	77.5 (534.3)	77.1 (531.6)	43.6 (300.6)
$W\sqrt{\theta}/\delta$, lb/sec (kg/sec)	32.6 (14.79)	32.6 (14.79)	32.0 (14.51)	32.0 (14.51)	32.0 (14.51)	29.2 (13.24)
W_a, lb/sec (kg/sec)	57.1 (25.90)	55.2 (25.04)	129.2 (58.60)	127.0 (57.60)	128.9 (58.47)	72.6 (32.93)
Burner Inlet						
Temperature, °R (°K)	1226 (681.1)	1318 (732.2)	1329 (738.3)	1392 (773.3)	1331 (739.4)	1080 (600.0)
Pressure, psia (kpa)	129.8 (894.9)	130.6 (900.5)	303.3 (2091)	305.6 (2107)	302.8 (2087)	146.6 (1011)
HP Turbine Inlet						
Temperature, °R (°K)	2223 (1235)	2396 (1331)	2360 (1311)	2474 (1374)	2360 (1311)	1749 (971.7)
Pressure, psia (kpa)	124.0 (854.9)	124.7 (859.8)	289.4 (1995)	291.6 (2010)	288.9 (1992)	139.2 (959.8)
IP Turbine Inlet						
Temperature, °R (°K)	1814 (1008)	1961 (1089)	1931 (1073)	2028 (1127)	1931 (1073)	1418 (787.8)
Pressure, psia (kpa)	49.5 (341.3)	49.8 (343.3)	115.8 (798.4)	116.8 (805.3)	115.6 (797.0)	55.8 (384.7)
LP Turbine Inlet						
Temperature, °R (°K)	1557 (865.0)	1688 (937.8)	1667 (926.1)	1753 (973.9)	1666 (925.6)	1232 (684.4)
Pressure, psia (kpa)	25.0 (172.4)	25.2 (173.7)	59.3 (408.9)	59.8 (412.3)	59.1 (407.5)	30.4 (209.6)
Engine Jet Exit						
W_g, lb/sec (kg/sec)						
Primary jet	57.7 (26.1)	55.8 (25.3)	130.6 (59.2)	128.5 (58.3)	130.3 (59.1)	73.0 (33.1)
Fan discharge	313.9 (142.4)	303.1 (137.5)	695.7 (315.6)	682.6 (309.6)	711.1 (322.5)	475.6 (215.7)
Area, in.^{2} (m^2)						
Primary jet	509.6 (0.3288)					
Fan discharge	1692.4 (1.092)					
Exhaust total temp, °R (°K)						
Primary jet	1194 (663.3)	1300 (722.2)	1323 (735)	1394 (774.4)	1320 (733.3)	1067 (592.8)
Fan discharge	510 (283.3)	551 (306.1)	581 (322.8)	610 (338.9)	583 (323.9)	548 (304.4)
Exit velocity, ft/sec(m/sec)						
Primary jet	1536 (468.2)	1600 (487.7)	1261 (384.4)	1305 (397.8)	1298 (395.6)	622 (189.6)
Secondary jet	1011 (308.2)	1050 (320.0)	821 (250.2)	845 (257.6)	865 (263.6)	575 (175.3)

Table 3a-V.
PD218-Q estimated performance.

Altitude—sea level — Mach No. —0.0
T_{amb}—59°F (288°K) — T_2—518.7°R (288.17°K)
P_{amb}—14.7 psi (101.4 kpa) — P_2—14.7 psi (10.1 kpa)

	Thrust		sfc		Fuel flow		FNTAM		LP rotor speed		IP rotor speed		HP rotor speed	
	(lb)	(kN)	($lb/hr/lb_t$)	(g/N-sec)	(lb/hr)	(kg/sec)	(lb)	(kN)	(rpm)	(rps)	(rpm)	(rps)	(rpm)	(rps)
Takeoff	21,964	97.7	0.335	0.0095	7347	0.926	21,964	97.7	3138	52.3	8507	141.8	12,995	216.6
Max continuous	19,871	88.4	0.327	0.0093	6497	0.819	19,871	88.4	3006	50.1	8265	137.8	12,770	212.8
Max cruise	18,585	82.7	0.323	0.0091	5997	0.756	18,585	82.7	2925	48.8	8104	135.1	12,630	210.5
	15,610	69.4	0.314	0.0089	4900	0.617	15,610	69.4	2714	45.2	7706	128.4	12,287	204.8
	13,286	59.1	0.309	0.00875	4104	0.517	13,286	59.1	2512	41.9	7364	122.7	12,008	200.1
	11,064	49.2	0.307	0.00870	3395	0.428	11,064	49.2	2273	37.9	6997	116.6	11,710	195.2
	8,954	39.8	0.309	0.00875	2769	0.349	8,954	39.8	1999	33.3	6598	110.0	11,381	189.7
	7,006	31.2	0.317	0.0090	2220	0.280	7,006	31.2	1722	28.7	6167	102.8	11,035	184.0
	4,896	21.8	0.347	0.0098	1700	0.214	4,896	21.8	1400	23.3	5596	93.3	10,631	177.2
	3,015	13.4	0.399	0.0113	1204	0.152	3,015	13.4	1081	18.0	4801	80.0	10,010	166.8

	Corrected airflow										
	(lb/hr)	(kg/sec)	BPR	$P_{2.4}/P_2$	$T_{2.4}/T_2$	P_3/P_2	T_3/T_2	$P_{2.2}/P_2$	$T_{2.2}/T_2$	P_5/P_2	T_5/T_2
Takeoff	824.8	0.1039	5.39	5.24	1.68	20.64	2.56	1.43	1.12	1.44	2.55
Max continuous	786.6	0.0991	5.48	4.92	1.65	19.04	2.50	1.39	1.11	1.38	2.47
Max cruise	761.8	0.0960	5.54	4.72	1.63	18.04	2.46	1.36	1.10	1.35	2.42
	700.5	0.0883	5.71	4.23	1.58	15.73	2.36	1.31	1.09	1.27	2.32
	648.2	0.0817	5.83	3.84	1.53	13.93	2.28	1.26	1.08	1.21	2.24
	593.1	0.0747	5.94	3.46	1.49	12.23	2.20	1.22	1.07	1.16	2.16
	534.7	0.0674	6.03	3.09	1.44	10.60	2.11	1.18	1.05	1.12	2.10
	474.1	0.0597	6.08	2.72	1.39	9.06	2.03	1.14	1.04	1.09	2.04
	396.8	0.0500	6.11	2.26	1.33	7.33	1.92	1.10	1.03	1.06	2.00
	311.5	0.0392	6.44	1.71	1.24	5.31	1.78	1.06	1.02	1.03	1.99

Table 3a-VI.
PD218-Q estimated performance.

Altitude – 1000 ft (304.8 m) Mach No. – 0.25
T_{amb} – 55.4°F (286.1°K) T_2 – 522°R (290°K)
P_{amb} – 14.17 psia (97.7 kpa) P_2 – 14.8 psi (10.2 kpa)

	Thrust		sfc		Fuel flow		FNTAM		LP rotor speed		IP rotor speed		HP rotor speed	
	(lb)	(kN)	(lb/hr/lb_t)	(g/N-sec)	(lb/hr)	(kg/sec)	(lb)	(kN)	(rpm)	(rps)	(rpm)	(rps)	(rpm)	(rps)
Takeoff	16,716	74.4	0.436	0.0123	7282	0.918	17,333	77.1	3155	52.6	8506	141.8	12,997	216.6
Max continuous	14,896	66.3	0.432	0.0122	6439	0.811	15,446	68.7	3022	50.4	8266	137.8	12,776	212.9
Max cruise	13,794	61.4	0.431	0.01221	5945	0.749	14,303	63.6	2940	49.0	8108	135.1	12,639	210.7
	11,261	50.1	0.431	0.01221	4857	0.612	11,677	51.9	2729	45.5	7714	128.6	12,296	204.9
	9,304	41.4	0.437	0.0124	4066	0.512	9,647	42.9	2534	42.2	7372	122.9	12,016	200.3
	7,488	33.3	0.449	0.0127	3364	0.424	7,764	34.5	2306	38.4	7010	116.8	11,719	195.3
	5,783	25.7	0.475	0.0135	2746	0.346	5,996	26.7	2028	33.8	6625	110.4	11,394	189.9
	4,243	18.9	0.520	0.0147	2205	0.278	4,400	19.6	1735	28.9	6210	103.5	11,056	184.3
	2,747	12.2	0.620	0.0176	1702	0.214	2,848	12.7	1430	23.8	5674	94.6	10,671	177.9
	1,441	6.4	0.846	0.0240	1219	0.154	1,494	6.6	1084	18.1	4914	81.9	10,115	168.6

	Corrected airflow										
	(lb/hr)	(kg/sec)	BPR	$P_{2.4}/P_2$	$T_{2.4}/T_2$	P_3/P_2	T_3/T_2	$P_{2.2}/P_2$	$T_{2.2}/T_2$	P_5/P_2	T_5/T_2
Takeoff	836.1	0.105	5.52	5.21	1.68	20.44	2.55	1.42	1.12	1.42	2.53
Max continuous	799.9	0.101	5.63	4.89	1.65	18.87	2.49	1.38	1.11	1.35	2.45
Max cruise	776.7	0.098	5.71	4.69	1.63	17.89	2.45	1.36	1.10	1.31	2.40
	719.1	0.091	5.92	4.21	1.57	15.60	2.35	1.30	1.09	1.23	2.30
	669.7	0.084	6.10	3.83	1.53	13.82	2.27	1.26	1.08	1.18	2.22
	619.2	0.078	6.28	3.45	1.49	12.14	2.19	1.21	1.06	1.13	2.14
	565.7	0.071	6.45	3.09	1.44	10.55	2.11	1.17	1.05	1.09	2.07
	510.3	0.064	6.62	2.73	1.39	9.05	2.02	1.13	1.04	1.05	2.01
	446.2	0.056	6.88	2.30	1.33	7.41	1.92	1.09	1.03	1.02	1.96
	375.9	0.047	7.67	1.77	1.25	5.49	1.79	1.05	1.02	0.99	1.95

Table 3a-VII.

PD218-Q estimated performance.

Altitude—35,000 ft (10.668 km) Mach No. —0.82

T_{amb} — -65.8°F (218.9°K) T_2 —446.8°R (248°K)

P_{amb} —3.46 psi (23.9 kpa) P_2 —5.38 psi (37.1 kpa)

	Thrust		sfc		Fuel flow		FNTAM		LP rotor speed		IP rotor speed		HP rotor speed	
	(lb)	(kN)	(lb/hr/lb$_t$)	(g/N-sec)	(lb/hr)	(kg/sec)	(lb)	(kN)	(rpm)	(rps)	(rpm)	(rps)	(rpm)	(rps)
Max continuous	5141	22.8	0.634	0.0180	3258	0.410	21,847	97.1	3344	55.7	8515	141.9	12,694	211.6
Max cruise	4903	21.8	0.627	0.0178	3075	0.387	20,837	92.7	3287	54.8	8382	139.7	12,555	209.3
	4216	18.7	0.619	0.0175	2611	0.329	17,917	79.6	3121	52.0	8073	134.6	12,224	203.7
	3597	16.0	0.621	0.0176	2235	0.282	15,286	67.9	2955	49.3	7812	130.2	11,953	199.2
	2984	13.3	0.632	0.0179	1885	0.238	12,682	56.8	2787	46.5	7518	125.3	11,681	194.7
	2405	10.7	0.651	0.0184	1565	0.197	10,221	45.4	2647	44.1	7196	119.9	11,394	189.9
	1846	8.2	0.691	0.0196	1275	0.161	7,847	34.9	2487	41.5	6853	114.2	11,097	185.0
	1319	5.9	0.774	0.0219	1020	0.128	5,603	24.9	2304	38.4	6495	108.3	10,779	179.7
	878	3.9	0.915	0.0259	804	0.101	3,733	16.6	2144	35.7	6098	101.6	10,436	173.9

	Corrected airflow										
	(lb/hr)	(kg/sec)	BPR	$P_{2.4}/P_2$	$T_{2.4}/T_2$	P_3/P_2	T_3/T_2	$P_{2.2}/P_2$	$T_{2.2}/T_2$	P_5/P_2	T_5/T_2
Max continuous	950.9	0.120	5.44	6.04	1.79	24.91	2.79	1.52	1.15	1.50	2.74
Max cruise	941.1	0.119	5.50	5.92	1.77	24.14	2.74	1.50	1.14	1.46	2.67
	907.0	0.114	5.72	5.51	1.72	21.86	2.64	1.45	1.13	1.35	2.52
	872.1	0.110	5.96	5.11	1.68	19.80	2.55	1.40	1.11	1.25	2.40
	835.7	0.105	6.26	4.70	1.63	17.75	2.47	1.35	1.10	1.15	2.29
	799.1	0.101	6.63	4.28	1.59	15.69	2.38	1.30	1.09	1.06	2.18
	760.4	0.096	7.09	3.85	1.54	13.69	2.29	1.24	1.07	0.98	2.07
	720.0	0.091	7.63	3.42	1.49	11.79	2.20	1.19	1.06	0.90	1.98
	682.6	0.086	8.30	3.02	1.44	10.04	2.10	1.14	1.05	0.84	1.89

3b. Summary of Engine Configurations Studied

During Task I of the contract, three engine configurations were selected for a preliminary design effort. This selection was based on the results of an optimization study to determine the effect of bypass ratio, tip speed, fan aerodynamics, and blade row spacing on overall engine noise production. The selected engines were:

- A 5:1 bypass ratio, single-stage fan engine designated as PD218-5A1, as shown in Figure 3b-1
- A 5:1 bypass ratio, two-stage fan engine designated PD218-5B1, as shown in Figure 3b-2
- A 3:1 bypass ratio, two-stage engine designated PD218-3B1, as shown in Figure 3b-3

These engines have three-rotor systems and incorporate the same design considerations and mechanical arrangement features that are discussed in detail in Subsection 3d, PD218-Q Engine Description. The design point used for all engine aerodynamic components was the altitude cruise condition of 35,000 ft (10.7 km) at Mach 0.8.

Table 3b-I summarizes and facilitates comparison of engine and component configurations for the three Task I study engines.

Table 3b-I.

Engine and component configuration summary for Task I study engines.

Design point: 35,000 ft (10.7 km) at Mach 0.8

	PD218-5A1	PD218-5B1	PD218-3B1
Engine			
Bypass ratio	5:1	5:1	3:1
Overall pressure ratio	24.1:1	24.1:1	25.6:1
Turbine inlet temp, °F (°K)	1750 (1230)	1750 (1230)	1700 (1200)
Fan compressor			
No. of stages	1	2	2
Corrected airflow, lb/sec (kg/sec)	935 (424)	935 (424)	708 (321)
Pressure ratio, primary	1.45:1	1.45:1	1.65:1
Pressure ratio, bypass	1.50:1	1.50:1	1.70:1

Table 3b-I. (cont)

Fan compressor (continued)	PD218-5A1	PD218-5B1	PD218-3B1
Corrected tip speed, rotor inlet, ft/sec (m/sec)	1196 (364.5)	825 (251.5)	964 (293.8)
Corrected specific weight flow, rotor inlet, lb/sec/ft^2 (kg/sec/m^2)	39.5 (1.66)	39.5 (1.66)	39.5 (1.66)
Corrected rotor speed, rpm (rps)	3683 (61.38)	2559 (42.65)	3440 (57.33)
IP compressor			
No. of stages	8	8	7
Corrected flow, lb/sec (kg/sec)	114.2 (51.8)	114.2 (51.8)	116.5 (52.8)
Pressure ratio	4.08:1	4.08:1	3.8:1
First blade corrected tip speed, ft/sec (m/sec)	1050 (320)	1050 (320)	1050 (320)
Corrected specific weight flow, rotor inlet, lb/sec/ft^2 (kg/sec/m^2)	37.6 (1.58)	37.6 (1.58)	37.6 (1.58)
Corrected rotor speed, rpm (rps)	8664 (144.4)	8664 (144.4)	8565 (142.75)
HP compressor			
No. of stages	8	8	8
Corrected flow, lb/sec (kg/sec)	35.0 (15.9)	35.0 (15.9)	37.9 (17.2)
Pressure ratio	4.08:1	4.08:1	4.08:1
First blade corrected tip speed, ft/sec (m/sec)	1000 (304.8)	1000 (304.8)	1000 (304.8)
Corrected specific weight flow, rotor inlet, lb/sec/ft^2 (kg/sec/m^2)	37.2 (1.57)	37.2 (1.57)	37.9 (1.60)
Corrected rotor speed, rpm (rps)	10,368 (172.8)	10,368 (172.8)	9,948 (165.8)

Table 3b-I. (cont)

	PD218-5A1	PD218-5B1	PD218-3B1
Annular combustor			
Heat load, BTU/hr-ft^3-atm (joules/N-m-sec)	2.5×10^6 (25.5×10^6)	2.5×10^6 25.5×10^6)	2.5×10^6 (25.5×10^6)
Length/height ratio	2.97	2.97	2.97
Circumferential temp distribution, T_{max}/T_{avg}	1.12	1.12	1.12
No. of fuel nozzles	16	16	16
No. of igniters	2	2	2
HP turbine			
No. of stages	1	1	1
Design work, BTU/lb (joules/g)	110.9(257.9)	110.9(257.9)	113.3(263.5)
Stage inlet temp, °F(°K)	1750(1230)	1750(1230)	1700(1200)
Blade aspect ratio	2.15	2.15	2.0
IP turbine			
No. of stages	1	1	1
Design work, BTU/lb (joules/g)	68.39(159.1)	68.39(159.1)	67.1(156.1)
Stage inlet temp, °F(°K)	1344(1002)	1344(1002)	1285(969)
Blade aspect ratio	2.62	2.62	2.76
LP turbine			
No. of stages	4	6	4
Design work, first-stage, BTU/lb(joules/g)	21.77(50.6)	14.4(33.5)	19.53(45.4)
Design work, last-stage, BTU/lb(joules/g)	22.20(51.6)	15.2(35.4)	20.05(46.6)
First-stage inlet temp, °F(°K)	1091(862)	1091(862)	1036(576)
Last-stage inlet temp, °F(°K)	845(725)	816(709)	814(708)

Table 3b-I. (cont)

	PD218-5A1	PD218-5B1	PD218-3B1
LP turbine (continued)			
First-stage blade aspect ratio	4.44	4.0	4.48
Last-stage blade aspect ratio	6.07	6.42	6.31

The estimated weight breakdown for the Task I study engines is summarized in Table 3b-II. The accessory equipment items include the accessory drive gearbox, the fuel and control system, the lubrication system, the ignition system, and all associated plumbing.

Table 3b-II.
Weight estimate summary for Task I study engines.

(Weight in pounds*)

Engine component	PD218-5A1			PD218-5B1			PD218-3B1		
	Rotating	Static	Total	Rotating	Static	Total	Rotating	Static	Total
Fan compressor assembly	328.0 (148.8)	480.9 (218.1)	808.9 (366.9)	633.4 (287.3)	861.0 (390.5)	1494.4 (677.8)	604.4 (274.1)	697.3 (316.3)	1301.7 (590.4)
IP compressor assembly	194.7 (88.3)	262.8 (119.2)	457.5 (207.5)	194.7 (88.3)	279.1 (126.6)	473.8 (214.9)	181.2 (82.2)	283.0 (128.4)	464.2 (210.6)
HP compressor assembly	226.4 (102.7)	169.1 (76.7)	395.5 (179.4)	226.4 (102.7)	169.1 (76.7)	395.5 (179.4)	232.0 (105.2)	179.1 (81.2)	411.1 (186.5)
Diffused and combustor assembly	—	244.4 (110.9)	244.4 (110.9)	—	244.4 (110.9)	244.4 (110.9)	—	250.1 (113.4)	250.1 (113.4)
HP turbine assembly	163.6 (74.2)	98.3 (44.6)	261.9 (118.8)	163.6 (74.2)	98.3 (44.6)	261.9 (118.8)	165.9 (75.3)	105.0 (47.6)	270.9 (122.9)
IP turbine assembly	195.9 (88.9)	201.0 (91.2)	396.9 (180.0)	195.9 (88.9)	216.8 (98.3)	412.7 (187.2)	198.4 (90.0)	246.0 (111.6)	444.4 (201.6)
Fan turbine assembly	570.3 (258.7)	514.4 (233.3)	1084.7 (492.0)	943.7 (428.1)	860.6 (390.5)	1804.6 (818.5)	579.5 (262.9)	547.5 (248.3)	1127.0 (511.2)
Accessory equipment	—	—	480.8 (218.1)	—	—	482.8 (219.0)	—	—	482.8 (219.0)
Subtotal	1678.9 (761.6)	1970.9 (894.0)		2357.7 (1069.4)	2729.6 (1238.1)		1961.4 (889.7)	2308.0 (1046.9)	
Total engine weight (without margin)			4130.6 (1873.6)			5570.1 (2526.5)			4752.2 (2155.6)
Estimated engine weight (including 10% margin)			4544 (2061.1)			6127 (2779.1)			5227 (2370.9)

*Numbers in parenthesis represent mass in kilograms.

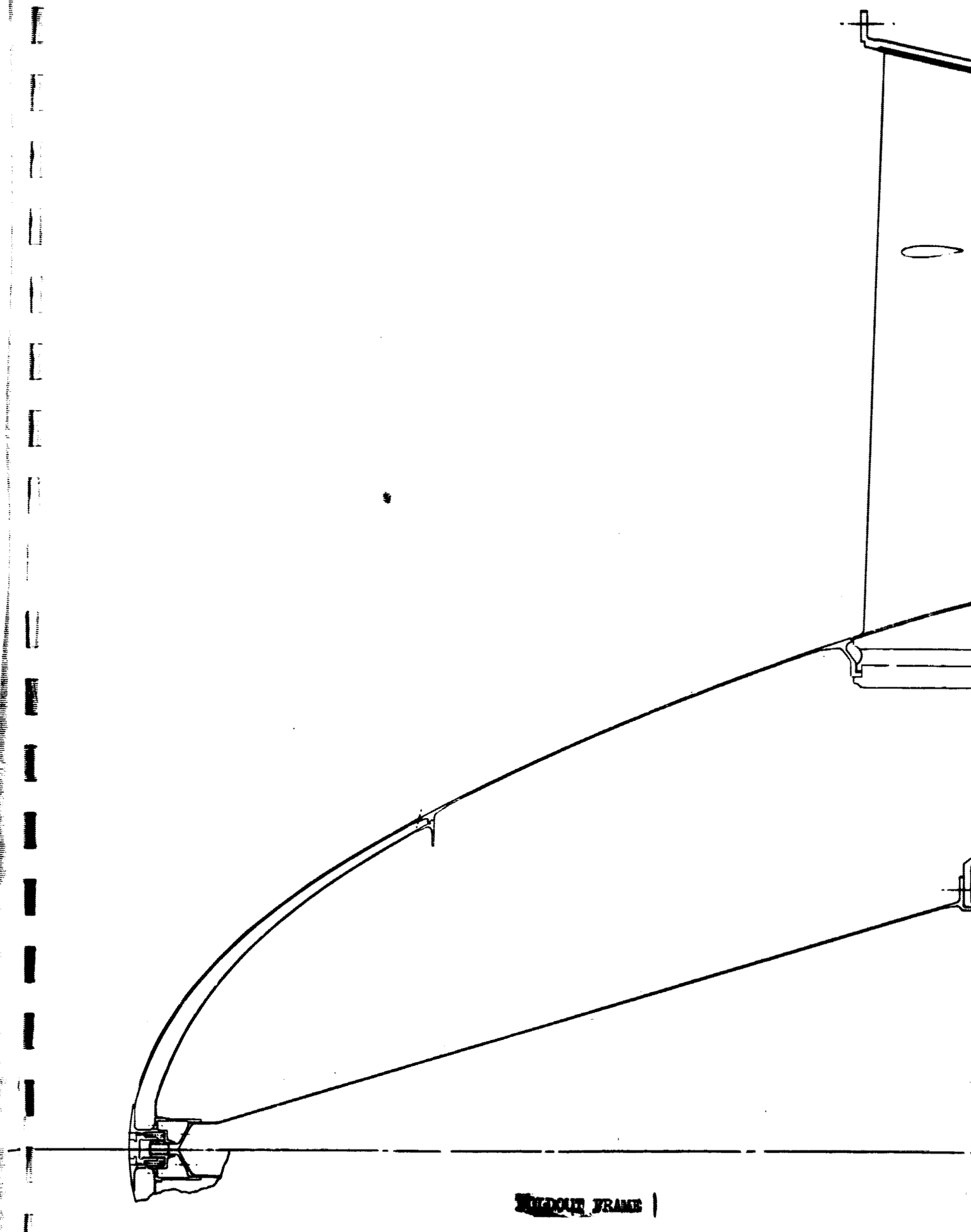

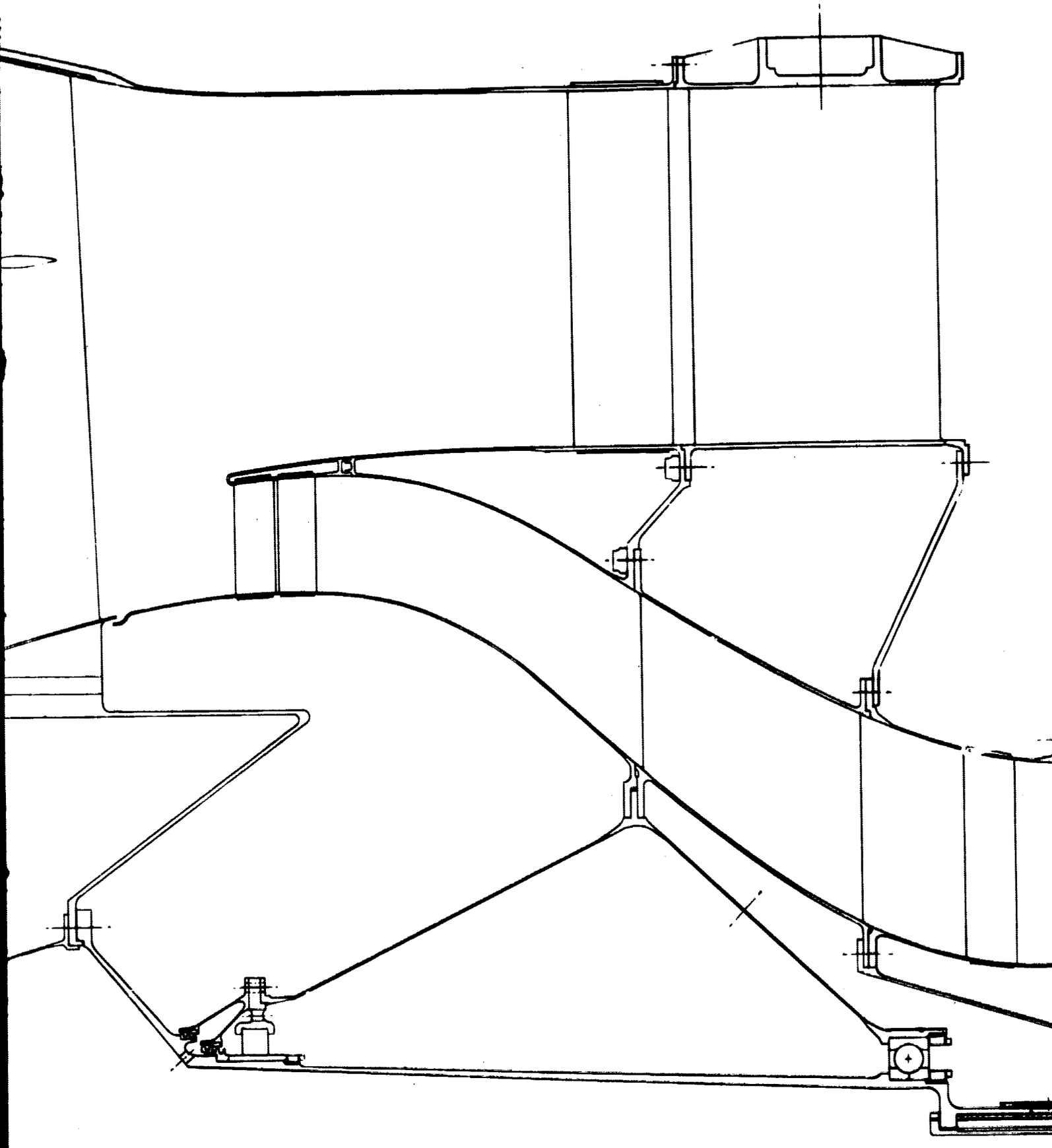

FOLDOUT FRAME 2

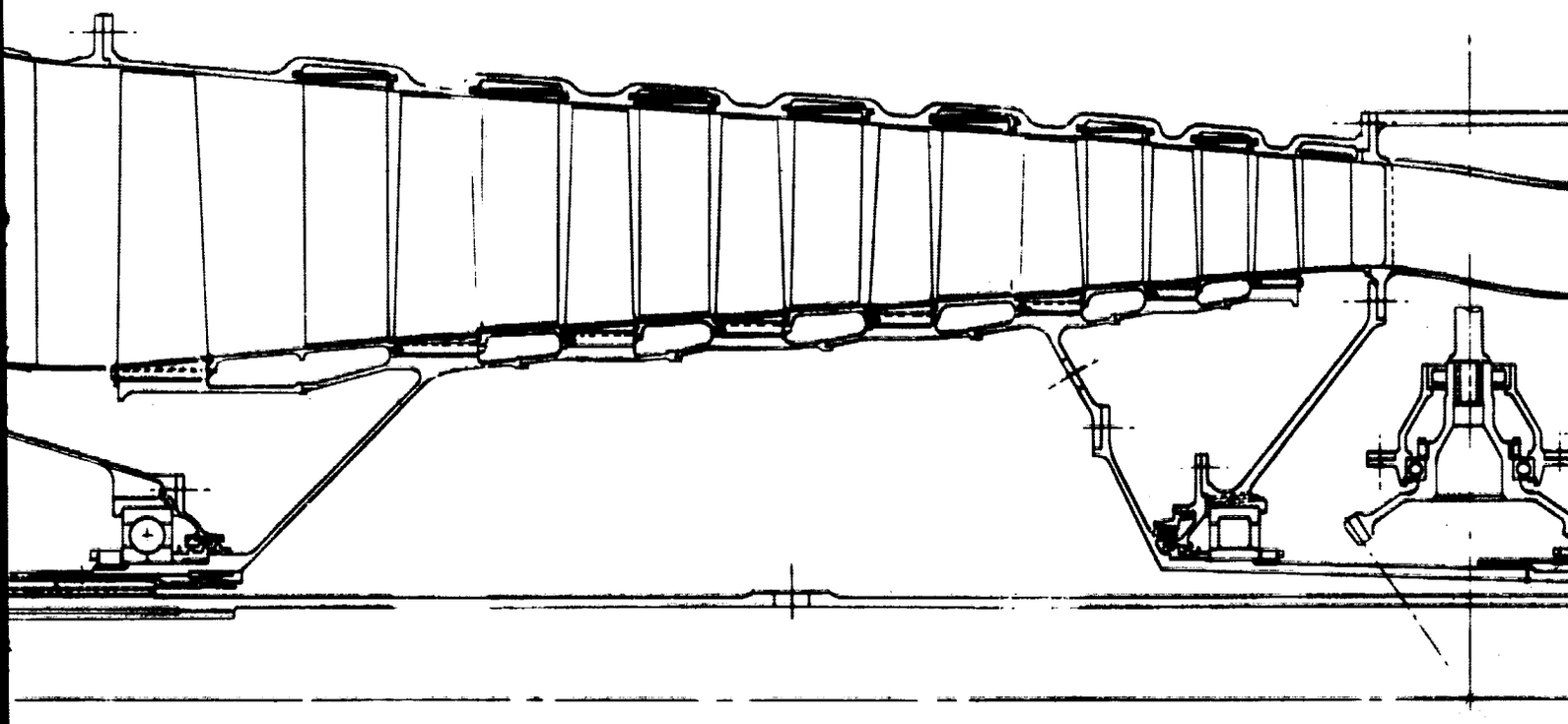

FOLDOUT FRAME 3

FOLDOU

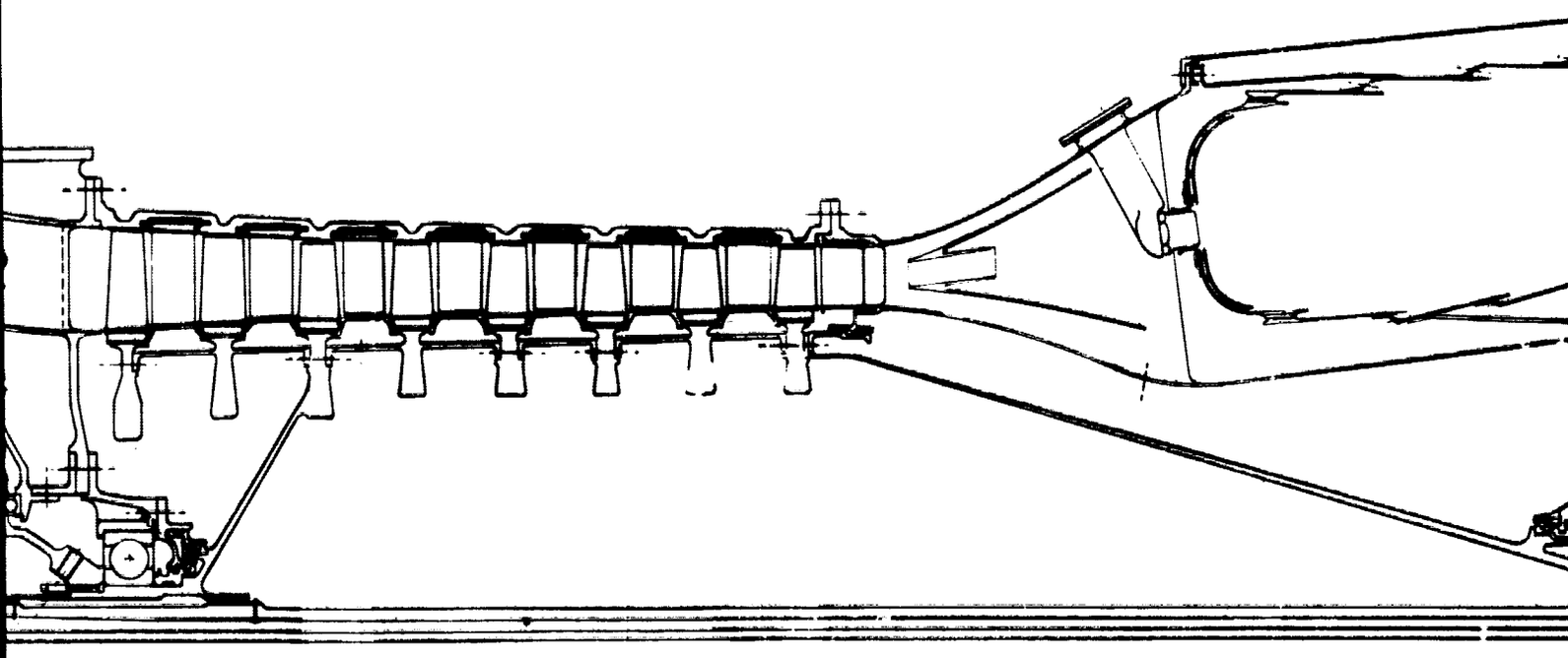

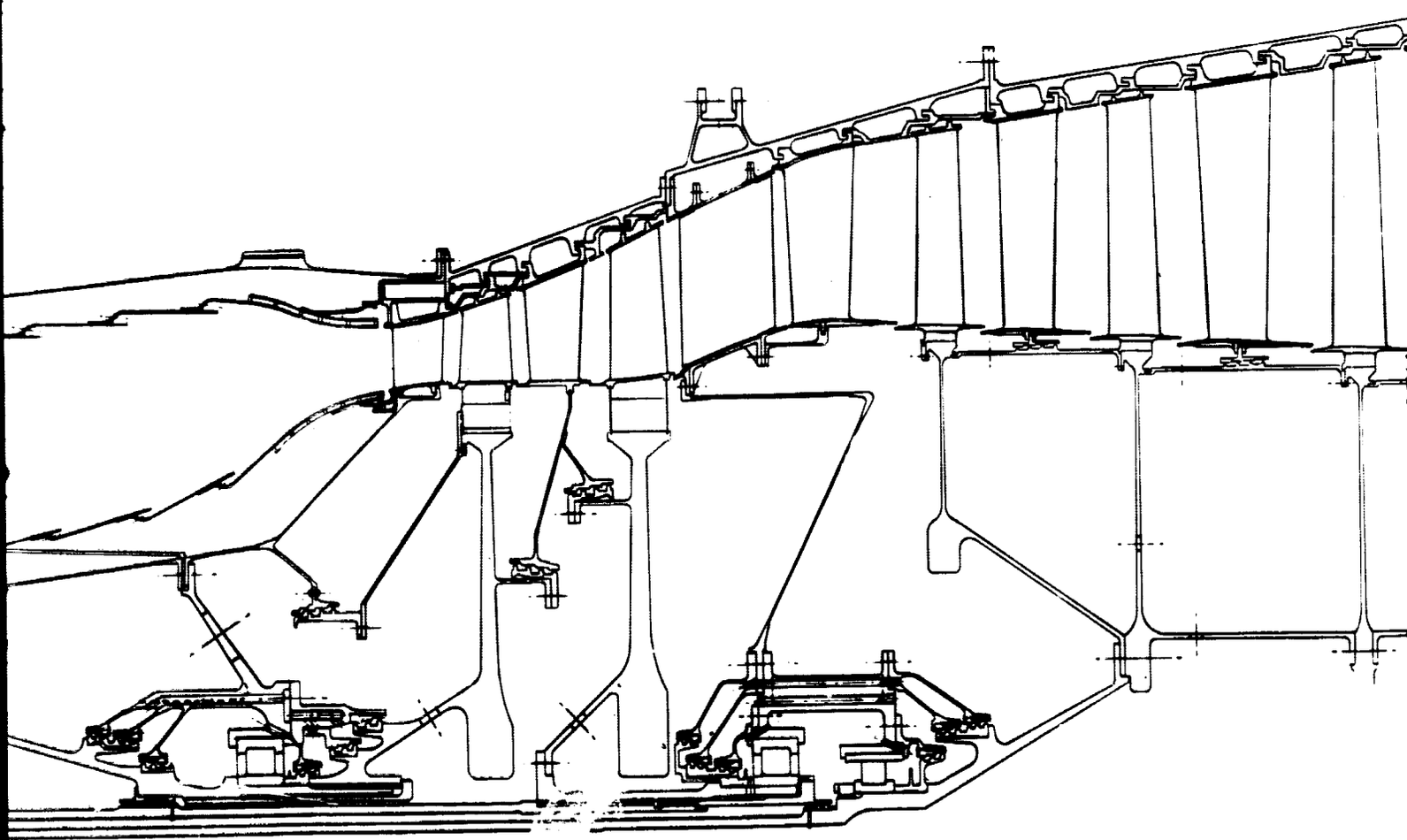

FOLDOUT FRAME 5

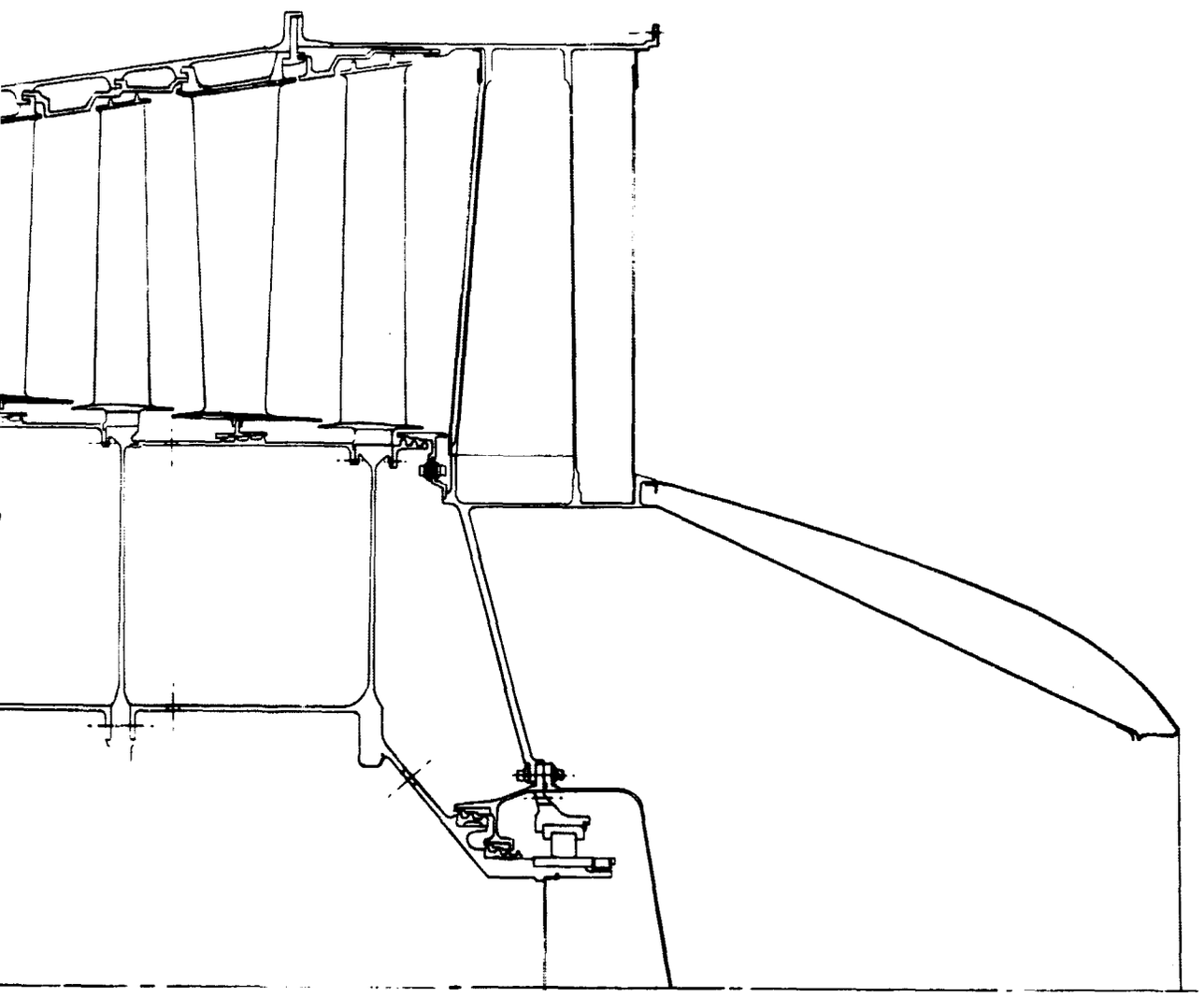

Figure 3b-1. PD218-5A1 engine cross section.

FOLDOUT FRAME 6

PRECEDING PAGE BLANK NOT FILMED.

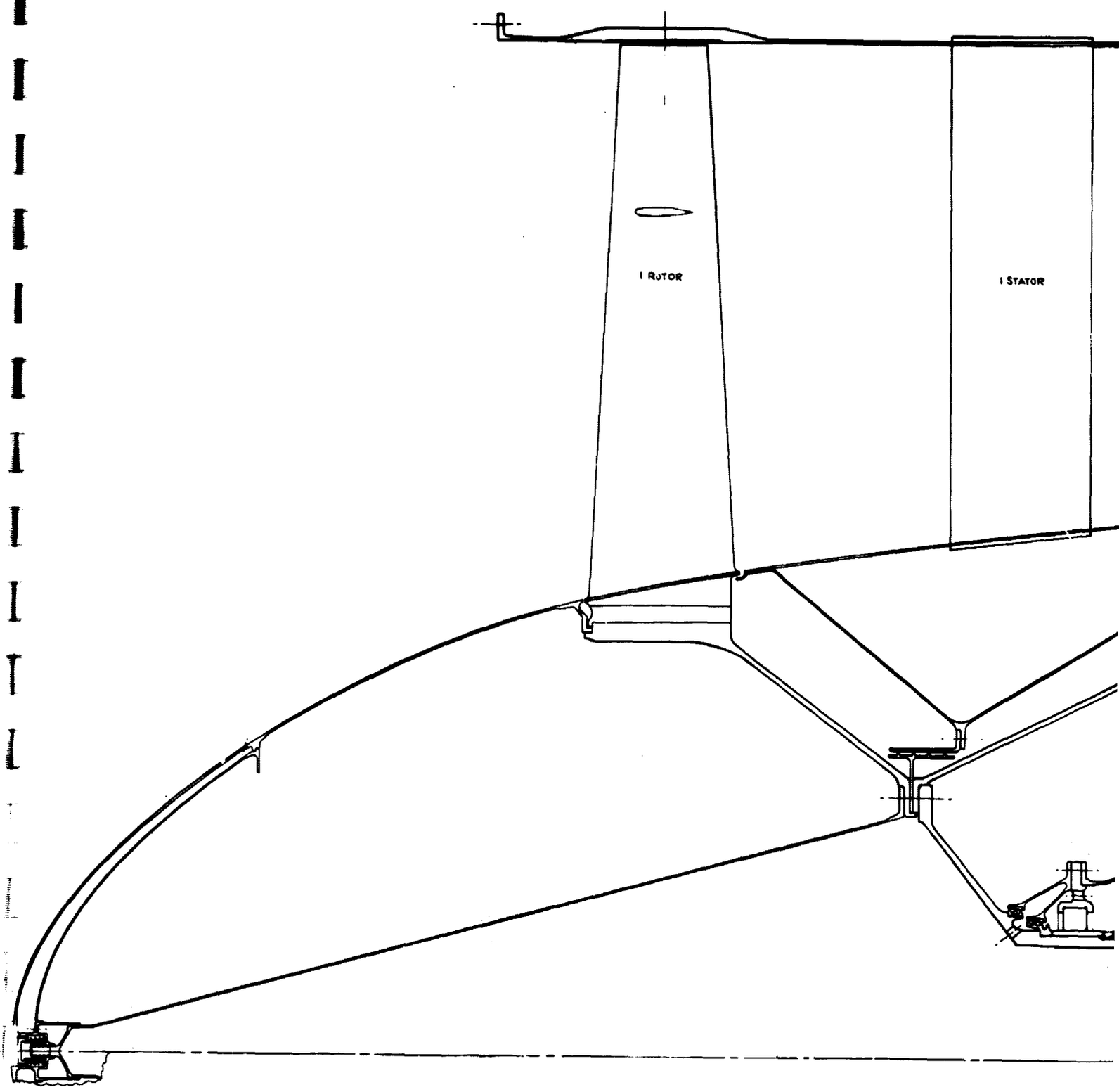

FOLDOUT FRAME 1

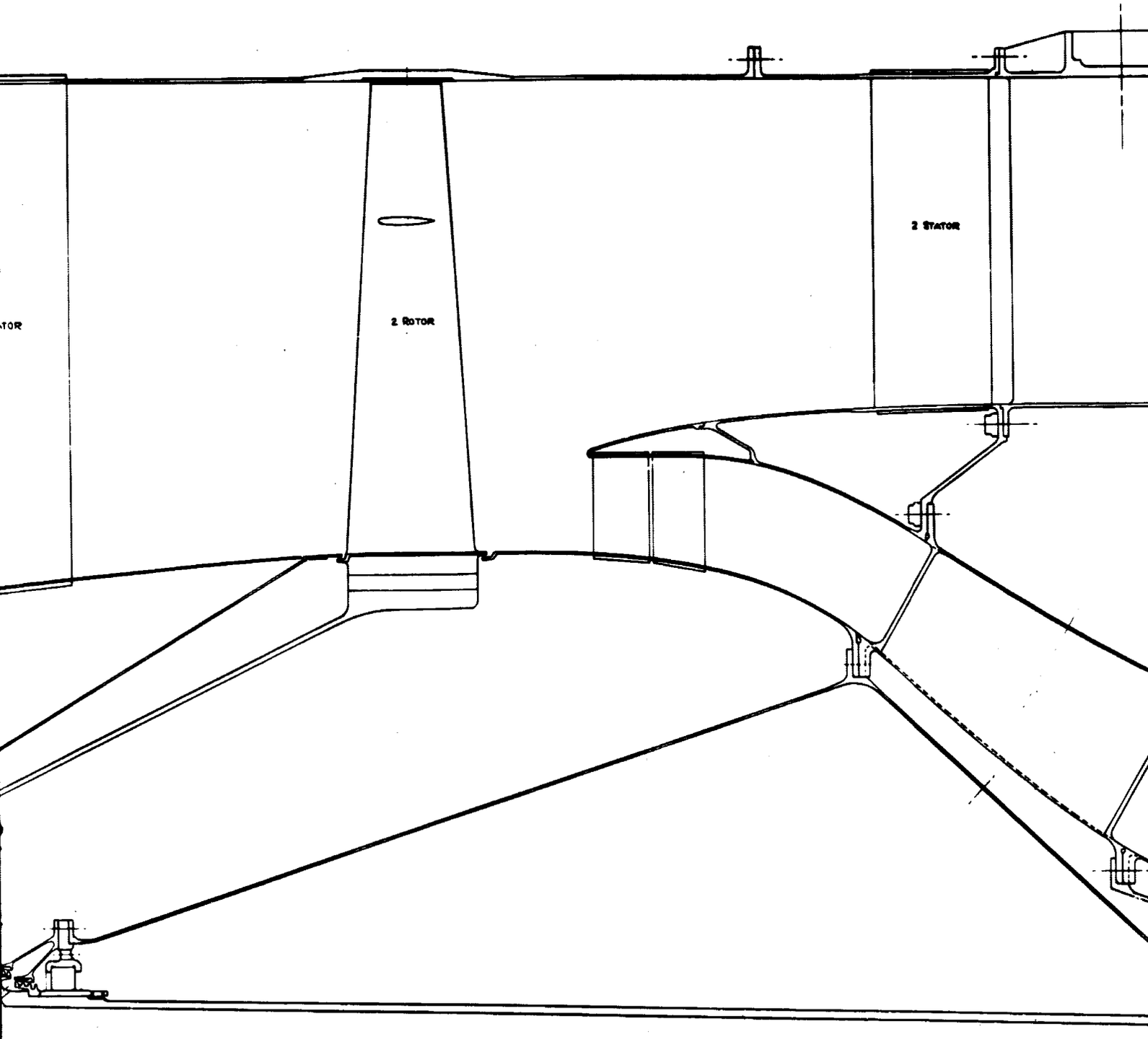

FOLDOUT FRAME 2

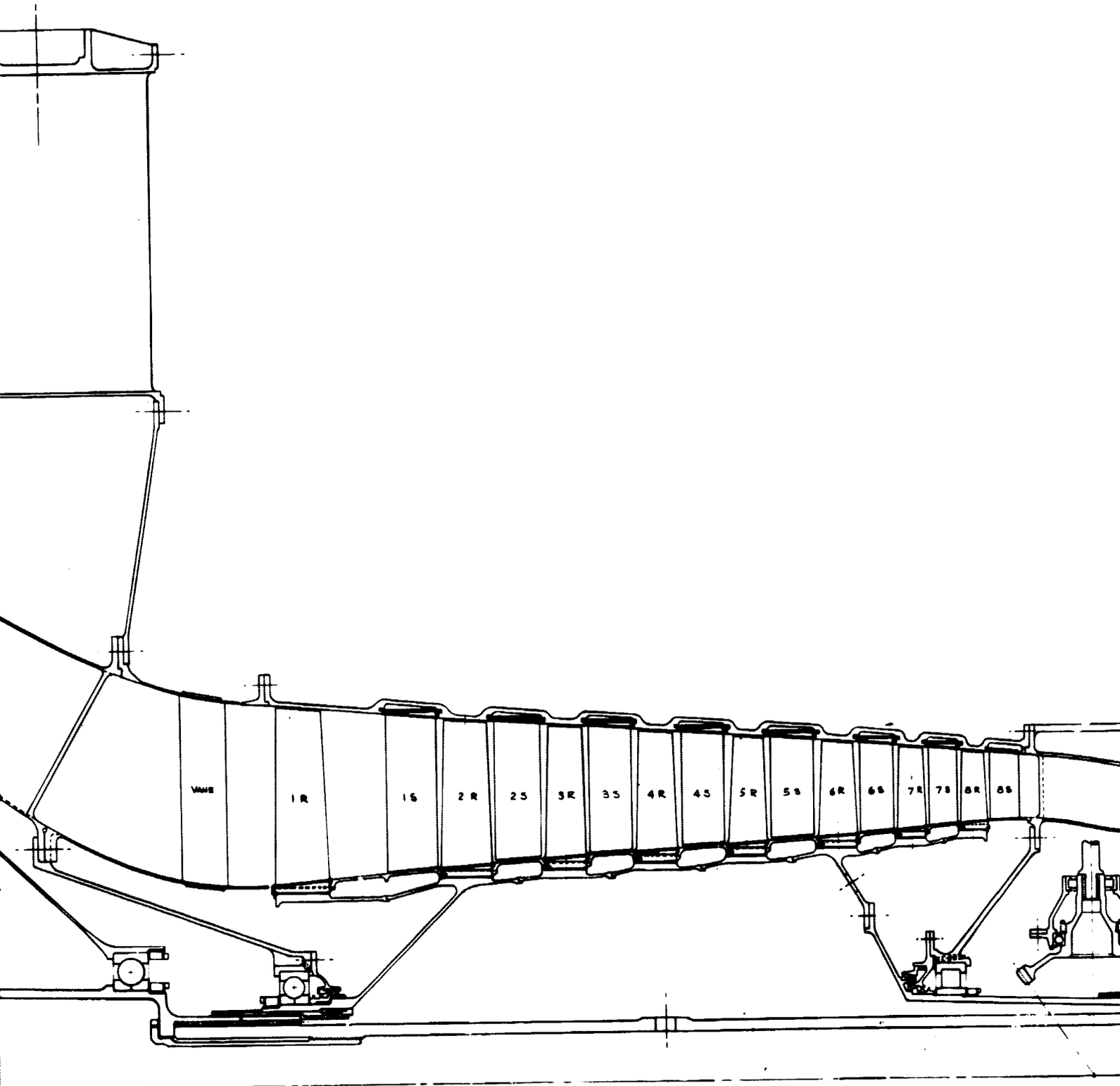

FOLDOUT FRAME 3

FOLDOUT FRAME

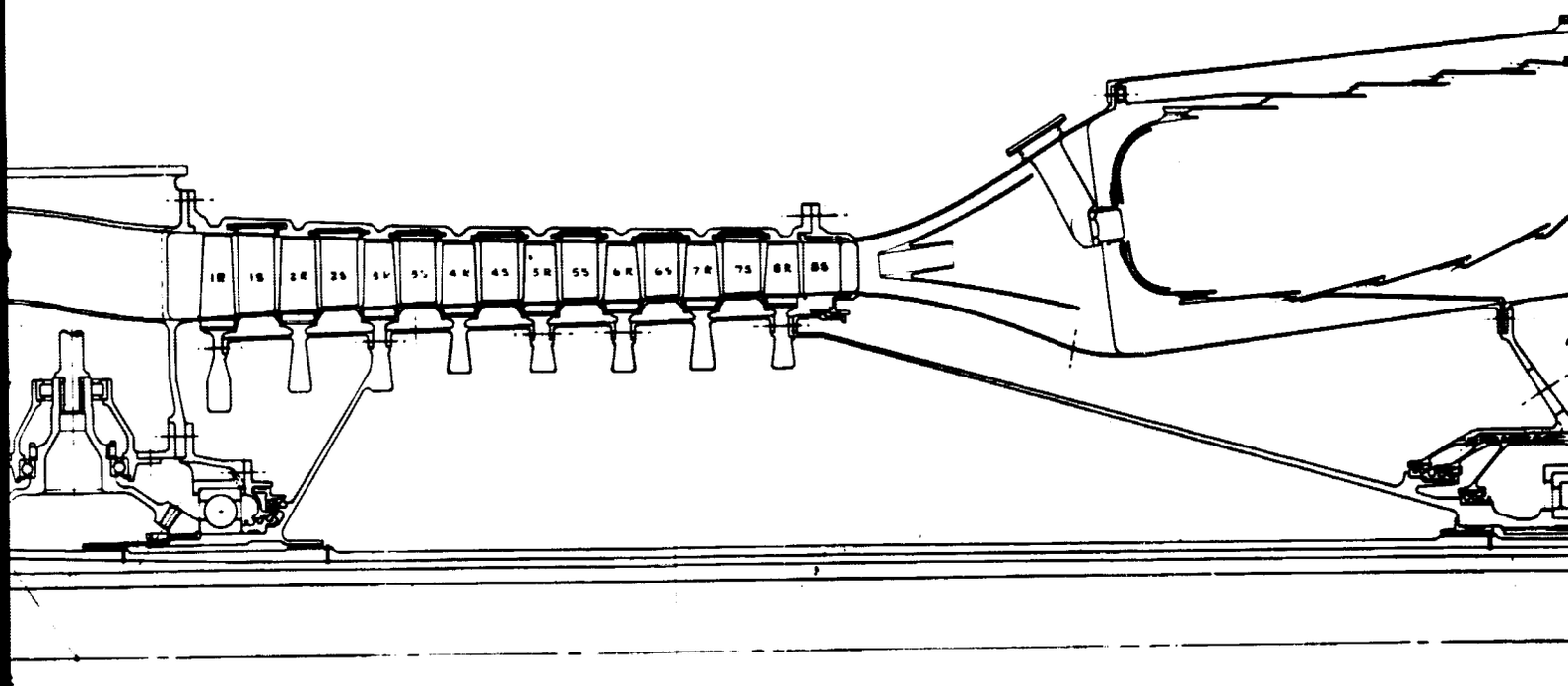

FRAME

FOLDOUT FRAME 4

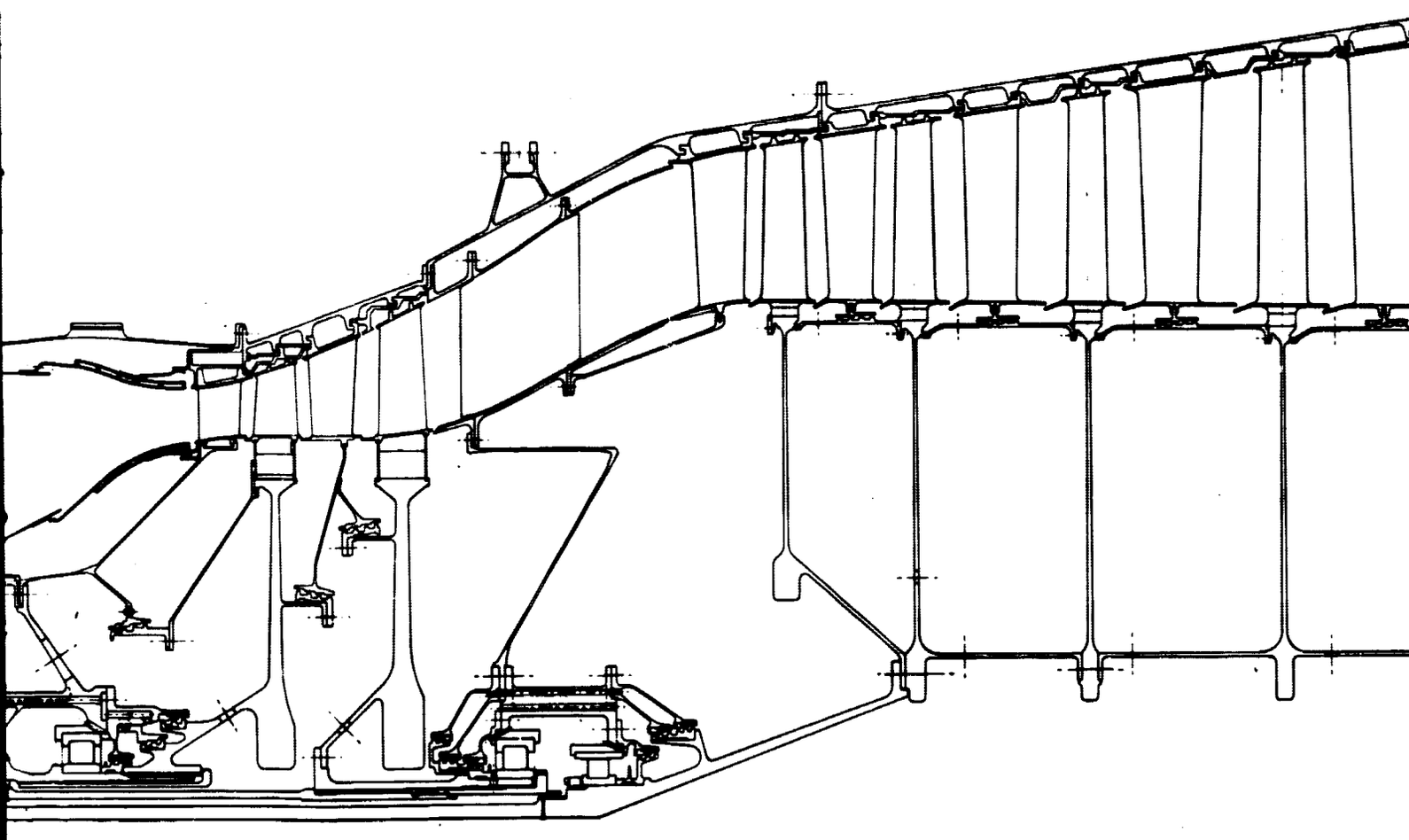

FOLDOUT FRAME 5

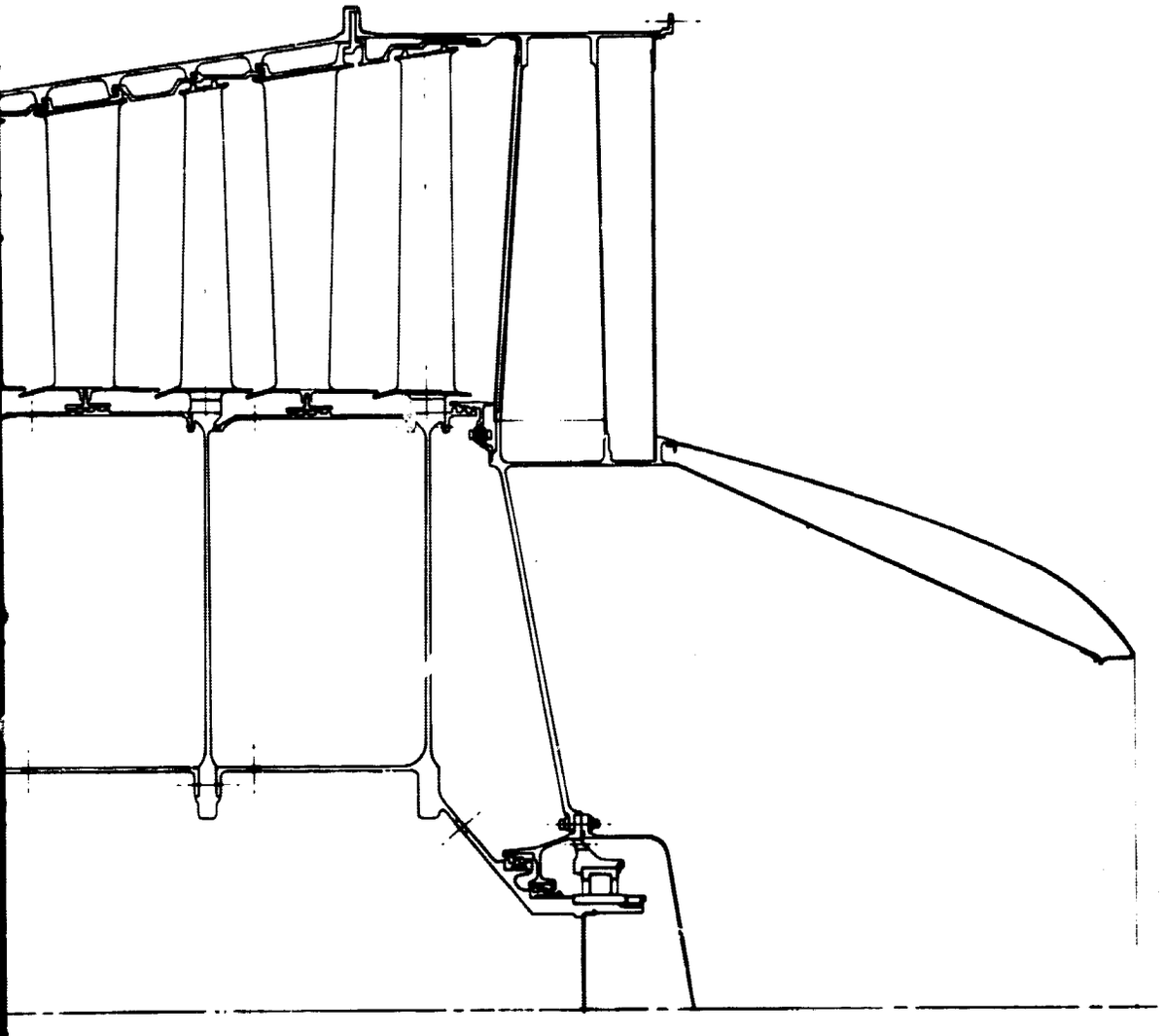

Figure 3b-2. PD218-5B1 engine cross section. 3b-7

FOLDOUT FRAME 6

PRECEDING PAGE BLANK NOT FILMED.

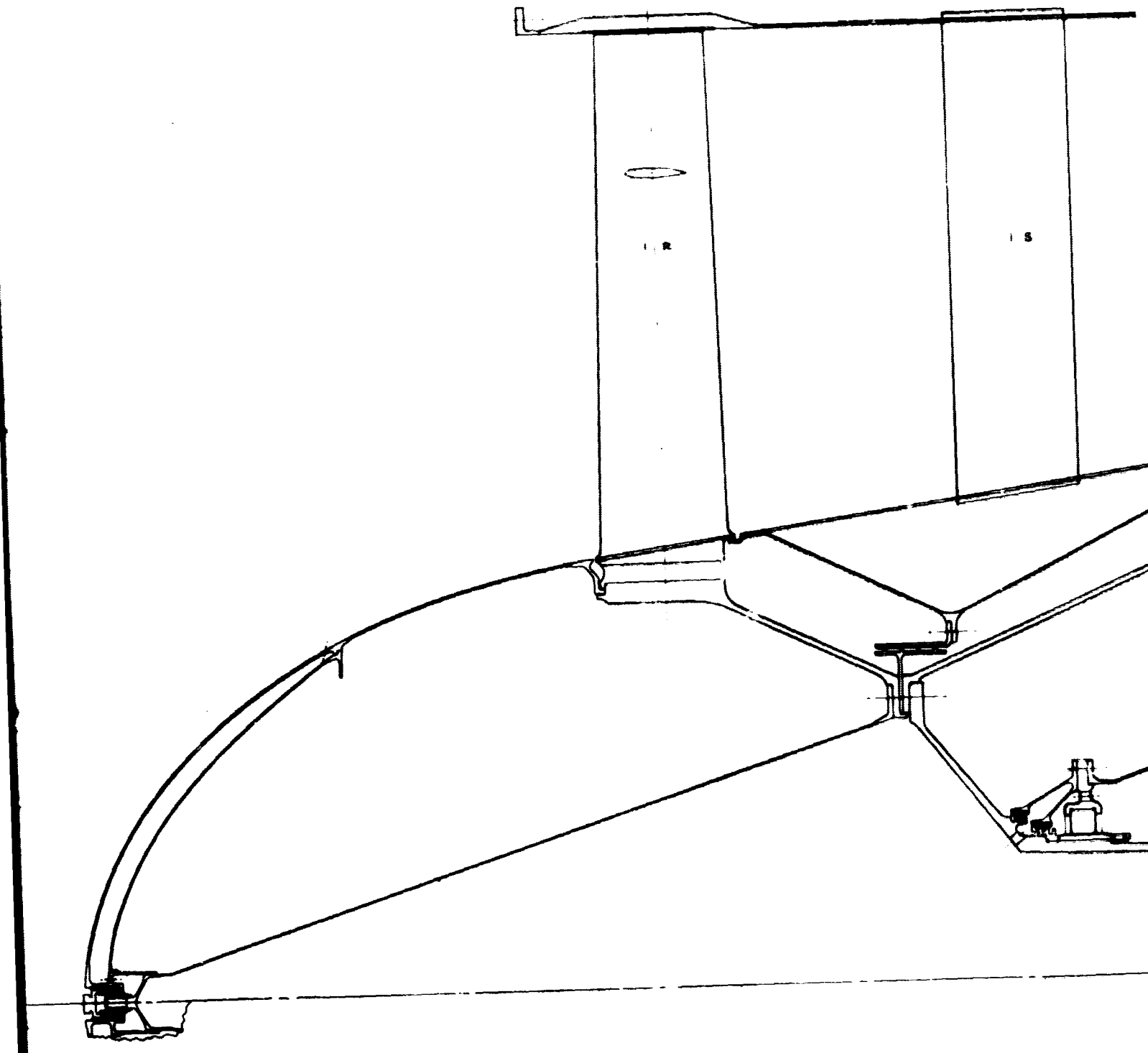

FOLDOUT FRAME 1

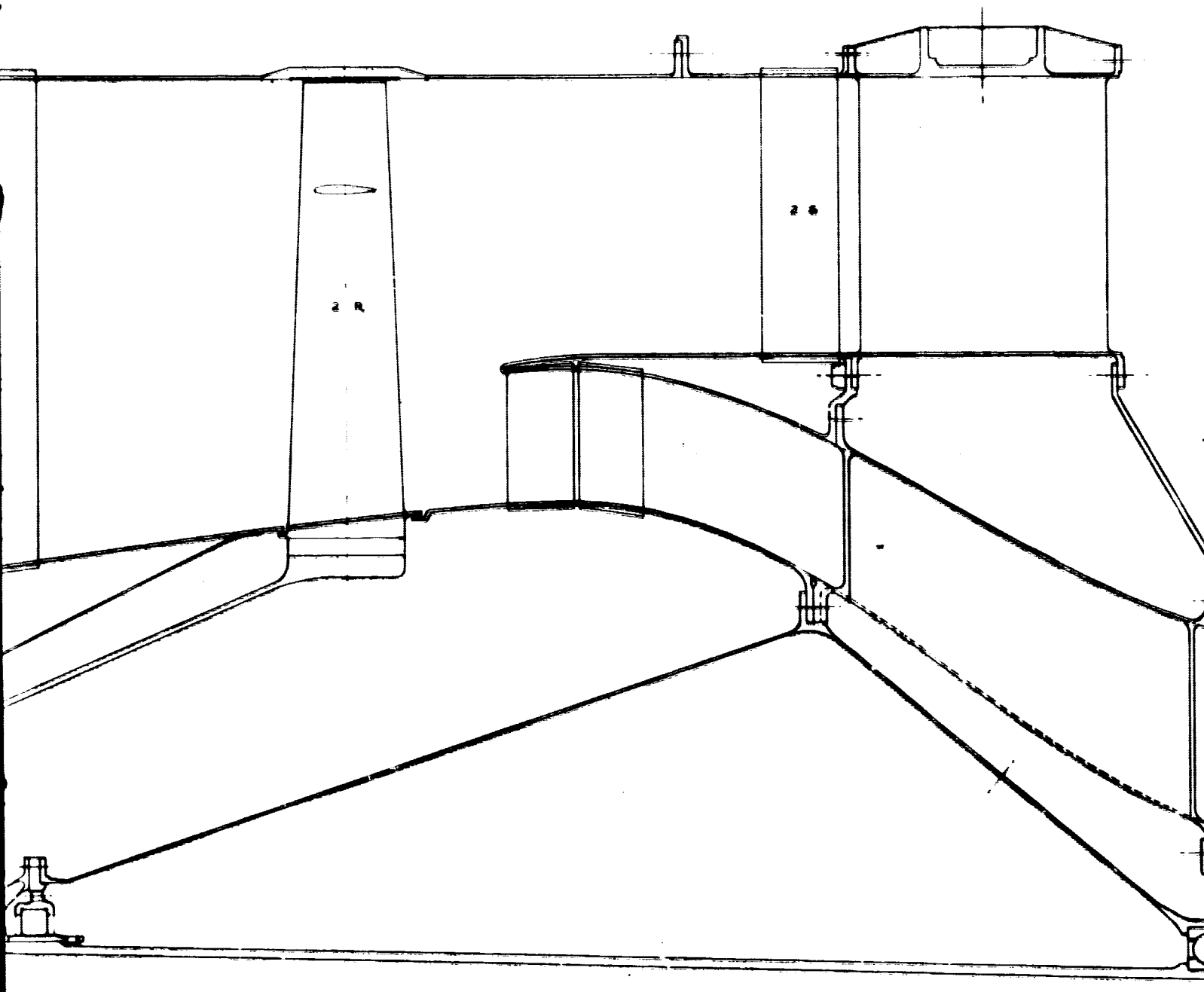

FOLDOUT FRAME 2

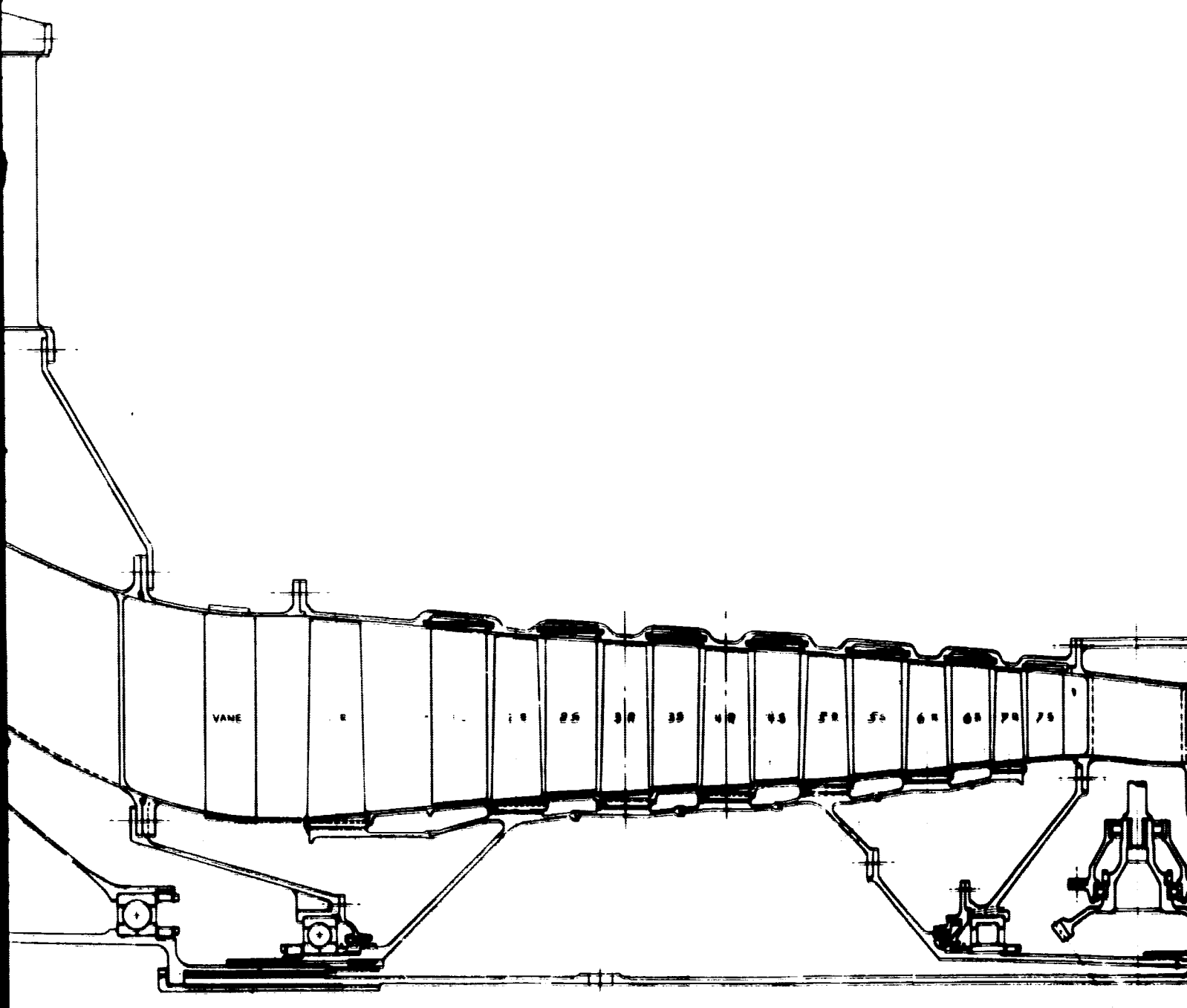

FOLDOUT FRAME 3

FOLDOUT F

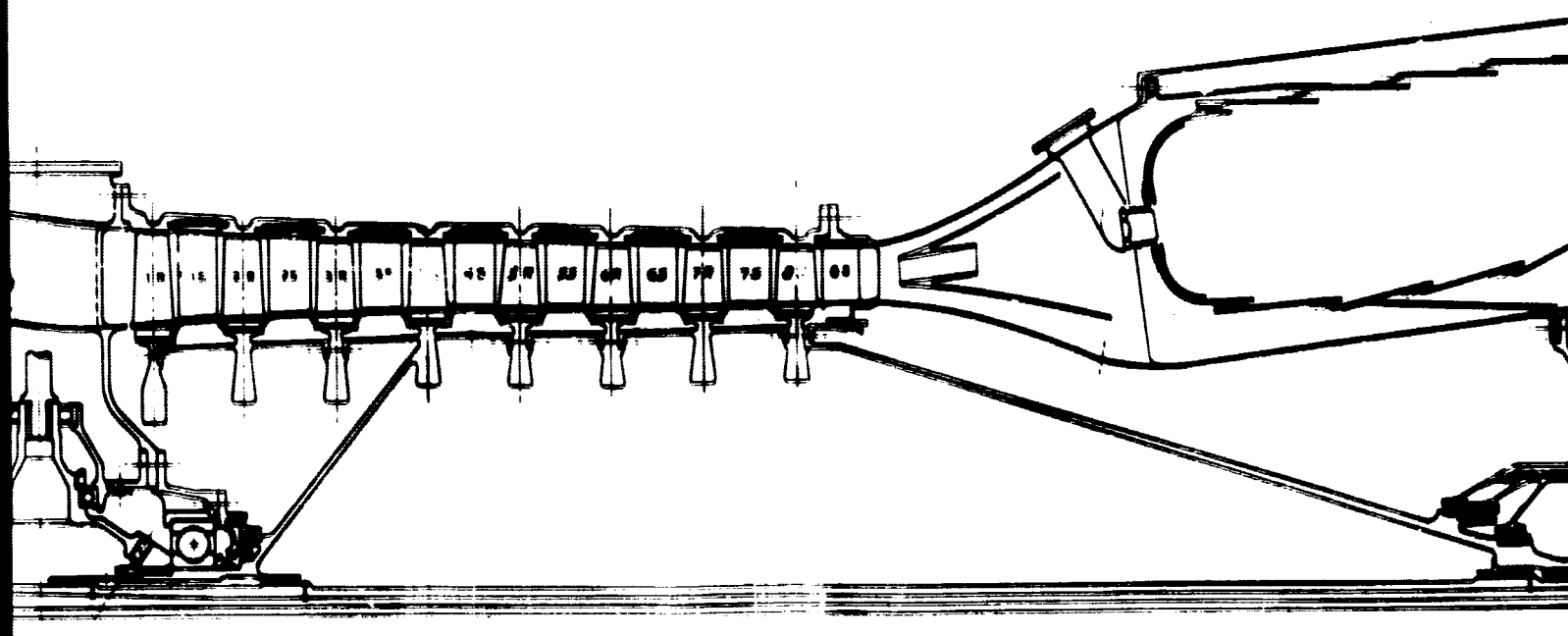

LDOUT FRAME

FOLDOUT FRAME 4

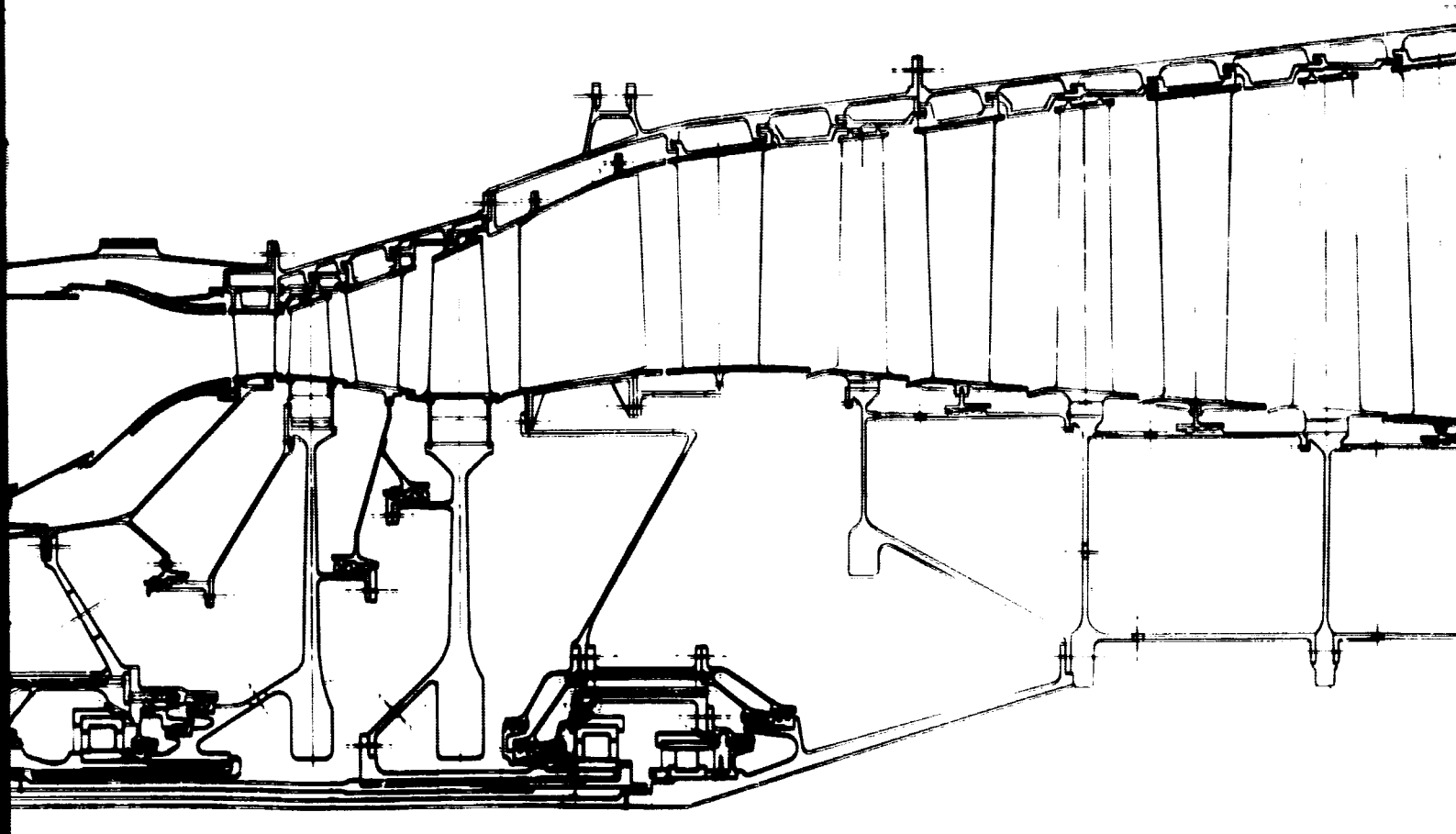

FOLDOUT FRAME 5

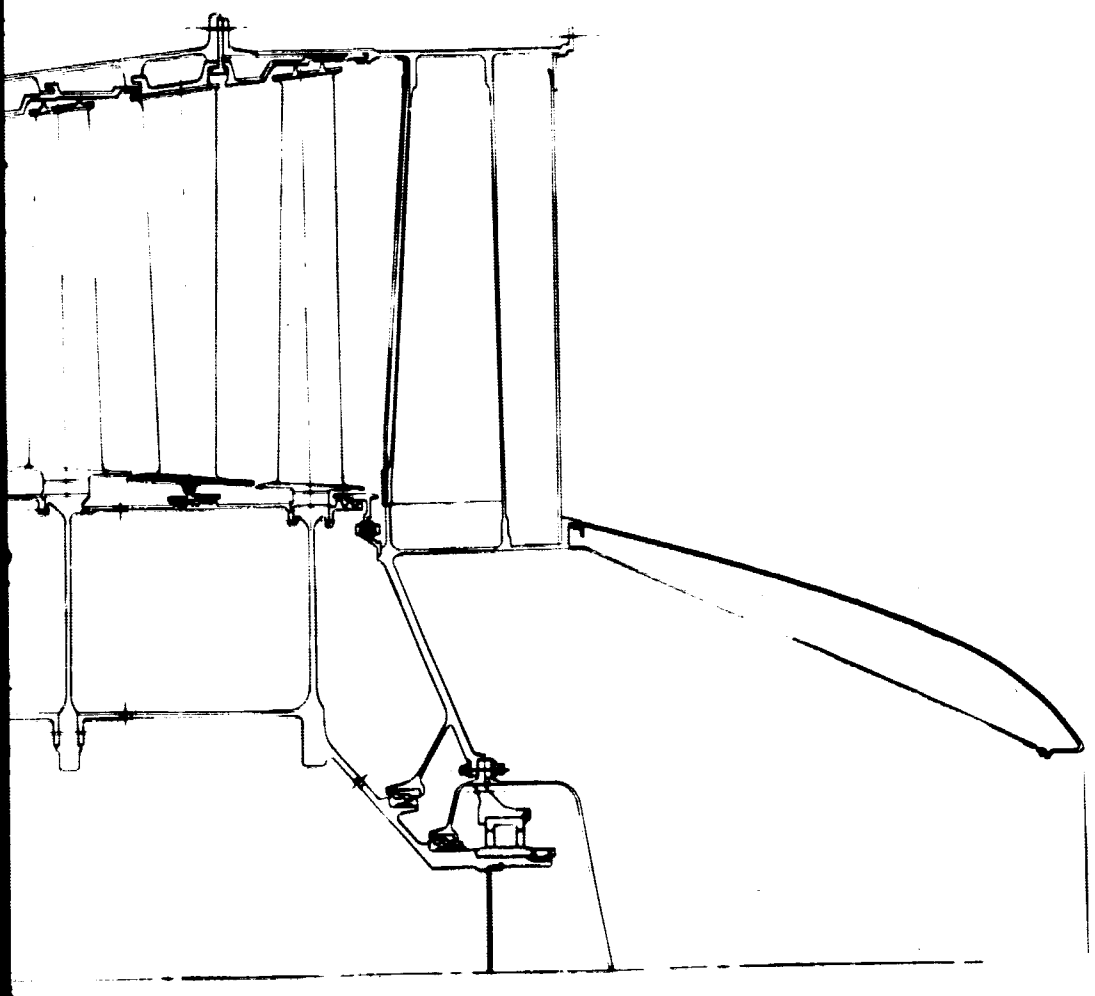

Figure 3b-3. PD218-3B1 engine cross section. 3b-9

FOLDOUT FRAME 6

During the Task II portion of the program, a preliminary design of the PD218-Q was completed. The PD218-Q is a three-rotor, fan engine as shown in Figure 3b-4. The design point for this engine is the altitude cruise condition of Mach 0.82 at 35,000 ft (10.7 km). At this condition, the engine is designed to produce 4900 lb (21.8 kN) uninstalled thrust at a bypass ratio (BPR) of 5.5:1 with an overall pressure ratio of 24.1:1. The design turbine inlet temperature at this condition is 1763°F (1234°K).

The engine has a single-stage fan compressor supported on two bearings. The eight-stage intermediate pressure (IP) compressor and its single-stage drive turbine are supported on three bearings. The eight-stage high pressure (HP) compressor and its overhung, single-stage drive turbine are supported on two bearings. A five-stage turbine mounted on two bearings drives the fan compressor and uses the fan thrust bearing through an axially locked, splined joint.

PRECEDING PAGE BLANK NOT FILMED.

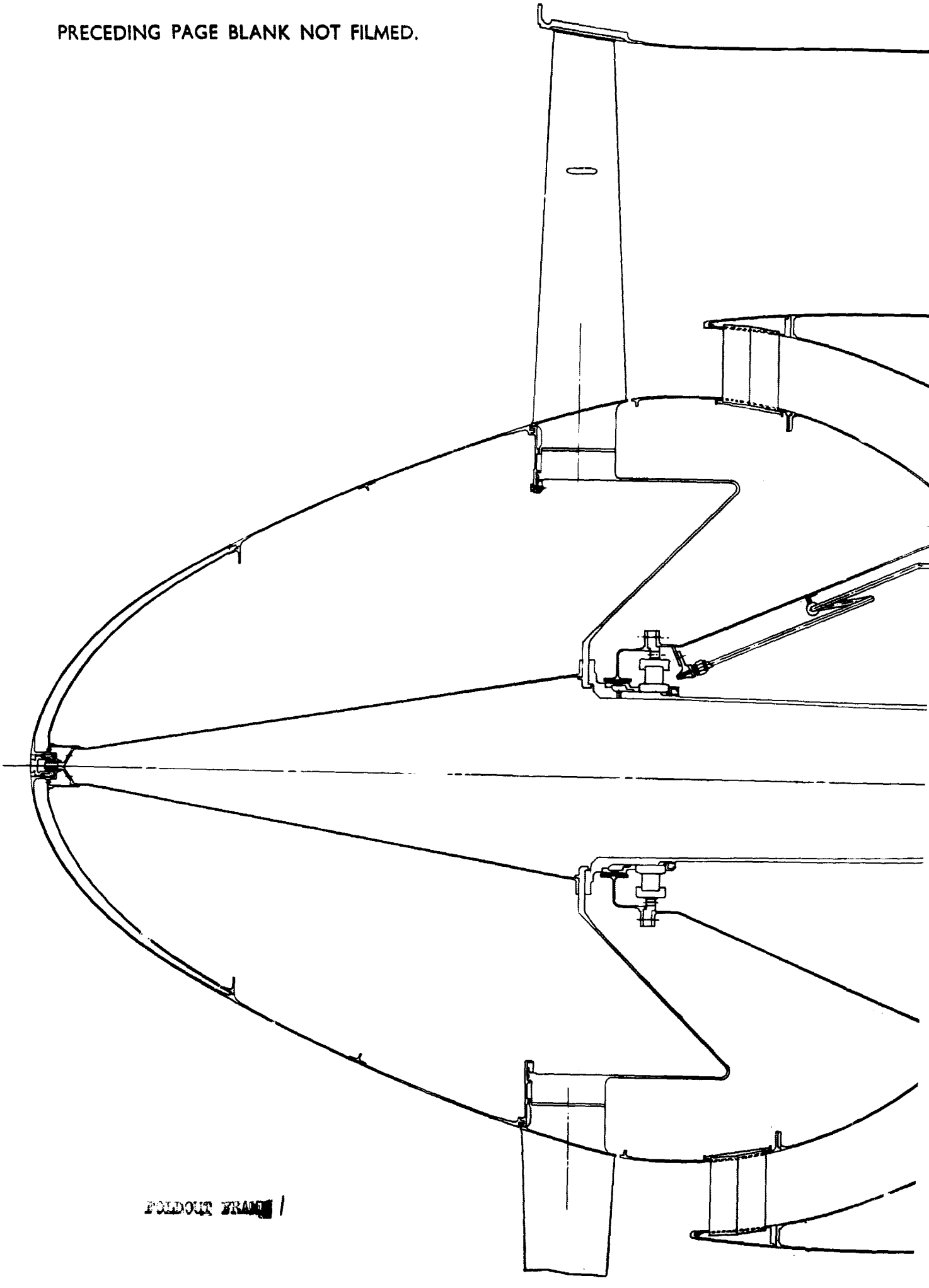

FOLDOUT FRAME 1

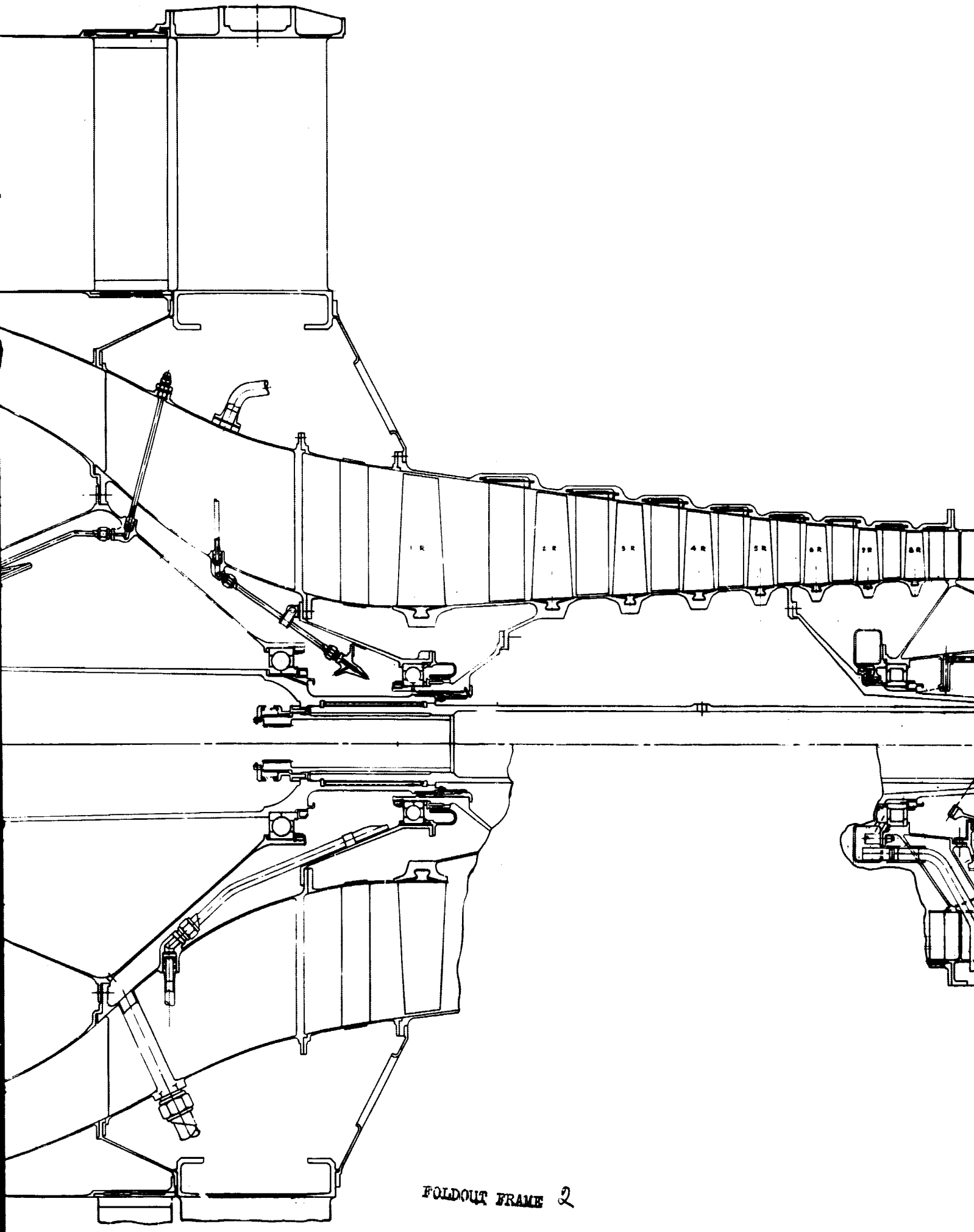

FOLDOUT FRAME 2

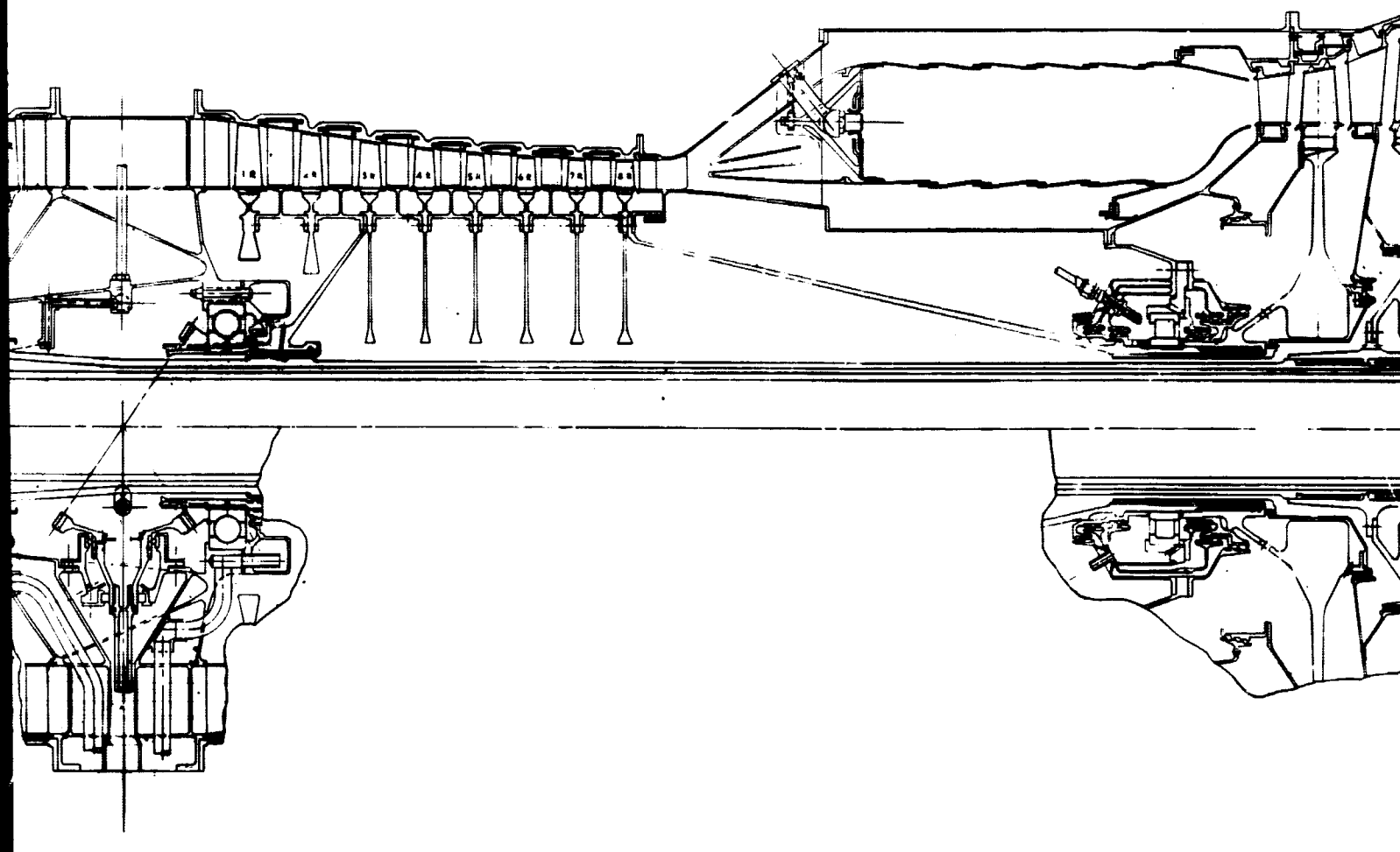

FOLDOUT FRAME 3

FOLDOUT

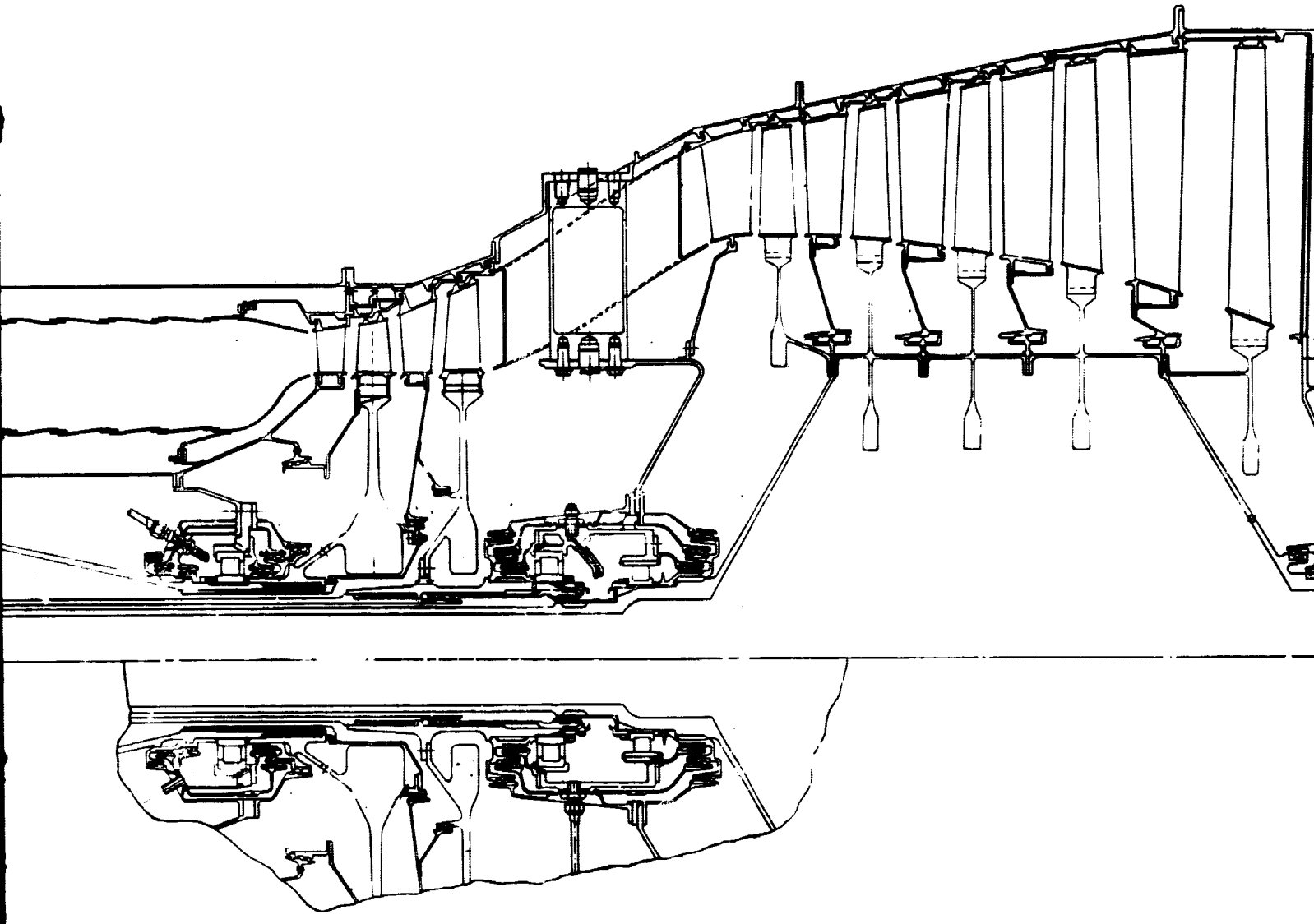

FOLDOUT FRAME 4

Figur

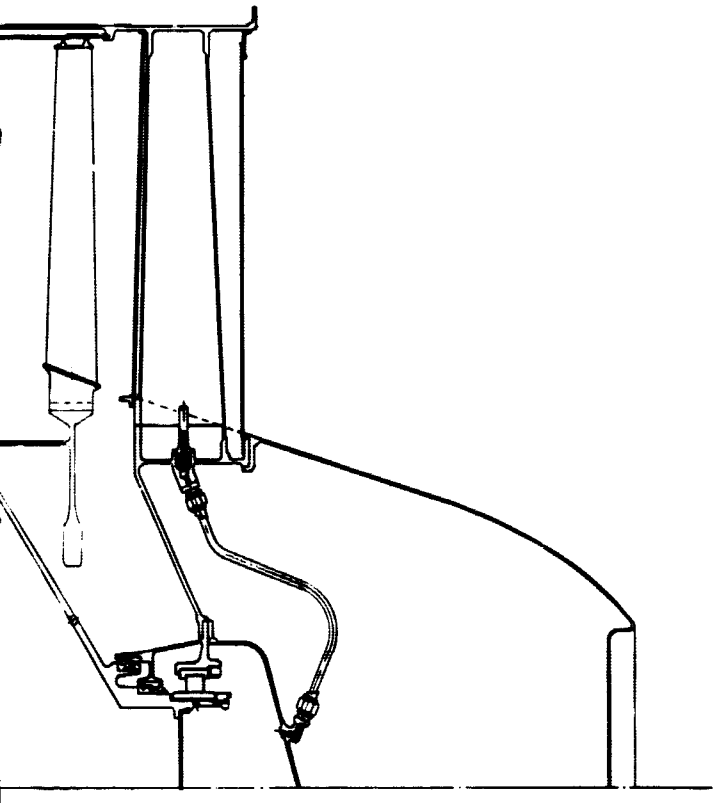

FOLDOUT FRAME 5

Figure 3b-4. PD218-Q engine cross section.

3c. Noise Evaluation

The noisiness of aircraft engines is usually evaluated on the perceived noise (PNdB) scale which measures human response to noise levels and spectral shape and the PNdB rating was used in this evaluation. Two basic noise prediction methods were used—the Smith and House[1]* technique for fan, compressor, and turbine noise, and the SAE AIR 876A method for fan and primary jet noise. These prediction methods include modifications based on Allison and Rolls-Royce test experience.

ANALYSIS METHOD

Fan and Compressor Noise

White Noise

The broad band or white noise which arises primarily from the fluctuating lift forces on blades or vanes resulting from turbulence in the input airflow is described as:

White noise peak 1/3 octave band level at 100 ft linear (db)

$$= 78.5 + 50 \log \frac{V_{rel}}{1000} + 10 \log W_a + \Delta F + 10 \log \delta + a \qquad (1)$$
$$+ 10 \log \frac{V_a}{V_{rel}} - 15 \log \frac{T_{row}}{T_{ref}} + \sum K_r$$

where

V_{rel} = maximum relative velocity, fps
W_a = airflow, lb/sec
ΔF = attenuation term to account for local Mn effect
δ = mean solidity
a = incidence relative to design incidence
V_a = mean axial velocity, fps
T_{row} = static inlet temperature, °R
T_{ref} = reference temperature, 518.7°R (543°K)
$\sum K_r$ = accumulated local ΔF attenuations (not including stage being calculated) between source and free field

*Superscripts refer to references in Section V.

Discrete Noise

The characteristic tonal quality of fan noise is due to the discrete tones generated as a result of blade or vane wake interaction. The discrete noise at the blade passage frequency is described as:

$$\text{Fundamental tone at 100 ft (db)} = 85 + 50 \log \frac{V_{rel}}{1000} - 10 \log \left[\left(\frac{S}{C} \right)^2 \cdot \frac{1}{W_a} \right] + \Delta F - 15 \log \frac{T_{row}}{T_{ref}} + \sum K_r \quad (2)$$

where

$\left(\frac{S}{C}\right)$ = the spacing ratio of space to upstream projected chord on a streamline preceding the maximum V_{rel} point

$\sum K_r$ = accumulated ΔF attenuations as in Equation (1) for forward propagated noise, but extended to include a 5-db per stage reduction for rearward noise

Harmonics of the fundamental tone are also generated. The level of these tones has a 10 log $(N)^2$ relationship to the fundamental tone where N refers to the harmonic number.

Mach Noise

As the blade tip relative Mach number reaches and exceeds unity, shock waves form from the blade tips and become a new source of noise. This noise is a function of shock strength and takes the form of discrete tones harmonically related as multiples of fan rotational frequency so that the major effect is a "filling in" of the spectrum below the normal discrete tone at blade passage frequency.

Test data indicate that Mach noise is propagated only forward and that the maximum increase in PNdB occurs at relative Mach numbers of 1.2 to 1.3.

The Mach noise effect as a function of fan blade tip relative Mach number and fan airflow has been derived from test data and is used to adjust fan noise as computed by the method of Smith and House to account for this extra noise source.

Jet Noise

Jet noise prediction is based on the procedure outlined in SAE AIR 876 A with two modifications. The first modification is the extension of the curve, maximum OASPL versus jet

relative velocity, below the 1000 fps (304.8 m/sec) level. An accumulation of Allison and other test data provided a basis for the curve extension shown in Figure 3c-1.

The second modification was necessary to account for the spectral shape resulting from the use of coaxial and coplanar nozzles. New Strouhal number relationships, shown in Figures 3c-2 and 3c-3, have been derived to account for different nozzle configurations.

Turbine Noise

Turbine noise prediction is based on unpublished Rolls-Royce data which describe discrete and peak white noise as functions of turbine blade tip speed. White and discrete noise are both normalized for mass flow while the discrete level is further adjusted for the ratio of upstream vane-blade clearance to blade chord (S/C). Spectral shaping is applied to the white noise and discrete noise is added on an octave band basis prior to computing overall turbine PNdB.

Noise Summation

The previously defined prediction methods provide noise estimates for the individual noise sources of the uninstalled engine at 100 or 200 ft (30.5 or 61 m) sideline distances operating

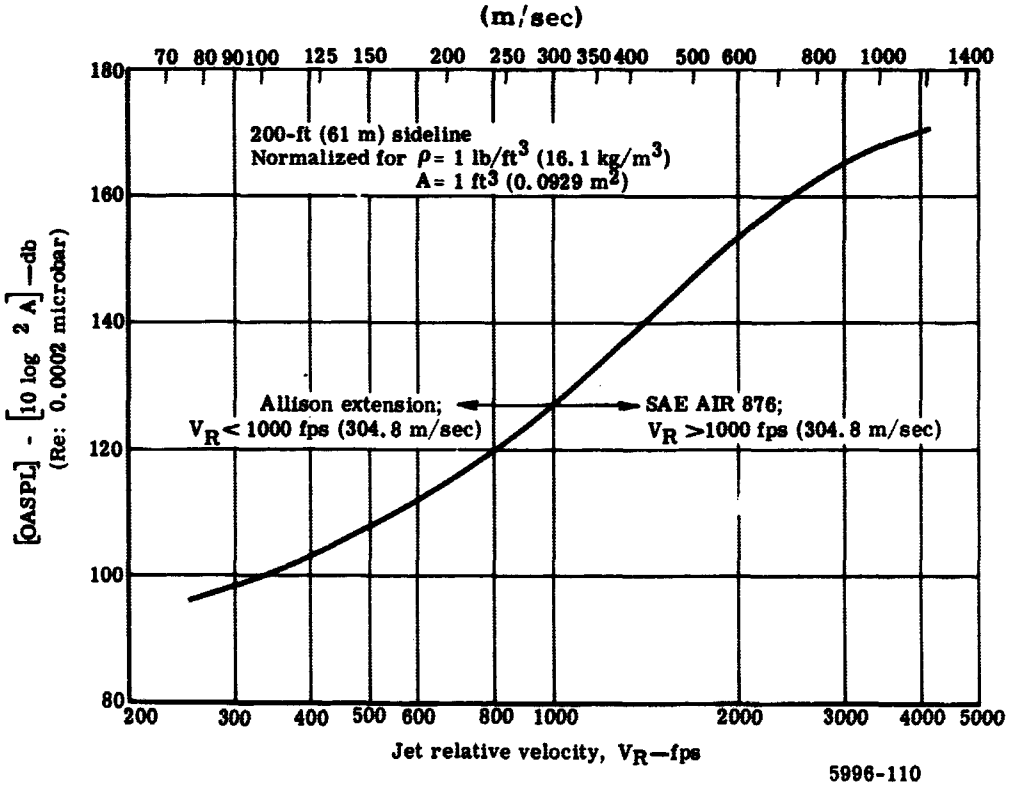

Figure 3c-1. Effect of jet noise on jet relative velocity.

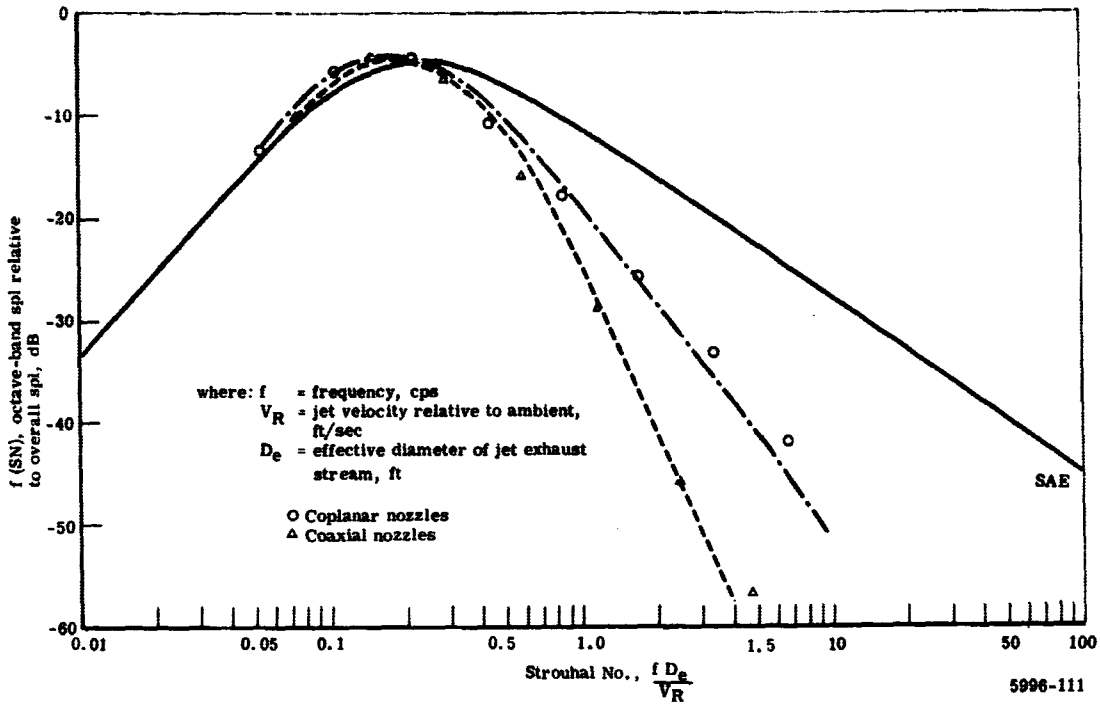

Figure 3c-2. Octave band jet noise versus S_n—ground.

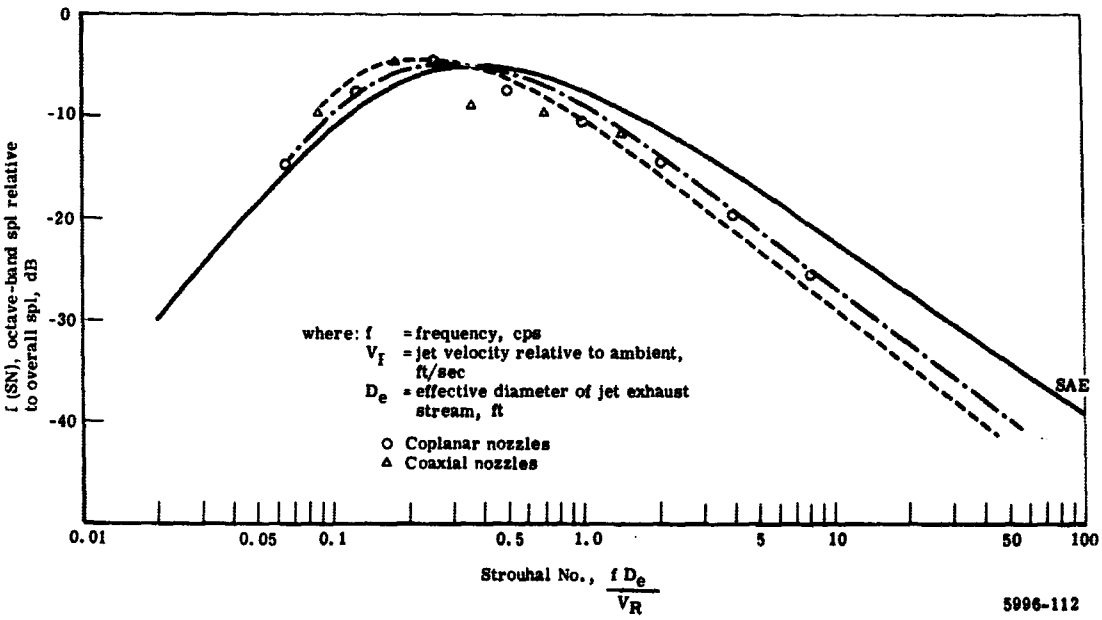

Figure 3c-3. Octave band jet noise versus S_n—flight.

at sea level static, standard day conditions. To properly evaluate an observer's reaction to the overall noise emitted during aircraft takeoff and approach, the following are considered in the Allison computer program developed for this study.

- Installation Effects
  The noise source levels are adjusted to reflect an installed engine exhaust nozzle configuration. The ducting did not include acoustic treatment.
- Distance
  In addition to the inverse square law and excess air attenuation applied to the individual source levels, a minus 2-db correction is applied to forward fan, fan jet, and primary jet noise to account for the change from hemispherical radiation on the ground to spherical radiation in the air. Those sources which propagate through a jet (rear fan and turbine) are modified to account for jet core effects on directivity.
- Directivity
  Directivity patterns for the five noise sources—fan front, fan rear, fan jet, turbine, and primary jet—have been derived from a variety of published fan and bypass engine data[2,3,4,5,6] Knowledge of the individual directivity patterns permits superposition of the noise fields to obtain a single noise field about the engine axis. To establish the proper slant distance between the engine and the observer, the combined noise field is oriented as required to account for aircraft attitude during takeoff and approach conditions

Correlation with Measured Noise

An indication of the noise prediction accuracy obtained with the existing prediction techniques is shown in Figure 3c-4[7]. The three predicted PNdB values for a four-engine (JT3D-3B's) transport fall well within the scatter of FAA data that have been normalized for four engines and average four-engine aircraft gross weights.

DESIGN CHANGE EFFECTS

The noise analysis method described in the previous subsection was used to evaluate design alternates with respect to noise generation of components and the overall engine. The major design considerations evaluated were fan hub-to-tip ratios, single-stage and multistage fans, and two- and three-spool engine configurations. The results of these evaluations are presented in the following paragraphs.

Hub-To-Tip Ratio

To determine the possible benefits from varying the hub-to-tip ratio (H/T), a parametric study was made on a variable H/T configuration consisting of a single fan stage and an OGV

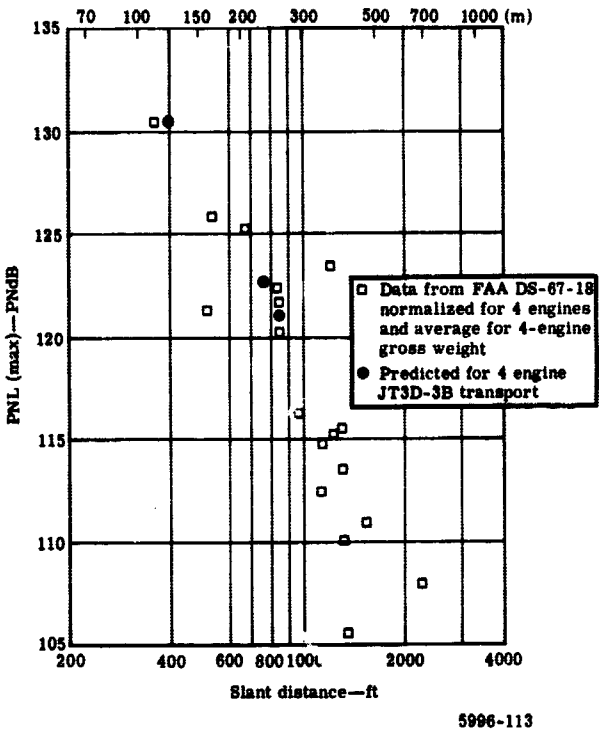

Figure 3c-4. Correlation of predicted and measured noise.

spaced at three chords. The design details are given in Table 3c-I. Since the fan tip V_{rel} has an inverse relationship to H/T, a decrease in noise output would be expected with an increase in H/T. As shown in Figure 3c-5, a noise reduction does occur, but only in the rearward noise. Forward noise remains constant because the higher Mach number inflow reduces the fan forward propagated noise so that the white noise from the OGV becomes dominant. In effect, the fan swallows its noise. A similar study on a two-stage fan resulted in a 2-PNdB rearward noise reduction for an H/T change of 0.35 to 0.45. The higher H/T is desirable because of the resulting decrease in fan V_{rel} and lower noise in the rear arc.

Tip Mach Number Effects

The production of extra discrete tones at supersonic tip relative speeds is the primary observable Mach number effect. This noise is confined to the front arc only and consists primarily of N discrete tones (N = number of blades) distributed between rotor rotational frequency and blade passage frequency. Based on test experience and initial analysis, the peak effect is expected to occur between Mach 1.2 and 1.3 with only a perceptible effect at or below Mach 1.1. Test data obtained in a long duct fan rig show the gross effect to be 2 to 3 PNdB; however, there may be some question about the applicability of PNdB because of the gross change in tonal quality. At Mach 1.1, the change was less than 0.5 PNdB.

Table 3c-I.

Fan optimize' ..n study—noise prediction.

Hub/tip ratio	0.477	0.425	0.340
Hub diameter, ft (m)	3.02 (0.921)	2.62 (0.799)	2 08 (0.634)
Tip diameter, ft (m)	6.36 (1.939)	6.18 (1.881)	5 97 (1.820)
Fan rpm (rps)	3760 (62.7)	4230 (70.5)	5240 (87.3)
No. of blades	55	45	31
Fan axial chord, in. (mm)	3.80 (96.52)	3.99 (101.35)	4.10 (104.14)
OGV axial chord, in. (mm)	4.00 (101.6)	4.00 (101.6)	4.00 (101.6)
Space/fan axial chord	3.00	3.00	3.00
OGV V_{rel}, ft/sec (m/sec)	828 (252.4)	828 (252.4)	828 (252.4)
Fan V_{rel}, ft/sec (m/sec)	1340 (408.4)	1460 (445.0)	1650 (502.9)
Fan solidity	1.13	1.13	1.13
OGV solidity	1.13	1.13	1.13
Fan ' l velocity, ft/sec (m/sec)	609 (185.6)	609 (185.6)	609 (185.6)
OGV axial velocity, ft/sec (m/sec)	576 (175.6)	576 (175.6)	576 (175.6)

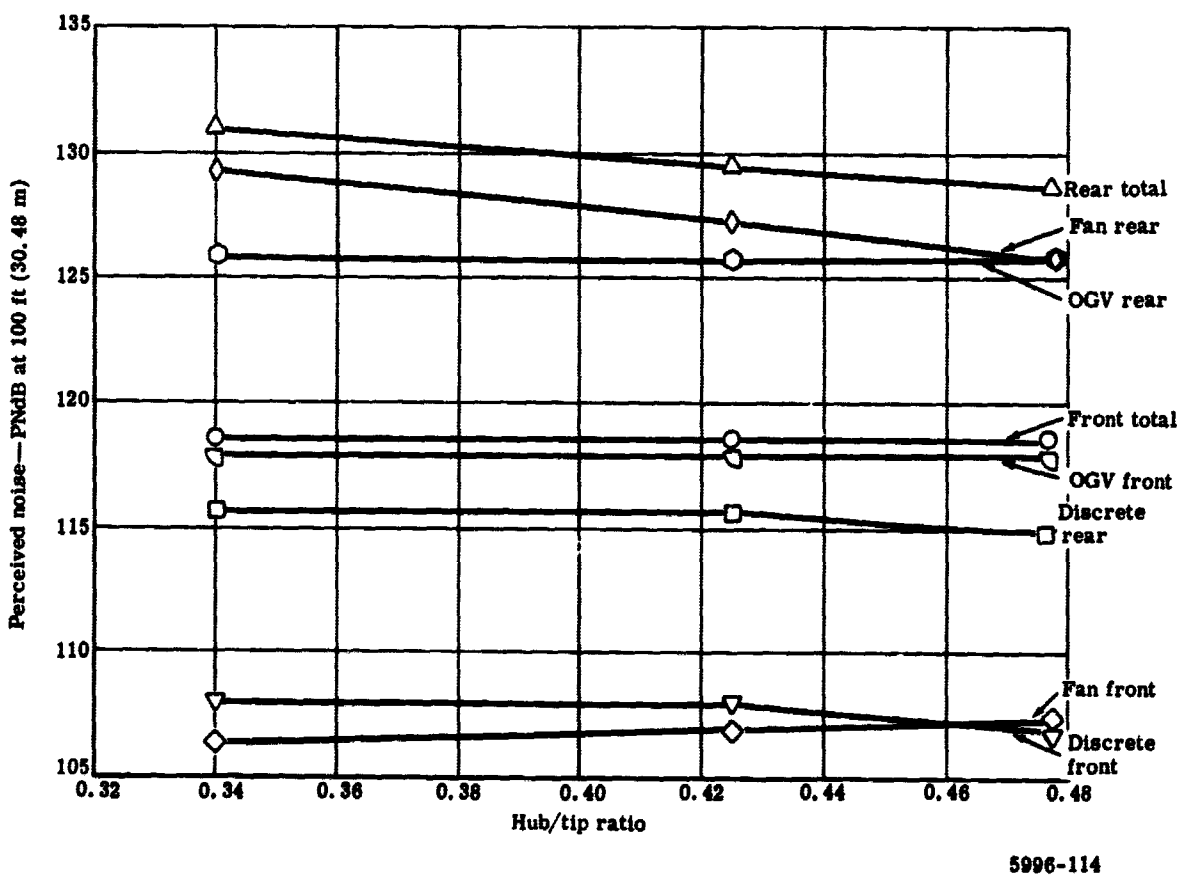

Figure 3c-5. Fan H/T ratio versus perceived noise level.

Single-Stage Versus Multistage Fans

The multistage fan has many disadvantages when compared with the single-stage fan, even when normalized to the same H/T ratio. The factors which adversely affect the multistage fan are as follows.

- The benefits gained by removing the IGV's in reducing turbulence into the fan rotor are lost largely because of turbulent flow into the second and succeeding stages which is generated by upstream stages.
- The additional stages represent new noise sources not present in the single-stage unit.
- Engine length and weight are penalized when the rotor-to-stator spacings required to avoid severe discrete tone level increases are added. Table 3c-II gives a comparison of one- and two-stage fans (with two chord spacings) at a takeoff condition. The single-stage fan is quieter by about 4 PNdB in both the front and rear arcs. The fan intermediate vane is primarily responsible for both the front and rear arc noisiness of the two-stage design. The vane produces high level white noise which receives little forward attenuation because of the low speed of the first-stage fan. This vane also acts as an IGV for the second-stage fan, thus aggravating the generation of both white and discrete noise by the second-stage fan. Acoustic convection (ΔF) also plays an important but subtle role in controlling the forward arc noise. For example, comparing the tip speeds of the single-stage fan and the first fan stage in the two-stage design—1227 versus 930 fps (374 versus 283.5 m/sec)—the initial reaction would be to expect lower noise levels from the 930-fps (283.5-m/sec) fan. This is true in the rear arc; however, acoustic convection at the higher tip speed actually results in a lower forward level for the high-speed fan. In addition to affecting the fan noise, the higher speed fan also produces a greater attenuation of vane noise so that the total effect is compounded and the high-speed fan has lower fan and vane noise in the front arc.

Two-Spool Versus Three-Spool Designs

In the approach condition, noise generated by the compressor becomes an important factor in the forward arc noise because of the decreased local acoustic convection attenuation at the low fan speed. The flexibility allowed by the three-spool concept permits control of this noise generation (not available in the two-spool design) by slowing down the intermediate pressure rotor. An additional low pressure stage was added to each of the preliminary design engine intermediate pressure rotors to allow lower tip speeds, thus decreasing the noise production or emission.

INITIAL STUDY ENGINES

A detailed noise analysis was made for the three basic study engines to evaluate the overall engine noise levels and determine the contribution of the individual noise sources to these levels.

Table 3c-II.

Comparison of single- and two-stage fans.

5.0:1 bypass ratio

PNdB at 1000-ft (304.8 m) takeoff power

	Single-stage			Two-stage		
	Foward	Rear	Tip speed, fps (m/sec)	Forward	Rear	Tip speed, fps (m/sec)
First fan white	81.3	92.5	1227 (374)	82.6	82.7	930 (283.5)
First stator white	—	—	—	88.5	88.6	—
First stator discrete	—	—	—	77.9	78.1	—
Second fan white	—	—	—	8[illegible].2	99.2	930 (283.5)
Second fan discrete	—	—	—	75.6	90.4	—
OGV white	83.6	93.1	—	73.8	90.6	—
OGV discrete	68.8	78.5	—	59.1	75.6	—
Total	87.0	97.8*	—	91.7	101.4*	—

*Normalized by removing primary jet influence.

Overall engine noise for the three study engines was compared, on a PNdB basis, to that produced by the JT3D-3B engine to provide an indication of the relative quieting potential of the basic study engines.

The three study engines were three-spool engines sized to produce approximately 5175 lb (23 kN) of thrust at Mach 0.8 and 35,000 ft (10.7 km). The designs differed in the numbers of fan stages and bypass ratios. One- and two-fan stages were used at a BPR of 5:1 and a two-stage fan was used at a BPR of 3:1. These engines had the following design features to ensure minimum noise generation:

- No IGVs
- Low fan tip speed
- Wide blade-to-vane spacings (not less than one chord) for both the fan and intermediate compressor
- Optimum number of vanes relative to the number of fan blades at the intermediate compressor inlet
- Low blade tip speed on the intermediate compressor
- Wide vane-to-blade spacings in the low pressure turbine

The results of the initial engine studies are given in Table 3c-III and show the favorable effect of increasing bypass ratio and of using a single-stage fan design. The PD218-5A1 single-stage fan engine is 4 to 5 PNdB more quiet on takeoff and 1 to 3 PNdB more quiet during approach than the two-stage fan engines and was clearly the best choice for further study.

- An increase in BPR to 5.5 resulted in a noise reduction of about 1 PNdB for both the takeoff and approach conditions.
- An increase and decrease in takeoff turbine inlet temperature of +50 and -25°F (+27.8 and -13.9°K) resulted in less than 1-PNdB change in noise level.
- A reduction of primary exhaust nozzle area during approach to permit a lower fan speed indicated a possible gain of about 2 PNdB at an optimum exhaust nozzle area reduction of 40%.
- A high performance version of the engine was designed and studied to determine the effective noise reduction achieved beyond that gained by the effect of bypass ratio and elimination of IGVs. In this version, the OGV spacing was reduced to one chord length, the H/T was reduced to 0.425, the fan tip speed was 1350 fps (412 m/sec) at takeoff, and provisions were made for normal spacing in the IP compressor and the intermediate turbine. The fan pressure ratio of the tip was increased to 1.6, the overall pressure ratio was increased to 25.8, and the turbine inlet temperature at the beginning of cruise was increased to 1825°F (1270°K). Optimum numbers of vanes were used in the fan primary exit stator. The results of this study indicate that about 430 lb (195 kg) of engine weight and 1.3% in fuel consumption are sacrificed to achieve an improvement of 2 PNdB on takeoff and 3 PNdB on approach. The takeoff thrust of the high performance engine is lower because of a lower thrust lapse rate from sea level to altitude cruise condition.
- Another version of the PD218-5A engine was designed specifically to achieve a low primary jet noise level while maintaining low fan and vane noise. This engine, designated PD218-5.5A2, had a 5.5 BPR to extract noise energy from the primary exhaust. Table 3c-III shows that while a reduction in primary jet noise will be marginally profitable in reducing bare engine noise, it will be a requirement to achieve the full benefit of duct treatment for further noise reductions. The noise levels generated by this engine are given in Table 3c-IV and show that while the total engine noise was nearly unaffected, hot jet noise was reduced by 6 PNdB. The results of this study show clearly that the engine design must be biased to provide the lowest possible jet noise floor if duct treatment is to be considered as part of the noise solution.

Table 3c-III.

Engine total and source noise (PNdB) for flyover at takeoff and approach powers.

(single engine levels)

Engine	PD218-3B1 (two-stage fan)				PD218-5A1 (single-stage fan)				PD218-5B1 (two-stage fan)			
Condition	Takeoff 1000 ft (304.8 m)		Approach, 325 ft (99.1 m)		Takeoff, 1000 ft (304.8 m)		Approach, 325 ft (99.1 m)		Takeoff, 1000 ft (304.8 m)		Approach, 325 ft (99.1 m)	
	Front	Rear	Front	Rear	Front	Rear	Front	Rear	Front	Rear	Front	Rear
Total noise	88.3	104.8	99.6	104.3	93.0*	100.9	98.8	97.1	91.7	104.0	99.5	100.9
Mach contribution	—	—	—	—	6.0	—	—	—	—	—	—	—
Fan white	84.0	99.9	95.2	98.0	81.3	92.5	90.5	90.2	86.5	99.3	94.0	95.5
Fan discrete	70.9	89.5	86.2	90.0	—	—	—	—	75.6	90.4	85.8	88.0
Vane white	85.3	92.0	96.0	99.4	85.1	93.1	94.3	94.1	88.6	92.1	95.6	97.8
Vane discrete	77.2	79.4	83.1	79.2	68.8	78.5	77.9	78.3	78.0	80.1	80.2	76.3
IP compressor total	60.2	—	90.3	—	73.4	—	94.1	—	65.0	—	90.6	—
Turbine	—	83.9	—	89.0	—	85.8	—	84.4	—	71.9	—	76.0
Fan jet	—	86.7	—	78.2	—	82.4	—	73.6	—	82.4	—	73.6
Hot jet	—	93.6	—	68.2	—	91.1	—	67.8	—	91.1	—	68.0

*Includes the estimated PNdB Mach effect

Table 3c-IV.
PD218-5.5A2 engine total and source noise (PNdB) for flyover at takeoff and approach powers.

(single engine)

	Takeoff, 1000 ft (304.8 m) at Mach 0.25		Approach, 325 ft (99.1 m) at Mach 0.25	
	Front	Rear	Front	Rear
Total noise	93.2	100.0	99.0	97.3
Mach contribution	6	—	0	—
Fan white	81.5	92.5	90.7	90.4
Vane white	85.3	93.2	94.5	94.4
Vane discrete	69.1	78.6	78.2	78.5
IP compressor total	74.7	—	95.1	—
Turbine		85.3		84.2
Fan jet		86.8		73.2
Hot jet		85.3		63.7

OPTIMIZATION STUDIES FOR PD218-Q ENGINE

IP Compressor

As given in Table 3c-III, the IP compressor is an important noise source for a single-stage fan engine during approach. The following configurations were evaluated in an effort to reduce the IP compressor noise contribution during approach.

- 0.5 reaction
- 0.6 reaction with no bleed
- 0.6 reaction with 15% bleed
- Increased area flow path

Table 3c-V presents the results obtained from the optimization study and shows that within the aerodynamic restraints imposed, only a small improvement was possible.

Fan

Three additional fan configurations were evaluated to determine the possible benefits of:

- Reduced turning at the hub, 1075 fps (327.7 m/sec) tip speed at sea level takeoff
- Reduced tip speed with reduced turning, 1000 fps (304.8 m/sec) at sea level takeoff
- Increased flow per unit area, 1075 fps (327.7 m/sec) tip speed at sea level takeoff

Table 3c-V.

Forward arc noise during approach for several IP compressor designs.

Single engine levels in PNdB at 325 ft (99.1 m) and Mach 0.25

Configuration	PD218-5.5A1 (base)	Increased area flow path	0.5 reaction	0.6 reaction	
				No bleed	With bleed
Total forward noise (including fan)	98.8	98.0	99.5	98.8	98.8

All fans studied were for an engine having a 5.5 BPR. Table 3c-VI presents the results of this evaluation. Clearly, no one fan is best for all conditions. In the case of the reduced turning fan, the tip speed was increased slightly to minimize the amount of turning required at the fan root. It was hoped that this would reduce the approach velocity to the fan OGV, thereby reducing the vane white noise contribution that predominates especially on approach. The vane white noise was reduced but this was accompanied by an increase in the fan blade noise contribution, thus offsetting the gain for the most part. When the fan tip speed was reduced, the fan noise contribution was reduced and was accompanied by an offsetting increase in the vane noise contribution. The latter occurred because the fan root was required to do more turning, causing the vane approach velocity to be higher.

The flow per unit area was increased from 39.5 to 41 lb/sec/ft^2 (1.66 to 1.73 kg/sec/m^2) at the higher tip speed. When this was done, the relative velocities to the blade and vane were increased, resulting in an increase in noise production. This effect was offset at approach because of a more favorable incidence; the noise remained virtually unchanged when compared with the reduced turning fan.

Engine

The engine is designed to have a 5.5:1 BPR to achieve the lowest practical level of primary exhaust jet noise. The IP compressor incorporates the larger inlet area (reduced specific flow) so that it can be minimized as a noise source on approach. A compromise solution was achieved in the design of the fan where the fan tip speed was reduced to 1020 fps (310.9 m/sec) at sea level takeoff and the inlet flow per unit area was increased slightly to 40 lb/sec/ft^2 (1.69 kg/sec/m^2). This resulted in a fan design that also minimized the velocity to the fan OGV.

Table 3c-VI.

Takeoff noise from fan and vanes in PNdB at 1000 ft (304.8 m) and Mach 0.25.

	PD218-5.5A2		Reduced turning fan		Reduced speed fan		Increased flow per unit area	
	Front	Rear	Front	Rear	Front	Rear	Front	Rear
Total noise (fan and vane)	92.9	95.9	90.6	95.2	85.7	94.5	93.6	97.6
Mach contribution	6.0	—	4.5	—	0	—	6.0	—
Fan white	81.5	92.7	81.8	92.7	82.4	91.5	82.7	93.9
Vane white	85.3	93.4	84.1	91.8	83.0	91.5	85.9	95.2
Vane discrete	69.1	78.8	67.3	76.2	68.0	76.8	67.6	77.2
Approach noise from fan and vanes								
Total noise (fan and vane)	96.0	95.9	95.8	95.6	96.4	96.3	95.9	95.8
Fan white	90.7	90.4	91.3	91.1	90.5	89.8	92.0	92.0
Vane white	94.5	94.4	93.7	93.5	95.3	95.2	93.7	93.4
Vane discrete	78.2	78.5	76.8	76.9	77.5	77.5	77.7	78.0

Table 3c-VII presents the single-engine total and source noise levels for the PD218-Q engine and also shows the total noise levels for the JT3D-3B engine. This comparison indicates that the PD218-Q engine would provide a 13- to 14-PNdB reduction over current JT3D-powered transports. On a four-engine basis, the maximum levels generated by the PD218-Q engine would be 105.6 PNdB at takeoff power and 1000-ft (304.8-m) altitude and 104.1 PNdB at approach power and 325-ft (99.1-m) altitude.

PERCEIVED NOISE AT FLIGHT PATH LOCATIONS

Typical aircraft characteristics for the 325,000 lb (147 Mg) DC 8/707 transport used in this study were obtained from McDonnell-Douglas and Boeing. Data for four-engine takeoff flight paths were calculated for flaps, gears, speeds, and power settings shown in Figure 3c-6. The initial weight at the start of roll was 325,000 lb (147 Mg). For takeoff power, thrust versus velocity characteristics were defined by the engine data at constant actual turbine inlet temperature. The aircraft data used are as follows:

Wing area	2884 ft^2 (267.9 m^2)
Ground roll lift coefficient	0.513
Ground roll drag coefficient	0.0444
Rolling friction coefficient	0.015
Maximum lift coefficient for takeoff	1.742

First segment climb lift coefficient	1.187
First segment climb drag coefficient	0.1073
Gear retracted base drag coefficient	0.0281
Gear retracted induced drag coefficient	0.0566
Wing angle of attack at a lift coefficient of zero	-4.9 degrees (-0.086 radians)
Lift curve slope	13.333

The three initial study engines were sized for a thrust of 5175 lb (23 kN) at the beginning of cruise—Mach 0.8 and 35,000-ft (10.7-km) altitude and rated cruise turbine inlet temperature—and the PD218-Q engine was sized to produce 4900 lb (21.8 kN). Takeoff thrust ratings were 21,000 lb (93.4 kN) for the PD218-3B1 and 24,050 lb (107 kN) for the PD218-5A1 and PD218-5B1 engines. The PD218-Q engine is rated at 21,960-lb (97.7-kN) takeoff thrust. The JT3D-3B engine was assumed to have 18,000-lb (80.1-kN) thrust. Ram recovery and horsepower/bleed extraction were 1.0 and 0.0, respectively.

Figure 3c-7 shows representative plots of altitude versus distance from start of roll for four engine configurations. The solid lines show the flight path for constant power. The flight paths indicated by the dotted lines are for a power cutback at a 1000-ft (304.8-m) height to the thrust required for a 1000-fpm (5.1-m/sec) climb rate. The approach path was constant for

Table 3c-VII.
PD218-Q single-engine total and source noise in PNdB for flyover at takeoff and approach powers.

	Takeoff, 1000 ft (304.8 m) and Mach 0.25		Approach, 325 ft (99.1 m) and Mach 0.25	
	Front	Rear	Front	Rear
PD218-Q engine				
Total noise	87.5	99.6	98.1	97.1
Mach contribution	1.0	—	0	—
Fan white	81.4	91.4	90.0	89.5
Vane white	84.5	92.5	94.5	94.4
Vane discrete	68.2	77.0	77.1	77.5
IP compressor total	69.1	—	92.3	—
Turbine		83.4		83.4
Fan jet		82.2		74.3
Hot jet		87.9		66.7
JT3D-3B total noise (single engine)	96.9	112.3	111.0	112.6

all engines. The approach glide slope was defined as three degrees and passes through an altitude of 325 ft (99.1-m), one mile (1.61 km) from the end of the runway and clears a 50-ft (15.24-m) obstacle over the end of the runway. Altitude, velocity, power setting, flight path angle, and engine axis inclination to the flight path angle were calculated along these flight paths for determining engine ground level noise. As expected from the flight path comparison, the increased climbout performance of the study engines provided an additional noise reduction at the standard flight path monitor locations which are shown pictorially in Figure 3c-8.

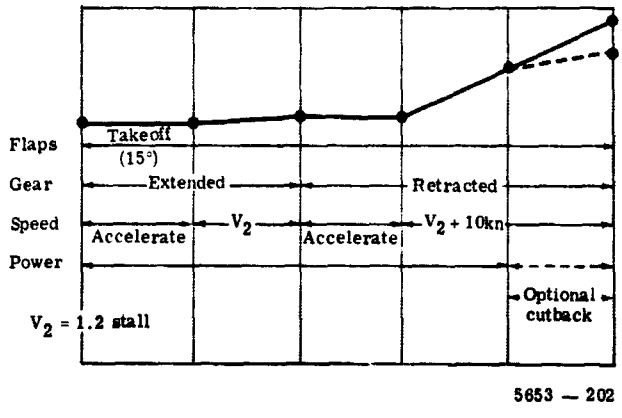

Figure 3c-6. Flap, gear, aircraft speed, and power setting for DC-8/707 transport.

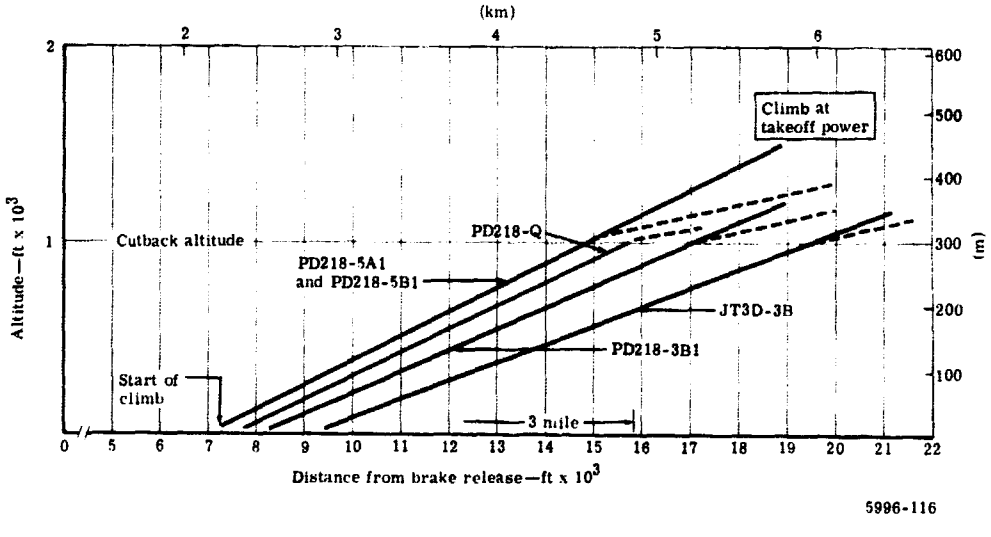

Figure 3c-7. Quiet engine study flight path comparison.

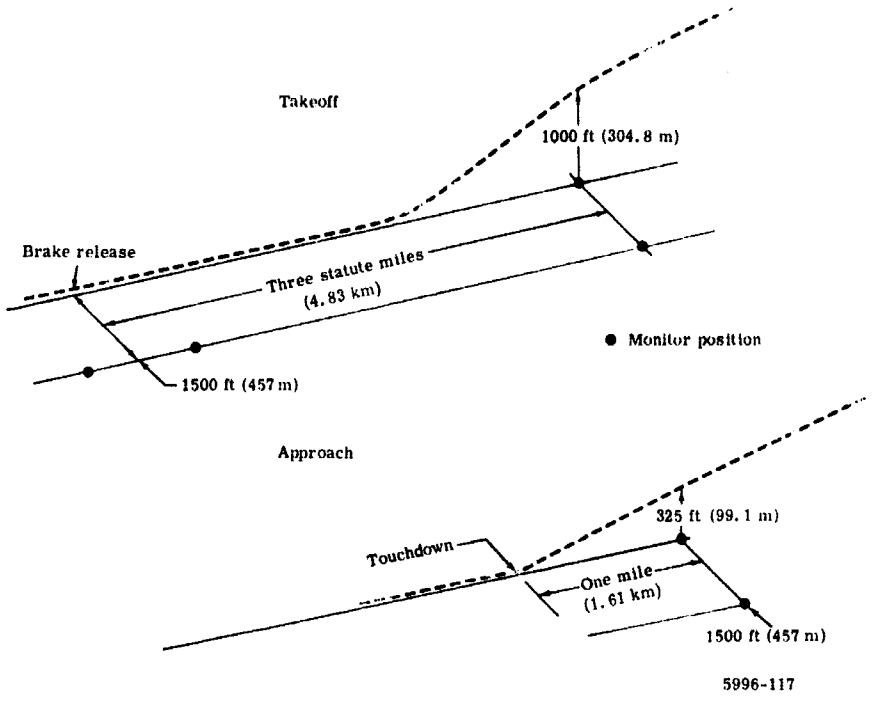

Figure 3c-8. Standard noise monitor positions.

The expected perceived noise at the standard flight , th monitor locations is given in Table 3c-VIII. The levels for the takeoff static comparison are probably high since ground attenuation effects were not included in the calculations. However, the increment between engines provides a valid comparison. At the takeoff static condition, the study engines give a reduction of 6 to 11 PNdB as compared with the JT3D-3B. The reductions are more dramatic when the flight path effect is considered. The rapid climb capability of the PD218-Q, PD218-5A1, and PD218-5B1 engines produces reductions of about 20 to 23 PNdB after cutback. The PD218-3B1 engine, which has a climb-out path only slightly better than the JT3D-3B engine, gives a reduction of 11 PNdB. This reduction occurs with full takeoff power, since the PD218-3B1 engine cutback, like the JT3D-3B, occurs too late to provide a reduction at the 3-mile (4.83 km) point.

At approach, the noise reduction varies from 9 to 15 PNdB with the PD218-Q and PD218-5A1 engines providing the maximum reductions. The approach is made at a 3-degree pitch-up attitude so that these noise levels will not necessarily agree with those given in Tables 3c-III and 3c-VII.

Noise breakdowns at the standard measurement positions are given in Table 3c-IX.

Table 3c-VIII.

Engine flight path comparison (PNdB and altitude).

Engine	Ground static takeoff power, 1500-ft (457.2-m) sideline		Takeoff 3 miles (4828 m) from brake release				Approach one mile (1609 m) from runway	
			Full takeoff without cutback		Takeoff with cutback			
	Front	Rear	Overhead	1500-ft (457.2-m) sideline	Overhead	1500-ft (457.2-m) sideline	Overhead	1500-ft (457.2-m) sideline
JT3D-3B								
PNdB	100.7	119.4	124.3	112.1			119.1	98.7
Altitude—ft (m)	0	0	667 (203.3)	693 (211.2)			321 (97.8)	300 (91.4)
PD218-3B1								
PNdB	90.4	112.7	113.6	103.9			110.6	91.4
Altitude—ft (m)	0	0	882 (268.8)	912 (278)			321 (97.8)	300 (91.4)
PD218-5A1								
PNdB	97.0*	109.5	106.7	99.4	100.9	93.2	103.4	83.6
Altitude—ft (m)	0	0	1140 (348)	1180 (360)	1070 (326.1)	1076 (328.0)	321 (97.8)	300 (91.4)
PD218-5B1								
PNdB	95.9	112.7	109.7	102.6	103.9	96.5	107.2	87.9
Altitude—ft (m)	0	0	1140 (348)	1140 (348)	1070 (326.1)	1076 (328.0)	321 (97.8)	300 (91.4)
PD218-Q								
PNdB	91.0*	108.3	106.8	98.6	100.8	92.6	103.4	83.6
Altitude—ft (m)	0	0	995 (304)	1030 (315)	1005 (306.3)	1010 (307.8)	321 (97.8)	300 (91.4)

*Includes Mach noise effect.

Table 3c-IX.

Engine total and source noise levels at standard measurement positions.

(Single engine levels in PNdB)

	PD218-Q					PD218-5A1				
	Takeoff			Approach		Takeoff			Approach	
	Static	Cutback				Static	Cutback			
	1500 ft (457.2 m)	Overhead	1500 ft (457.2 m)	Overhead	1500 ft (457.2 m)	1500 ft (457.2 m)	Overhead	1500 ft (457.2 m)	Overhead	1500 ft (457.2 m)
Total noise	102.3	94.8	86.6	97.4	77.6	103.5	94.9	87.2	97.4	77.6
Fan white	92.7	87.3	78.9	89.8	70.0	93.6	88.4	80.6	90.6	70.8
Vane white	93.8	89.3	80.8	94.7	75.1	94.2	89.0	81.2	94.5	74.8
Fan discrete										
Vane discrete	77.2	76.1	67.8	77.8	59.3	78.5	75.9	68.1	78.6	60.1
Turbine	80.8	79.0	68.4	84.0	58.7	83.0	79.6	69.6	84.8	62.7
Fan jet	89.9	77.3	70.8	74.6	58.1	90.1	76.2	70.2	73.9	57.4
Hot jet	92.1	79.9	72.4	67.4	50.2	95.0	79.7	72.7	68.6	51.4

	PD218-5B1					PD218-3B1				
	Takeoff			Approach		Takeoff			Approach	
	Static	Cutback				Static	Cutback			
	1500 ft (457.2 m)	Overhead	1500 ft (457.2 m)	Overhead	1500 ft (457.2 m)	1500 ft (457.2 m)	Overhead	1500 ft (457.2 m)	Overhead	1500 ft (457.2 m)
Total noise	106.7	97.9	90.5	101.2	81.9	106.7	107.6	97.9	104.6	85.4
Fan white	100.9	95.3	87.5	95.8	76.2	99.8	101.7	91.9	101.2	81.6
Vane white	94.5	87.6	80.0	98.1	78.6	92.6	94.5	84.7	98.8	79.2
Fan discrete	92.1	85.2	77.4	88.3	70.0	89.1	92.2	80.3	93.9	75.6
Vane discrete	81.7	74.5	66.7	77.6	59.2	80.1	81.7	71.8	79.5	61.0
Turbine	67.6	68.6	57.4	78.5	54.9	81.0	86.7	74.8	89.4	67.4
Fan jet	90.1	75.6	69.5	73.9	57.4	92.9	88.6	81.2	78.8	62.4
Hot jet	95.0	79.9	72.9	68.7	51.5	97.4	97.4	88.8	68.9	51.7

EFFECTS OF DUCT TREATMENT

Although all previous noise predictions were made without considering acoustic duct treatment for noise suppression, the possibility for further noise reduction through application of acoustic techniques should not be overlooked. For example, engine design choices which reduce noise from sources difficult to suppress (i.e., jet noise) at the expense of those which lend themselves rather easily to treatment (i.e., fan exit noise) offer a better opportunity of achieving the lowest possible installed engine noise. Data presented in NASA progress reports (Reference 8) were studied with respect to the quiet engine (PD218-Q) and the following observations were made.

Inlet Treatment

Forward radiated noise from the PD218-Q engine fan inlet consisting of fan and vane white noise and IP compressor noise is of primary concern during approach. With maximum treatment of a conventional inlet (L/D = 0.5), only about a 1- or 2-PNdB reduction could be expected. Increasing the (treated) inlet length to an L/D of 1 could result in a 4- to 5-PNdB reduction of forward radiated noise. This is a conservative estimate based on a configuration which consists of a 1-in. (25-mm) deep honeycomb structure with a porous surface such as Feltmetal bonded or welded on the inside of the cowl. Reference 8 indicates that this amount of treatment could give at least a 5-PNdB reduction in transmitted noise.

A significant portion of the predicted forward radiation during approach originates in the IP compressor. Reduction of the IP compressor noise by treatment of the IP compressor transition duct is readily possible. A modest duct treatment of a L/D = 1 inlet and of the IP compressor transition duct could produce a net reduction in forward noise of 4 to 7 PNdB.

An unresolved but important question regarding inlet duct treatment is to what extent will the porous skin required for duct treatment increase the free-stream turbulence which is presented to the fan. If the turbulence increase is significant, a portion of expected benefits from the inlet and exhaust ducts will not be realized because the white noise generation will be increased.

Fan Discharge Duct Treatment

The major contribution to the rearward noise for both takeoff and approach is the fan and vane noise transmitted through the fan exit duct. Treating both the inner and outer walls of this duct should produce attenuations of 10 to 14 PNdB. However, since only fan and vane noise are reduced, the total engine noise would not be lowered by the same increment because the unattenuated jet and turbine noise become the dominant noise sources.

EFFECT OF DUCT TREATMENT ON STUDY ENGINES

Evaluation of the ducts shown in Figure 3c-9 was done by applying the duct attenuations to the individual sources and then flying the engines at the referee altitudes and power conditions. The referee conditions were 1000 ft (304.8 m) and Mach 0.25 for takeoff and 325 ft (99.1 m) and Mach 0.25 for approach. Table 3c-X gives a comparison of the engines with and without duct treatment. With the duct treatment considered, the takeoff (not cutback) levels for the four engines now range from 105 PNdB for the PD218-3B1 to 101 PNdB for the PD218-Q engine; these are reductions of 13 and 18 PNdB. On approach the range is 102 PNdB for the PD218-3B1 to 97 PNdB for the PD218-Q engine; these are reductions of 16 to 21 PNdB.

Figure 3c-9. Treated duct locations.

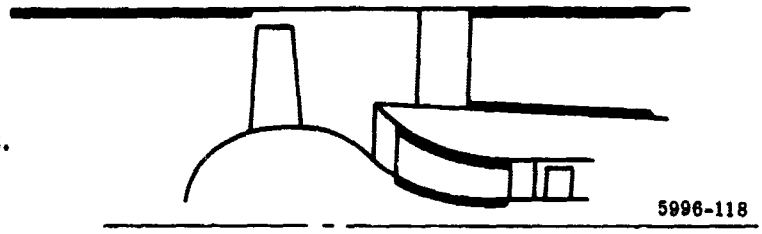

Table 3c-X
Comparison of engines with and without duct treatment.

(Four engine flyover levels in PNdB)

	Takeoff power at 1000 ft (304.8 m) and Mach 0.25				Approach power at 325 ft (99.1 m) and Mach 0.25			
	Treated ducts		Nontreated ducts		Treated ducts		Nontreated ducts	
	Front	Rear	Front	Rear	Front	Rear	Front	Rear
JT3D-3B	—	—	103	118	—	—	117	119
PD218-3B1	90	105	94	111	100	102	106	110
Reduction		13				16		
PD218-5A1	94*	103	99*	107	98	98	105	103
Reduction		15			21			
PD218-5B1	93	103	98	110	100	98	106	107
Reduction		15			19			
PD218-Q	88*	101	94*	106	97	95	104	103
Reduction		18			21			

*Includes Mach noise effect.

NOISE EXPOSURE CONTOURS

Another method of comparison of the effect of a given noise reduction is to develop noise exposure contours. The noise exposure contour shows the boundary along the flight path which encloses a given level of noise. The contour development is shown graphically in Figure 3c-10. The noise exposure contour is useful both in planning land usage and in judging the population reaction to a change in aircraft noise levels. The reduction of the area exposed to high noise levels is one of the most significant aspects of the quiet engine.

Each of the study engines was flown in a 325,000-lb (147-Mg) gross weight aircraft through the takeoff and approach flight paths. The noise exposure contours at 90, 95, and 100 PNdB were determined for each engine-aircraft combination. Each of the study engines was cut back to the power required to produce a 1000-fpm (5.1-m/sec) rate of climb at 1000-ft (304.8-m) altitude because this resulted in the least noise exposure. The JT3D-3B was flown out at takeoff power because the total exposed area was minimized as a result.

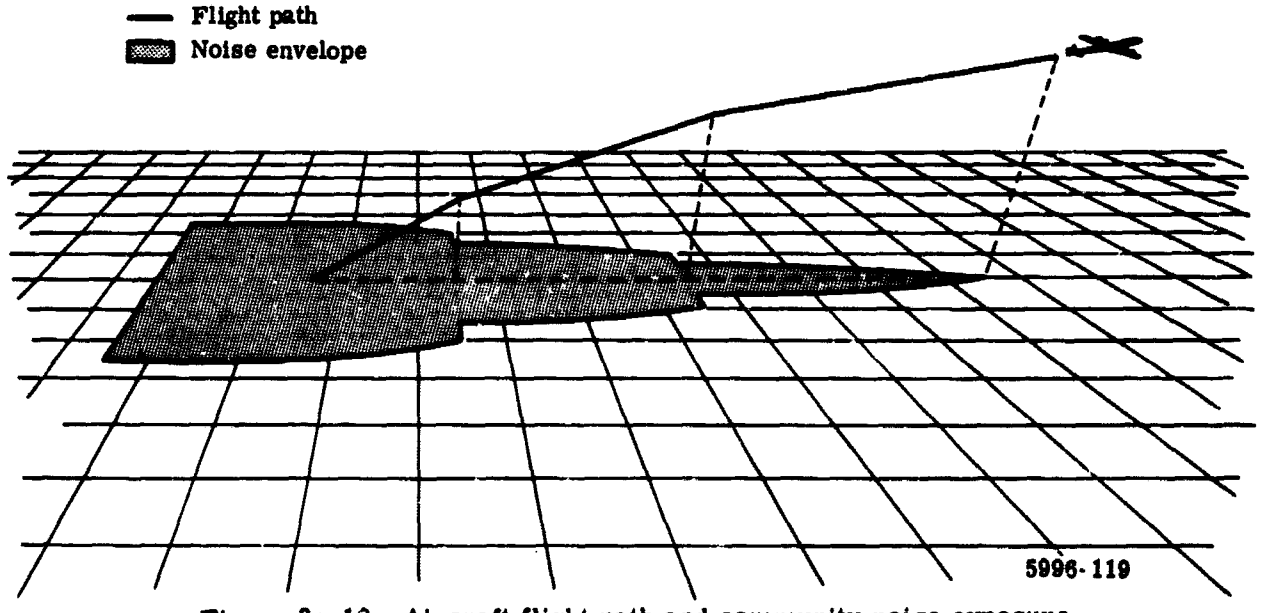

Figure 3c-10. Aircraft flight path and community noise exposure.

The noise exposure contours derived for the JT3D-3B and study engines are presented in Figures 3c-11 through 3c-20. Since it is at best very difficult to make definitive judgements based on the plotted data, the area in acres enclosed by each of the exposure contours was derived for direct comparison. The areas bounded by levels of 90, 95, and 100 PNdB over the full takeoff path are given in comparison to the JT3D-3B data in Table 3c-XI and show a reduction in exposed area of at least 4 to 1 for the PD218-Q powered aircraft. The comparison of the areas bounded by 90, 95, and 100 PNdB on approach shows that the PD 218-Q engine reduces the exposed area to 1/10 of that produced by the JT3D-3B, as indicated in Table 3c-XII. From Table 3c-XIII, the reduction in area during takeoff is even more dramatic when the airport is excluded, assuming an airport boundary of 10,000 ft (3048 m) from start of takeoff.

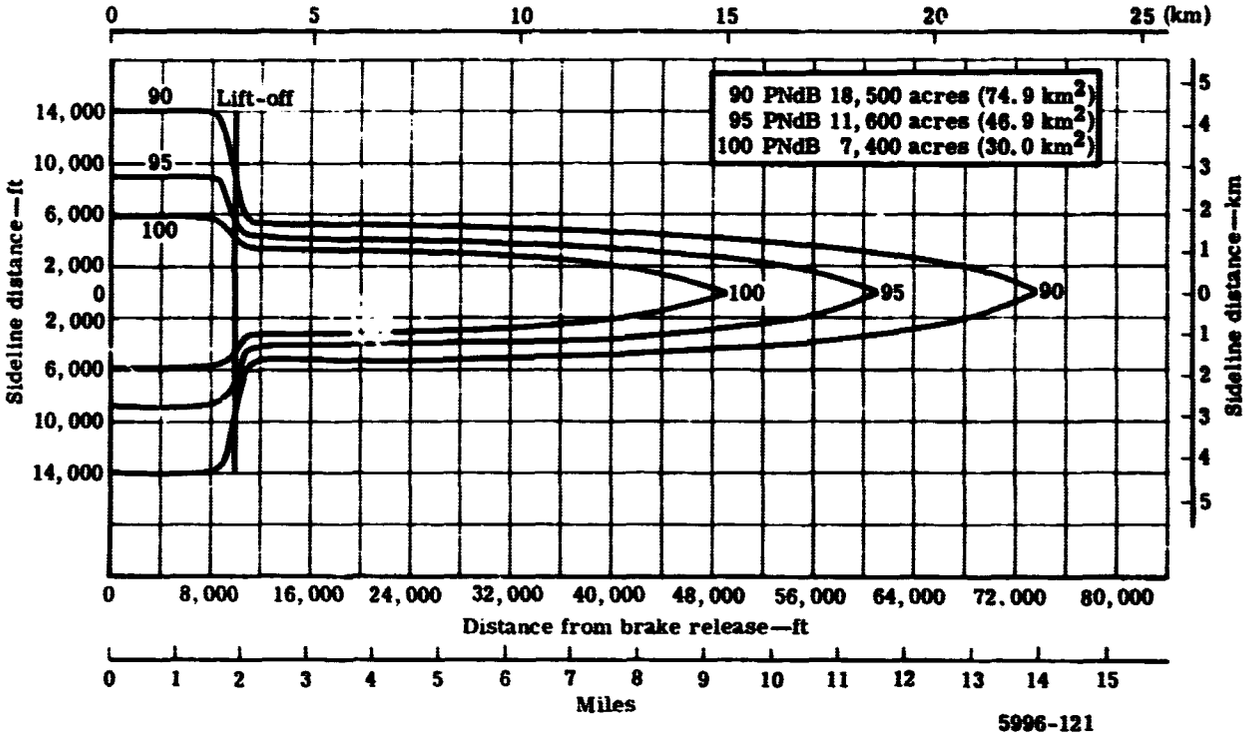

Figure 3c-11. PNdB contour for JT3D takeoff.

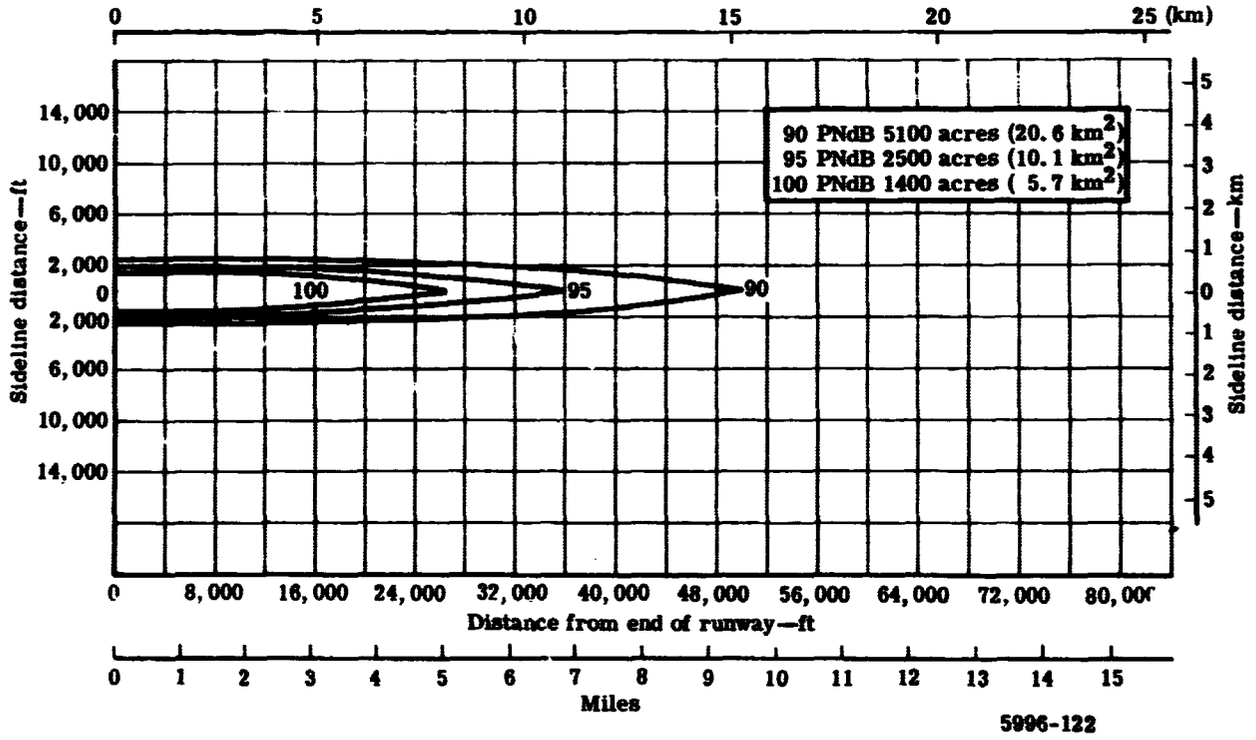

Figure 3c-12. PNdB contour for JT3D approach.

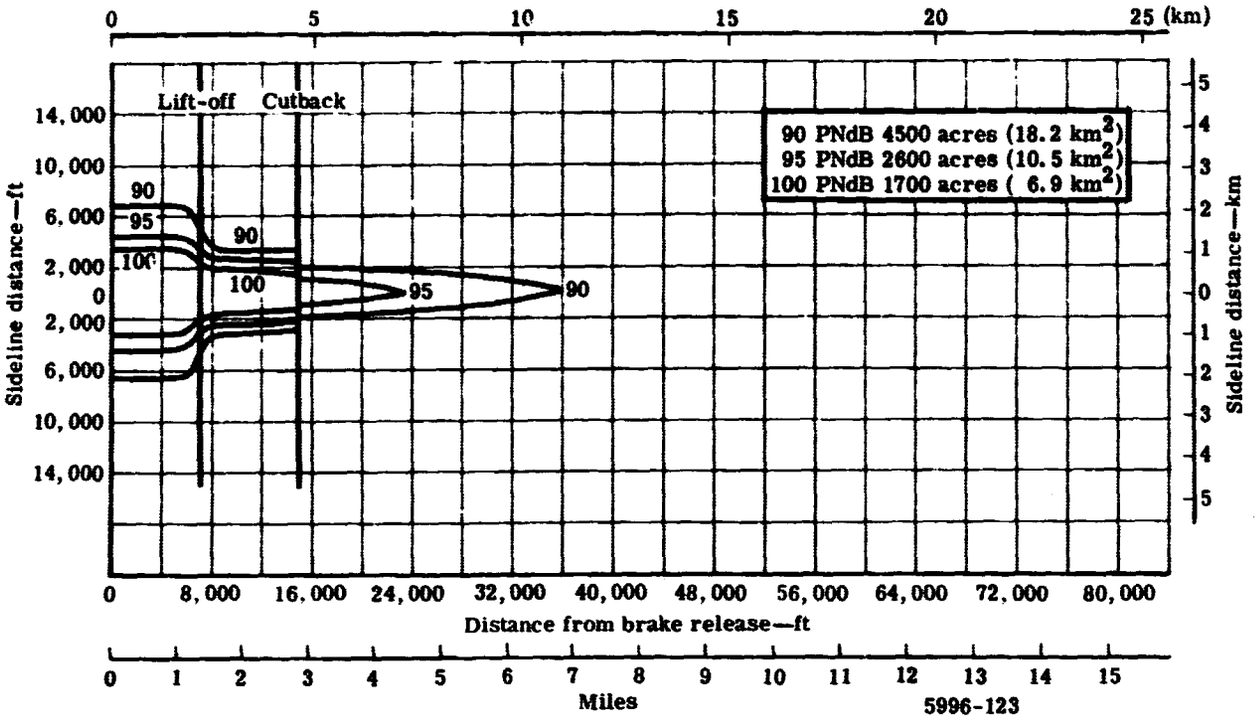

Figure 3c-13. PNdB contour for PD218-5A1 takeoff.

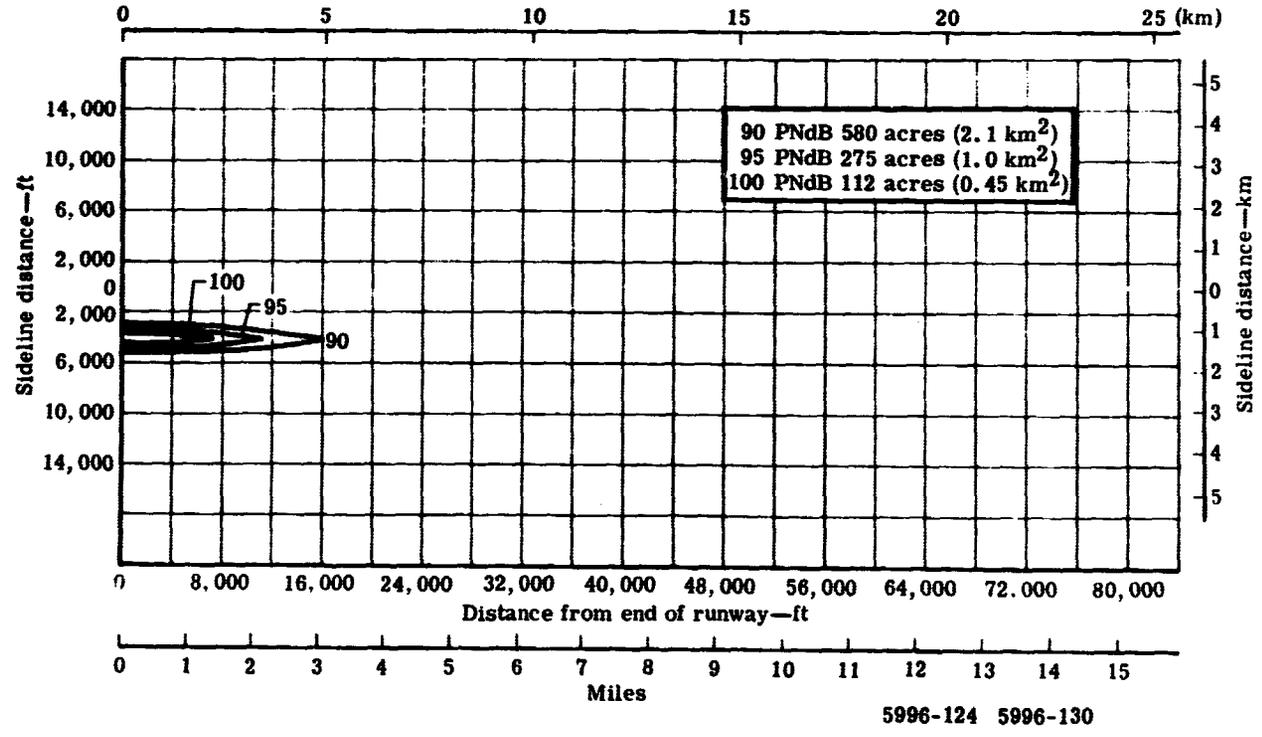

Figure 3c-14. PNdB contour for PD218-5A1 approach.

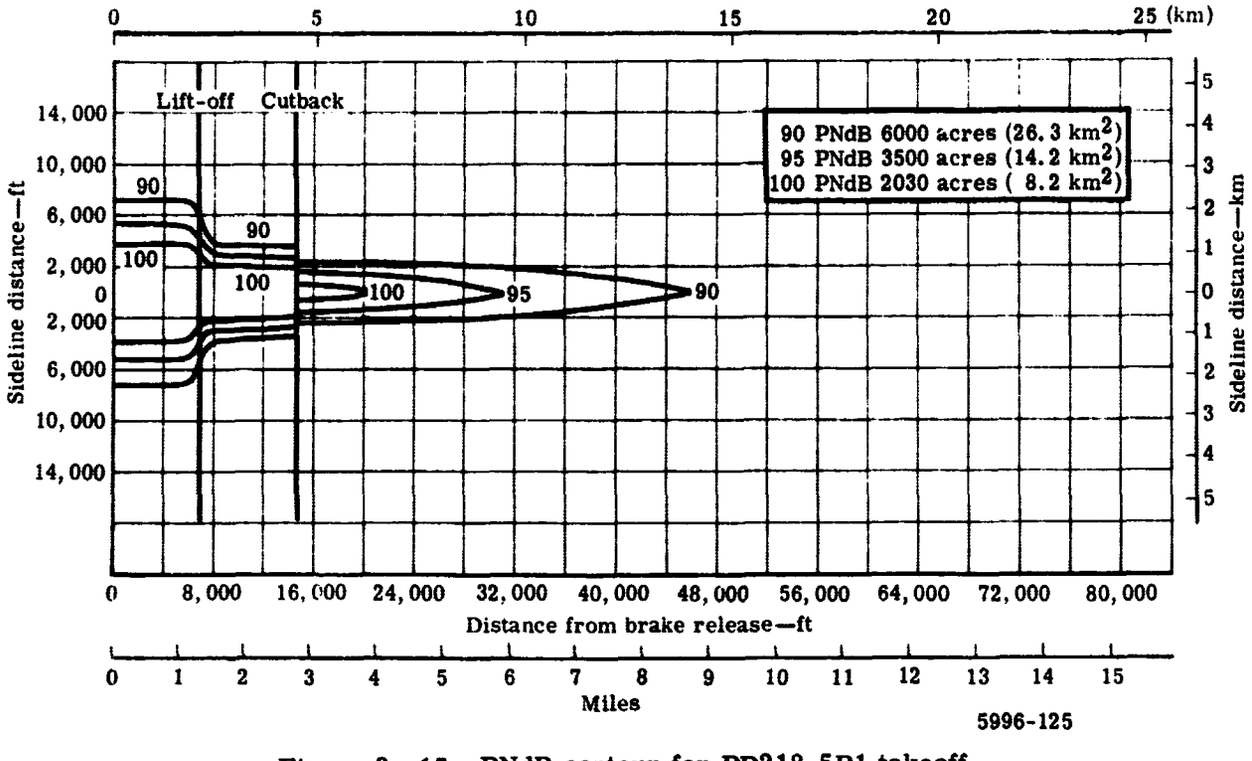

Figure 3c-15. PNdB contour for PD218-5B1 takeoff.

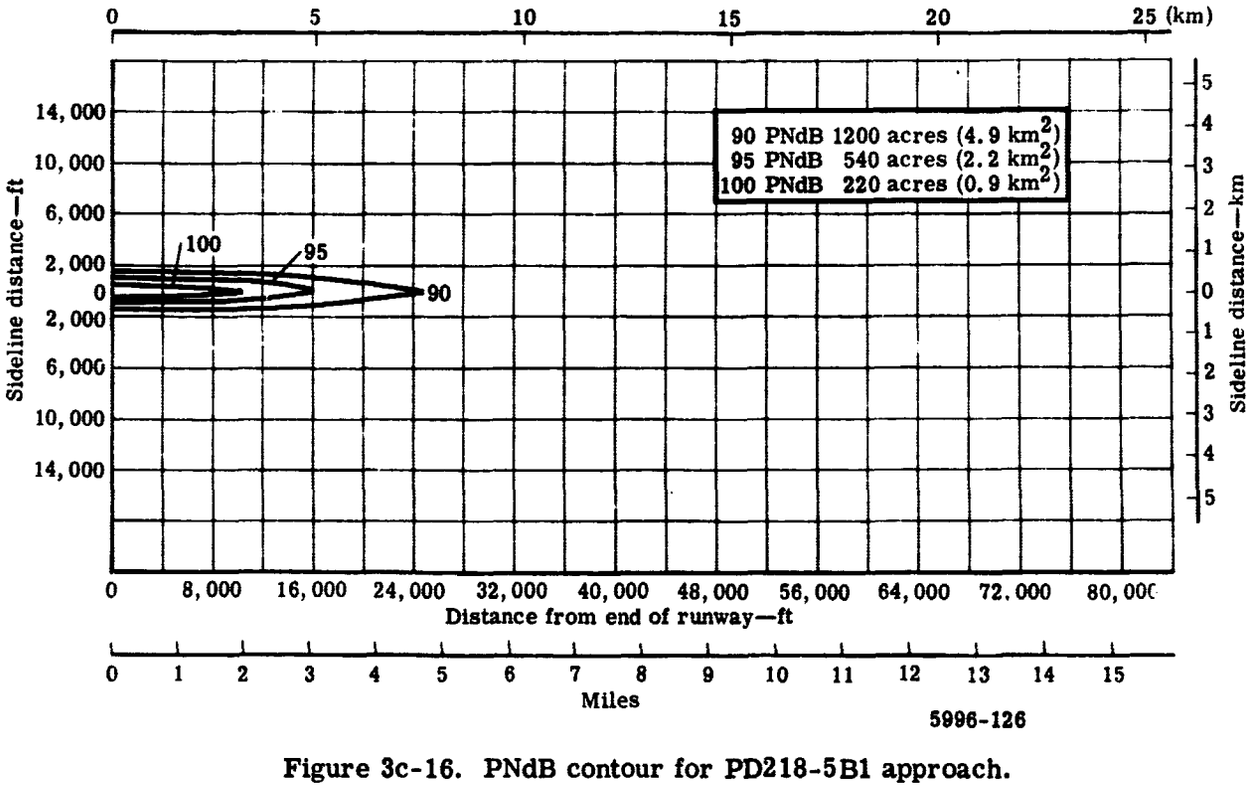

Figure 3c-16. PNdB contour for PD218-5B1 approach.

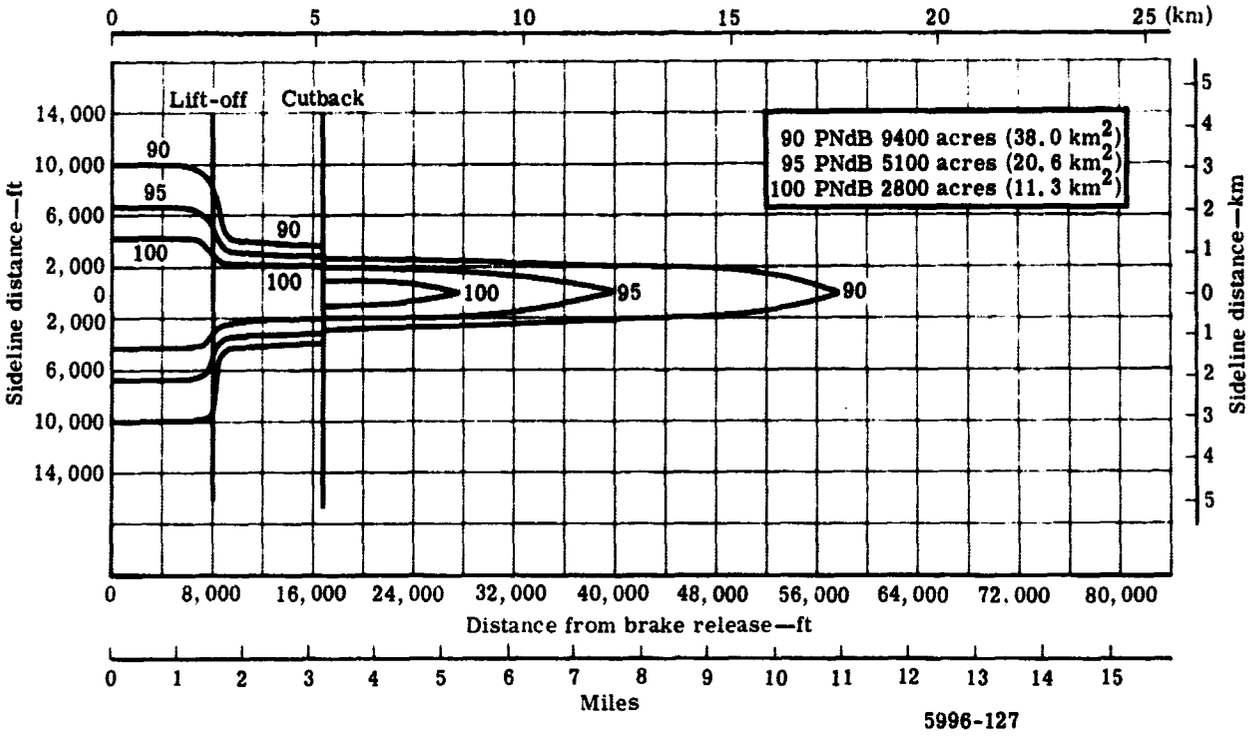

Figure 3c-17. PNdB contour for PD218-3B1 takeoff.

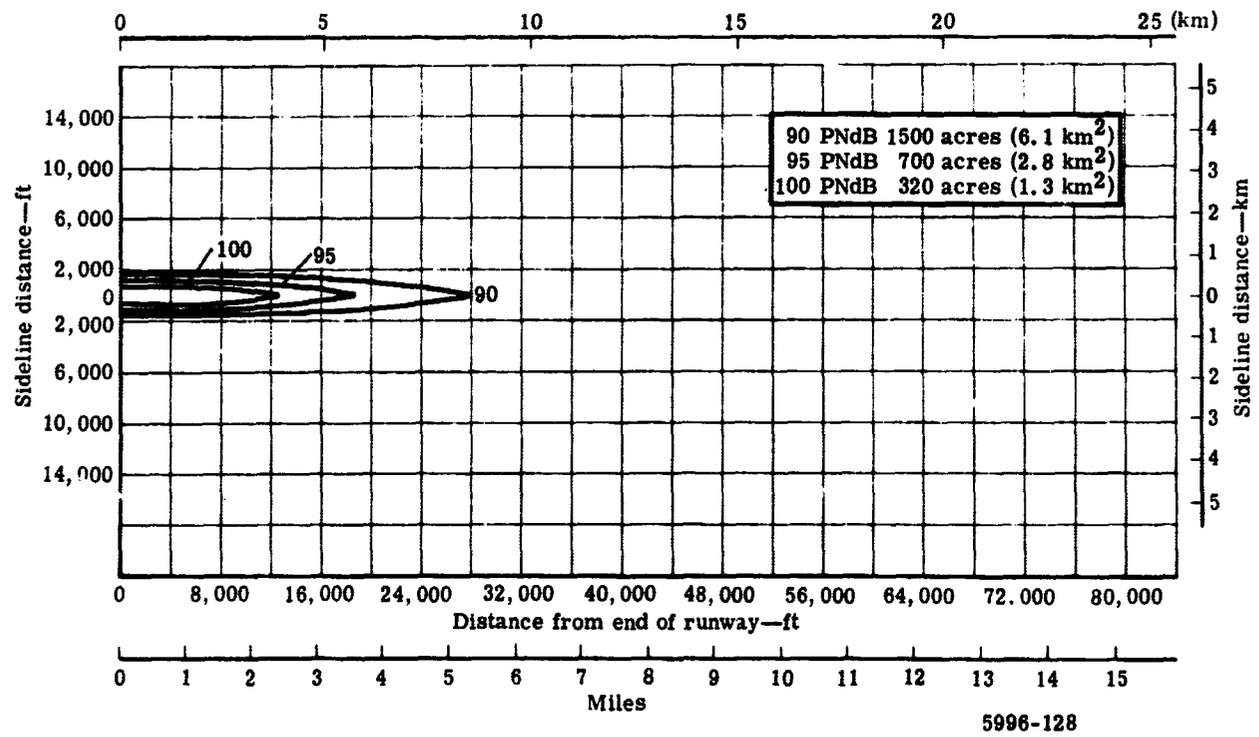

Figure 3c-18. PNdB contour for PD218-3B1 approach.

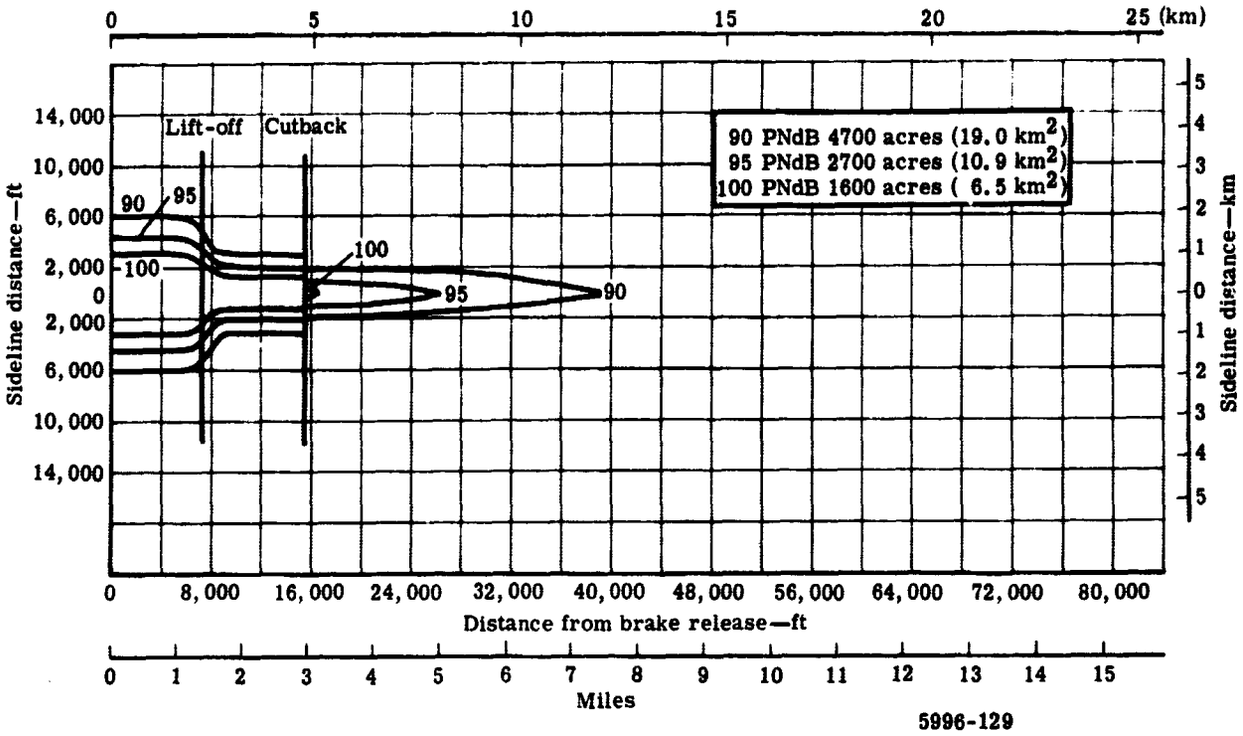

Figure 3c-19. PNdB contour for PD218-Q takeoff.

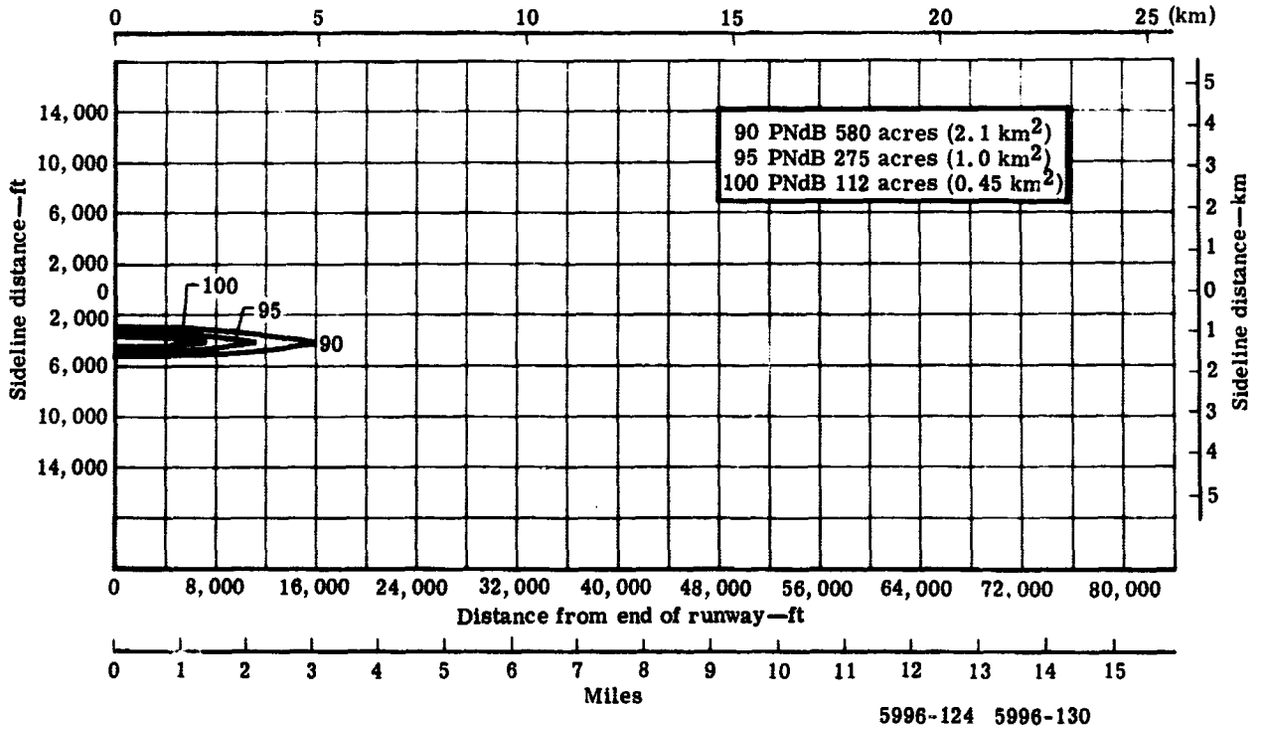

Figure 3c-20. PNdB contour for PD218-Q approach.

Table 3c-XI.

Area in acres (km^2) enclosed by the 90-, 95-, and 100-PNdB contours during takeoff.

Contour level	JT3D-3B	PD218-5A1	PD218-5B1	PD218-3B1	PD218-Q
90	18,500 (74.9)	4500 (18.2)	6000 (26.3)	9400 (38)	4700 (19)*
95	11,600 (46.9)	2600 (10.5)	3500 (14.2)	5100 (20.6)	2700 (10.9)
100	7,400 (29.9)	1700 (6.9)	2030 (8.2)	2800 (11.3)	1600 (6.5)

*The PD218-Q, though quieter at similar altitudes, suffers in relation to the PD218-5A1 engine because of its smaller size which results in a less rapid climb-out prior to cutback.

Table 3c-XII.

Area in acres (km^2) enclosed by the 90-, 95-, and 100-PNdB contours during approach.

Contour level	JT3D-3B	PD218-5A1	PD218-5B1	PD218-3B1	PD218-Q
90	5100 (20.6)	580 (2.3)	1200 (4.9)	1500 (6.1)	580 (2.3)
95	2500 (10.1)	275 (1.1)	540 (2.2)	700 (2.8)	275 (1.1)
100	1400 (5.7)	112 (0.44)	220 (0.9)	320 (1.3)	112 (0.44)

Table 3c-XIII.

Area in acres (km^2) beyond airport boundary enclosed by the 90-, 95-, and 100-PNdB contours during takeoff.

Contour level	JT3D-3B	PD218-5A1	PD218-5B1	PD218-3B1	PD218-Q
90	12,000 (48.6)	1900 (7.7)	3200 (12.9)	5300 (21.4)	2300 (9.3)
95	7,600 (30.8)	740 (3.0)	1400 (5.7)	2500 (10.1)	1000 (4.0)
100	4,800 (19.4)	360 (1.5)	540 (2.2)	1100 (4.5)	400 (1.6)

EFFECTIVE PERCEIVED NOISE LEVELS

An alternate method of evaluating noise levels is the effective perceived noise scale (EPNdB). The EPNdB level depends on the severity of pure tone (discrete frequency) protrusion above background noise levels and the duration of noise levels within 10 PNdB of the peak level recorded at the monitoring location. The procedure for estimating EPNdB has been outlined by the FAA.[9]

Pure tone protrusions result in an increase in EPNdB over the noise level ordinarily predicted in PNdB. The pure tones of the PD218-Q engine have been completely submerged by proper spacing and the selection of the proper number of stators so that discrete blade passing frequencies will not propagate. The sound pressure level produced over the full range of 1/3 octave bands predicted for the PD218-Q are shown in Figure 3c-21. This demonstrates that no tone correction is required in determining EPNdB from PNdB.

The flyover noise level was determined as a function of time for takeoff as shown in Figure 3c-22 and for approach as shown in Figure 3c-23. The resulting time when noise levels were within 10 PNdB of the peak level at the 3-mile (4.83 km) point during takeoff was found to be 5 sec when full power was continued throughout the climb and 3 sec when power was reduced to that necessary to maintain a 1000-fpm (5.1 m/sec) climb. Time duration at 1 mile (1.61 km) on approach was found to be 4 sec. Applying the EPNdB correction of $+10 \log \frac{t}{15}$, the following corrections and EPNdB levels for a four-engine aircraft were determined:

Condition	Peak PNdB	Time within 10 PNdB of peak	Correction	EPNdB
Takeoff with full power, 3 miles (4.83 km)	105.6	5	-4.8	100.8
Takeoff with cutback power, 3 miles (4.83 km)	105.6	3	-7.0	98.6
Approach, 1 mile (1.61 km), at 5000-lb (22.24-kN) thrust	103.4	4	-5.7	97.7

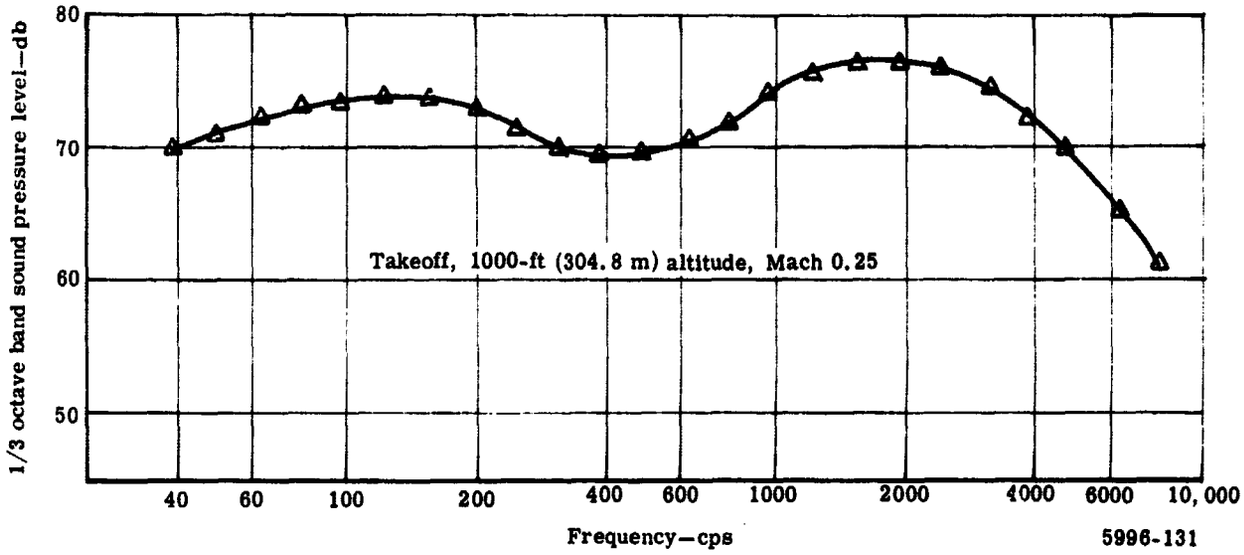

Figure 3c-21. Flyover 1/3 octave band spectrum for PD218-Q engine.

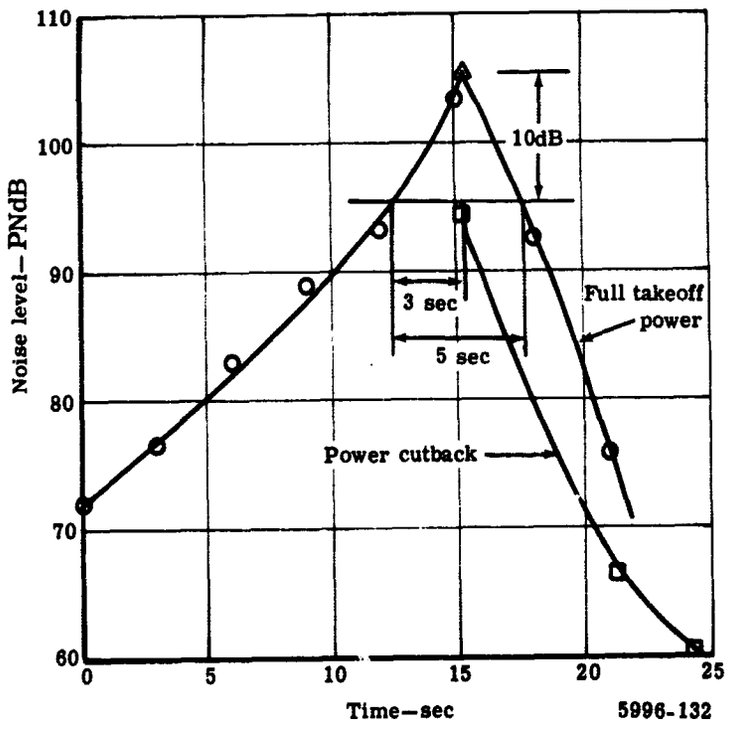

Figure 3c-22. PD218-Q takeoff noise duration time for four-engine aircraft 3 miles (4.83 km) from brake release.

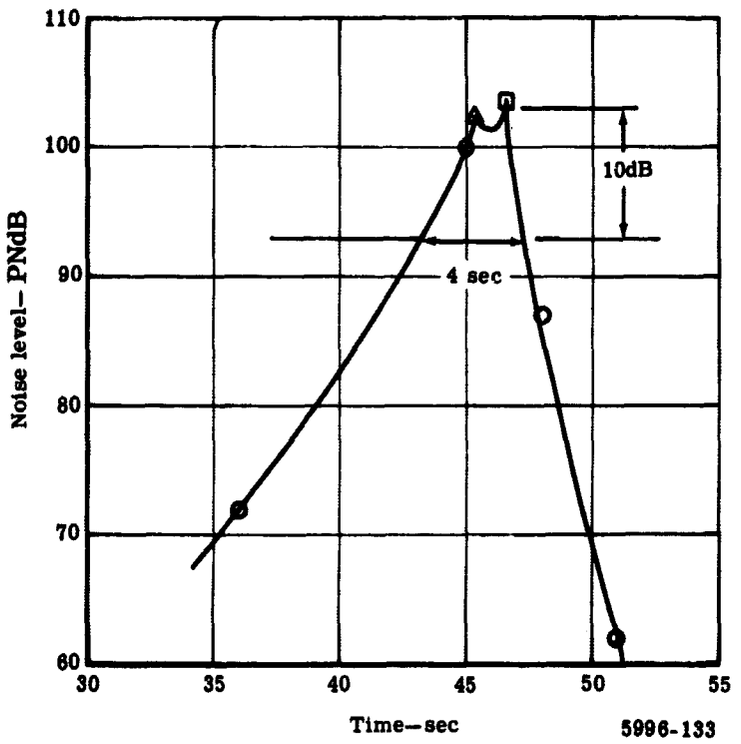

Figure 3c-23. PD216-Q approach noise duration time for four-engine aircraft 1 mile (1.61 km) from end of runway.

3d. PD218-Q Engine Description

The PD218-Q is a three-rotor, fan engine as shown in Figure 3d-1. The design point for this engine is the altitude cruise condition of Mach 0.82 at 35,000 ft (10.7 km). At this condition, the engine is designed to produce 4900 lb (21.8 kN) uninstalled thrust at a bypass ratio (BPR) of 5.5:1 with an overall pressure ratio of 24.1:1. The design turbine inlet temperature at this condition is 1763°F (1234°K).

The engine has a single-stage fan compressor supported on two bearings. The eight-stage intermediate pressure (IP) compressor and its single-stage drive turbine are supported on three bearings. The eight-stage high pressure (HP) compressor and its overhung, single-stage drive turbine are supported on two bearings. A five-stage turbine mounted on two bearings drives the fan compressor and uses the fan thrust bearing through an axially locked, splined joint.

A detailed description of the individual engine components follows.

PRECEDING PAGE BLANK NOT FILMED.

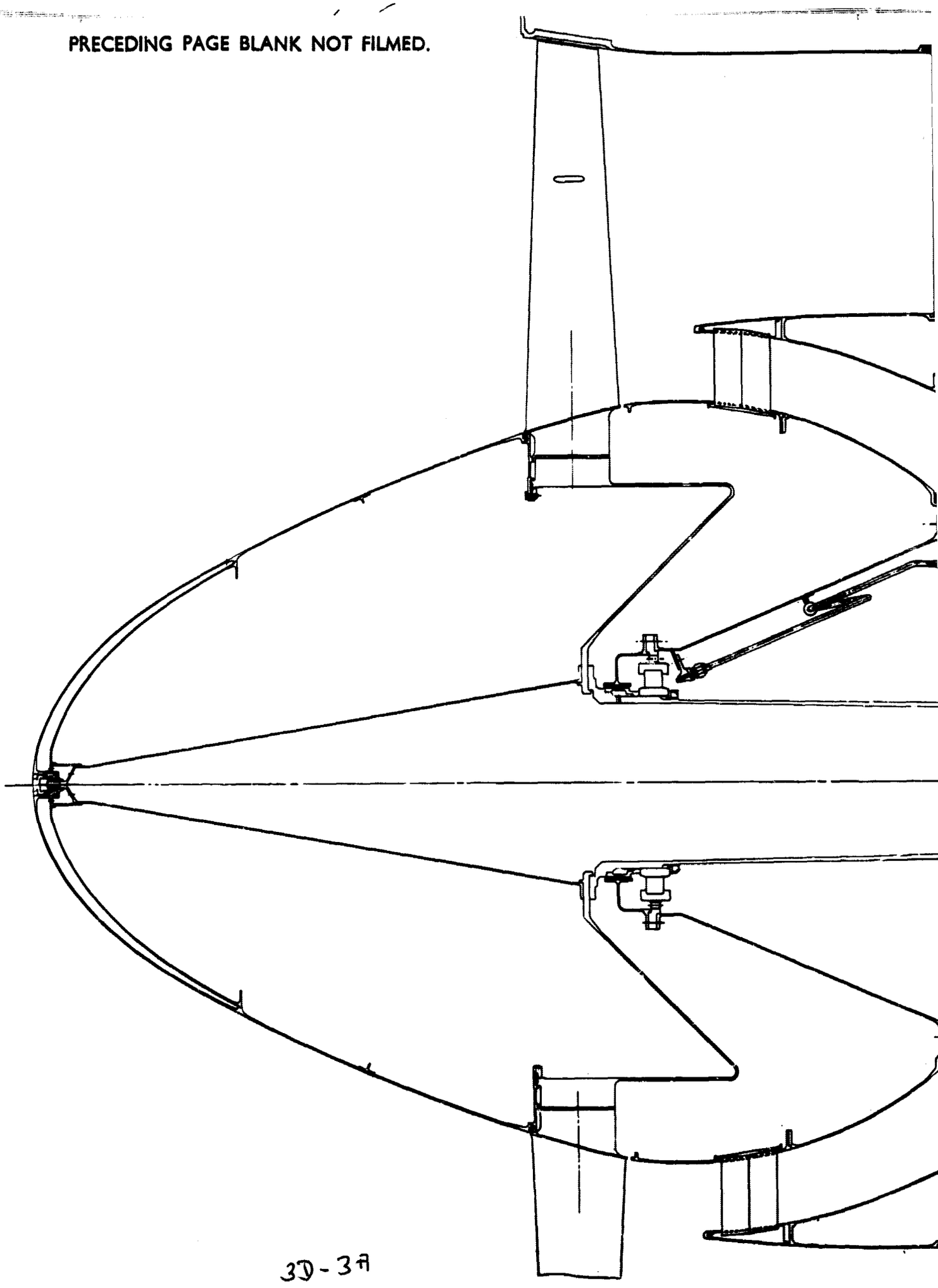

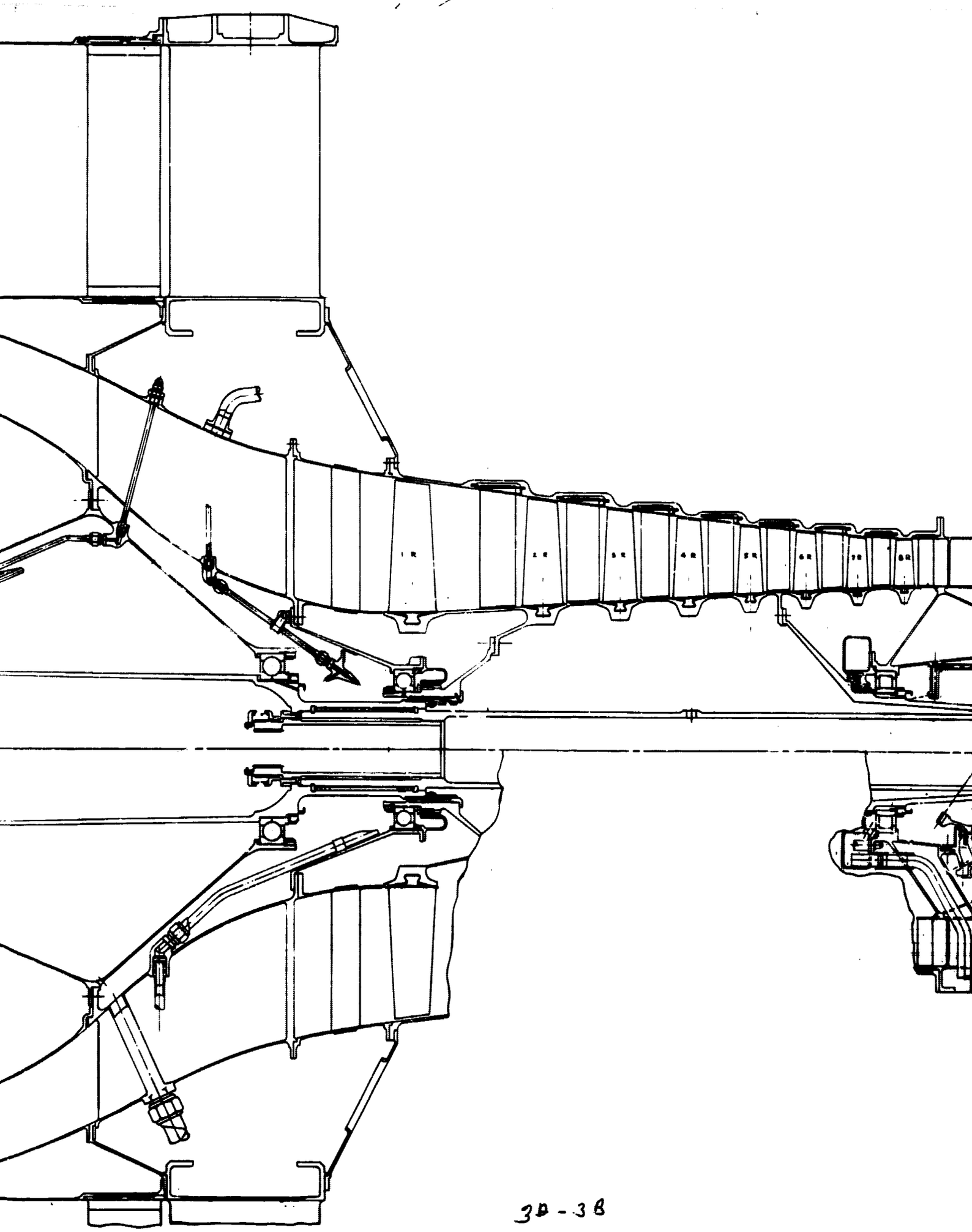

3D-3B

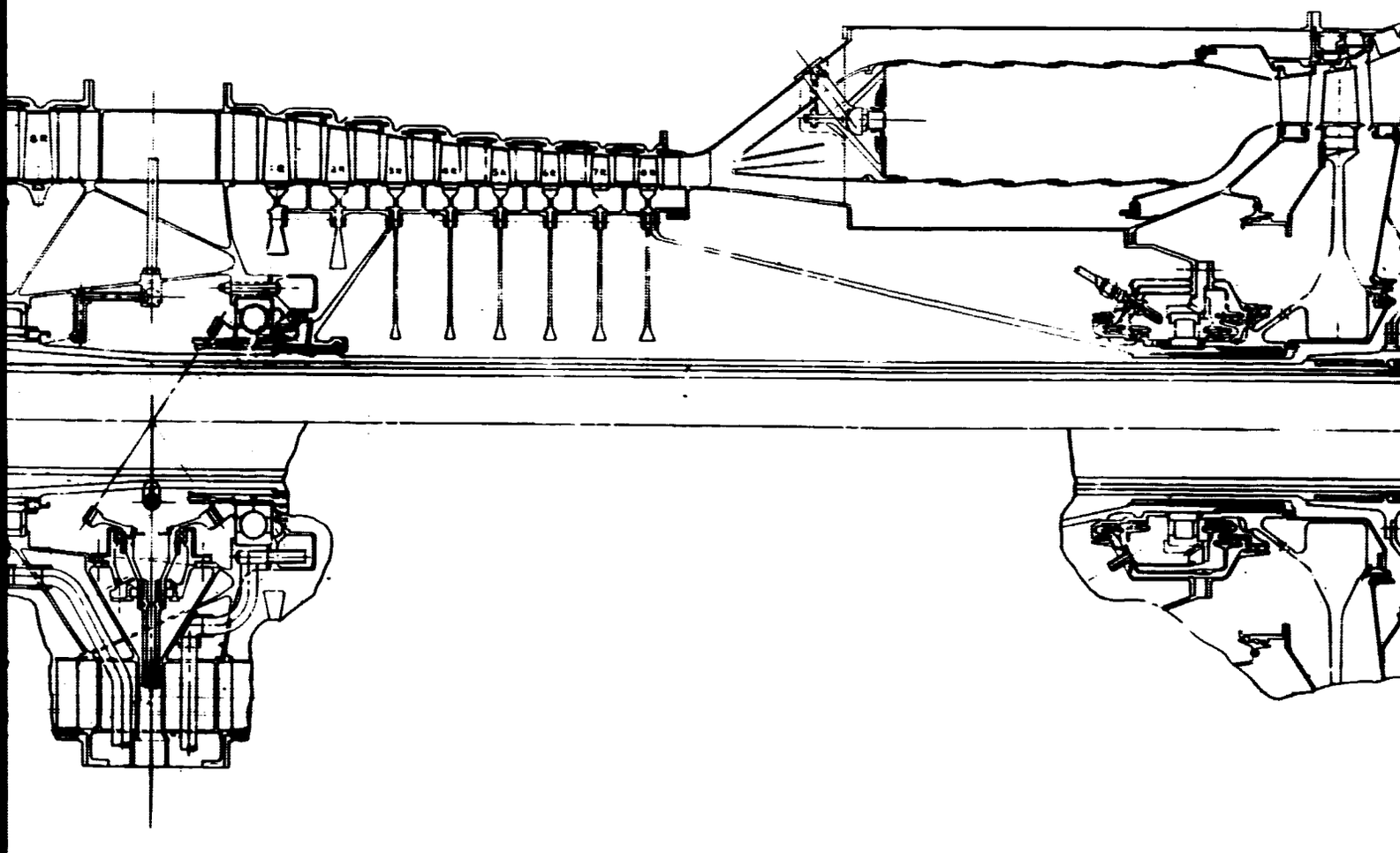

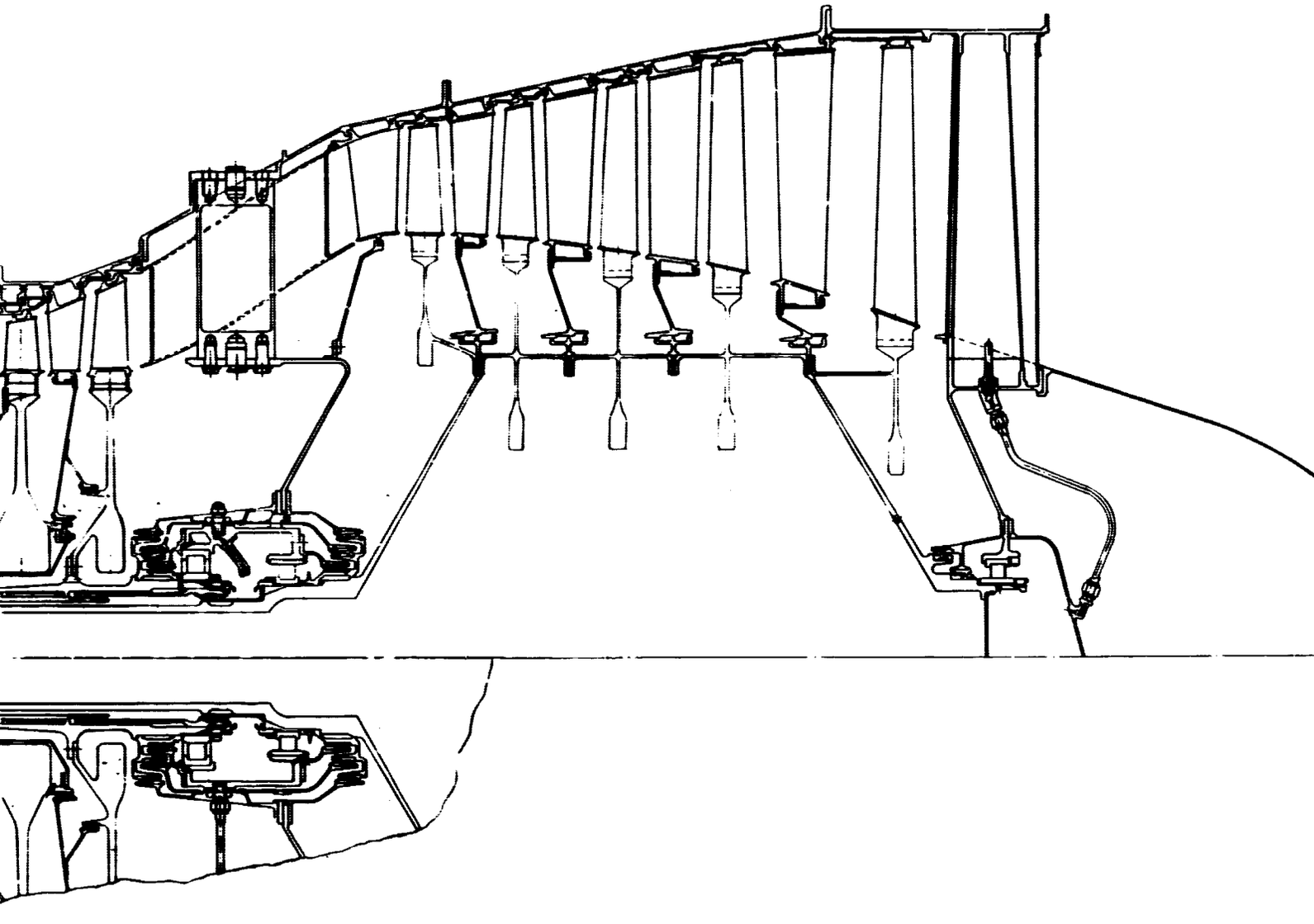

Figure 3d-1. PD218-Q engine cr

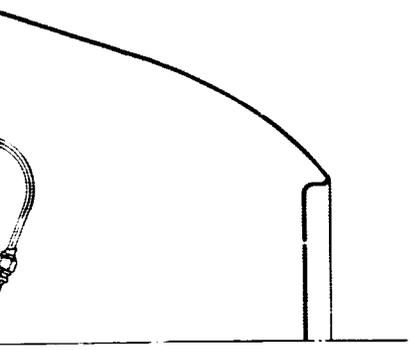

PD218-Q engine cross section. 3d-3 E

3d1. WEIGHT ANALYSIS

The basic dry weight of the engine is 4780 lb (2168.2 kg). A weight breakdown by major engine sections is given in Table 3d1-I. The specific items included in these major sections are as follows (as shown in Figure 3d-1):

1. Fan section—rotating members—fan blades, fan disk, nose spinner, and nose spinner support

2. Fan section—static members—fan outer case, fan exit stator vanes (bypass), outer fan exit support struts, and front engine mount

3. Front support structure—rotor support structure including front fan and IP compressor bearings and seals, fan EGV's (primary), fan to IP compressor inlet transition, and IP compressor IGV's

4. IP compressor—rotor drum and blades, outer case, and vane assemblies

5. Intermediate support structure—bearing support structure, bearings and seals for IP compressor rear bearing and HP compressor front bearing, and accessories drive shaft and gears

6. HP compressor—rotor disks, blades, and spacers; outer case and vane assemblies

7. Combustor—diffuser, combustor liner, inner and outer cases, HP turbine bearing compartment, bearing, seals, and bearing support structure

8. HP turbine—disks, blades, vanes, vane attachment ring, blade tip rub strip, and outer case for HP and IP turbine

9. IP turbine—disks, blades, vanes, blade tip rub strip, seals, and seal supports

10. LP (fan) turbine—disks, blades, vanes, seals and seal supports, blade tip rub strips, and outer case

11. Turbine bearing support and transition—support structure, bearings, and seals for IP turbine bearing and front LP turbine bearing; flow path transition from IP turbine exit to LP turbine inlet; outer case and rear engine mount

12. Turbine exit—bearing support structure, bearing, and seals for LP turbine rear bearing; inner and outer cases

13. Shafting—HP turbine to HP compressor drive shaft, HP turbine tie bolt, and HP compressor forward shaft; IP turbine to IP compressor drive shaft, IP turbine bearing support shaft and tie bolt, and IP compressor forward shaft; LP turbine to fan drive shaft, fan shaft, and tie bolt, and LP turbine rear shaft

14. Accessories—accessories drive gearbox, engine fuel and control system (including fuel pump, fuel control, fuel nozzles and manifold, etc), ignition system, lubrication system (including pump, oil tank, oil/fuel heat exchanger), engine bleed valve, and all engine-associated plumbing

The engine design and weight reflect provisions to mount and/or to drive the following items (these items are not included in the engine weight):

- Engine inlet cowl
- Fan exit ducting, exhaust nozzle, and thrust reverser
- Turbine exit ducting and exhaust nozzle
- Engine inlet and exhaust acoustic treatment
- Engine starter
- Hydraulic pump
- Alternator

Table 3d1-I.
PD218-Q weight estimate.

Engine Section	Weight lb	Weight kg
1. Fan section—rotating members	472.7	214.4
2. Fan section—static members	375.7	170.4
3. Front support structure	368.7	167.2
4. IP compressor	279.1	126.6
5. Intermediate support structure	65.9	29.9
6. HP compressor	293.2	133.0
7. Combustor	209.0	94.8
8. HP turbine	201.4	91.4
9. IP turbine	153.1	69.4
10. LP (fan) turbine	1265.8	574.2
11. Turbine bearing support and transition	222.2	100.8
12. Turbine exit	118.2	53.6
13. Shafting	476.1	216.0
14. Accessories	278.9	126.5
Total engine weight	4780.0	2168.2

3d2. FAN

Aerodynamic Design

General

The single-stage axial flow fan unit for the engine consists of a single transonic rotor. This rotor is followed by two rows of primary (hot flow path) stator vanes which return the flow to the axial direction and one row of axial exit vanes in the bypass duct. An aerodynamically designed transition duct is provided between the fan and the IP compressor. At the altitude design point of 35,000 ft (10.7 km) at Mach 0.82, the fan match point requirements are:

- Corrected airflow, $W_a\sqrt{\theta}/\delta$ = 940.8 lb/sec (426 kg/sec)
- Pressure ratio, R_c = 1.45 (primary) and 1.50 (bypass)

Complete listings of the symbols used and aerodynamic design information are given in Tables 3d2-I and 3d2-II. The estimated performance map is shown in Figure 3d2-1. Double circular arc blading is used throughout. A linear chord taper from 4.89 in. (124 mm) at the hub to 6.175 in. (157 mm) at the tip is employed for the rotor; the stators are of constant chord design. A circumferential vibration damper is provided at an engine cold radius of 30.1975 in. (767 mm), corresponding to 65% of the blade span. IGV's are not required in this design. The exit vanes are designed for strip-stock fabrication for ease of manufacture.

Table 3d2-I.
PD218-Q aerodynamic design symbols.

A_a	=	annulus area
D	=	diameter
D_f	=	Lieblien diffusion factor
N	=	shaft speed
R_c	=	pressure ratio
R	=	radius (engine)
U	=	wheel speed
W_a	=	airflow
V	=	velocity
V_z	=	axial velocity

V_θ = tangential velocity

α = relative air angle

β = absolute air angle

δ = pressure correction term, = P in psia/14.7

σ = solidity

θ = temperature correction term, = T in °R/518.7

Subscripts

0 = absolute

1 = inlet

2 = exit

H = hub

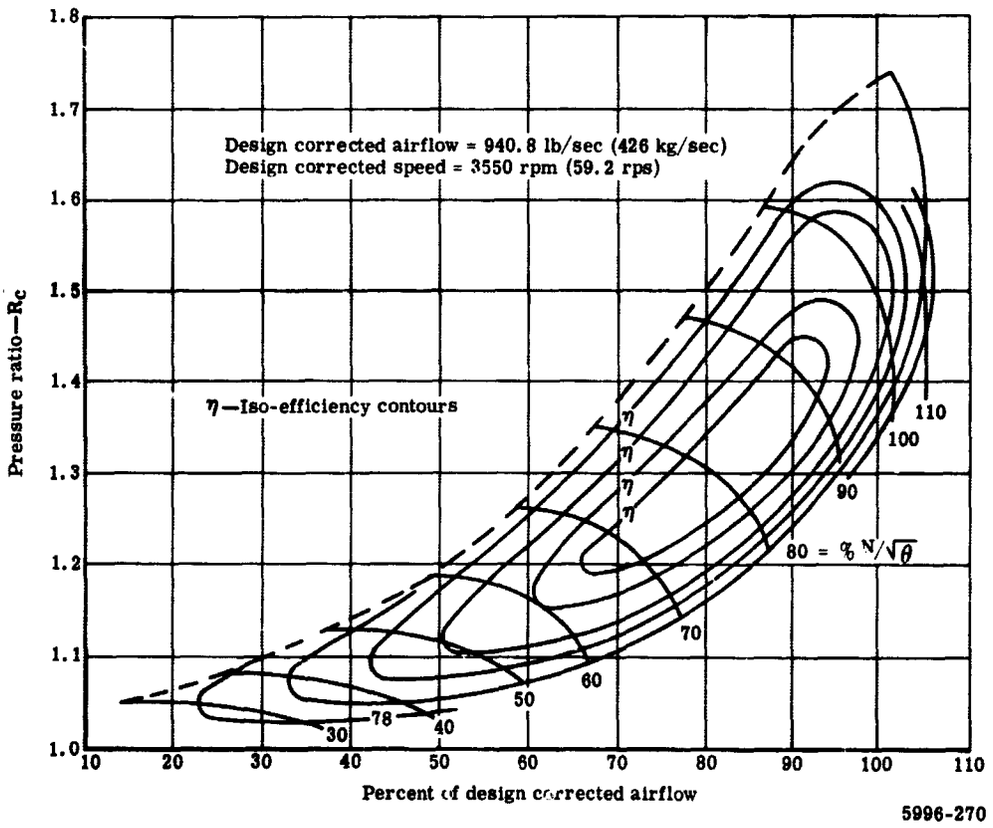

Figure 3d2-1. PD218-Q fan estimated performance.

R	=	relative
T	=	tip
z	=	axial direction
max	=	maximum
mean	=	mean-line conditions

Table 3d2-II.
PD218-Q fan aerodynamic design values.

Corrected specific annulus flow*	40.0 lb/sec-ft^2 (195.2 kg/sec-m^2)
Corrected airflow	940.8 lb/sec (426 kg/sec)
Pressure ratio, primary	1.45:1
Pressure ratio, bypass	1.50:1
Bypass ratio	5.5:1
Corrected speed	3550 rpm (59.2 rps)
Inlet total pressure	5.4 psia (37,250 pascals)
Inlet total temperature	-12.9°F (248°K)
Corrected inlet tip speed	1158 fps (353 m/sec)
Inlet annulus area	23.5 ft^2 (2.18 m^2)
Inlet tip diameter	74.0 in. (1.88 m)
Inlet H/T diameter ratio	0.466
Rotational direction, from rear	Clockwise

*Based on aerodynamic boundaries, not mechanical dimensions.

Inclusion of quieting techniques within the basic aerodynamic system has resulted in a configuration which will achieve overall performance requirements with lower predicted noise generation than present designs. Engineering information obtained during Tasks I and II of the Quiet Engine Definition Program provided a basis for selection of the final design.

Parametric Studies

Parametric studies conducted early in the program pointed out major design variables and their effects on noise production. It became apparent that the major contributions to overall fan noise are generated in three areas: rotor tip, stator hub, and blade-wakes.

Frictional energy transfer associated with high Mach numbers on the blading tends to significantly increase noise generation. Rotor white noise varies as a logarithmic function of rotational speed, and Mach wave noise occurs when the rotor tip relative Mach numbers become supersonic. A quiet fan must, therefore, operate at relatively low speed.

The substantial reduction in rotor tip Mach number noise realized by selection of a reduced shaft speed results in two major aerodynamic effects, both of which tend to compromise performance.

- At reduced rpm, the rotor hub is forced to provide its design pressure rise at low wheel speeds. This may result in the necessity of turning the air past the axial direction at the hub, a situation which is aerodynamically unstable and which increases the approach velocity and, therefore, the noise generated at the stator hub.
- Low shaft speeds are undesirable from engine size and weight considerations. This is due to the greater number of turbine stages and larger connecting shafting to accommodate the higher fan torque resulting from the reduced speed. The larger shafting also aggravates the bearing DN design parameter of the higher speed outer concentric shafts of the multispool engine design.

Two methods are available to remedy the first effect described. The first method is to raise the H/T diameter ratio commensurate with acceptable hub turning. If the flow per unit of annular area is held constant, this method results in an increase in engine diameter and weight. The second method is to reduce the rotor hub pressure rise requirements and incorporate a radial pressure gradient. This could result in adverse velocity gradients at the inlet to the transition duct, a situation which could compromise duct performance.

Vane discrete noise is generated through interaction of the blade wakes with the vanes. Blade emersion in high Mach number flow fields produces high energy turbulence within the wakes. Acoustic energy is released when these wakes interact with downstream vane rows. In general, wake turbulence may be minimized by proper selection of the following blading design parameters:

- Solidity
- Thickness-to-chord (T/C) ratio
- Aspect ratio
- Incidence angle

Blading with insufficient solidity tends to generate excessive whirl, which is associated with inefficient air turning; too much blade solidity reduces the flow capacity. In addition, the strength of passage shock waves is, to a high degree, controlled by the choice of solidity. A variable chord distribution is required to more nearly optimize solidity at all radial stations of the blade. The quiet engine fan rotor employs a linear chord taper ratio of 1.264, increasing from hub to tip.

Excessive blade thickness is undesirable from the standpoint of turbulence production because the wakes become thicker. The same is true for blades with long chords associated with a low aspect ratio. From stress considerations, the thicker blading is best and some degree of compromise is required.

The optimum T/C distribution for the quiet engine fan rotor was found to be a linear variation from 8% at the hub to 3% at the tip. For the stators, 8% (constant radially) was found to be satisfactory.

High aspect ratio blading, although considered quieter, is susceptible to inlet distortion and mechanical tip clearance problems. In addition, the hub and tip ramp angles increase for a given inlet-to-outlet area ratio. The transition from the fan to the IP compressor then becomes more difficult. In view of these considerations, the rotor mean aspect ratio for the final design was set at 3.4. The resulting hub and tip ramp angles were 17.2 and -8.7 degrees (0.3 and 0.152 radian), respectively.

Minimum loss incidence is related to minimum wake thickness and, hence, noise production. A radially constant 3-degree (0.0524-radian) incidence distribution was used in designing the fan rotor. This establishes a wide operating range between surge and choke, and losses are minimized at the design point. The first primary stator vane employs a design incidence of 3 degrees (0.0524 radian). Both the bypass and second primary vanes were designed to zero incidence.

In addition to minimum wake thickness considerations, the studies indicated that the axial spacing between blade rows in regions where the rotor relative Mach number is highest would promote better mixing of the blade wakes. The axial spacing of the rotors and stators was set at one chord length in the primary duct and three chord lengths in the bypass section. The aerodynamic parametric design study resulted in five basic fan configurations. The principal design variables of each design are listed in Table 3d2-III. Each design is discussed separately in the following paragraphs.

Table 3d2-III.

PD218-Q parametric design configurations (cruise design point).

	A	B	C	D	E
$W_a\sqrt{\theta}/\delta A_a$, lb/sec-ft^2	39.5	39.5	39.5	41.0	40
(kg/sec-m^2)	(192.8)	(192.8)	(192.8)	(200)	(195.1)
$U_t/\sqrt{\theta}$, fps	1196	1196	1101	1196	1158
(m/sec)	(364.5)	(364.5)	(335.5)	(364.5)	(352.5)
R_c primary	1.45	1.41	1.45	1.45	1.45
R_c bypass	1.50	1.50	1.50	1.50	1.50
Inlet D_H/D_T	0.466	0.466	0.466	0.466	0.466
V_{max}/V_{mean} at duct inlet	1.06	1.19	1.08	1.035	1.02
α_2 at rotor hub, degrees	1.8	13.6	-3.7	-4.2	0.57
(radian)	(0.0314)	(0.2375)	(-0.0646)	(-0.0733)	(0.0095)
D_f at rotor tip	0.415	0.433	0.451	0.409	0.421
Bypass ratio	5.5	5.5	5.5	5.5	5.5

- Configuration A—This design served as a basis for the Task II comparison studies. It was established as a refinement of the 5:1 bypass ratio, single-stage fan design generated during Task I. The increased bypass ratio together with elimination of past-axial turning resulted in decreased noise production at the stator, although rotor tip Mach numbers at takeoff were higher than desired.
- Configuration B—In this design an attempt was made to reduce the hub pressure rise requirement by employing a larger radial pressure gradient. The severe velocity gradient at the inlet to the transition duct was considered to be unacceptable, although noise characteristics at the stator hub were favorable.
- Configuration C—In this design a nominal pressure gradient was used in conjunction with a reduced shaft speed. Although the rotor noise was reduced, excessive vane white noise resulted from the past-axial turning. Also, the rotor tip diffusion factor was excessive.
- Configuration D—To investigate the effects of specific flow on fan noise characteristics, flow per unit area was increased to 41.0 lb/sec-ft^2 (200 kg/sec-m^2) in this configuration. The tip speed, radial pressure gradient, and inlet H/T radius ratio remained the same as those of Configuration A. Moderately high off-design tip Mach numbers on the rotor were still present, however, the rotor tip diffusion factor was reduced significantly.

- Configuration E—This configuration was selected as the final design. It has the following features.
  - Rotor tip loading is reduced by using a specific flow of 40.0 lb/sec-ft^2 (195.1 kg/sec-m^2) together with a pressure gradient in the bypass section.
  - Past-axial turning is eliminated by using a moderate pressure gradient in the primary section. This results in reduced vane noise and acceptable duct performance.
  - Rotor tip Mach noise at takeoff is reduced significantly by limiting the inlet tip speed to 1158 fps (352.5 m/sec) at the cruise design point.

  The required aerodynamic performance is achieved using a minimum-risk type design which will not require extensive development time.

Vector Diagrams

As a result of the high streamline curvatures associated with single-stage energy addition at high rotational speed, a full radial equilibrium solution of the equations of motion was used. This calculation satisfied the system of dynamic and state equations. This calculation is available as a computerized solution in which blade losses are calculated internally based on an empirical correlation developed to predict the radial distribution of blade element efficiency.

A summary of aerodynamic and geometric design data is given in Tables 3d2-IV and 3d2-V. The fan flow path and transition duct are shown in Figure 3d2-2.

Mechanical Design

The single-stage fan is supported on two bearings. The fan rotor is designed to provide adequate spacing for noise reduction and critical speed margins for the low-pressure rotor system. This permits revisions to be made during engine development without disrupting the remainder of the engine. In the event of an in-flight fan failure, the two-bearing support system will isolate the major failure damage and carry resulting loads directly to the mounts. Figure 3d2-3 shows the fan rotor and stator assembly. Details of the fan blade, wheel, bypass stators, and primary exit stators are shown in Figures 3d2-4 through 3d2-7, respectively.

As shown in Figure 3d2-3, removal of the fan rotor assembly is accomplished by first removing the spinner retaining locknut and spinner. The spinner support, disk, and blade assembly can then be unbolted and removed. The fan stator assembly is removed by unbolting the strut at the aft strut support and unbolting the inner duct and bearing support from the forward compressor structure. The tie bolt can then be disengaged and removed. This allows the fan stator and fan stub shaft assembly to be removed.

The bypass stators, due to the centrifugal action of the fan, are the only parts besides the fan blades that are likely to suffer from foreign object damage. Ease of removal of the bypass stators, therefore, was one of the primary objectives of this design. Removal is accomplished

Table 3d2-IV.
PD218-Q fan blade and vane physical properties.

	Radius, in. (m)	Mean aspect ratio	Camber angle, deg (rad)	Setting angle, deg (rad)	Incidence angle, deg (rad)	T/C ratio	Solidity, σ	Chord, in. (m)	Leading and trailing edge radii, in. (m)	Axial chord, in. (m)
Rotor, 50 blades	18.287 (0.464)	↑	51.19 (0.8940)	13.14 (0.2295)	↑ ↑	0.0800	2.2125	4.890 (0.1241)	↑ ↑	4.762 (0.1210)
	22.052 (0.561)		42.56 (0.7430)	22.70 (0.3960)		0.0695	1.851	5.150 (0.1308)		4.751 (0.1208)
	26.556 (0.674)	3.411	31.50 (0.5500)	33.93 (0.5915)	3.0 (0.0524)	0.0572	1.632	5.465 (0.1390)	0.0244 (0.000616)	4.534 (0.1151)
	30.938 (0.786)		17.91 (0.3125)	45.47 (0.7930)		0.0460	1.480	5.770 (0.1467)		4.046 (0.1028)
	34.858 (0.886)		8.10 (0.1412)	53.96 (0.9400)		0.0355	1.375	6.040 (0.1534)		3.554 (0.0898)
	36.735 (0.933)	↓	0.85 (0.0148)	59.07 (1.0310)	↓ ↓	0.0300	1.335	6.175 (0.1570)	↓ ↓	3.174 (0.0801)
First primary vane, 125 vanes	19.028 (0.484)	↑	20.46 (0.3570)	27.91 (0.4870)	↑ ↑	0.0790	1.029	0.9837 (0.0250)	↑ ↑	0.8693 (0.02205)
	19.936 (0.506)		21.18 (0.3890)	28.51 (0.4975)		0.0800	0.981	0.9833 (0.0250)		0.8641 (0.02195)
	20.806 (0.530)	3.49	21.68 (0.3785)	29.01 (0.5060)	3.0 (0.0524)	0.0800	0.940	0.9831 (0.0250)	0.00491 (0.0001248)	0.8597 (0.02185)
	21.642 (0.551)		22.05 (0.3845)	29.49 (0.5140)		0.0800	0.904	0.9829 (0.0250)		0.8556 (0.02175)
	22.451 (0.571)	↓	22.38 (0.3900)	29.91 (0.5220)	↓ ↓	0.0800	0.871	0.9827 (0.0250)	↓ ↓	0.8518 (0.02165)
Second primary vane, 125 vanes	18.781 (0.477)	↑	29.92 (0.5210)	8.17 (0.1426)	↑	0.0804	1.036	0.9778 (0.0248)	↑ ↑	0.9679 (0.02460)
	19.737 (0.502)		30.96 (0.5400)	8.28 (0.1445)		0.0805	0.985	0.9770 (0.0248)		0.9668 (0.02458)
	20.636 (0.525)	3.61	31.93 (0.5570)	8.37 (0.1460)	0 (0)	0.0806	0.941	0.9762 (0.0248)	0.00491 (0.0001248)	0.9658 (0.02455)
	21.487 (0.546)		32.87 (0.5740)	8.46 (0.1478)		0.0806	0.903	0.9754 (0.0248)		0.9648 (0.02452)
	22.300 (0.566)	↓	33.75 (0.5890)	8.53 (0.1490)	↓ ↓	0.0807	0.870	0.9747 (0.0248)	↓ ↓	0.9639 (0.02447)
Bypass vane, 81 vanes	23.384 (0.593)	↑	49.90 (0.8700)	17.21 (0.3050)	↑	0.0800	2.205	3.990 (0.1016)	↑ ↑	3.820 (0.0964)
	27.073 (0.688)		49.78 (0.8690)	16.58 (0.2890)		0.0800	1.905	4.000 (0.1016)		3.833 (0.0966)
	30.[illegible]3 (0.770)	3.241	48.08 (0.8400)	15.56 (0.2715)	0 (0)	0.0796	1.705	4.008 (0.1019)	0.020 (0.000505)	3.861 (0.0975)
	33.313 (0.846)		46.23 (0.8070)	14.55 (0.2540)		0.0796	1.555	4.017 (0.1020)		3.889 (0.0982)
	36.346 (0.924)	↓	45.09 (0.8020)	14.12 (0.2465)	↓ ↓	0.0796	1.425	4.019 (0.1020)	↓ ↓	3.897 (0.0985)

Table

PD218-Q fan aero

	Inlet radius		Exit radius		Wheel speed $U_1/\sqrt{\theta}$		$U_2/\sqrt{\theta}$		Axial velocity $V_{z_1}/\sqrt{\theta}$		$V_{z_2}/\sqrt{\theta}$		Relative velocity $V_{R_1}/\sqrt{\theta}$		$V_{R_2}/\sqrt{\theta}$		Absolute velocity $V_{\theta_1}/\sqrt{\theta}$		$V_{\theta_2}/\sqrt{\theta}$
	in.	m	in.	m	fps	mps	fps	mps	fps	mps	fps	mps	fps	mps	fps	mps	fps	mps	fps
Rotor	17.56	0.4460	19.01	0.4825	544.0	165.8	589.0	179.5	632.2	192.8	669.9	204.1	862.1	262.5	681.6	207.9	668.8	203.9	896.4
	21.71	0.5515	22.39	0.5690	672.6	205.0	693.7	211.3	636.9	194.2	601.0	183.1	932.4	284.0	614.0	187.0	645.8	197.0	839.5
	26.55	0.6750	26.57	0.6745	822.3	250.5	823.0	250.7	626.1	191.0	557.9	170.0	1033.9	315.5	620.9	189.1	626.7	191.0	784.0
	31.17	0.7910	30.70	0.7800	965.7	294.5	951.2	290.0	610.5	186.1	528.7	161.0	1142.8	349.0	710.8	216.5	611.1	186.1	712.5
	35.27	0.8970	34.45	0.8760	1092.5	333.3	1067.3	325.0	595.3	181.5	508.0	154.9	1245.8	380.0	832.0	253.5	598.6	182.1	654.4
	37.00	0.9405	36.30	0.9210	1151.4	351.5	1124.6	342.5	589.8	179.8	458.2	139.5	1295.8	395.0	894.2	272.5	594.4	181.0	582.8
First primary vane	19.13	0.4860	18.93	0.481					660.0	201.2	536.0	163.3					879.6	268.0	590.4
	20.01	0.5080	19.86	0.5045					638.8	194.5	533.8	162.5					862.6	263.0	588.4
	20.87	0.5310	20.75	0.5270					621.6	189.3	532.0	162.1					849.3	258.5	587.7
	21.70	0.5515	21.95	0.5575					607.2	185.1	530.5	161.9					838.3	255.5	588.0
	22.50	0.5720	22.40	0.5690					594.6	181.0	529.4	161.1					828.3	252.5	589.1
Second primary vane	18.93	0.4810	18.63	0.4740					536.0	163.3	501.3	152.9					590.4	180.0	518.4
	19.86	0.5450	19.61	0.4980					533.8	162.5	507.4	154.8					588.4	179.2	520.4
	20.75	0.5270	20.53	0.5210					532.0	162.1	512.8	156.3					587.7	179.2	523.3
	21.50	0.5490	21.39	0.5435					530.5	161.9	518.1	157.9					588.0	179.2	527.2
	22.40	0.5690	22.20	0.5640					529.4	161.1	523.7	159.5					589.1	179.3	532.0
Bypass vane	23.38	0.5940	23.38	0.5935					616.4	188.0	502.1	153.0					831.6	253.5	502.1
	27.07	0.6880	27.07	0.6880					610.7	186.1	564.6	172.0					815.0	248.5	564.6
	30.31	0.7700	30.31	0.7700					588.6	179.1	553.9	168.8					764.0	232.5	553.9
	33.32	0.8460	33.32	0.8455					555.7	169.5	517.6	157.9					702.1	214.0	517.6
	36.35	0.9240	36.35	0.9240					472.5	144.0	403.2	122.9					592.5	180.7	403.2

FOLDOUT FRAME

Table 3d2-V.

Q fan aerodynamic design data.

solute velocity			Absolute angle				Relative angle				Tangential velocity				Inlet relative Mach No.	Exit absolute Mach No.	Diffusion factor D_f	Percent choke margin
	$V_{0_2}/\sqrt{\theta}$		β_1		β_2		α_1		α_2		$V_{\theta_1}/\sqrt{\theta}$		$V_{\theta_2}/\sqrt{\theta}$					
nps	fps	mps	deg	rad	deg	rad	deg	rad	deg	rad	fps	mps	fps	mps				
03.9	896.4	273.5			41.00	0.7160	40.71	0.7110	0.57	0.0099			582.3	177.5	0.802	0.811	0.356	9.13
07.0	839.5	255.9			44.13	0.7710	46.56	0.8140	10.43	0.1821			583.1	177.5	0.865	0.746	0.504	7.19
01.0	784.0	238.7			44.63	0.7790	52.71	0.9200	26.01	0.4540			550.8	168.0	0.957	0.686	0.562	8.41
86.1	712.5	217.0			42.05	0.7340	57.70	1.008	41.90	0.7310			476.8	145.2	1.056	0.619	0.523	8.89
62.1	654.4	199.2			38.91	0.6790	61.41	1.071	52.30	0.9140			410.0	125.0	1.150	0.566	0.459	9.23
31.0	582.8	177.8			37.99	0.6630	62.88	1.098	59.14	1.016			357.8	109.0	1.195	0.504	0.421	6.29
58.0	590.4	180.0	41.26	0.7200	23.49	0.4100					579.1	176.3	232.9	71.0		0.515	0.520	9.02
63.0	588.4	179.2	42.16	0.7365	24.03	0.4200					578.5	176.1	238.0	72.5		0.512	0.519	10.70
58.5	587.7	179.2	42.91	0.7490	24.54	0.4280					577.9	176.0	242.9	74.1		0.510	0.517	12.21
55.5	588.0	179.2	43.56	0.7610	25.08	0.4380					577.4	176.0	248.3	75.8		0.509	0.516	13.51
52.5	589.1	179.3	44.13	0.7700	25.59	0.4460					576.8	176.0	253.5	77.2		0.509	0.513	14.79
00.0	518.4	158.0	23.49	0.4100							232.9	71.0				0.450	0.313	23.14
79.2	520.4	158.8	24.03	0.4200							238.0	72.5				0.450	0.322	23.63
79.2	523.3	159.4	24.54	0.4285							242.9	74.1				0.452	0.330	24.09
79.2	527.2	160.8	25.08	0.4380							248.3	75.8				0.454	0.337	24.77
79.3	532.0	162.1	25.59	0.4460							253.5	77.2				0.458	0.345	26.07
03.5	502.1	153.1	42.16	0.7360							558.2	170.0				0.431	0.548	5.30
88.5	564.6	172.0	41.47	0.7230							539.7	164.4				0.484	0.481	8.12
72.5	553.9	168.8	39.60	0.6910							487.0	148.5				0.474	0.462	11.63
14.0	517.6	157.9	37.66	0.6580							428.9	130.7				0.442	0.459	16.01
00.7	403.2	122.9	37.11	0.6480							357.5	109.0				0.344	0.531	25.38

FOLDOUT FRAME 2

PRECEDING PAGE BLANK NOT FILMED.

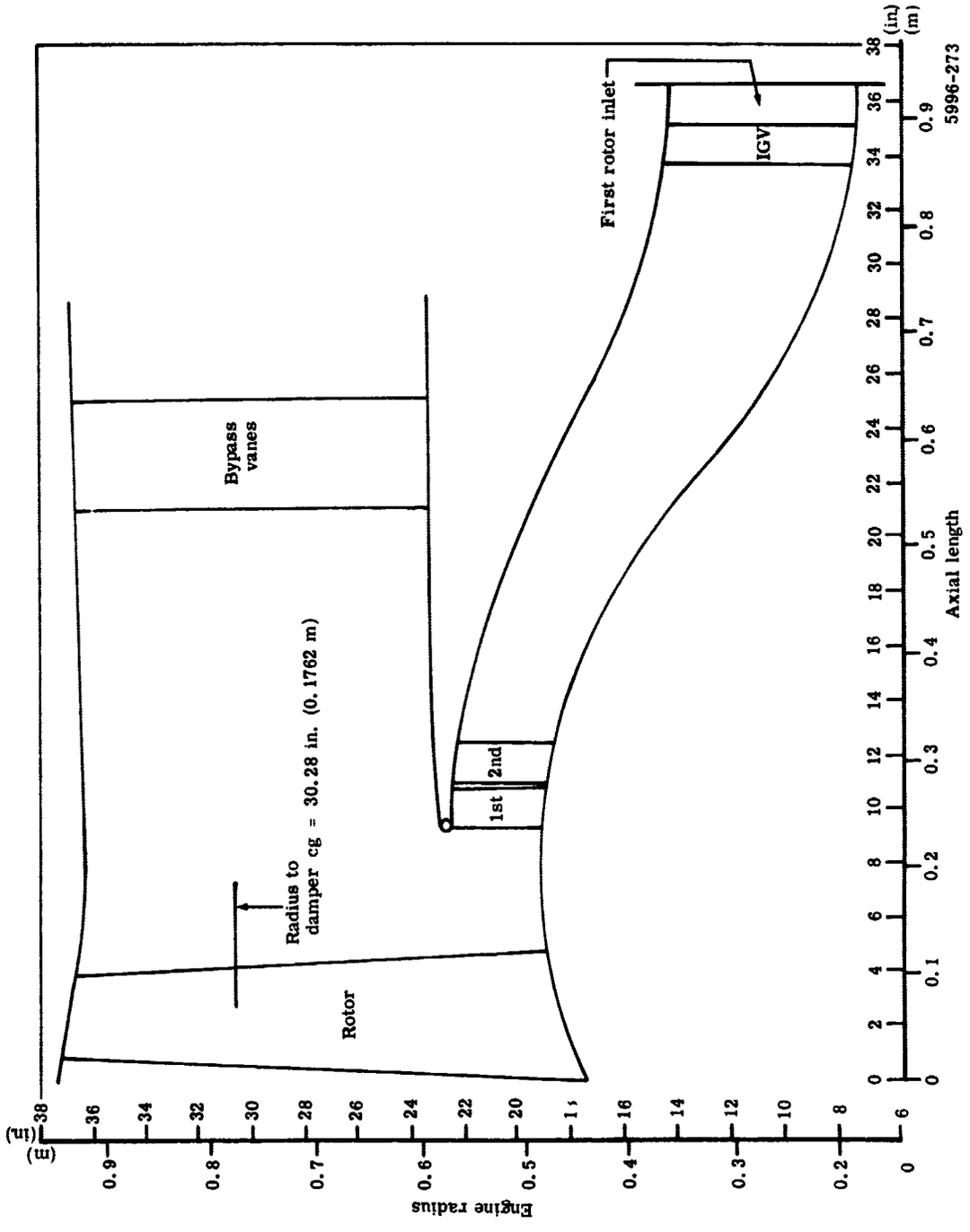

Figure 3d2-2. PD218-Q fan flow path.

by (1) unbolting the aft strut support at the inner diameter and the struts at their forward inner and outer diameters and (2) sliding the strut support and struts aft over the engine. This exposes the bypass stators so that they can be replaced one at a time by sliding them aft out of the fan duct.

There are 50 single-stage fan rotor blades. These blades are 6Al-4V titanium forgings. The airfoil steady-state stresses are as follows:

- Fan speed — 3286 rpm (54.8 rps)
- Metal temperature — 95°F (308°K)
- Airfoil hub stresses
  - Tensile — 22,800 psi (157.2 Mpa)
  - Tensile and bending — 26,000 psi (179.3 Mpa)

The blade is retained in the wheel by means of a single-serration dovetail attachment. The attachment nomenclature is shown in Figure 3d2-8. In addition to the blade load, the attachment system dead weight has been considered in sizing the wheel ring. The fan wheel and integral support hub are 6Al-4V titanium forgings.

The fan blade and wheel attachment stresses are given in Table 3d2-VI.

Table 3d2-VI.
PD218-Q fan blade and wheel attachment stresses.

	Design stress*	
Dovetail	psi	Mpa
Tensile	14,067	97.0
Shear	9,183	63.4
Bearing	29,487	203.5
Tooth bending	12,880	88.7
Tooth bending plus tensile		
100% speed	26,947	186.0
125% speed	42,000	289.5
Wheel		
Tensile	11,497	79.2
Shear	11,554	79.6
Bearing	29,487	203.5
Tooth bending	16,816	116.1
Tooth bending plus tensile		
100% speed	28,313	195.2
125% speed	44,239	305.0

*rpm = 3286 (54.8 rps); temperature = 95°F (308°K).

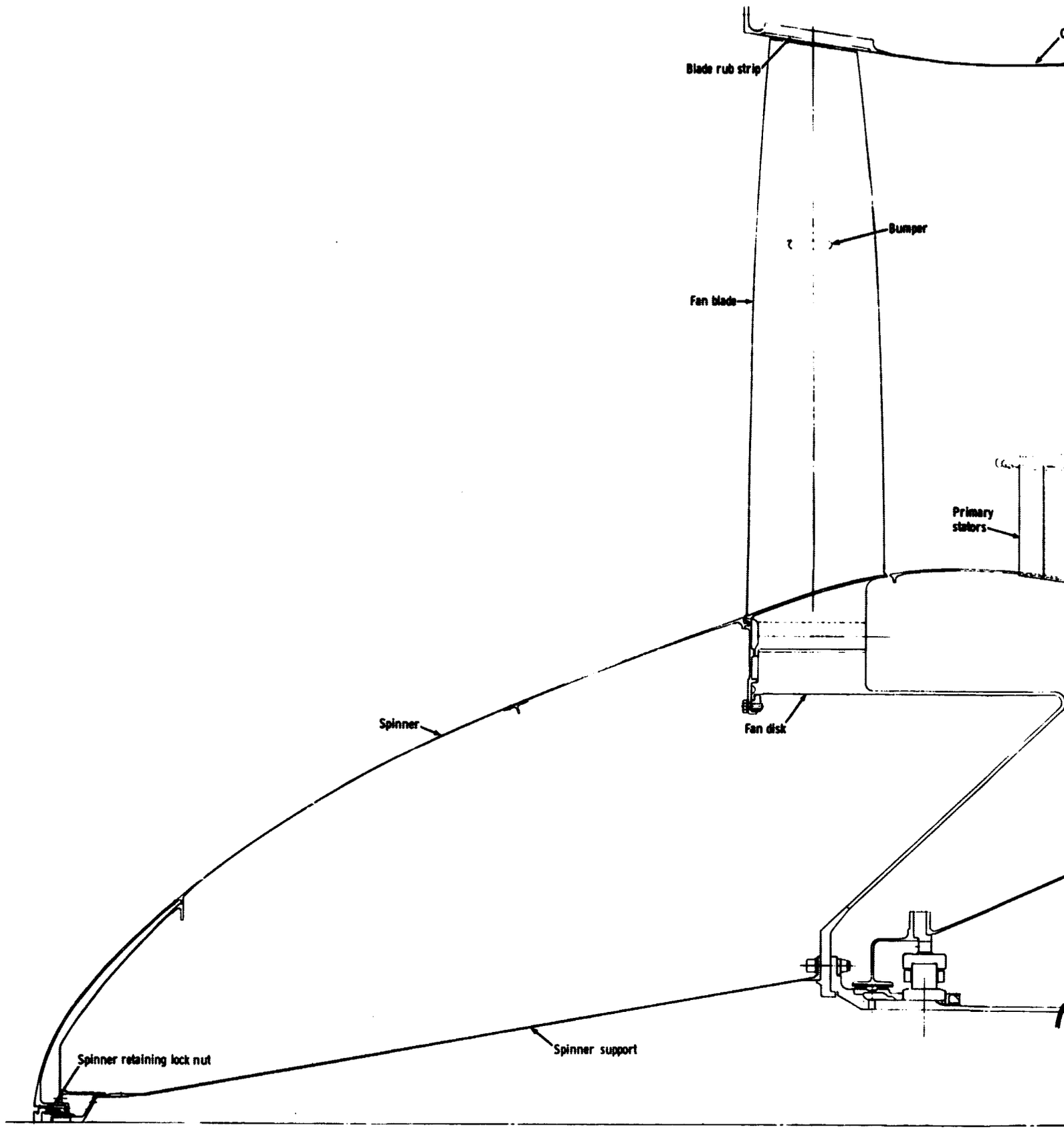

FOLDOUT FRAME 1

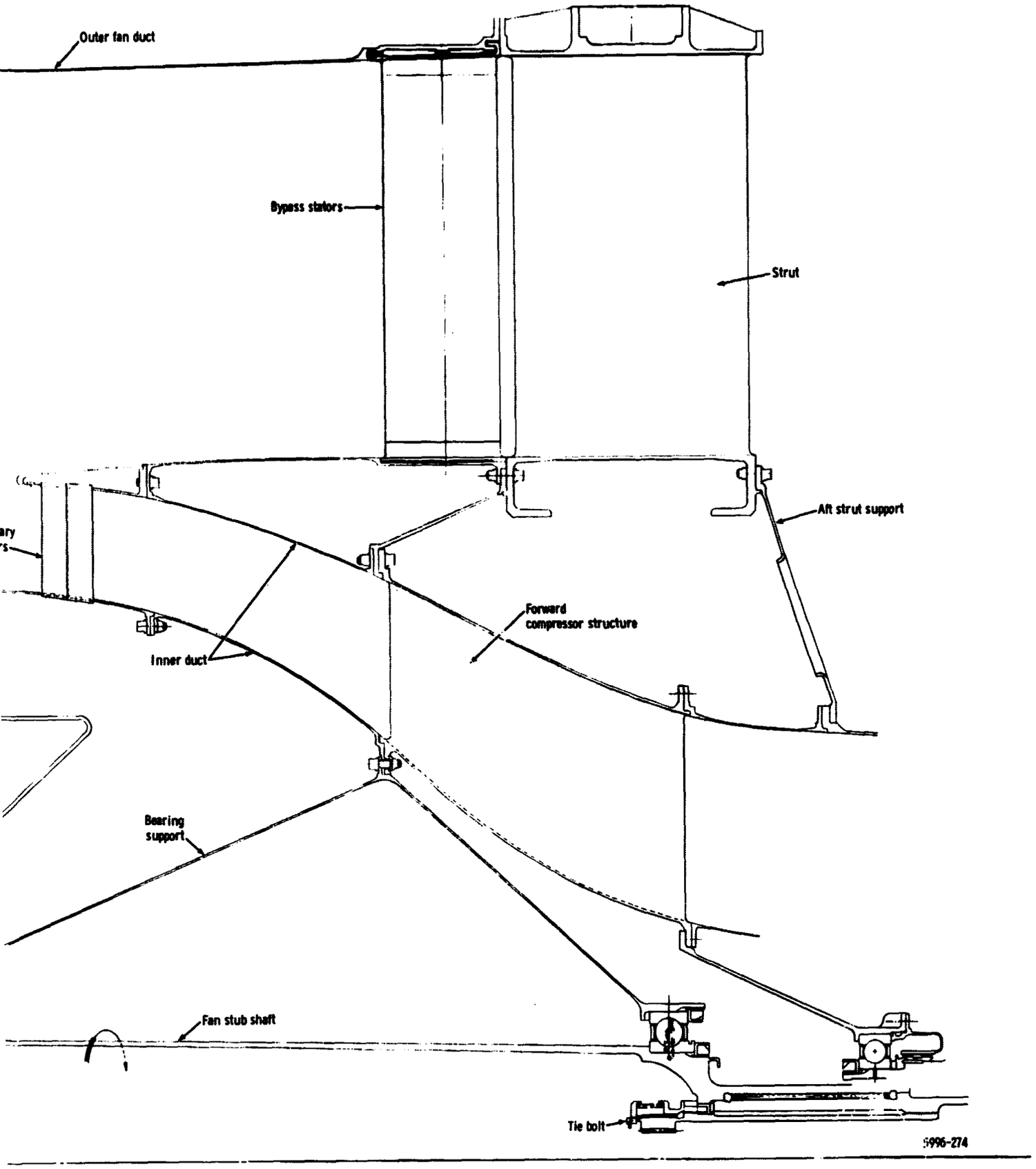

Figure 3d2-3. PD218-Q fan layout drawing.

FOLDOUT FRAME 2

PRECEDING PAGE BLANK NOT FILMED.

POINT J

.2000 R. T

GAGE PLAI

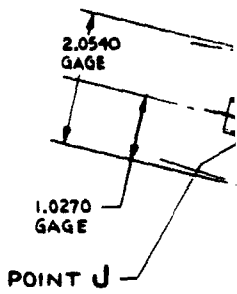

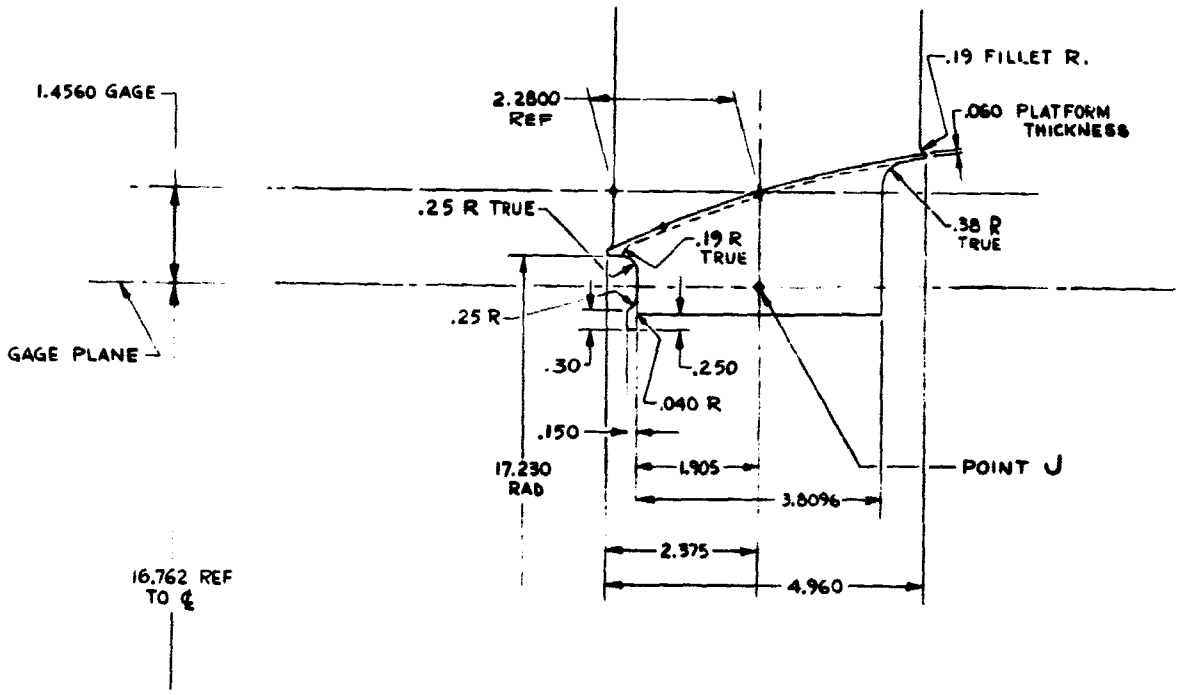

FOLDOUT FRAME 1

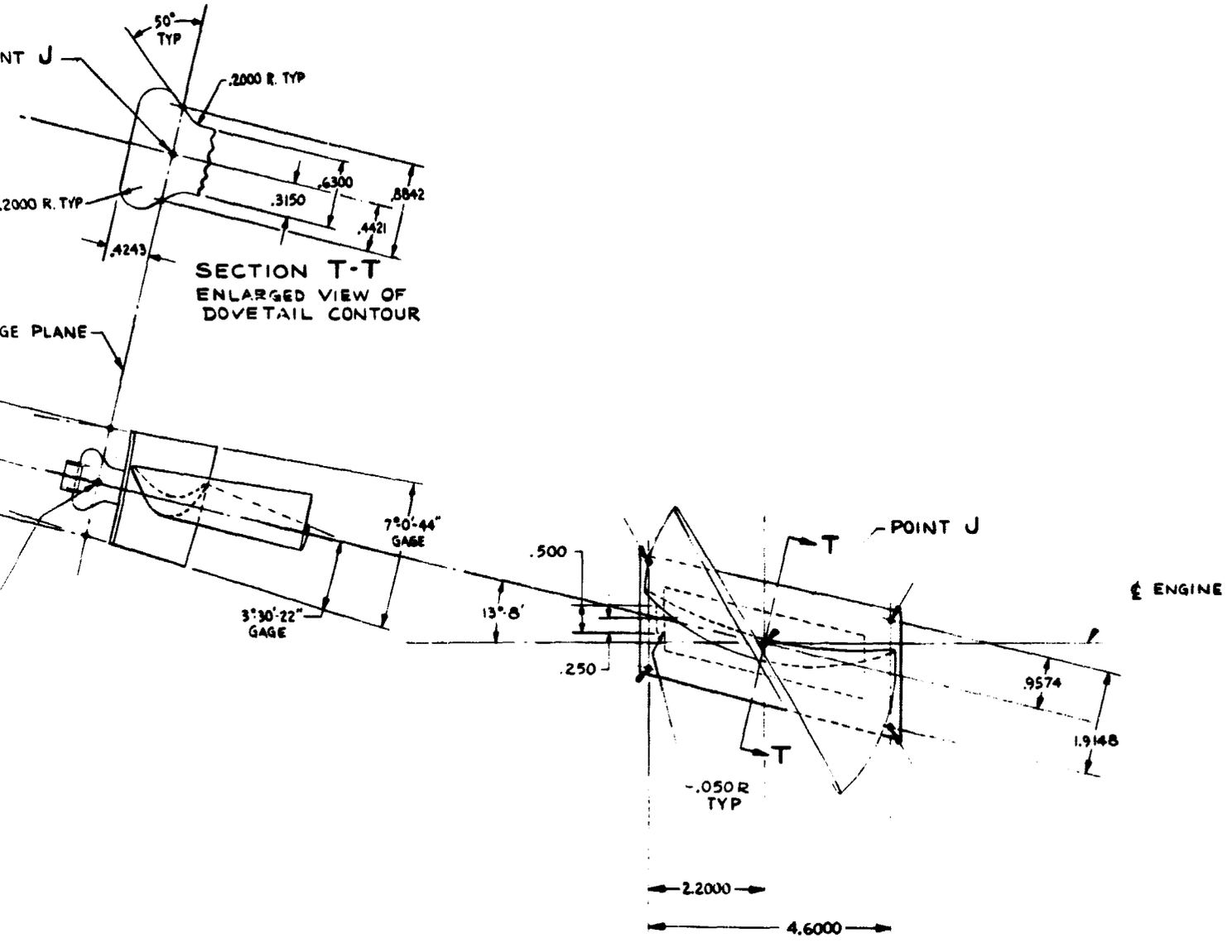

Figure 3d2-4. PD218-Q fan blade details.

FOLDOUT FRAME 2

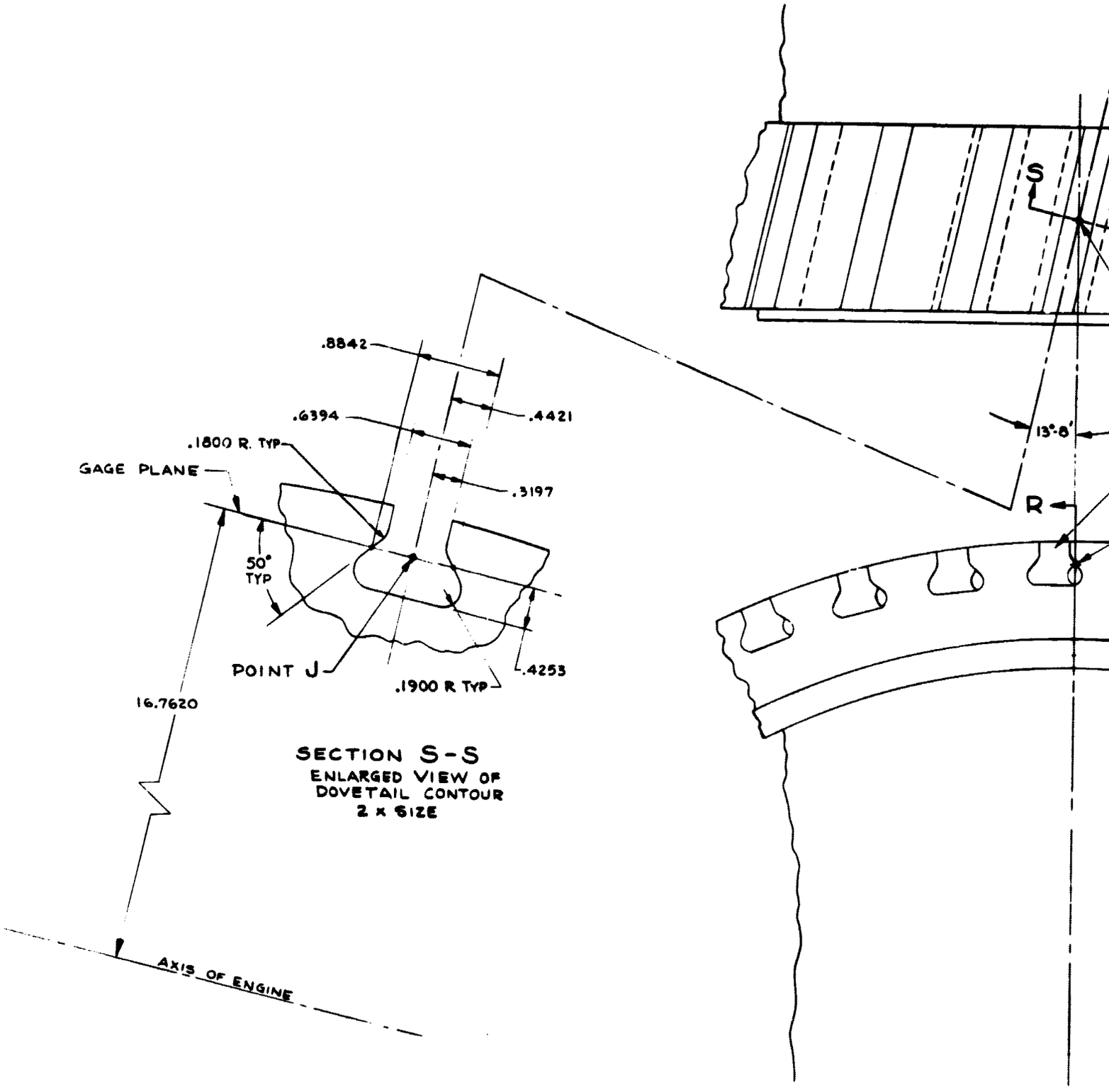

SECTION S-S
ENLARGED VIEW OF
DOVETAIL CONTOUR
2 x SIZE

FOLDOUT FRAME 1

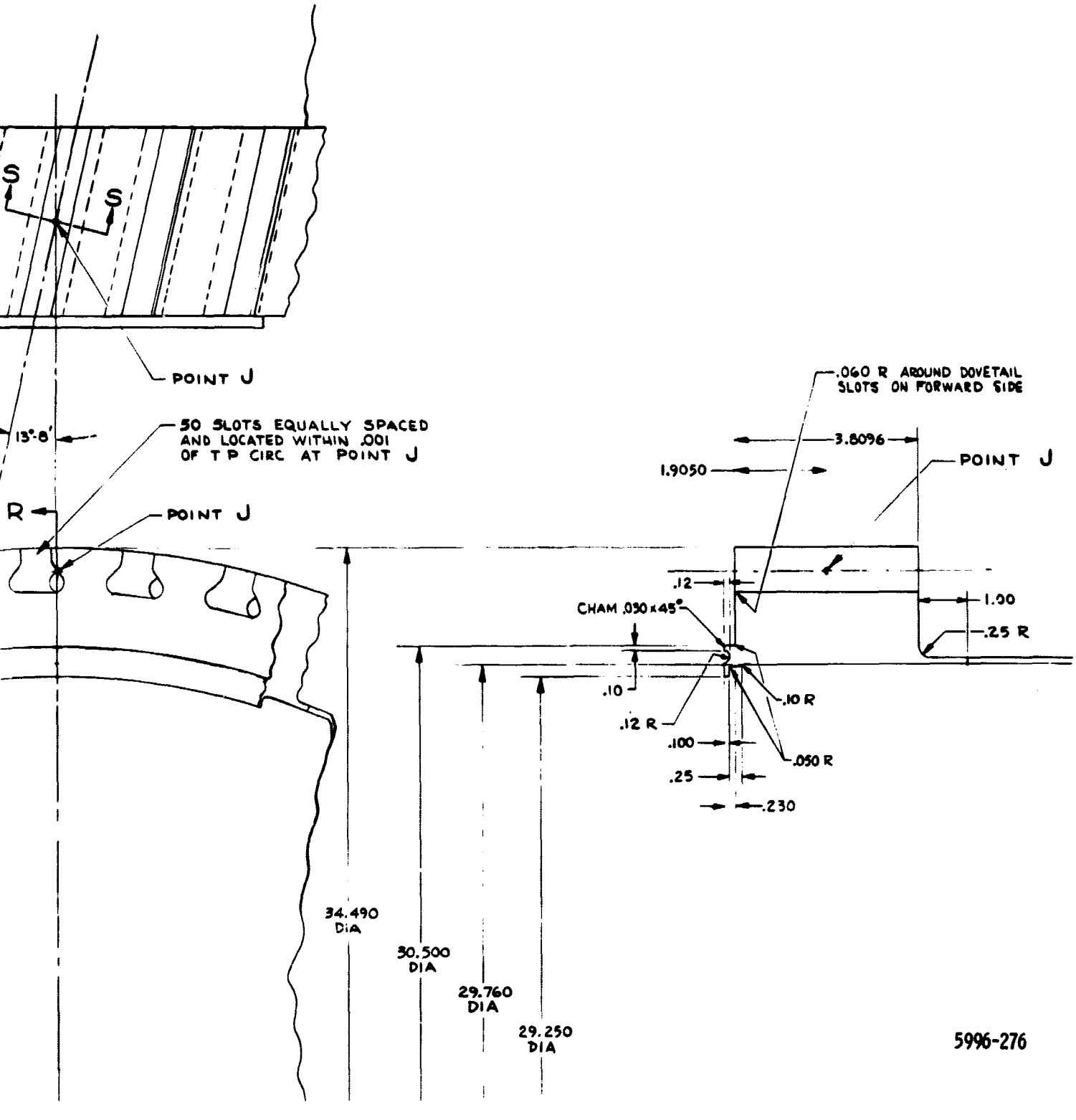

Figure 3d2-5. PD218-Q fan wheel details.

FOLDOUT FRAME 2

PRECEDING PAGE BLANK NOT FILMED.

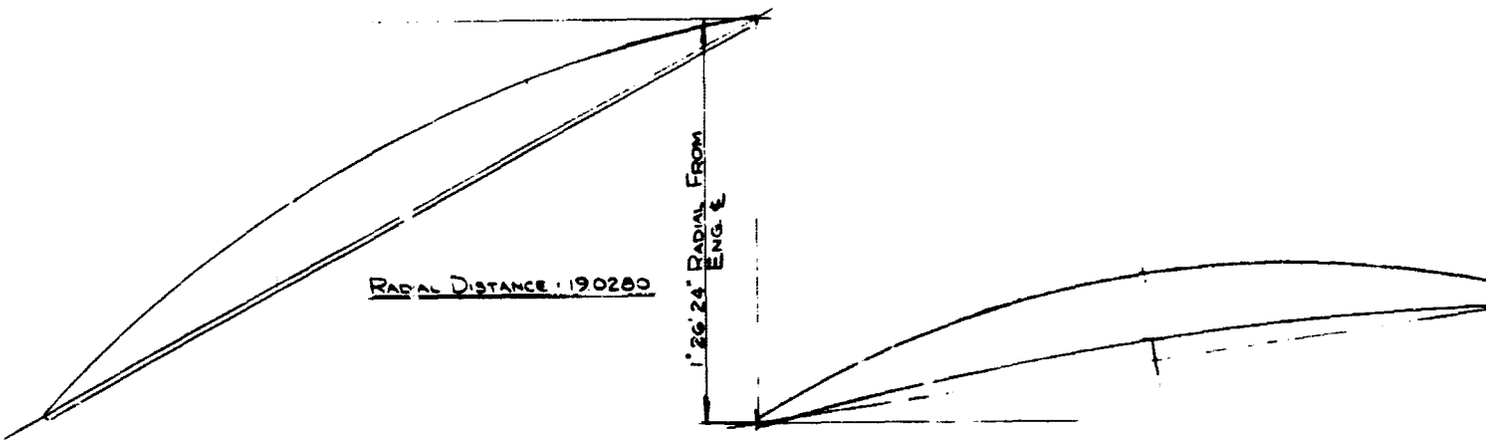

VIEW IN DIRECTION OF ARROW D

SCALE : 10 n SIZE

FOLDOUT FRAME

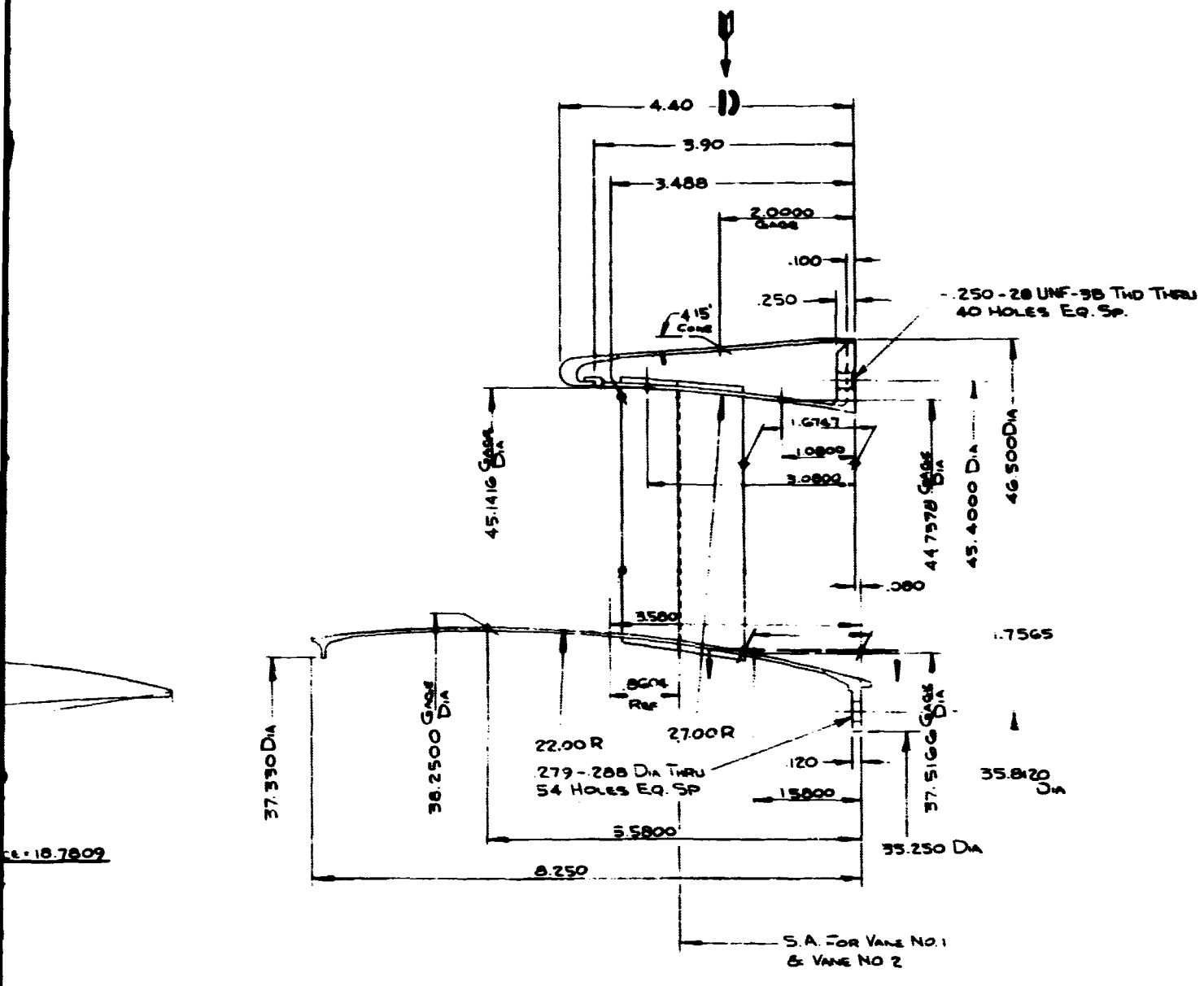

Figure 3d2-6. PD218-Q primary vane details.

FOLDOUT FRAME

PRECEDING PAGE BLANK NOT FILMED.

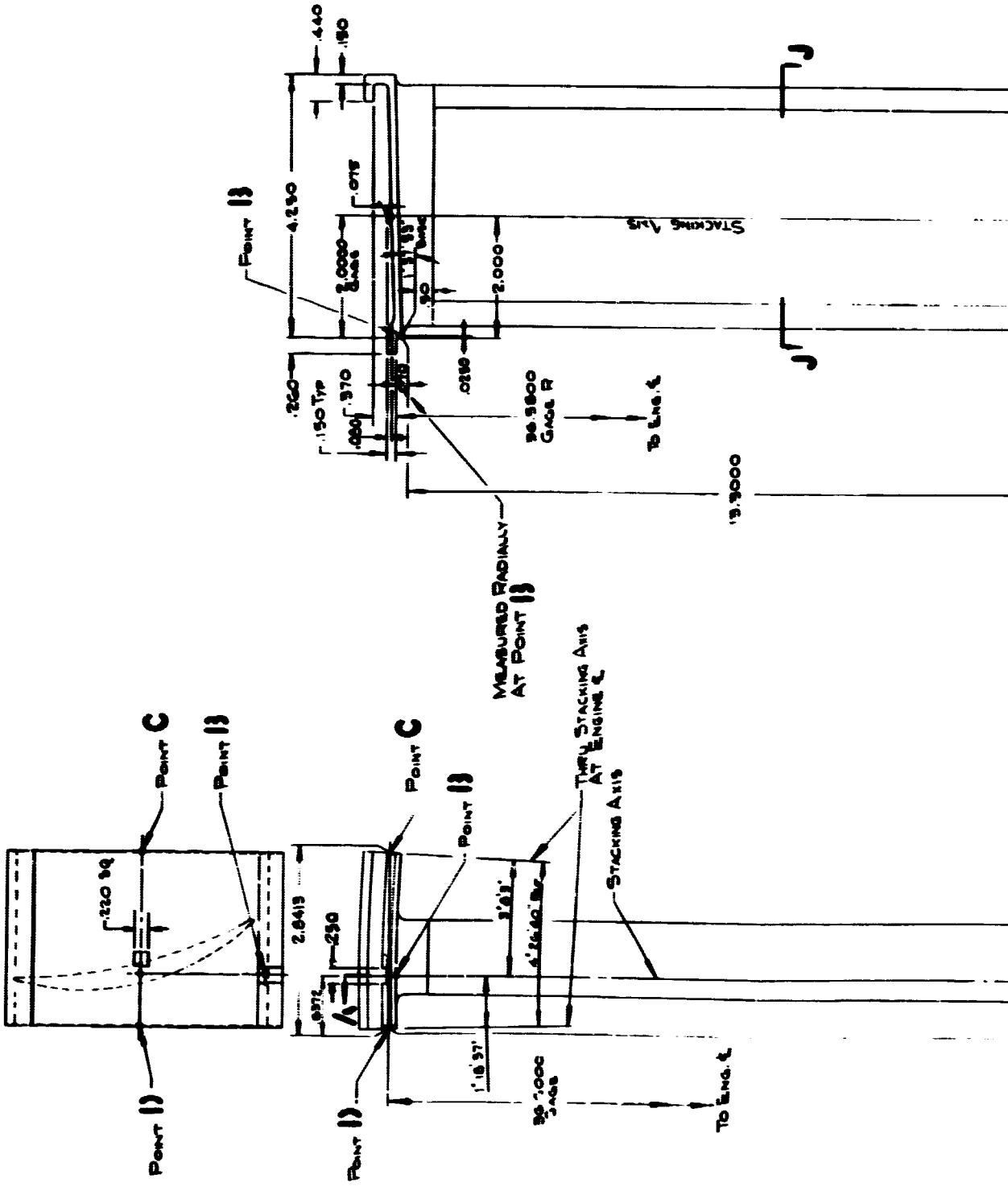

FOLDOUT FRAME 1

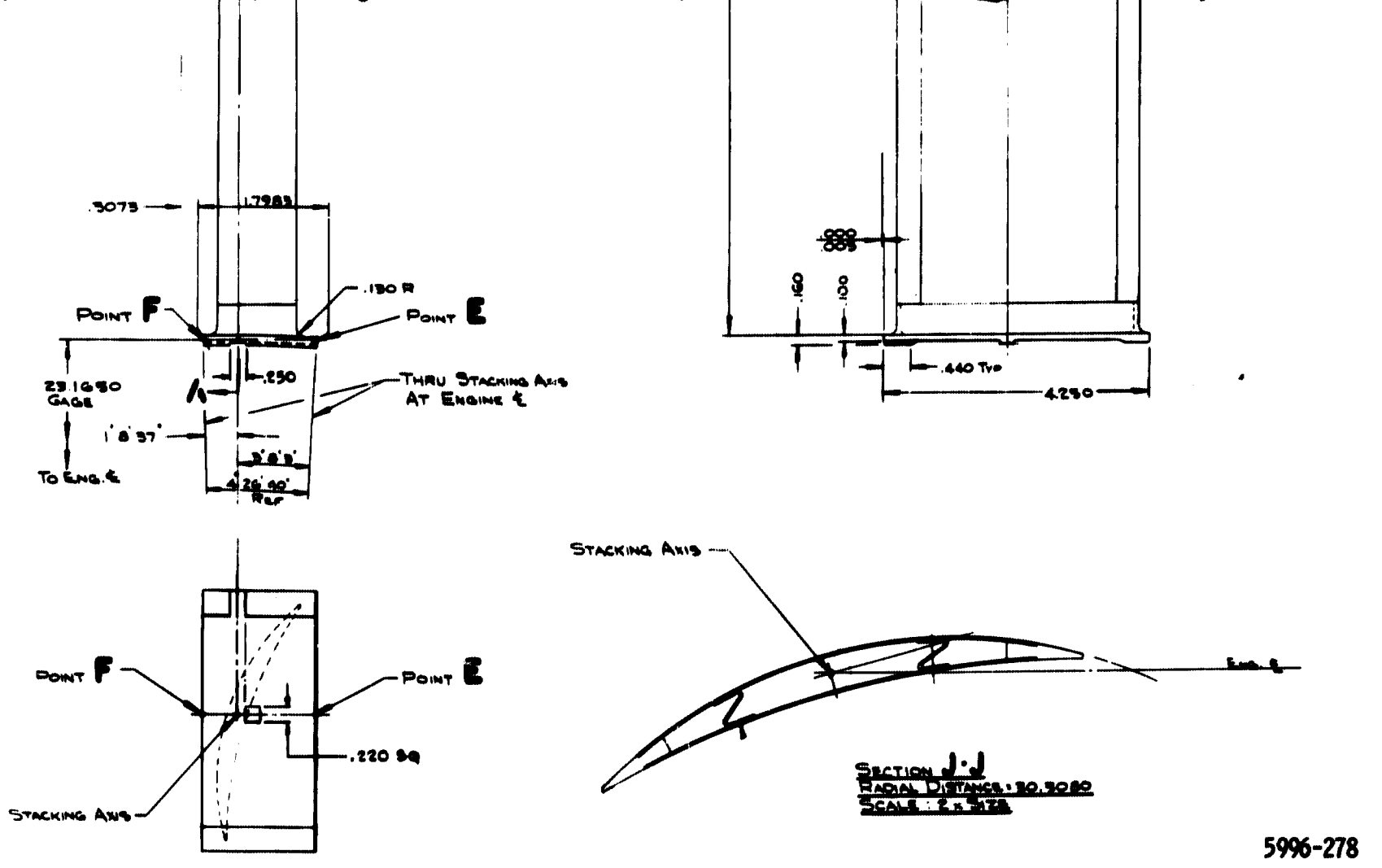

Figure 3d2-7. PD218-Q bypass vane details.

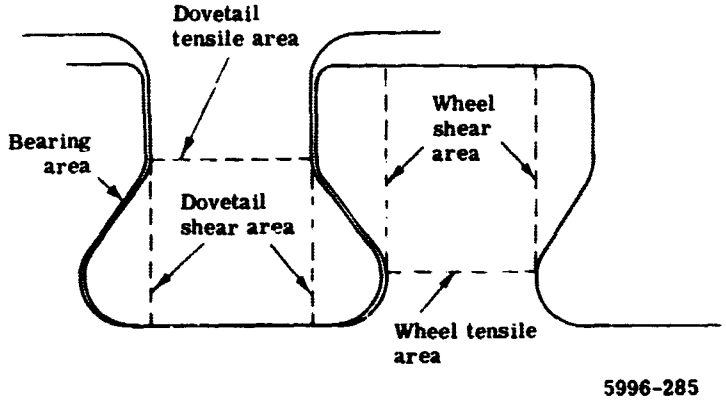

Figure 3d2-8. PD218-Q attachment stress nomenclature.

The fan wheel stresses and growth are as follows:

● Wheel speed	3286 rpm (54.8 rps)
● Metal temperature	100°F (311°K)
● Average tangential stress	68,000 psi (469.0 Mpa)
● Rim radial growth (mechanical and thermal)	0.064 in. (1.636 mm)

The outer fan duct contains a fiber glass stationary blade rub strip and is designed for fan blade containment. Refined empirical relationships have been developed from an appreciable amount of test data which use the energy of the separated airfoil to determine casing thickness. Applications of the containment thickness only apply to an area above the rotor blade. This duct of 7075 aluminum (AMS-4122) requires a minimum containment thickness of 0.323 in. (8.21 mm).

The bypass stator vanes are single vane fabrications made of hollow airfoil sections with internal stiffeners attached to forged inner and outer platforms. The vanes are attached to the outer fan casing at their OD and are supported on the ID by the inner bypass duct wall. A tangential load stop is provided at both the inner and outer platforms. See Figure 3d2-7.

The primary stator vanes are solid airfoils attached rigidly at the ID and OD to full 360-degree inner and outer bands. See Figure 3d2-6.

The bypass vane maximum gas bending stresses are as follows (81 vanes):

- Leading edge 24,507 psi (169.0 Mpa)
- Crown 15,102 psi (104.1 Mpa)
- Trailing edge 24,507 psi (169.0 Mpa)

The primary vane maximum gas bending stresses are as follows:

	Primary 1 (125 vanes)	Primary 2 (125 vanes)
Leading edge	16,600 psi (114.4 Mpa)	13,050 psi (90.0 Mpa)
Crown	23,800 psi (164.0 Mpa)	14,080 psi (97.0 Mpa)
Trailing edge	16,600 psi (114.4 Mpa)	13,050 psi (90.0 Mpa)

The materials selected for the fan section are listed in Table 3d2-VII.

Table 3d2-VII.
PD218-Q fan section materials list.

Item	Material	Specification
Fan blade	6Al-4V titanium	AMS-4967
Fan disk	6Al-4V titanium	AMS-4967
Fan stub shaft	6Al-4V titanium	AMS-4967
Spinner	7075 aluminum	AMS-4122
Spinner support	6061 aluminum	AMS-4025
Forward outer fan duct	7075 aluminum	AMS-4122
Fan EGV's	6Al-4V titanium	AMS-4967
Rear inner and outer duct	6Al-4V titanium	AMS-4967

Aeroelastic Study

A major consideration in the design of the quiet engine fan stage was the vibration and flutter characteristics of the fan blade. A bumpered blade configuration was selected which provided freedom from potentially damaging engine order resonances as well as substantial margins for both stalled and unstalled flutter. As shown in Figure 3d2-9, the lowest vibrational mode falls above fourth order at design speed, and no significant modal coincidence exists within the proposed operational range. The bypass vanes are placed sufficiently aft of the rotor blade so that they do not constitute an appreciable source of excitation for the high frequency, compiex blade modes that occasionally fall in the range of vane passage frequencies. The stalled flutter analysis results are shown in Figure 3d2-10. This graph shows the

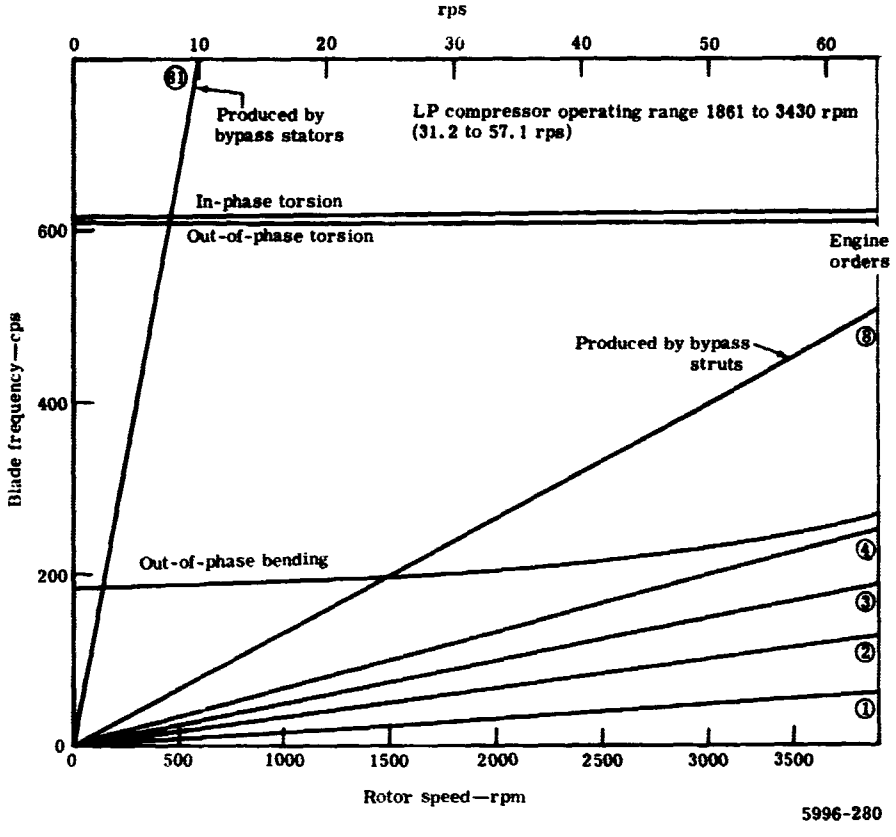

Figure 3d2-9. PD218-Q fan blade frequency versus rotor speed.

anticipated surge line characteristics of the blade and the boundary for stalled flutter in terms of incidence versus relative velocity. It can be seen that there is a very good margin between the surge line (which represents the highest blade operating incidence regime) and the minimum incidence angles required to produce torsional flutter. The flutter analysis also shows that there is over 100% margin for unstalled (low incidence) flutter.

The decision to incorporate bumpers on the fan blade was made after a careful study of the objectives of the quiet engine design. Several unbumpered configurations with varying T/C and aspect ratios were investigated. The results of this investigation showed that the basic airfoil constitutes a relatively conservative design, from the standpoint of blade dynamics, with adequate flutter margins in the unbumpered configuration. Each configuration did, however, have a coincidence of the first bending mode with the second order at the lower end of the fan operating speed range. At this low speed the blade loadings are reduced and the vibratory response is expected to be low. However, the increased reliability provided by the bumpers helps to ensure that the engine will operate satisfactorily with only minimum blade development effort. The feasibility of removing the bumper in a later version of the engine can be evaluated on the basis of experience gained during development testing.

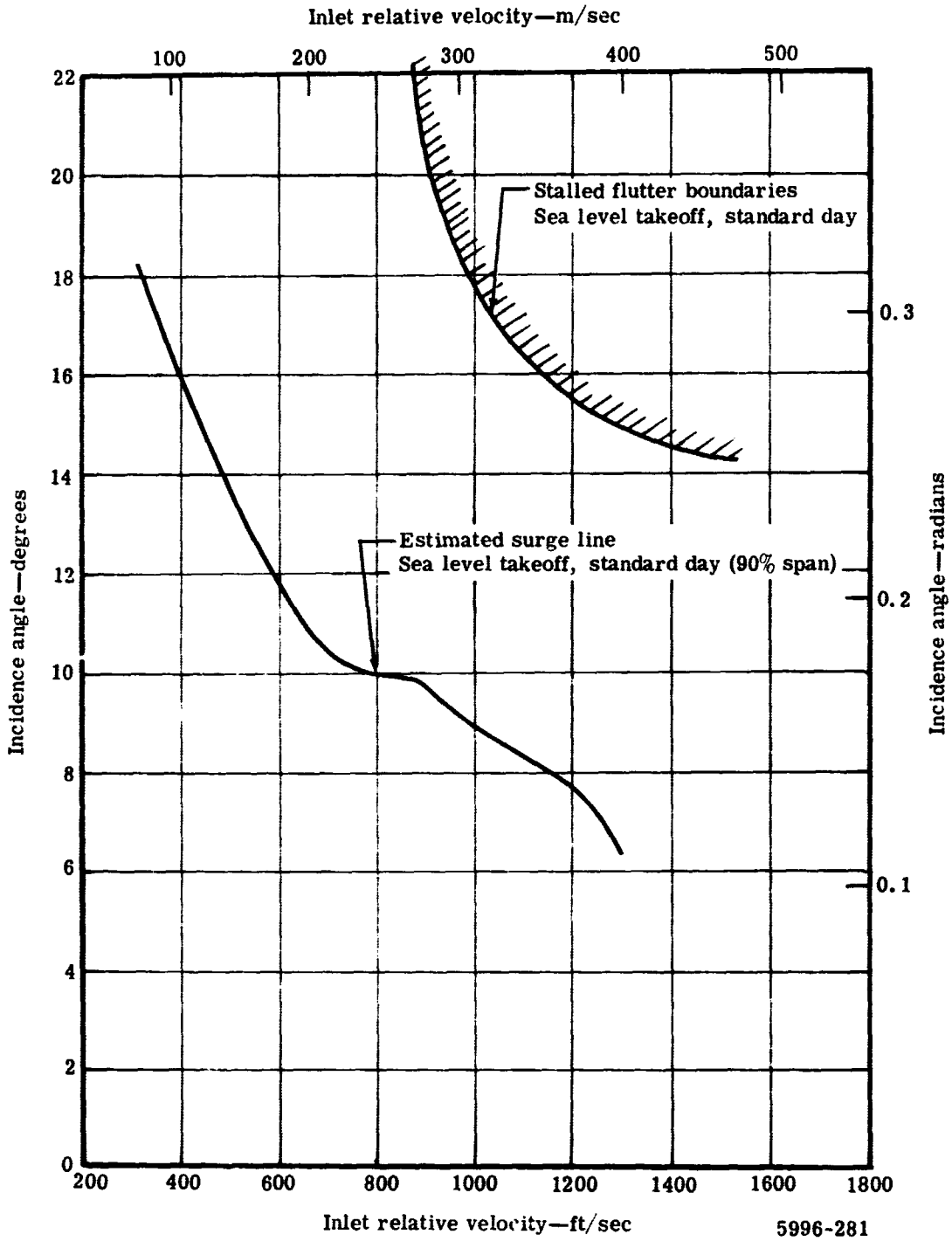

Figure 3d2-10. PD218-Q fan blade incidence angle versus inlet relative velocity.

The fan bypass and inner exit stator vanes are designed so that their lowest natural frequencies are well above the range of rotor unbalance excitations. Both stator vanes are completely stable with respect to flutter.

Several configurations of primary exit stator vanes with various chord lengths were investigated in an effort to find a configuration acceptable from both vibration and aerodynamic standpoints. A configuration which incorporates 125 vanes in each of the double-row exit stators was selected. This put coincidence of the vane fundamental modes with first and second engine order lines well out of the engine operating range. A frequency versus speed plot is shown in Figures 3d2-11 and 3d2-12 for the primary exit stators.

Both solid and hollow airfoil configurations were investigated for the bypass stator vanes. The hollow vane configuration was selected because of its inherent weight saving. Figure 3d2-13 indicates that there is a second bending and fiftieth engine order coincidence at 2100 rpm (35 rps). It is felt that this problem should be insignificant due to the low air velocities created at this low engine speed and the large separation of the bypass stators from the fan. In addition, the analysis assumes the bypass stators to be fixed-fixed while they probably approach a condition somewhere between fixed-fixed and fixed-pinned, thus making the analysis somewhat conservative. If testing of the engine shows that the vibrational stresses in the hollow bypass stators are excessive, the problem can be eliminated by changing to a solid airfoil which has no coincidence problem.

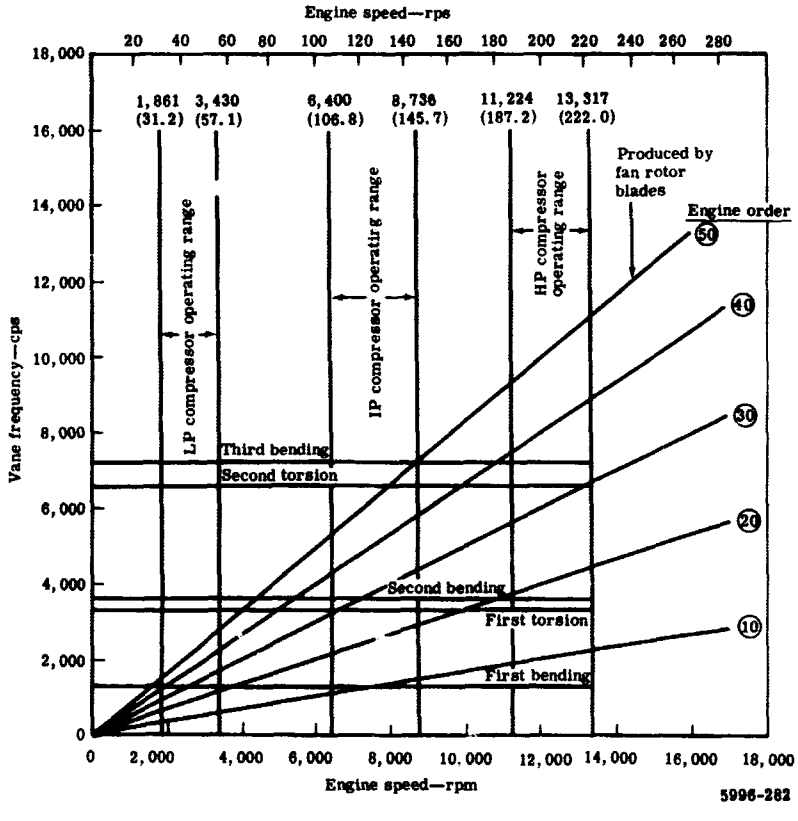

Figure 3d2-11. Frequency versus engine speed data for PD218-Q primary exit stator 1.

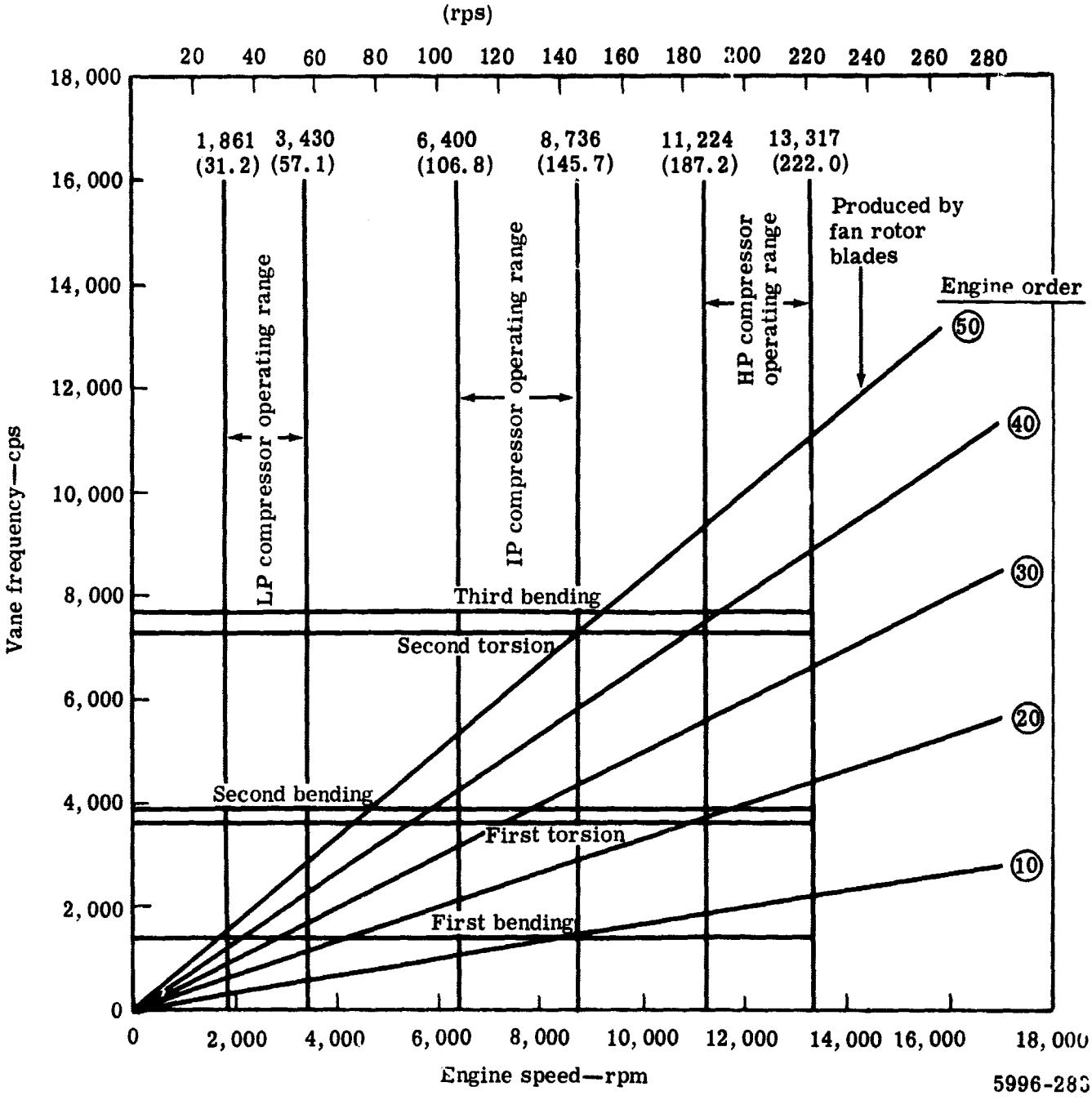

Figure 3d2-12. Frequency versus engine speed data for PD218-Q primary exit stator 2.

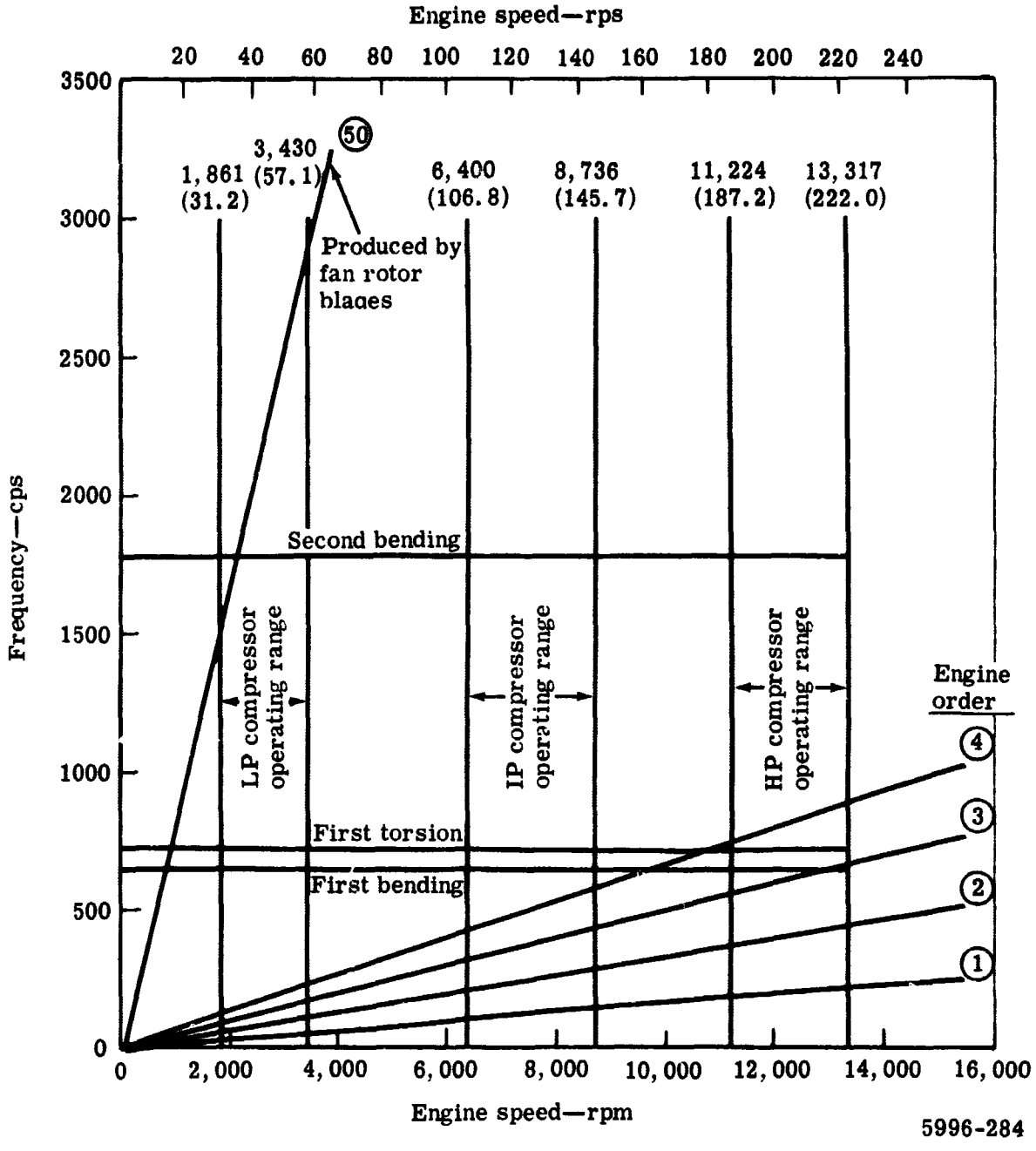

Figure 3d2-13. Frequency versus engine speed data for PD218-Q bypass stator vanes.

3d3. COMPRESSOR

Aerodynamic Design

General

The engine has two multistage compressors—an intermediate pressure (IP) compressor and a high pressure (HP) compressor. Each compressor has eight stages and is designed for a pressure ratio of 4.08:1 at the altitude cruise condition which is the design point. Both compressors have been designed using proven techniques and keeping design parameters within the range based on experience. This has been done to eliminate a costly and time consuming development program for these units.

Noise and mechanical design requirements were considered in the aerodynamic design. Bearing DN limitations were considered in choosing the HP compressor speed and H/T radius ratio.

IP Compressor

The IP compressor is designed for a corrected flow of 106.1 lb/sec (48.13 kg/sec) at a pressure ratio of 4.08:1. The corrected rotational speed of the eight-stage unit is 8520 rpm (142 rps) which produces an inlet stage corrected rotor tip speed of 1049 fps (319.7 mps). The overall design values are summarized in Table 3d3-I.

Table 3d3-I.
PD218-Q IP compressor design values.

Corrected airflow	106.1 lb/sec (48.13 kg/sec)
Pressure ratio	4.08
Corrected speed	8520 rpm (142 rps)
Inlet pressure	7.80 psia (53.781 kpa)
Inlet temperature	45°F (278.6°K)
Corrected specific inlet flow	32.7 lb/sec/ft^2 (159.6 kg/sec-m^2)
First rotor corrected inlet tip speed	1049 fps (319.7 m/sec)
Inlet annulus area	3.246 ft^2 (0.299 m^2)
Inlet tip diameter	28.22 in. (0.717 m)
First rotor inlet H/T radius ratio	0.502
Number of stages	8

Noise output of the IP compressor is a significant factor in the total engine noise level and care was taken to minimize the noise generation characteristics, particularly in the first stage. Also, rotor and stator inlet relative Mach numbers are major noise parameters and were minimized. In finalizing the design, the following variations were studied:

- Varying the level of prewhirl
- Reducing the annulus flow rate
- Reducing wheel speed
- Reducing the inlet stage temperature rise

The effect of these parameters is given in Table 3d3-II.

Varying the amount of prewhirl to the first rotor indicated that minimum noise generation is obtained at approximately 60% reaction. With less prewhirl, the rotor tip Mach number is predominant and causes the noise level to be higher. As the prewhirl is increased, the rotor incidence level is increased at off-design conditions.

At levels of prewhirl greater than that at 60% reaction, the incidence effects more than offset the reduced rotor relative Mach number, and the noise output is increased as indicated by comparing the first two columns of Table 3d3-II.

Decreasing the annulus specific flow produced the most significant reduction in total forward noise of the three variables analyzed. Reducing the flow rate from 37.7 to 32.7 lb/sec/ft^2 (184 to 159.6 kg/sec-m^2) produced a predicted reduction of 1 db in the total forward noise. Velocities relative to both the rotor and stator were reduced by this change and rotor incidence was decreased slightly as indicated in Table 3d3-II. Blade row turning was increased by this change but was still within acceptable limits.

A reduction in noise output could be realized by operating the intermediate compressor at lower rotational speed. As rotor inlet tip speed was reduced from 1050 to 948 fps (320 to 288.9 mps), total forward fan noise was reduced approximately 0.5 db; however, stage aerodynamic loading became excessive and would have required extra stages at the lower wheel speed. Therefore, it was determined that the inlet tip speed of 1050 fps (320 mps) represented a more favorable compromise between noise considerations and overall engine size and weight.

The final parameter studied was inlet stage work level. Since the first stage of the IP compressor is the primary source of forward radiated noise from the IP compressor, the loading of this stage was reduced by transferring some of its temperature rise to the later stages. The calculations indicated insignificant changes in velocities and incidence angles and, therefore, noise output.

This parametric study corroborated the initial selection of rotor inlet prewhirl, but indicated that a change in specific flow was advisable. This change has been incorporated in the final design. An increase in rotor inlet tip radius of approximately 0.7 in. (17.8 mm) was required to provide the increased area. Hub radius was not decreased; a decrease would have required an increase in length of the transition duct between the fan and IP compressor.

Further consideration of noise characteristics is reflected in axial separation of the IGV, first rotor, and first stator. The axial spacing between the IGV and first rotor is equal to one axial hub projected chord of the IGV, and the space between the first rotor and stator is equal to one axial hub projected chord of the first rotor blade. This spacing reduces the compressor discrete noise.

The IP compressor estimated performance map is shown in Figure 3d3-1. Stage design parameters for the IP compressor are given in Table 3d3-III. The vector diagram data are given in Table 3d3-IV. Blading data are given in Table 3d3-V.

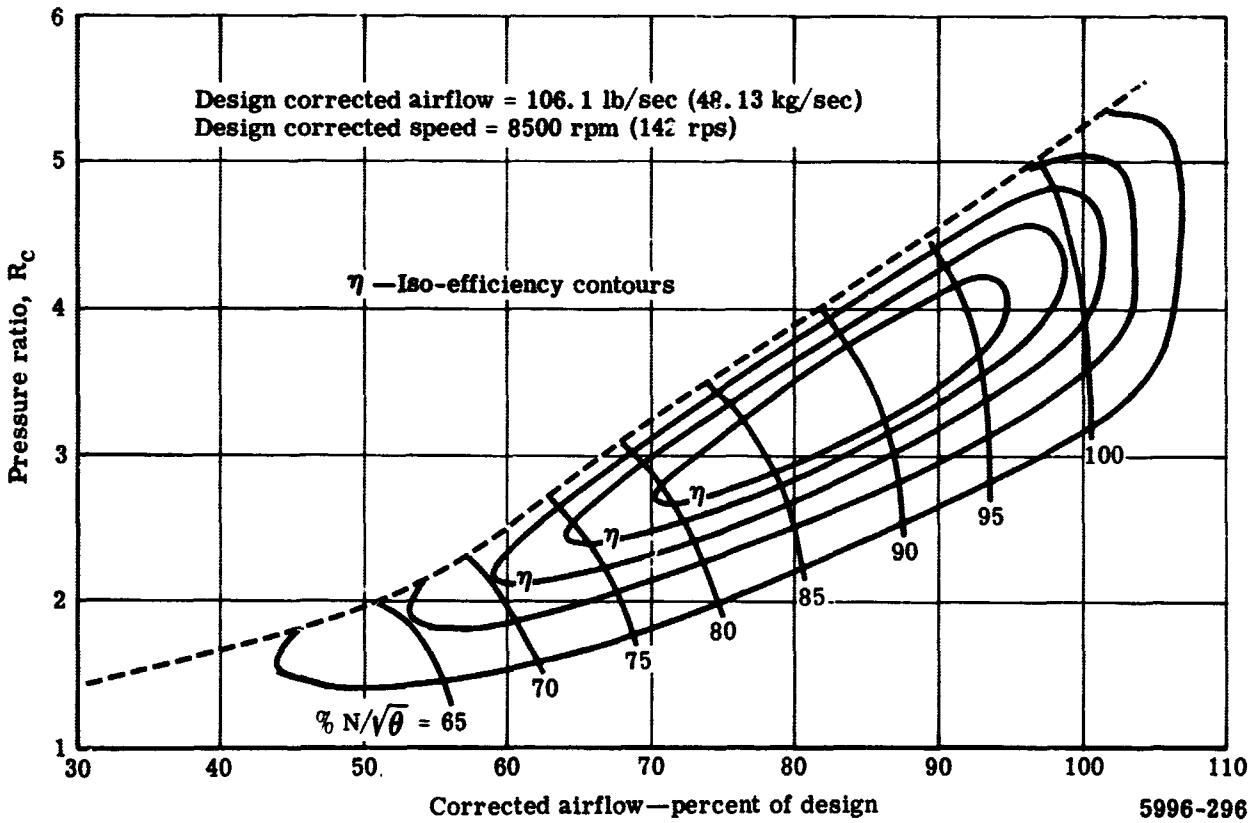

Figure 3d3-1. PD218-Q IP compressor estimated performance.

Table 3d3-III.

PD218-Q IP compressor stage design parameters.

Stage	Temp rise, ΔT_T, °F (°K)	Pressure ratio, R_S	Work factor, W_f	Diffusion factor		Rotor choke margin (%)	Stator choke margin (%)	Hub-to-tip dia ratio, D_H/D_T	Whirl change to axial velocity ratio at hub $(\Delta C_u/V_a)_H$
				Rotor tip, D_f	Stator hub, D_f				
1	27.6 (15.3)	1.178	0.95	0.265	0.289	0.128	0.154	0.502	0.681
2	32.4 (18)	1.200	0.90	0.323	0.383	0.113	0.132	0.569	0.677
3	36.1 (20)	1.210	0.85	0.346	0.394	0.105	0.112	0.614	0.746
4	38.0 (21.1)	1.208	0.85	0.357	0.395	0.116	0.123	0.653	0.745
5	39.6 (22)	1.203	0.85	0.368	0.400	0.107	0.111	0.690	0.745
6	40.8 (22.6)	1.197	0.85	0.373	0.299	0.118	0.138	0.724	0.745
7	42.1 (23.4)	1.192	0.85	0.398	0.425	0.132	0.129	0.754	0.745
8	39.3 (21.8)	1.168	0.85	0.429	—	0.164	0.188	0.773	0.719

Table 3d3-IV.

PD218-Q IP compressor vector diagram data.

	R_1		U_1		V_{z_1}		α_1		α'_1		M'_{n_1}	V_{z_2}		α_2		α'_2		M_{n_2}
	in.	mm	fps	mps	fps	mps	deg	rad	deg	rad		fps	mps	deg	rad	deg	rad	
First stage																		
Hub	7.10	180	527	160.8	486	148.5	5.36	0.094	44.75	0.781	0.625	495	151	37.30	0.652	16.90	0.2955	0.459
Mean	10.61	270	788	240.2	486	148.5	22.81	0.40	50.21	0.877	0.696	495	151	40.70	0.712	36.20	0.632	0.546
Tip	14.11	135.9	1049	319.7	486	148.5	34.63	0.606	55.71	0.974	0.796	495	151	45.40	0.783	47.90	0.836	0.642
Second stage																		
Hub	7.47	190	555	169.2	576	176	8.19	0.143	39.39	0.687	0.668	586	178	38.92	0.68	8.01	0.1401	0.666
Mean	10.31	262	766	233.6	576	176	22.75	0.397	42.34	0.74	0.701	586	178	41.84	0.731	22.40	0.3915	0.663
Tip	13.15	334	977	298	576	176	33.24	0.581	46.14	0.806	0.753	586	178	45.65	0.798	32.77	0.572	0.750
Third stage																		
Hub	7.73	196	575	175.2	596	182	6.16	0.1078	40.54	0.71	0.683	604	188	40.17	0.703	6.14	0.1071	0.680
Mean	10.15	258	755	230	596	182	19.24	0.336	42.55	0.745	0.707	604	188	42.17	0.738	19.09	0.3335	0.690
Tip	12.60	320	937	286	596	182	29.10	0.508	45.40	0.783	0.746	604	188	45.06	0.797	28.79	0.502	0.741
Fourth stage																		
Hub	7.95	202	591	180	611	186.5	6.34	0.1108	40.60	0.71	0.680	613	187	40.25	0.791	6.29	0.1099	0.676
Mean	10.07	256	748	228	611	186.5	17.56	0.3065	42.23	0.738	0.699	613	187	41.84	0.73	17.42	0.3042	0.684
Tip	12.19	310	904	275.5	611	186.5	26.35	0.460	44.54	0.78	0.729	613	187	44.18	0.771	26.11	0.456	0.724
Fifth stage																		
Hub	8.11	206	603	184	626	191	6.25	0.1091	40.52	0.71	0.675	630	192	40.36	0.705	6.17	0.108	0.669
Mean	9.93	252	737	225	626	191	15.93	0.2785	41.81	0.73	0.690	630	192	41.64	0.728	15.83	0.2765	0.676
Tip	11.75	298	873	266	626	191	23.77	0.415	43.76	0.765	0.713	630	192	43.52	0.761	23.65	0.414	0.706
Sixth stage																		
Hub	8.28	21	615	187.5	633	193	6.47	0.1112	40.65	0.711	0.664	638	194.5	40.44	0.706	6.39	0.1118	0.660
Mean	9.87	249.7	733	223.5	633	193	14.90	0.260	41.73	0.729	0.676	638	194.5	41.51	0.726	14.78	0.258	0.666
Tip	11.45	291	851	260	633	193	21.91	0.383	43.28	0.756	0.699	638	194.5	43.05	0.753	21.76	0.38	0.689
Seventh stage																		
Hub	8.44	214	626	192	643	196	6.51	0.114	40.72	0.712	0.656	629	191.8	41.29	0.721	6.69	0.1169	0.640
Mean	9.82	249.6	729	222	643	196	13.87	0.242	41.59	0.728	0.666	629	191.8	42.20	0.737	14.13	0.2465	0.655
Tip	11.20	284	832	254	643	196	20.10	0.3515	42.86	0.748	0.681	629	191.8	43.46	0.758	20.49	0.358	0.664
Eighth stage																		
Hub	8.54	216	634	196	616	188	8.82	0.154	41.20	0.72	0.615	578	176	43.00	0.751	9.42	0.1648	0.585
Mean	9.81	249.5	728	222	616	188	15.52	0.2716	42.14	0 736	0.624	578	176	43.97	0.768	16.48	0.288	0.626
Tip	11.07	281	823	251	616	188	21.26	0.372	43.39	0.757	0.638	578	176	45.20	0.790	22.56	0.394	0.609

Symbols

R—radius
U—wheel speed
V_z—axial velocity
α—absolute air angle
α'—relative air angle
M'_n—relative Mach number
M—absolute Mach number

Subscripts

1—inlet
2—exit

Table 3d3-V.

PD218-Q IP compressor blading data.

Blade row	Radius in.	Radius mm	Camber deg	Camber rad	Setting deg	Setting rad	Solidity	Chord in.	Chord mm	No. of airfoils
IGV										53
Hub	7.09	180	6.19	0.108	3.09	0.0526	1.66	1.503	38.2	
Mean	11.49	282	27.40	0.478	13.70	0.249	1.02	1.503	38.2	
Tip	14.75	375	43.00	0.751	21.50	0.376	0.80	1.503	38.2	
Rotor 1										25
Hub	7.09	180	35.42	0.619	27.03	0.472	1.58	2.816	71.5	
Mean	10.60	270	20.00	0.35	40.20	0.701	1.06	2.816	71.5	
Tip	14.11	359	12.45	0.2176	49.48	0.864	0.79	2.816	71.5	
Stator 1										32
Hub	7.31	186	33.55	0.585	17.08	0.298	1.38	2.004	50.9	
Mean	10.38	264	20.34	0.354	27.48	0.48	0.97	2.004	50.9	
Tip	13.42	342	12.59	0.22	36.16	0.631	0.75	2.004	50.9	
Rotor 2										31
Hub	7.47	190	39.45	0.689	19.69	0.343	1.46	2.233	56.7	
Mean	10.31	262	27.21	0.476	28.73	0.502	1.06	2.233	56.7	
Tip	13.15	334	19.80	0.346	36.24	0.634	0.83	2.233	56.7	
Stator 2										40
Hub	7.62	194	41.67	0.728	18.17	0.317	1.51	1.794	45.6	
Mean	10.24	260	29.76	0.519	26.92	0.47	1.12	1.794	45.6	
Tip	12.85	326	21.84	0.382	34.28	0.599	0.90	1.794	45.6	
Rotor 3										41
Hub	7.73	196	42.34	0.74	19.37	0.338	1.67	1.960	49.8	
Mean	10.15	258	30.78	0.536	27.16	0.474	1.27	1.960	49.8	
Tip	12.60	320.1	23.20	0.405	33.80	0.59	1.03	1.960	49.8	
Stator 3										50
Hub	7.84	199	42.61	0.744	18.89	0.33	1.63	1.597	40.6	
Mean	10.10	256	32.15	0.55	26.02	0.455	1.26	1.597	40.6	
Tip	12.35	314	24.64	0.431	32.43	0.566	1.03	1.597	40.6	
Rotor 4										48
Hub	7.95	202	42.25	0.738	19.48	0.340	1.67	1.745	44.4	
Mean	10.07	256	32.55	0.568	25.95	0.453	1.32	1.745	44.4	
Tip	12.19	310	25.28	0.442	31.90	0.557	1.09	1.745	44.4	
Stator 4										58
Hub	8.03	204	42.60	0.745	19.06	0.342	1.64	1.426	36.2	
Mean	9.99	254	33.20	0.579	25.2	0.440	1.31	1.426	36.2	
Tip	11.95	304	26.43	0.462	30.68	0.536	1.10	1.426	36.2	
Rotor 5										55
Hub	8.11	206	42.28	0.738	19.37	0.338	1.67	1.536	39.0	
Mean	9.93	252	33.50	0.584	25.06	0.437	1.36	1.536	39.0	
Tip	11.75	298	27.05	0.473	30.18	0.526	1.15	1.536	39.0	
Stator 5										66
Hub	8.20	208	42.49	0.74	19.16	0.332	1.64	1.278	32.4	
Mean	9.90	252	34.19	0.59	24.46	0.427	1.36	1.278	32.4	
Tip	11.60	294	27.96	0.488	29.37	0.512	1.16	1.278	32.4	
Rotor 6										63
Hub	8.28	210	42.19	0.736	19.56	0.342	1.67	1.372	34.9	
Mean	9.87	250	34.53	0.602	24.47	0.528	1.40	1.372	34.9	
Tip	11.45	291	28.67	0.502	28.95	0.505	1.21	1.372	34.9	
Stator 6										75
Hub	8.35	222	42.54	0.744	19.23	0.336	1.64	1.156	29.4	
Mean	9.84	250	35.19	0.614	23.91	0.418	1.40	1.156	29.4	
Tip	11.32	286	29.60	0.516	28.10	0.481	1.21	1.156	29.4	
Rotor 7										72
Hub	8.44	214	41.95	0.731	19.74	0.345	1.66	1.221	31.1	
Mean	9.82	250	35.02	0.612	24.07	0.421	1.43	1.221	31.1	
Tip	11.2	284	29.51	0.515	28.10	0.481	1.25	1.221	31.1	
Stator 7										81
Hub	8.48	215	40.85	0.714	20.88	0.365	1.61	1.063	27.1	
Mean	9.80	249	34.33	0.599	25.03	0.437	1.40	1.063	27.1	
Tip	11.12	283	28.96	0.505	28.87	0.504	1.24	1.063	27.1	
Rotor 8										73
Hub	8.54	217	39.66	0.694	21.37	0.373	1.57	1.150	29.2	
Mean	9.81	249	33.10	0.578	25.59	0.446	1.37	1.150	29.2	
Tip	11.07	281	27.78	0.484	29.50	0.515	1.21	1.150	29.2	

HP Compressor

Similar to the IP compressor, the philosophy was to design the HP compressor within state-of-the-art technology to minimize development time and cost. Therefore, the HP compressor was designed to demonstrated aerodynamic parameters. Table 3d3-VI presents a summary of HP compressor design values.

Table 3d3-VI.
PD218-Q HP compressor design values.

Corrected airflow	32.6 lb/sec (14.8 kg/sec)
Pressure ratio	4.08:1
Corrected speed	10,190 rpm (170 rps)
Inlet pressure	31.8 psia (219.271 kpa)
Inlet temperature	332°F (440°K)
Corrected specific inlet flow	32.4 lb/sec/ft^2 (158.1 kg/sec-m^2)
Corrected inlet tip speed	974 fps (296.9 m/sec)
Inlet annulus area	1.008 ft^2 (0.093 m^2)
Inlet tip diameter	21.92 in. (557 mm)
First rotor inlet H/T radius ratio	0.796
Number of stages	8

The choice of flow path for the HP compressor is based on consideration of several aspects of both total engine design parameters and compressor aerodynamic design. From an aerodynamic standpoint, it is desirable to design a flow path with a lower H/T radius ratio. However, due to certain mechanical limitations, an H/T radius ratio slightly higher than normally desired has been incorporated in the HP compressor. The following is an explanation of the design factor affecting this parameter.

- The lower H/T radius ratio design would result in lower hub and tip diameters, thus requiring higher rotational speeds to achieve the same wheel speeds. Higher rotational speeds compromise the DN value for the bearings of the HP compressor rotor. Because bearing diameter is restricted by the shafting requirements of the other rotors, the rotational speed of the HP compressor rotor must be limited to a value which will guarantee adequate bearing life.
- The higher rotational speed requires an HP turbine which is smaller in diameter and which requires a longer (axially) transition between turbines because of HP and IP turbine radial mismatch. This same consideration applies to the HP compressor and the IP compressor transition. In addition to adding engine length, it complicates the transition design mechanically.

An upper limit of 0.9 was chosen for compressor exit H/T radius ratio for aerodynamic reasons. Various compressor flow path shapes were considered before choosing the constant hub radius design. By maintaining the constant hub diameter of the HP compressor, the exit of the IP compressor was radially aligned with the inlet of HP compressor, thus making the shortest and most simple transition section while still maintaining the limit on exit radius ratio.

Table 3d3-VII presents the stage design parameters, Table 3d3-VIII presents the vector diagram data, and Table 3d3-IX gives the blading data for the HP compressor. The estimated performance map is shown in Figure 3d3-2.

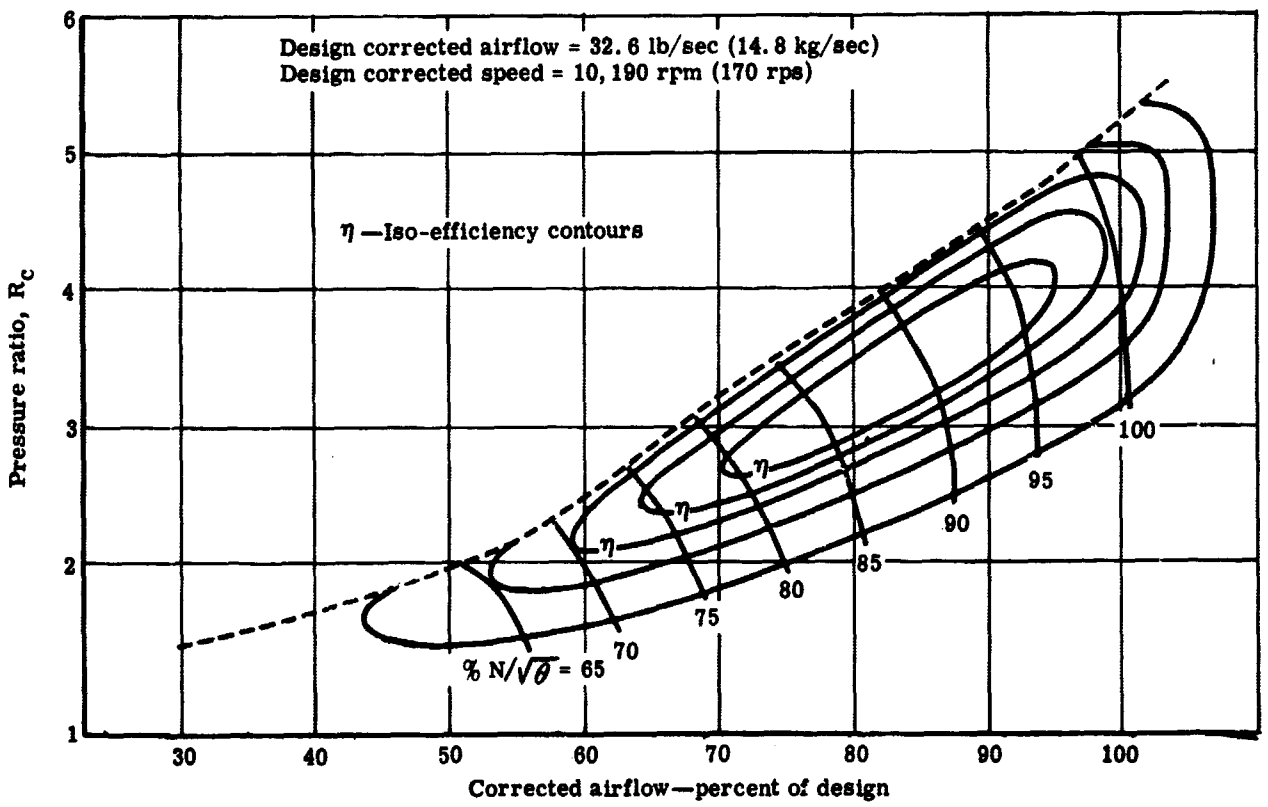

Figure 3d3-2. PD218-Q HP compressor estimated performance.

Table 3d3-VII.

PD218-Q HP compressor stage design parameters.

Stage	Temp rise, ΔT_T, °F (°K)	Pressure ratio, R_s	Work factor, W_f	Diffusion factor		Rotor choke margin (%)	Stator choke margin (%)	H/T dia ratio, D_H/D_T	Whirl change to axial velocity ratio at hub, $(\Delta C_u/V_a)_H$
				Rotor tip, D_f	Stator hub, D_f				
1	33.4 (18.5)	1.218	0.95	0.361	0.407	0.137	0.178	0.546	0.560
2	36.3 (20.1)	1.223	0.90	0.370	0.414	0.140	0.172	0.593	0.630
3	39.1 (21.7)	1.225	0.85	0.393	0.426	0.130	0.165	0.635	0.700
4	39.3 (21.8)	1.211	0.85	0.399	0.426	0.150	0.178	0.672	0.700
5	39.4 (21.9)	1.198	0.85	0.414	0.440	0.165	0.166	0.707	0.700
6	38.2 (21.2)	1.180	0.85	0.415	0.441	0.189	0.202	0.737	0.700
7	36.0 (20)	1.160	0.85	0.414	0.440	0.213	0.230	0.[illegible]	0.680
8	33.9 (18.8)	1.142	0.85	0.438		0.236	0.286	0.779	0.660

Table 3d3-VIII.
PD218-Q HP compressor vector diagram data.

	R_1		U_1		V_{z_1}		α_1		α'_1		M'_{n_1}	V_{z_2}		α_2		α'_2		M_{n_2}
	in.	mm	fps	mps	fps	mps	deg	rad	deg	rad		fps	mps	deg	rad	deg	rad	
First stage																		
Hub	8.59	218	763	232.1	494	150.6	26.24	0.459	46.50	0.811	0.659	499	150.4	46.20	0.806	26.04	0.454	0.652
Mean	9.78	248	868	264.2	494	150.6	32.33	0.564	48.40	0.845	0.686	499	150.4	48.09	0.839	32.12	0.561	0.679
Tip	10.96	278	974	296.3	494	150.6	37.47	0.654	50.33	0.876	0.716	499	150.4	50.05	0.881	37.19	0.648	0.708
Second stage																		
Hub	8.59	218	763	232.1	503	153.1	23.88	0.417	47.02	0.821	0.657	511	151.2	46.60	0.813	23.59	0.412	0.652
Mean	9.61	244	854	260	503	153.1	29.53	0.515	48.48	0.845	0.678	511	151.2	48.08	0.852	29.16	0.508	0.664
Tip	10.63	270	945	288	503	153.1	34.33	0.598	50.02	0.874	0.701	511	151.2	49.61	0.866	33.96	0.582	0.695
Third stage																		
Hub	8.59	218	763	232.1	519	151.6	21.14	0.3682	47.38	0.825	0.659	520	158.4	47.28	0.826	21.06	0.368	0.651
Mean	9.47	240	841	256.1	519	151.6	26.25	0.456	48.47	0.845	0.674	520	158.4	48.36	0.843	26.17	0.456	0.660
Tip	10.33	262	919	280	519	151.6	30.69	0.535	49.66	0.866	0.692	520	158.4	49.52	0.865	30.67	0.536	0.683
Fourth stage																		
Hub	8.59	218	763	232.1	522	159.1	20.86	0.3642	47.24	0.824	0.640	523	159.2	47.20	0.824	20.85	0.3642	0.633
Mean	9.35	238	829	252.2	522	159.1	25.34	0.442	48.17	0.842	0.653	523	159.2	48.13	0.841	25.32	0.442	0.643
Tip	10.10	256	896	273.8	522	159.1	29.30	0.512	49.19	0.859	0.867	523	159.2	49.12	0.858	29.33	0.511	0.659
Fifth stage																		
Hub	8.59	218	763	232.1	524	159.6	20.75	0.362	47.19	0.823	0.622	516	157.2	47.59	0.832	21.04	0.368	0.610
Mean	9.25	235	820	250	524	159.6	24.71	0.432	48.00	0.838	0.632	516	157.2	48.40	0.844	25.04	0.438	0.624
Tip	9.92	252	882	268.5	524	159.6	28.26	0.484	48.88	0.852	0.644	516	157.2	49.26	0.860	28.66	0.502	0.632
Sixth stage																		
Hub	8.59	218	763	232.1	509	151.0	21.85	0.382	47.73	0.834	0.592	502	153.0	48.13	0.841	22.07	0.386	0.582
Mean	9.19	233	816	248.5	509	151.0	25.43	0.445	48.50	0.846	0.602	502	153.0	48.87	0.853	25.75	0.449	0.599
Tip	9.79	248	871	265.8	509	151.0	28.72	0.502	49.31	0.860	0.621	502	153.0	49.66	0.867	29.07	0.507	0.602
Seventh stage																		
Hub	8.59	218	763	232.1	496	150.3	23.29	0.406	48.01	0.838	0.564	489	149	48.40	0.844	23.58	0.412	0.555
Mean	9.14	232	812	247.8	496	150.3	26.58	0.463	48.74	0.851	0.573	489	149	49.13	0.859	26.89	0.470	0.571
Tip	9.69	246	862	262.5	496	150.3	29.60	0.516	49.49	0.863	0.582	489	149	49.90	0.872	29.89	0.522	0.573
Eighth stage																		
Hub	8.59	218	763	232.1	482	147	24.82	0.434	48.32	0.843	0.539	461	140.1	49.58	0.866	25.83	0.452	0.523
Mean	9.10	231	808	246	482	147	27.84	0.886	49.03	0.856	0.547	461	140.1	50.29	0.878	28.91	0.505	0.545
Tip	9.61	244.1	855	260.4	482	147	30.59	0.533	49.78	0.869	0.556	461	140.1	51.01	0.891	31.76	0.554	0.540

Symbols

R—radius
U—wheel speed
V_z—axial velocity
α—absolute air angle
α'—relative air angle
M'_n—relative Mach number
M—absolute Mach number

Subscripts

1—inlet
2—exit

Table 3d3-IX.

PD218-Q HP compressor blading data.

Blade row	Radius in.	Radius mm	Camber deg	Camber rad	Setting deg	Setting rad	Solidity	Chord in.	Chord mm	No. of airfoils
IGV										65
Hub	8.59	218	31.12	0.543	15.56	0.272	1.13	0.933	23.6	
Mean	9.82	250	38.81	0.679	19.41	0.339	0.99	0.933	23.6	
Tip	11.05	281	45.47	0.794	22.74	0.397	0.88	0.933	23.6	
Rotor 1										48
Hub	8.59	218	28.22	0.494	32.38	0.565	1.05	1.182	30.1	
Mean	9.78	248	23.47	0.411	36.67	0.641	0.93	1.182	30.1	
Tip	10.96	278	19.76	0.345	40.48	0.705	0.82	1.182	30.1	
Stator 1										57
Hub	8.59	218	29.77	0.519	31.22	0.546	1.20	1.132	28.8	
Mean	9.70	246	25.04	0.437	35.48	0.62	1.06	1.132	28.8	
Tip	10.79	274	21.49	0.376	39.06	0.683	0.96	1.132	28.8	
Rotor 2										65
Hub	8.59	218	30.95	0.54	31.54	0.55	1.30	1.084	27.8	
Mean	9.61	244	26.38	0.469	35.29	0.616	1.16	1.084	27.8	
Tip	10.63	270	22.64	0.396	38.70	0.675	1.05	1.084	27.8	
Stator 2										74
Hub	8.59	218	33.00	0.576	30.10	0.525	1.42	1.036	26.3	
Mean	9.54	242	28.26	0.498	33.72	0.588	1.28	1.036	26.3	
Tip	10.49	266	24.60	0.43	37.10	0.648	1.16	1.036	26.3	
Rotor 3										84
Hub	8.59	218	33.74	0.588	30.51	0.532	1.53	0.981	25.0	
Mean	9.47	241	29.32	0.512	33.81	0.581	1.39	0.981	25.0	
Tip	10.33	262	25.61	0.437	36.85	0.644	1.27	0.981	25.0	
Stator 3										83
Hub	8.59	218	33.86	0.592	30.18	0.529	1.53	0.942	24.0	
Mean	9.40	238	29.74	0.519	33.33	0.581	1.40	0.942	24.0	
Tip	10.21	260	26.07	0.438	36.27	0.634	1.29	0.942	24.0	
Rotor 4										91
Hub	8.59	218	33.82	0.591	30.33	0.529	1.53	0.908	23.1	
Mean	9.35	238	29.93	0.522	33.21	0.580	1.41	0.908	23.1	
Tip	10.10	256	26.59	0.463	35.89	0.626	1.30	0.908	23.1	
Stator 4										90
Hub	8.59	218	33.70	0.589	30.25	0.528	1.55	0.846	21.5	
Mean	9.30	236	30.09	0.525	33.00	0.576	1.43	0.846	21.5	
Tip	10.00	254	27.03	0.472	35.48	0.62	1.33	0.846	21.5	
Rotor 5										95
Hub	8.59	218	33.58	0.585	30.40	0.531	1.51	0.854	21.7	
Mean	9.25	235	30.08	0.525	32.96	0.575	1.40	0.854	21.7	
Tip	9.92	252	26.99	0.471	35.38	0.618	1.31	0.854	21.7	
Stator 5										96
Hub	8.59	218	33.19	0.579	31.01	0.541	1.51	0.846	21.5	
Mean	9.22	234	29.57	0.516	33.62	0.588	1.40	0.846	21.5	
Tip	9.85	250	26.35	0.46	36.03	0.63	1.32	0.846	21.5	
Rotor 6										97
Hub	8.59	218	33.07	0.577	31.20	0.545	1.50	0.839	21.3	
Mean	9.19	234	29.86	0.522	33.57	0.586	1.39	0.839	21.3	
Tip	9.79	248	27.01	0.472	35.80	0.625	1.32	0.839	21.3	
Stator 6										95
Hub	8.59	218	32.16	0.561	32.02	0.559	1.46	0.834	21.2	
Mean	9.17	233	29.17	0.508	34.22	0.598	1.37	0.834	21.2	
Tip	9.74	248	26.12	0.456	36.29	0.634	1.29	0.834	21.2	
Rotor 7										93
Hub	8.59	218	31.73	0.554	32.15	0.561	1.45	0.839	21.3	
Mean	9.14	232	28.88	0.505	34.30	0.599	1.36	0.839	21.3	
Tip	9.69	246	26.34	0.46	36.32	0.634	1.28	0.839	21.3	
Stator 7										89
Hub	8.59	218	30.92	0.54	32.92	0.574	1.38	0.834	21.2	
Mean	9.12	232	28.16	0.491	35.02	0.611	1.30	0.834	21.2	
Tip	9.65	245	25.79	0.449	36.91	0.644	1.23	0.834	21.2	
Rotor 8										84
Hub	8.59	218	29.87	0.522	33.38	0.582	1.3	0.839	21.3	
Mean	9.10	231	27.16	0.474	35.44	0.619	1.23	0.839	21.3	
Tip	9.61	244	24.76	0.432	37.39	0.651	1.16	0.839	21.3	

Mechanical Design

IP Compressor

Figure 3d3-3 shows the general arrangement and supporting structure of the eight-stage IP compressor. A transition duct is provided between the fan exit and the IP compressor inlet to form the entrance to the gas generator. The primary fan exit vanes are made of 6Al-4V titanium and are located at the inlet of this duct to remove the swirl from the fan exit air to ensure laminar flow through the transition duct. The number of vanes has been selected so that the discrete noise from the blade wake interactions cannot propagate forward. Eight 6Al-4V titanium structural struts downstream of the intermediate vanes carry the fan and IP compressor thrust bearing loads from the inner support rings to the outer case support rings. These struts also provide access for oil pressure, oil scavenge, and breather air plumbing to the fan and IP compressor bearing compartment. The 6Al-4V titanium IGV's for the IP compressor are supported in the aft portion of the transition section. These vanes are spaced one chord length in front of the IP compressor rotor first-stage blade for noise reduction.

The rotor assembly consists of eight stages of blades, a first-stage disk, a forward stub shaft, a rotor disk and spacer drum, and a rear drive shaft. It is supported between two bearings. The rotor disk and spacer drum form an integral machined unit which contains the eight stages of blades. All of the blades in the IP compressor rotor are retained in tangential slots. The rear drive shaft is attached rigidly to the rotor drum and extends rearward where it is coupled to the IP turbine with a fixed set of splines.

A stress analysis of the IP compressor rotor blades was made and the results are given in Table 3d3-X. All eight stages are made of forged 6Al-4V titanium. No creep problems are anticipated at the blade metal temperatures given for the IP compressor blades. The disks and spacers of the IP compressor rotor are machined to form an integral unit from a 6Al-4V titanium forging. This drum-type construction provides a simple, lightweight, low cost rotor assembly which provides a smooth inner flow path between the blade rows. This construction will also provide a rotor wheel which will be easy to maintain and balance.

A stress analysis for the disk rings under the blade rows has been made and the results are given in Table 3d3-XI. Adequate low cycle fatigue life in excess of 12,000 cycles exists for these disks and the rotor drum. The connecting shaft from the IP turbine drive is a one-piece forging of D6 alloy steel and is a part of the IP compressor rotor assembly.

The IP compressor case is split axially in two halves. It is made of Inco 718 alloy steel. The first seven stages of stators are 180-degree (3.14-radian) segments of outer rings and vanes. The vanes are cantilever supported by the outer ring which is installed in T-slots in

the split compressor case. The chord-to-thickness ratios of the cantilevered vanes were adjusted to provide adequate stiffness for both blade frequency and bending stress. The eighth-stage stator is a complete ring assembled in the case and is retained by the intermediate transition and IP-HP compressor bearing support. All ring and vane assemblies are fabricated from 6Al-4V titanium. Table 3d3-XII lists the bending stress and axial deflection data for the IP compressor vanes.

Table 3d3-X.
PD218-Q IP compressor airfoil steady-state stress data.

Stage	Rotor speed rpm	Rotor speed rps	No. of blades	Metal temp °F	Metal temp °K	Airfoil hub centrifugal stress psi	Airfoil hub centrifugal stress Mpa
1	8382	139.7	25	185	358	16,520	113.8
2	8382	139.7	31	238	387	13,555	93.2
3	8382	139.7	41	290	416	13,000	89.4
4	8382	139.7	48	343	446	11,550	79.4
5	8382	139.7	55	395	474	10,200	70.2
6	8382	139.7	63	449	504	9,800	67.5
7	8382	139.7	72	476	520	8,900	61.3
8	8382	139.7	73	476	520	8,500	58.5

Table 3d3-XI.
Stress and growth of PD218-Q IP compressor wheels.

Stage	Rotor speed rpm	Rotor speed rps	Metal temp °F	Metal temp °K	Average tangential stress psi	Average tangential stress Mpa	Rim radial growth, mechanical and thermal in.	Rim radial growth, mechanical and thermal mm
1	8382	139.7	238	387	72,350	498	0.037	0.80
2	8382	139.7	273	407	71,370	491	0.040	1.02
3	8382	139.7	298	421	70,950	488	0.043	1.09
4	8382	139.7	316	431	70,650	486	0.045	1.14
5	8382	139.7	360	455	68,750	474	0.047	1.19
6	8382	139.7	400	477	62,700	432	0.047	1.19
7	8382	139.7	430	494	62,550	431	0.050	1.27
8	8382	139.7	430	494	63,550	438	0.051	1.30

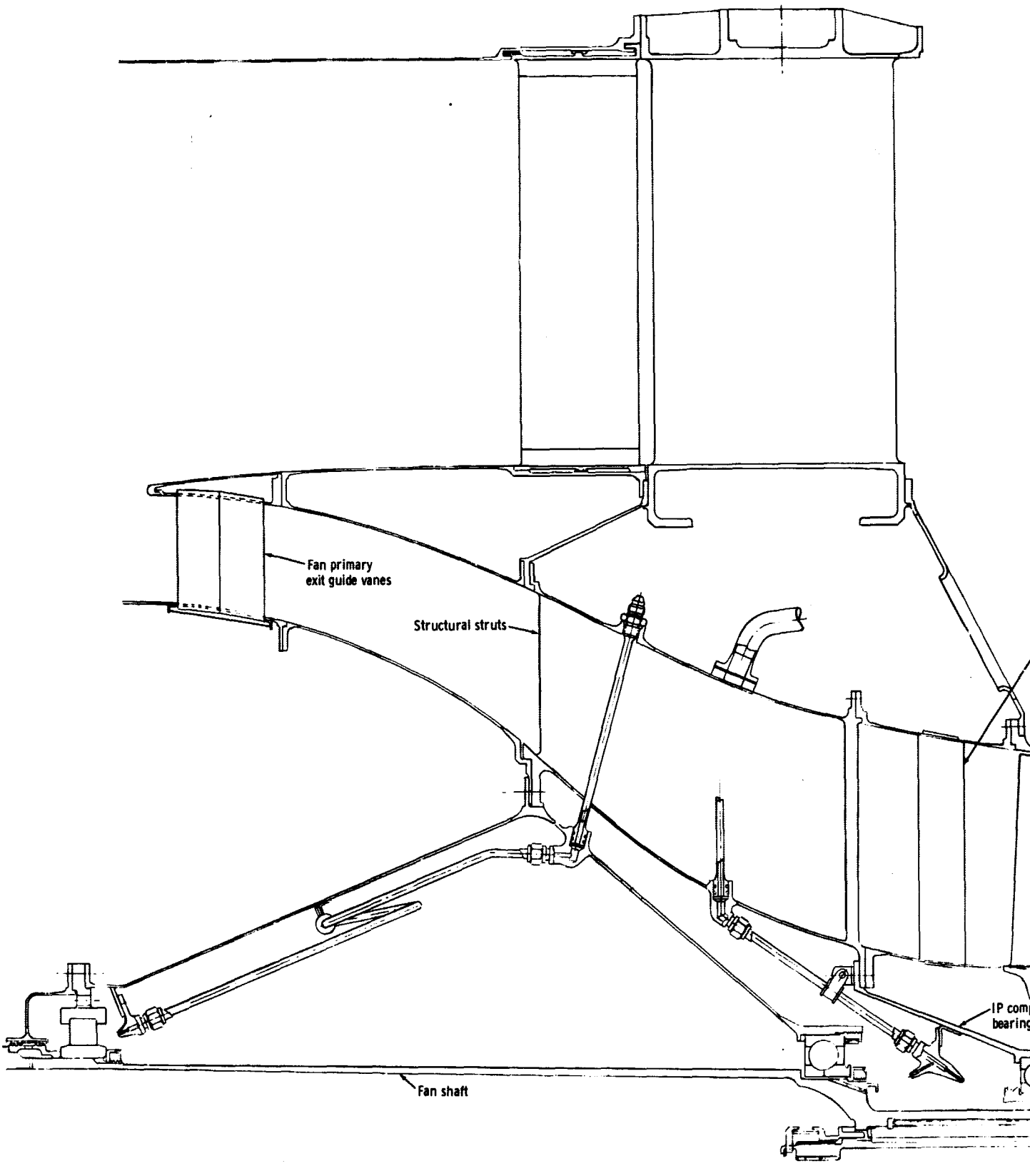

FOLDOUT FRAME /

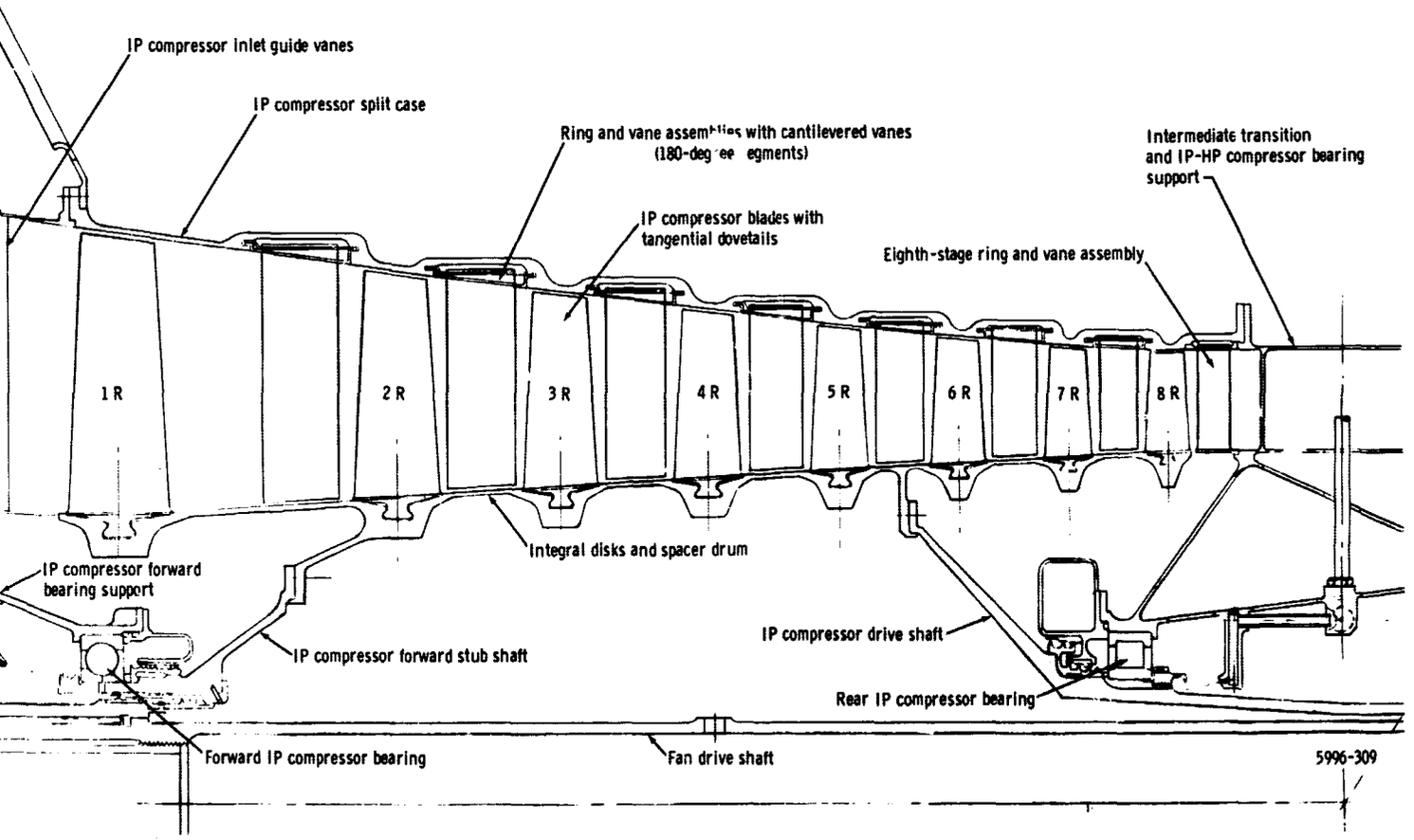

Figure 3d3-3. PD218-Q IP compressor.

FOLDOUT FRAME 2

Table 3d3-XII.
Stress and axial deflection data for PD218-Q IP compressor stator vanes.

Stage	Fixity	Bending stress psi	Bending stress pa × 10^8	Axial deflection in.	Axial deflection mm
1	Cantilevered at case	7,723	0.532	0.031	0.8
2	Cantilevered at case	21,534	1.481	0.063	1.600
3	Cantilevered at case	26,735	1.841	0.062	1.574
4	Cantilevered at case	36,133	2.482	0.090	2.281
5	Cantilvered at case	38,604	2.660	0.076	1.930
6	Cantilevered at case	39,562	2.721	0.063	1.600
7	Cantilevered at case	41,321	2.842	0.039	0.990
8	Fixed at case and inner band	40,396	2.781	0.025	0.635

The IP compressor case requires a minimum containment thickness of 0.060 to 0.030 in. (1.52 to 0.76 mm) from the first through eighth stages. These thickness values were computed using empirical relationships derived from an appreciable amount of test data. The IP compressor case thickness is in excess of these minimum values. Bosses are located at strategic points on the case to allow borescope inspection of the IP compressor.

HP Compressor

Figure 3d3-4 shows the general arrangement and supporting structure of the eight-stage HP compressor. The transition section forward of the HP compressor contains eight 6Al-4V titanium structural struts which carry the IP compressor roller and the HP compressor thrust bearing loads from the inner support rings to the outer case support rings. These struts also provide access for oil pressure, oil scavenge, and breather air plumbing from the accessory

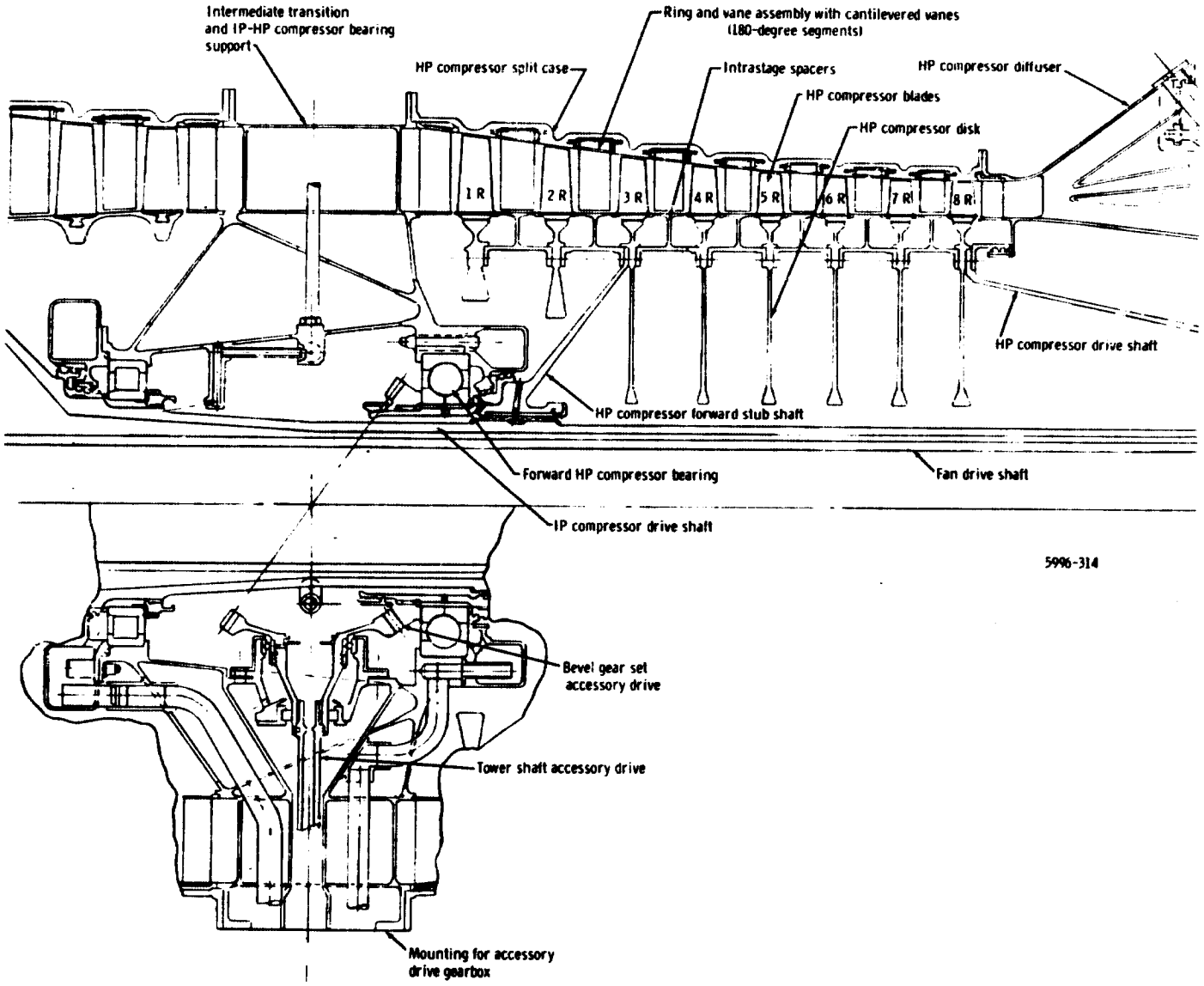

Figure 3d3-4. PD218-Q HP compressor.

drive gearbox to the bearing compartment. The bearing compartment also contains the power takeoff drive. This power takeoff, at the front of the HP compressor rotor, is through a tower shaft running at a right angle to the engine center line. The set of gears which drives the tower shaft provides the power for the accessory drive gearbox mounted on the outer diameter (OD) of this section.

The rotor assembly consists of eight stages of blades, eight rotor disks, seven spacers, a forward stub shaft and a rear conical drive shaft. The rotor assembly is supported on two bearings—a thrust bearing located at the front of the HP compressor and a radial bearing located at the end of the conical shaft just ahead of the HP turbine. The drive shaft is rigidly splined to the HP turbine.

The higher temperature regime in the HP compressor limits the use of 6Al-4V titanium to the first four stages of blades. Stages five through eight are of Inco 718 steel. Table 3d3-XIII lists the HP compressor airfoil stresses.

Table 3d3-XIII.
PD218-Q HP compressor rotor airfoil steady-state stresses.

Stage	Rotor speed		No. of	Temp		Airfoil hub centrifugal stress	
	rpm	rps	blades	°F	°K	psi	Mpa
1	12,555	209.3	48	509	538	18,320	126.2
2	12,555	209.3	65	576	520	15,590	107.1
3	12,555	209.3	84	644	557	12,800	88.2
4	12,555	209.3	91	712	650	13,000	89.6
5	12,555	209.3	95	780	689	22,050	151.8
6	12,555	209.3	97	848	727	20,700	142.6
7	12,555	209.3	93	916	764	22,350	153.8
8	12,555	209.3	84	916	764	22,540	155.1

All eight stages of HP compressor disks are forged from Inco 718 steel. Table 3d3-XIV lists the calculated stresses. These disks have a minimum low cycle fatigue life of 12,000 cycles. The blade attachments are of the single dovetail type and are located in the HP compressor disk in the conventional axial direction. The HP compressor blades are held in the axial position by Inco 718 steel spacers that also form the inner gas path for the cantilevered stators. The connecting one-piece, forged Inco 718 steel shaft from the HP turbine drive is also a part of the HP compressor rotor and case assembly.

Table 3d3-XIV.
Calculated stress for PD218-Q HP compressor rotor disks.

Stage	Rotor speed rpm	Rotor speed rps	Metal temp Rim °F	Metal temp Rim °K	Metal temp Bore °F	Metal temp Bore °K	Max calculated radial stress psi	Max calculated radial stress Mpa	Calculated bore tangential stress psi	Calculated bore tangential stress Mpa	Calculated average tangential stress psi	Calculated average tangential stress Mpa
1	12,555	209.3	480	522	480	522	46,205	318.1	108,260	746	91,900	631
2	12,555	209.3	530	550	530	550	45,190	311.9	108,240	746	89,130	615
3	12,555	209.3	580	577	580	577	46,840	322.1	126,840	872	81,680	563
4	12,555	209.3	640	611	610	594	43,570	300.6	124,620	858	78,380	539
5	12,555	209.3	690	639	610	594	48,750	336.0	128,040	882	80,900	557
6	12,555	209.3	750	672	610	594	48,980	337.5	129,210	890	78,500	541
7	12,555	209.3	800	700	610	594	48,250	332.5	136,460	940	77,850	536
8	12,555	209.3	800	700	610	594	47,070	324.5	130,370	898	75,650	522

The HP compressor case is split axially in two halves and is made of Inco 718 steel. As in the HP compressor rotor, the high temperature limits the use of 6Al-4V titanium to the first four stages of vanes. Stages five through eight are of Inco 718 steel. All eight stages of the HP compressor stator are 180-degree (3.14 radian) outer ring and vane segments and are cantilevered in T-slots in the HP compressor case halves. The chord-to-thickness ratio of the vanes was adjusted to avoid low order engine vibrational frequencies. Table 3d3-XV lists the bending stress and axial deflection of the HP compressor vanes.

Table 3d3-XV.
Calculated stress for PD218-Q HP compressor vanes.

Stage	Fixity	Bending stress psi	Bending stress Mpa	Axial deflection in.	Axial deflection mm
1	Cantilevered at case	43,792	302.0	0.056	1.421
2	Cantilevered at case	31,319	215.8	0.039	0.988
3	Cantilevered at case	40,366	277.9	0.037	0.800
4	Cantilevered at case	38,581	265.8	0.029	0.735
5	Cantilevered at case	38,694	266.2	0.010	0.254
6	Cantilevered at case	36,592	251.9	0.008	0.203
7	Cantilevered at case	33,512	230.5	0.007	0.178
8	Fixed at case and inner band	45,485	312.5	0.006	0.152

The HP compressor case requires a minimum containment thickness of 0.030 to 0.015 in. (0.76 to 0.38 mm) from the first through eighth stages. The HP compressor case thickness has been designed to exceed these values. Allison experience with cantilevered stators and this type of rotor construction indicates that the HP compressor has satisfactory strength margins. Borescope bosses will be located at strategic points on this case to allow borescope inspection of the HP compressor.

Materials

The materials list for the IP and HP compressors is given in Table 3d3-XVI.

Table 3d3-XVI.
PD218-Q compressor materials list.

Item	Material	Specification
IP compressor		
First- through eighth-stage blades	6Al-4V titanium	AMS-4967
First- through eighth-stage disks	6Al-4V titanium	AMS-4967
Drive shaft	D6 alloy steel	AMS-6431
First- through eighth-stage stator vanes	6Al-4V titanium	AMS-4967
First- through eighth-stage stator shroud rings	6Al-4V titanium	AMS-4911
Outer case	Inco 718 steel alloy	AMS-5662
HP compressor		
First- through fourth-stage blades	6Al-4V titanium	AMS-4967
Fifth- through eighth-stage blades	Inco 718 steel	AMS-5662
First- through eighth-stage blades	Inco 718 steel	AMS-5662
First- through eighth-stage blade retainers and vane root drum	Inco 718 steel	AMS-5662
Drive shaft	Inco 718 steel	AMS-5662
Fifth- through eighth-stage stator vanes	Inco 718 steel	AMS-5662
First- through fourth-stage stator vanes	6Al-4V titanium	AMS-4967
First- through fourth-stage stator shroud rings	6Al-4V titanium	AMS-4911
Fifth- through eighth-stage stator shroud rings	Inco 718 steel	AMS-5596
Outer case	Inco 718 steel	AMS-5662

3d4. DIFFUSER AND COMBUSTOR SYSTEM

Aerodynamic Design

General

The diffuser and combustor system is shown in Figure 3d4-1 and was designed to meet the following requirements:

- Efficient operation over the entire operating envelope
- Minimum turbine inlet temperature pattern consistent with pressure loss and sizing limitations
- Exhaust products free of smoke and carbon
- Maximum reliability, durability, producibility, and maintainability

The system consists of the following components:

- Annular three-passage diffuser and inner combustor casing
- Annular combustor
- 16 dual-orifice fuel nozzles
- Two shunted surface gap igniters
- Outer combustor casing

High pressure air enters the combustor section through a three-passage annular diffuser where the velocity is reduced to an acceptable level for combustion. The center passage provides air for the dome and first liner section cooling as well as fuel nozzle cooling. The inner and outer passages supply air in the proper proportions to provide the primary, trimmer, and dilution air required for efficient, uniform combustion. These passages also supply wall cooling air to ensure satisfactory endurance life. Fuel is introduced into the combustor liner through 16 equally spaced dual-orifice fuel nozzles. Ignition is accomplished by energizing two diametrically opposite, four-joule spark igniters which are located in close proximity to the fuel spray, as shown in Figure 3d4-2.

To meet the design requirements for the diffuser and combustor section, size was based on the following guidelines:

- Diffuser and combustor pitch diameters compatible with the compressor exit and turbine inlet diameters
- Diffuser sized to optimize combustor performance without airflow separation
- Combustor liner height compatible with diffuser and fuel nozzle features and combustion efficiency requirements

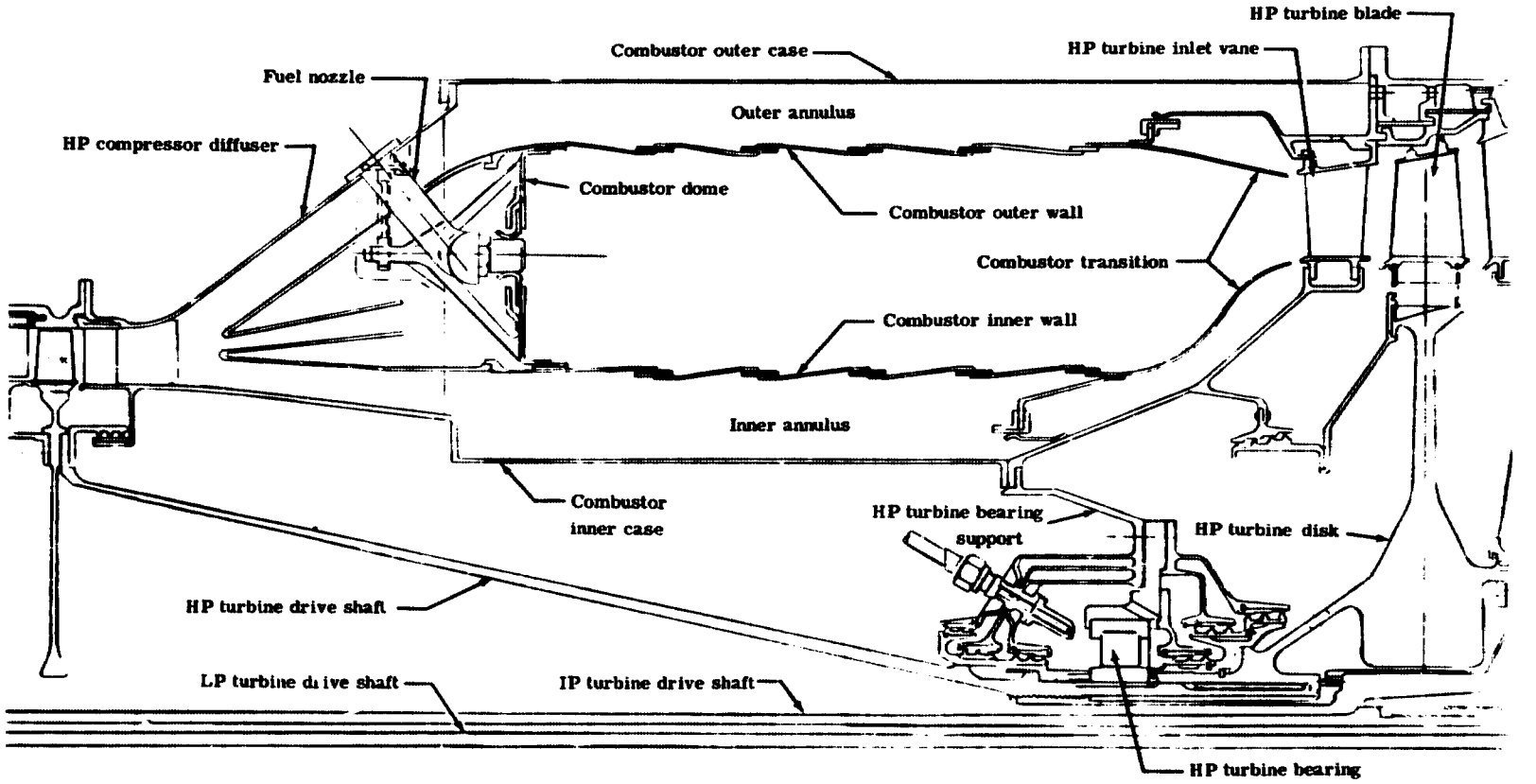

Figure 3d4-1. PD218-Q diffuser and combustor system.

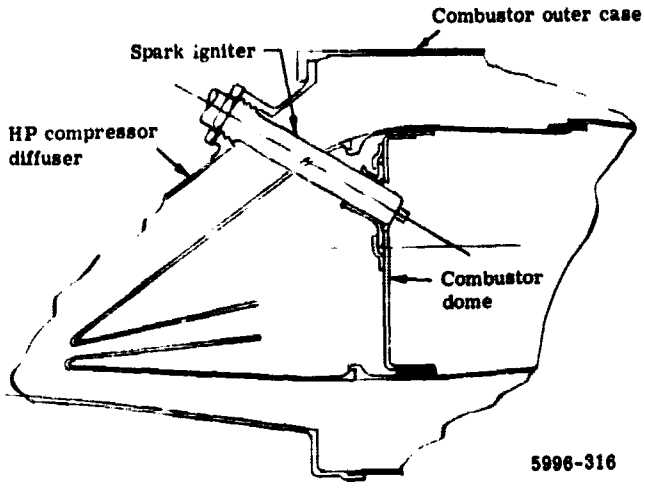

Figure 3d4-2. PD218-Q spark igniter location.

- Combustor annulus height and cross-sectional area consistent with minimum pressure loss
- Combustor length consistent with combustion efficiency and temperature traverse requirements

Based on these guidelines, diffuser and combustor section sizing is as follows:

Diffuser length	7.4 in. (188mm)
Diffuser area ratio	1.87
Combustor pitch diameter	22.0 in. (559mm)
Combustor liner height	4.2 in. (107mm)
Combustor length	14.6 in. (371mm)
Inner annulus height	0.860 in. (21.8mm)
Outer annulus height	0.730 in. (18.5mm)

Diffuser

The optimum diffuser geometry and peak pressure recovery losses were established by considering the momentum losses and the reaction rates which affect combustor performance. The diffuser length was optimized for size based on the following parameters at the design point:

Airflow	54.2 lb/sec (24.6 kg/sec)
Compressor discharge pressure	129.8 psia (894.9 kpa)
Compressor discharge temperature	1226°R (681 °K)

Average diffuser inlet velocity	554 fps (168.9 m/sec)
Diffuser inlet velocity ratio (V_{max}/V_{avg})	1.2
Diffuser inlet Mach number	0.325
Diffuser inlet area	57.2 in.^{2} (0.0369 m^2)
Pressure recovery	37%
Diffuser area ratio	1.87
Diffuser length-to-inlet width ratio	12.3
Diffuser exit Mach number	0.138
Total diffuser pressure loss	2.0%

The selection of the diffuser area ratio of 1.87 and a diffuser length-to-inlet width ratio of 12.3 is in keeping with the desire to provide efficient diffusion and a design exit velocity profile that has a small circumferential variation.

The predicted compressor discharge pressure and velocity ratio profiles are shown in Figure 3d4-3. At the maximum predicted velocity ratio of 1.2, the selected diffuser area ratio and length-to-inlet width ratio combination provides adequate stall margin.

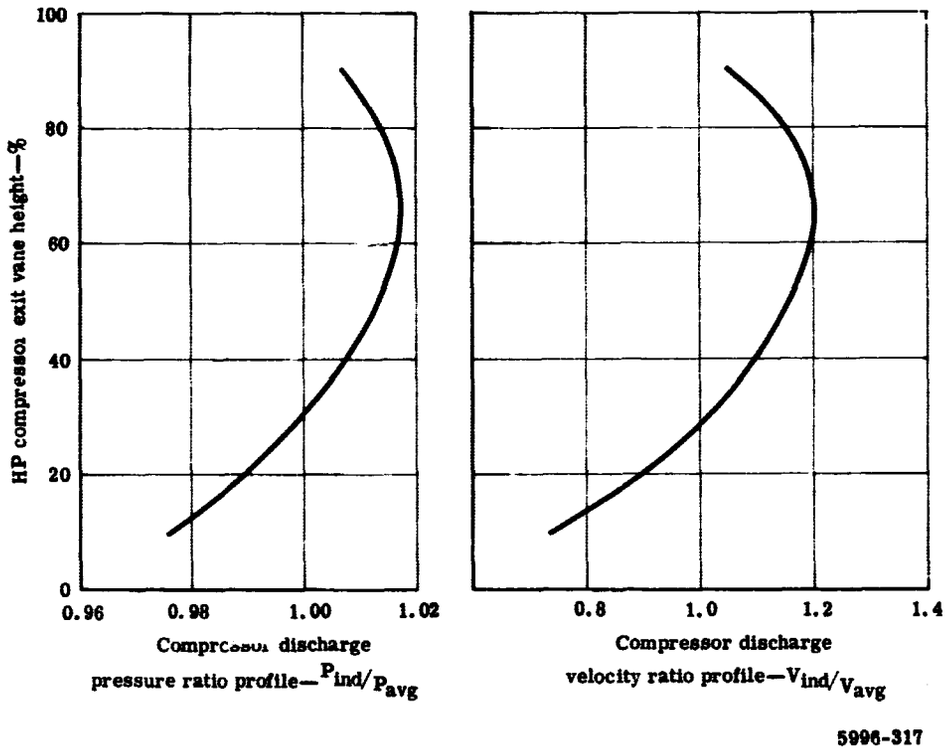

Figure 3d4-3. Predicted PD218-Q compressor discharge pressure and velocity ratio profiles.

The potential advantage of the three-passage diffuser used in this design over the conventional, solid nose, two-passage diffuser is that the dome air for the main combustion cone is taken from the center passage, which is least affected by changes in inlet velocity profile. The first 6 in. (152.4 mm) of the diffuser reduces the velocity to 250 fps (76.2 m/sec). The airflow is then dumped at the trailing edge of the struts to provide an additional reduction of the velocity to 130 fps (39.6 m/sec). This adds stability to the flow in the transition area between the strut trailing edges and the inner and outer annulus passages around the combustor liner.

Combustor

The predicted combustor performance for the design selected is as follows:

Altitude	35,000 ft (10.7 km)	Sea level
Flight Mach number	0.82	0
Combustion efficiency	99.8%	99.8%
Pattern factor, $\frac{T_{max}-T_{avg}}{T_{avg}-T_{in}}$	0.175	0.175
Combustor pressure loss, $P_t/P_{t_{in}}$	3.0%	2.9%
Exhaust smoke density (AIA scale)	—	25

Diffuser and Combustor

The selected diffuser and combustor system has been designed to meet all of the anticipated performance design requirements. This system is conservatively sized and is based on state-of-the-art technology. A performance summary is as follows:

- Design point efficiency—99.8%
- Sea level static efficiency—99.8%
- Space rate—2.7×10^6 BTU/hr-ft^3-atm (27.56 joules/N-m-sec)
- Velocity
  - Liner Reference—96.0 fps (29.3 m/sec)
  - Annulus—130 fps (39.6 m/sec)
- System pressure loss—5.0%

Mechanical Design

Diffuser

The diffuser case is a weldment of Inco 718 steel and contains eight structural struts. These struts along with the inner and outer walls of the diffuser case provide the structural

stiffness required to transmit the HP turbine roller bearing loads to the outer case. The struts also provide access for oil pressure, oil scavenge, pressurizing air, and vent dump air plumbing to the HP turbine bearing compartment.

Combustor

Sixteen pressure-atomizing, dual-orifice fuel nozzles are equally spaced on the combustor pitch diameter and are fed from an external fuel manifold. The fuel nozzles are supported in individual fuel nozzle housings of cast Inco 718 steel; these housings are cantilevered from their respective boss supports on the OD of the diffuser case. This arrangement provides easy access for inspection of fuel nozzles, reduces the tendency of fuel line coking, and minimizes the possibilities of internal fuel leaks.

The inner combustor case is an Inco 718 steel weldment. This case transmits the HP turbine inlet vane and bearing loads to the diffuser case.

The outer combustor case is an Inco 718 steel weldment. This case transmits thrust and maneuver loads, and provides the outer cover to carry the internal pressure loads of the combustor.

The annular combustor liner is a sheet metal weldment of corrugated strip cooling construction and is made of Hastelloy X material (AMS-5536). The inner wall and dome are 0.040 in. (1.016mm) thick and the outer wall is 0.062 in. thick. Hastelloy X material was selected because of its good high temperature strength and oxidation resistance. Precision castings of cobalt base AMS-5382 material are used where added strength and wear resistance are required.

The outer wall stock thickness of 0.062 in. (1.575mm) was selected based on pressure loading calculations. The buckling load carried by the OD of the liner is the governing load factor which is dependent on stock thickness and operating temperature. A computer program is used to determine buckling loads for a thin-wall cylindrical shell with supported ends loaded by hydrostatic pressure; this is for evaluating liner wall stock thickness. Figure 3d4-4 shows the margin of safety predicted by this calculation. This margin of safety is consistent with other annular designs which have demonstrated structural integrity at their design buckling load.

All of the overlapped liner joints will be a combination of resistance welding and nickel brazing to improve the thermal conductivity across the joint, increase joint strength, and increase the resistance of the joint to vibratory fatigue.

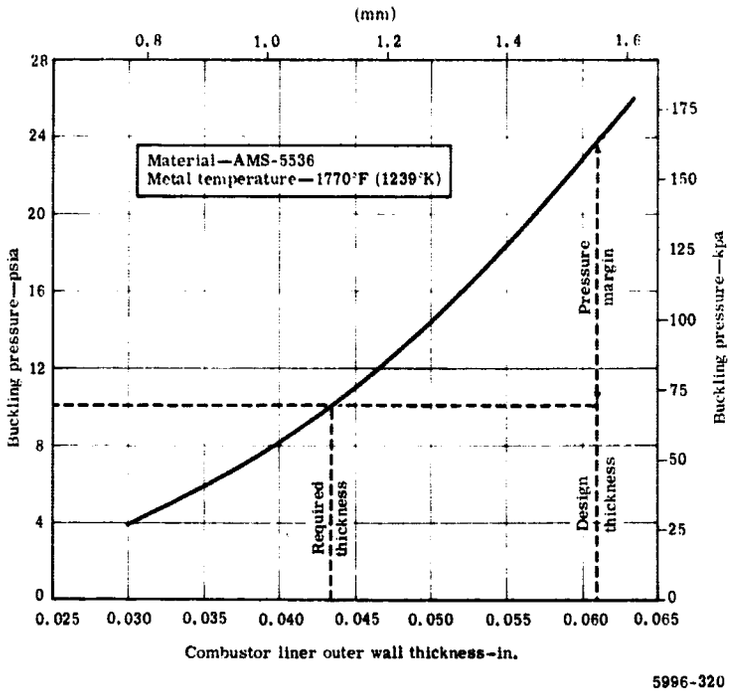

Figure 3d4-4. PD218-Q combustor liner required wall stock thickness.

The combustor liner is supported by pilot diameters on the diffuser splitters and is located axially by eight radial pins. These pins are located in the diffuser strut to eliminate blockage in the flow path. The axial growth is compensated for in the liner-to-turbine locating arrangement.

Radial and axial thermal growth of the liner and first-stage turbine nozzle support are compensated for by seal rings between the liner transition section and the mating turbine parts. This sealing arrangement also allows for accurate control of the compressor discharge air which is required for cooling.

Radial thermal growth differences between the diffuser-mounted fuel nozzles and igniter plugs and the combustor liner are compensated for by floating ferrules in the liner dome.

Materials

The combustor materials list is given in Table 3d4-I.

Table 3d4-I.
PD218-Q combustor materials list.

Item	Material	Specification
Diffuser case	Inco 718	AMS-5662 and -5596
Inner combustor case	Inco 718	AMS-5662 and -5596
Outer combustor case	Inco 718	AMS-5662 and -5596
Fuel nozzle housing	Cast Inco 718	AMS-5383
Combustor liner	Hastelloy X	AMS-5536 and -5382
HP turbine bearing support	Inco 718	AMS-5662

3d5. TURBINE

Aerodynamic Design

HP Turbine

The HP turbine is a shrouded, single-stage unit and is basically similar to the first stages of previous Allison turbines. The H/T diameter ratio denoted in Table 3d5-I is identical with that of the shrouded, air-cooled first-stage of the T56 engine. The ratio selected for the HP turbine provides the greatest possible blade length to obtain the best flow coefficient for the level of stage loading. Figure 3d5-1 shows the typical relationship of stage efficiency to the stage loading and flow coefficients for the HP turbine. The loading coefficient relates stage work to the square of mean-line wheel speed and is inversely proportional to velocity ratio. The flow coefficient relates average axial velocity through the stage to the mean-line wheel velocity. The location of the HP turbine design point in Figure 3d5-1 indicates that the design is selected for high efficiency. When proper allowances are made for tip clearances and pumping the cooling air for this stage, the desired efficiency is achieved.

Table 3d5-I.
PD218-Q HP turbine design point data.

Design work	112.0 BTU/lb (260,330 joules/kg)
Equivalent design work	26.78 BTU/lb (62,247 joules/kg)
Design flow	55.07 lb/sec (24.98 kg/sec)
Equivalent design flow	13.51 lb/sec (6.13 kg/sec)
Stage inlet temperature	1763°F (1235°K)
Stage inlet pressure	124.0 psia (855 kpa)
H/T diameter ratio at rotor exit	0.846
Number of blades	
Stator	46
Rotor	72

The HP turbine design point conditions are listed in Table 3d5-I. The aerodynamic design of the HP turbine at this design point is based on experience gained from previous air-cooled turbine stages. HP turbine velocity diagram data are given in Table 3d5-II. Free-vortex whirl distribution exists at a level of stage reaction which provides the optimum combination of efficiency and rotor relative temperature.

The estimated performance and operating range for the HP turbine are shown in Figure 3d5-2. The map shows the performance over a broad range; however, the operating range from idle to maximum thrust changes very little from the design point. This characteristic can be expected with the HP turbine of a three-spool engine.

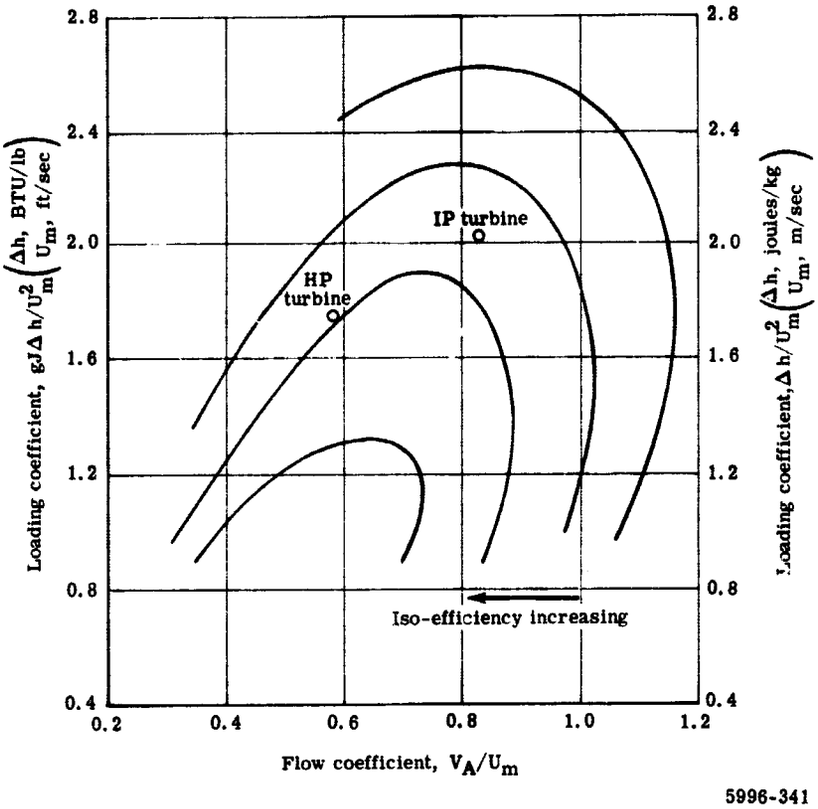

Figure 3d5-1. Typical relationship of stage efficiency to stage loading and flow coefficients for PD218-Q HP and IP turbines.

IP Turbine

The IP turbine is also a shrouded, single-stage unit located immediately aft of the HP turbine. This alignment was possible because of the combination of speeds and level of loading coefficient selected for the HP and IP turbines. The loading and flow coefficients selected for the IP turbine are shown in Figure 3d5-1. At this level the design efficiency will be ensured after proper allowances are made for tip clearances and pumping cooling air for the stage. The H/T diameter ratio selected for the IP turbine is comparable to other shrouded, air-cooled second-stage designs which have met similar efficiency requirements.

The IP turbine design conditions are listed in Table 3d5-III. The aerodynamic design of the IP turbine is similar to that for the HP turbine, as indicated by the similar velocity diagram data in Table 3d5-IV.

Table 3d5-II.
PD218-Q HP turbine velocity diagram data.

	D_1		U_1		V_{a_1}		V_{u_1}		W_{u_1}		V_1		W_1		$\beta_{1_{abs}}$		$\beta_{1_{rel}}$		$M_{1_{abs}}$	$M_{1_{rel}}$
	in.	m	fps	mps	fps	mps	fps	mps	fps	mps	fps	mps	fps	mps	deg	rad	deg	rad		
Stator exit																				
Hub	22.0	0.559	1205.2	367.3	641.9	195.7	1947.8	593.7	742.6	226.3	2050.8	625.1	981.6	299.2	18.24	0.318	40.84	0.713	0.980	0.469
Mean	23.68	0.601	1296.9	395.3	641.9	195.7	1810.0	551.7	513.1	156.4	1920.4	585.3	821.7	250.5	19.53	0.341	51.36	0.896	0.909	0.389
Tip	25.35	0.644	1388.7	423.3	641.9	195.7	1690.4	515.2	301.7	92.0	1808.2	551.1	709.2	216.2	20.79	0.363	64.83	1.131	0.849	0.333

	D_2		U_2		V_{a_2}		V_{u_2}		W_{u_2}		V_2		W_2		$\beta_{2_{abs}}$		$\beta_{2_{rel}}$		$M_{2_{abs}}$	$M_{2_{rel}}$
	in.	m	fps	mps	fps	mps	fps	mps	fps	mps	fps	mps	fps	mps	deg	rad	deg	rad		
Rotor exit																				
Hub	22.0	0.559	1205.2	367.3	786.2	239.6	378.9	115.5	1584.1	482.8	872.7	266.0	1768.4	539.0	64.27	1.122	26.40	0.461	0.434	0.879
Mean	24.0	0.610	1314.8	400.8	786.2	239.6	347.3	105.9	1662.1	506.6	859.5	262.0	1838.6	560.4	66.17	1.155	25.31	0.442	0.427	0.913
Tip	26.0	0.660	1424.3	434.1	786.2	239.6	320.6	97.7	1744.9	531.8	849.0	258.8	1913.8	583.3	67.82	1.184	24.25	0.423	0.422	0.950

Symbols

D—diameter
U—blade tangential velocity
V—absolute gas velocity
W—relative gas velocity
β—gas angle
M—Mach number

Subscripts

1—stator exit
2—rotor exit
a—axial component
u—tangential component
abs—absolute
rel—relative

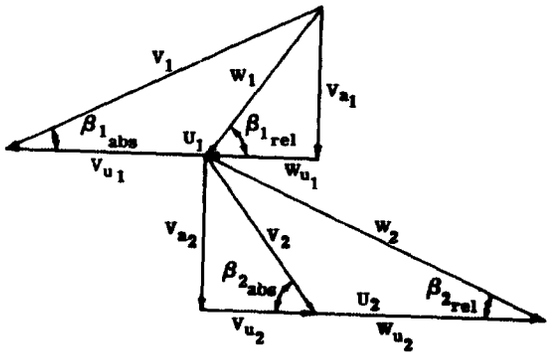

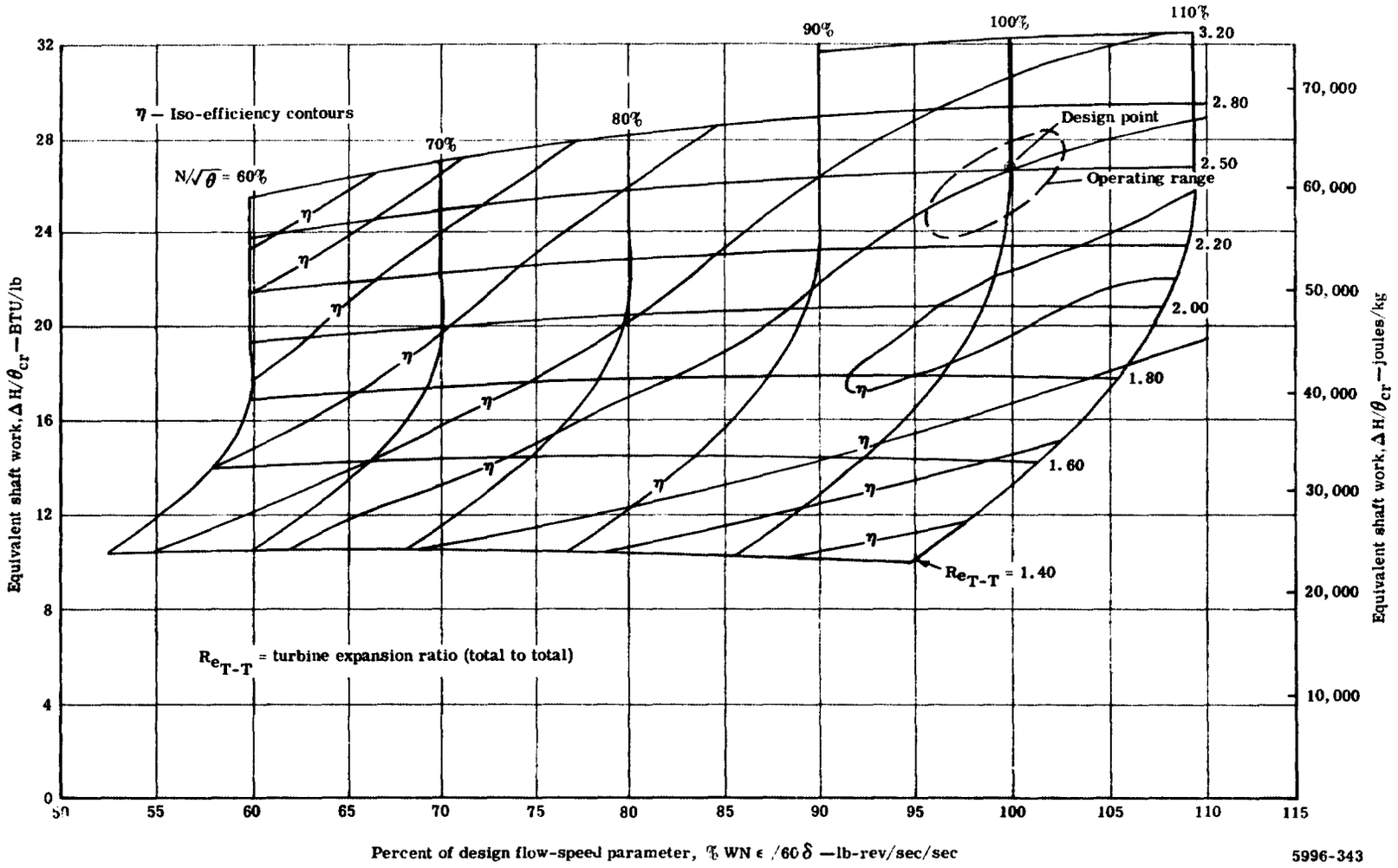

Figure 3d5-2. PD218-Q HP turbine performance map.

Table 3d5-III.
PD218-Q IP turbine design data.

Design work	69.55 BTU/lb (161,660 joules/kg)
Equivalent design work	20.28 BTU/lb (47,140 joules/kg)
Design flow	56.78 lb/sec (25.75 kg/sec)
Equivalent design flow	31.55 lb/sec (14.31 kg/sec)
Stage inlet temperature	1354° F (1007°K)
Stage inlet pressure	49.45 psia (341 kpa)
H/T diameter ratio at rotor exit	0.771
Number of blades	
Stator	72
Rotor	86

The predicted IP turbine performance map is shown in Figure 3d5-3. The characteristics indicated are similar to those for other Allison single-stage turbines. The operating range from idle to maximum thrust varies from the design point more than that for the HP turbine operating range; however, this is typical of the second spool of a multispool engine.

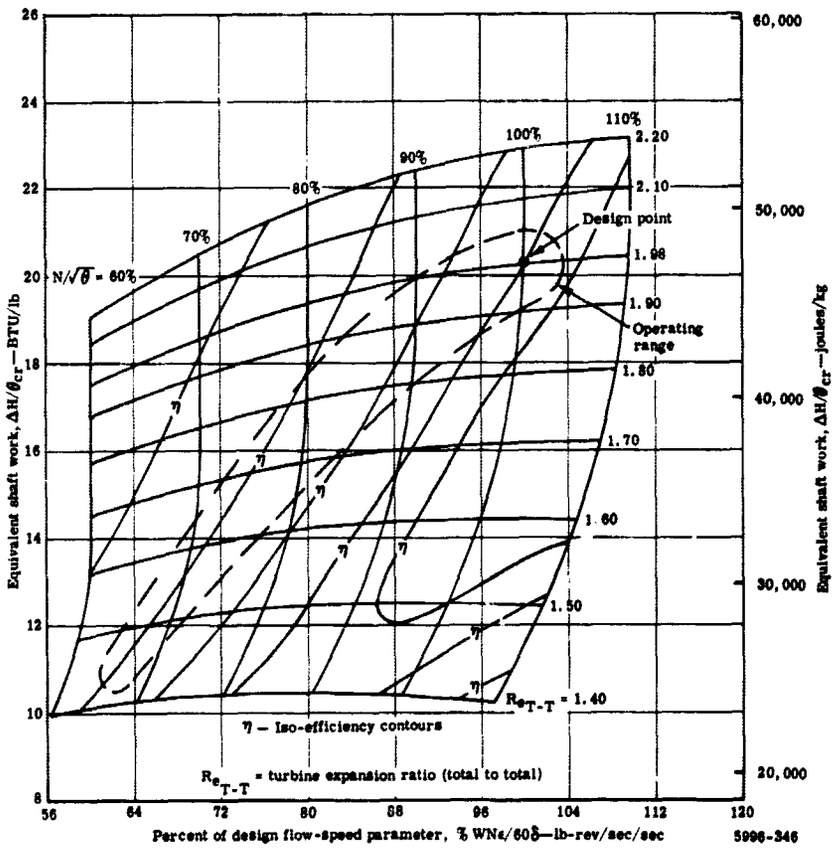

Figure 3d5-3. PD218-Q IP turbine performance map.

Table 3d5-IV.
PD218-Q IP turbine velocity diagram data.

	D_1		U_1		V_{a_1}		V_{u_1}		W_{u_1}		V_1		W_1		$\beta_{1_{abs}}$		$\beta_{1_{rel}}$		$M_{1_{abs}}$	$M_{1_{rel}}$
	in.	m	fps	mps	fps	mps	fps	mps	fps	mps	fps	mps	fps	mps	deg	rad	deg	rad		
Stator exit																				
Hub	22.1	0.561	808.3	246.4	777.7	237.0	1666.4	507.9	858.2	261.6	1838.9	560.5	1158.1	353.0	25.02	0.437	42.18	0.736	0.963	0.610
Mean	24.8	0.630	907.0	276.5	777.7	237.0	1485.0	452.6	578.0	176.2	1676.3	510.9	968.9	295.3	27.64	0.482	53.38	0.932	0.871	0.504
Tip	27.5	0.699	1005.8	306.6	777.7	237.0	1339.2	408.2	333.4	101.6	1548.6	472.0	846.1	257.9	30.14	0.526	66.79	1.166	0.797	0.436

	D_2		U_2		V_{a_2}		V_{u_2}		W_{u_2}		V_2		W_2		$\beta_{2_{abs}}$		$\beta_{2_{rel}}$		$M_{2_{abs}}$	$M_{2_{rel}}$
	in.	m	fps	mps	fps	mps	fps	mps	fps	mps	fps	mps	fps	mps	deg	rad	deg	rad		
Rotor exit																				
Hub	22.2	0.564	811.9	247.5	802.3	244.5	485.7	148.0	1297.6	395.5	937.8	285.8	1525.6	465.0	58.8	1.026	31.73	0.554	0.505	0.821
Mean	25.5	0.648	932.6	284.3	802.3	244.5	422.8	128.9	1355.5	413.2	906.9	276.4	1575.1	480.1	62.2	1.086	30.62	0.534	0.487	0.847
Tip	28.8	0.732	1053.3	321.0	802.3	244.5	374.4	114.1	1427.7	435.2	885.3	269.8	1637.7	499.2	65.0	1.134	20.33	0.512	0.475	0.879

Symbols

D—diameter
U—blade tangential velocity
V—absolute gas velocity
W—relative gas velocity
β—gas angle
M—Mach number

Subscripts

1—stator exit
2—rotor exit
a—axial component
u—tangential component
abs—absolute
rel—relative

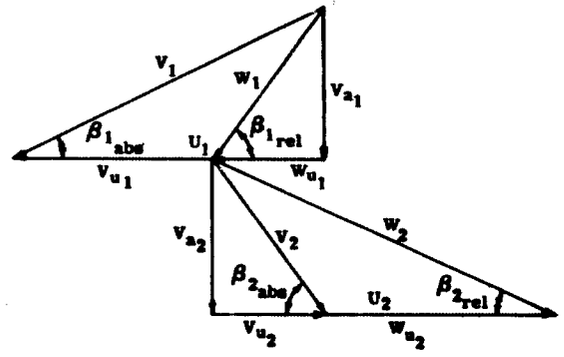

LP Turbine

The turbine flow path for the engine is shown in Figure 3d5-4. The HP and IP turbines were designed with the divergence at the tip and a constant hub diameter to provide a smooth entrance to the transition duct as well as a shorter overall turbine length. The transition duct provides the change in diameter from the IP turbine exit to the LP turbine inlet in the shortest possible length consistent with performance requirements. The LP turbine flow path was positioned so that the performance of each stage could be optimized. The last stage was compromised slightly in diameter from a smooth flow path to facilitate installation requirements. The aspect ratios for the complete turbine are comparable to those for previous engines. The axial clearances between blade rows are more than adequate for mechanical considerations. The last stage contains an even larger axial clearance to suppress the noise from the LP turbine exit.

The LP turbine is a five-stage unit. At the diameters shown in Figure 3d5-4, the LP turbine satisfies the speed, work, and performance requirements of the fan. The individual stage loadings are shown in Figure 3d5-5. The split between stages was selected so that the middle stages were loaded slightly higher than the first and last stages. This allowed more work to be done in the stages with the slightly higher mean-line wheel speeds and, thereby, reduced the swirl at the LP turbine exit to a minimum. This work split also results in improved off-design performance which is essential for a fan turbine. With the work selected for each stage, an H/T diameter ratio was selected to give the proper flow coefficient at the resulting loading coefficient. When proper allowances are made for Mach number, tip clearance, duct losses, and LP turbine exit losses, the desired efficiency is achieved.

The basic design of the LP turbine follows the philosophy of previous Allison fan turbines. The requirement of low speed and minimum turbine size results in low wheel velocities of the rotor and, consequently, high pitch-line loading and low hub reaction. Turbine test results at Allison indicate that the work requirements of this turbine can be accomplished efficiently with five stages. However, four stages were considered initially in view of the minimum size requirement. When this smaller unit was compared with previous designs, the predicted performance was 3% below the design efficiency goal. Turbine size, therefore, was compromised for the higher performance desired.

The conditions at the LP turbine design point are listed in Table 3d5-V. The velocity diagram data for the five stages are given in Table 3d5-VI. These data reflect the requirements imposed on the LP turbine at the design conditions. The low velocities through the blade rows and the level of reaction in each stage are a direct result of the low wheel speed of the unit.

Table 3d5-V.

PD218-Q LP turbine design data.

Stage	1	2	3	4	5
Design work, BTU/lb (joules/kg)	19.80 (46,023)	20.30 (47,185)	20.20 (46,953)	20.10 (46,720)	16.39 (38,097)
Equivalent design work, BTU/lb (joules/kg)	6.70 (15,573)	7.21 (16,759)	7.56 (17,572)	7.95 (18,479)	6.88 (15,992)
Design flow, lb/sec (kg/sec)	57.65 (26.15)	57.65 (26.15)	57.65 (26.15)	57.65 (26.15)	57.65 (26.15)
Equivalent design flow, LP turbine inlet conditions, lb/sec (kg/sec)	60.41 (27.40)	60.41 (27.40)	60.41 (27.40)	60.41 (27.40)	60.41 (27.40)
Stage inlet temperature, °F (°K)	1097 (865)	1023 (824)	945 (780)	868 (737)	790 (694)
Stage inlet pressure, psia (pa)	24.3 (167,540)	19.6 (135,140)	15.5 (106,870)	12.2 (84,120)	9.5 (65,500)
H/T diameter ratio at rotor exit	0.796	0.757	0.704	0.647	0.545
Number of stator vanes	96	102	78	76	74
Number of rotor blades	128	124	116	112	104

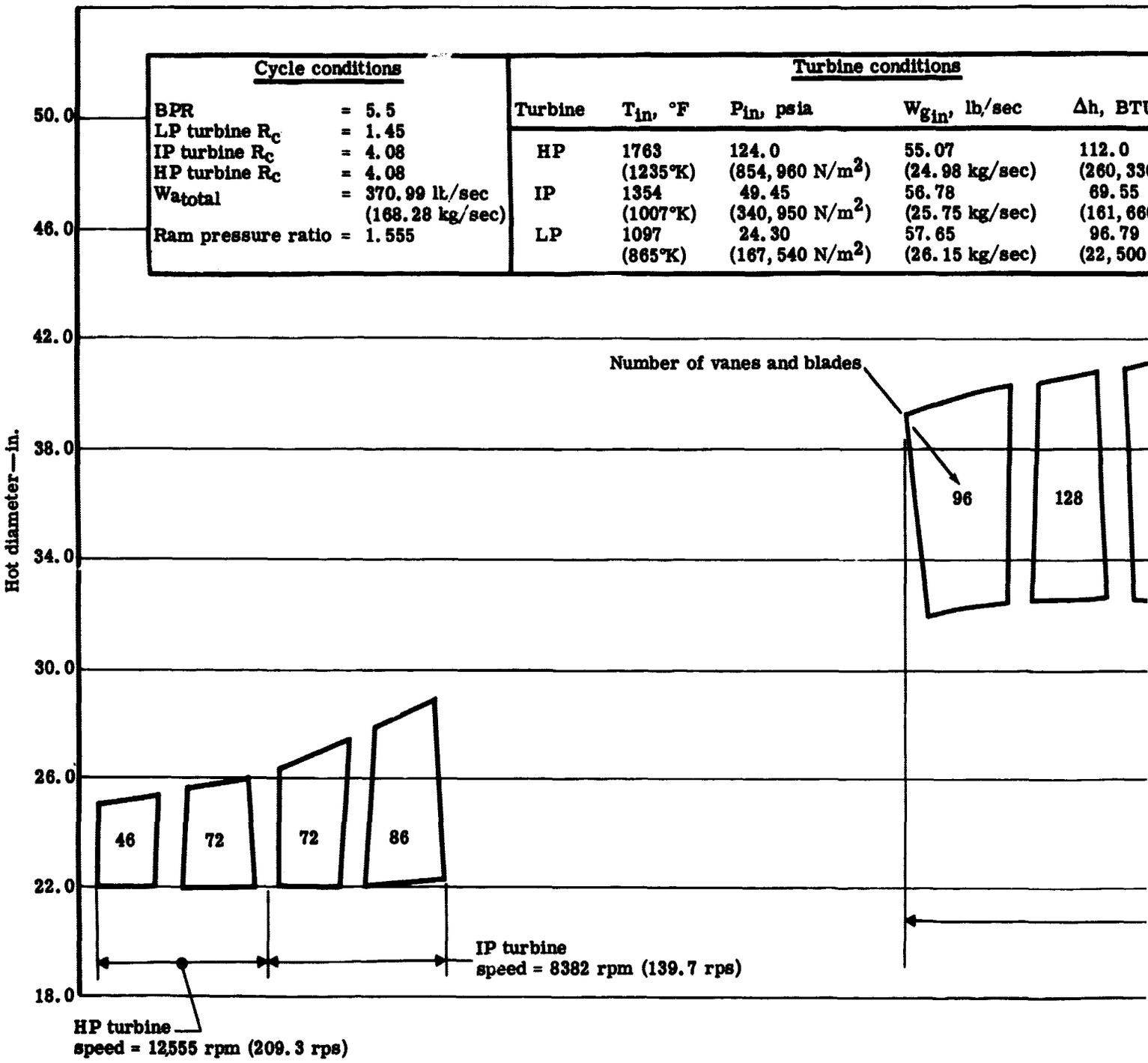

FOLDOUT FRAME 1

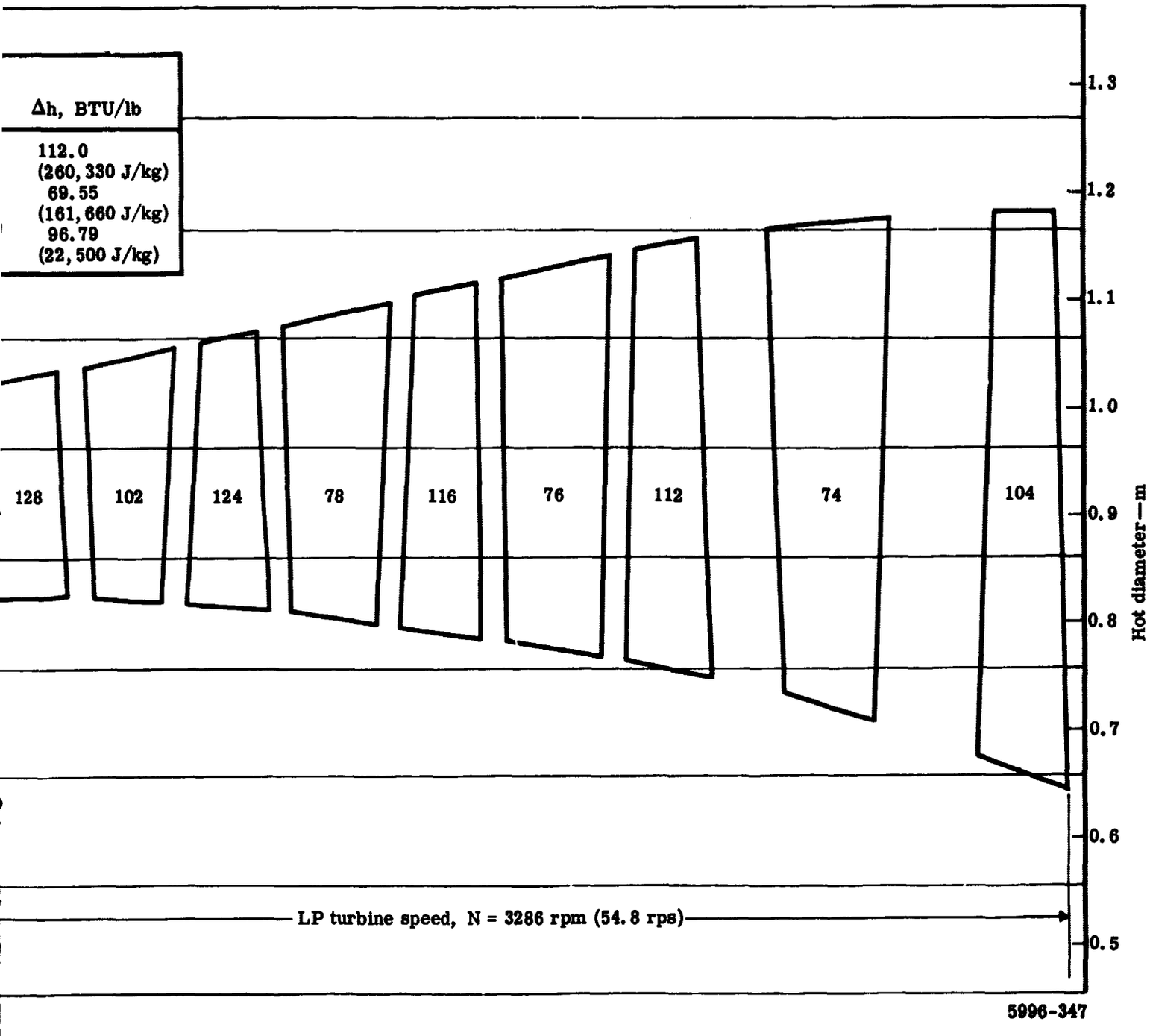

Figure 3d5-4. PD218-Q preliminary turbine flow path—35, 000 ft (10.7 km) at Mach 0.82.

FOLDOUT FRAME 2

PRECEDING PAGE BLANK NOT FILMED.

Table 3d5-VI.

PD218-Q LP turbine velocity d

	D_1		U_1		V_{a_1}		V_{u_1}		W_{u_1}		
	in.	m	fps	mps	fps	mps	fps	mps	fps	mps	fps
Stator exit											
Stage 1											
Hub	32.45	0.824	465.3	141.8	507.5	154.7	829.5	252.8	364.2	111.0	972.
Mean	36.37	0.924	521.5	159.0	507.5	154.7	740.0	225.6	218.5	66.6	897.
Tip	40.30	1.024	577.8	176.1	507.5	154.7	667.9	203.6	90.1	27.5	838.
Stage 2											
Hub	32.30	0.820	463.1	141.2	501.4	152.8	863.7	263.3	400.6	122.1	998.
Mean	36.95	0.939	529.8	161.5	501.4	152.8	755.0	230.1	225.2	68.6	906.
Tip	41.60	1.057	596.5	181.8	501.4	152.8	670.6	204.4	74.2	22.6	837.
Stage 3											
Hub	31.50	0.800	451.6	137.6	465.6	141.9	896.4	273.2	444.8	135.6	1010.
Mean	37.40	0.950	563.2	171.7	465.6	141.9	755.0	230.1	218.8	66.7	887.
Tip	43.30	1.010	620.8	189.2	465.6	141.9	652.1	198.8	31.3	9.5	801.
Stage 4											
Hub	30.28	0.769	434.2	132.3	446.3	136.0	942.2	287.2	508.1	154.9	1042.
Mean	37.64	0.956	539.7	164.5	446.3	136.0	758.0	231.0	218.3	66.5	879.
Tip	45.00	1.143	645.2	196.7	446.3	136.0	634.0	193.2	-11.2	-3.4	775.
Stage 5											
Hub	27.85	0.707	399.3	121.7	428.5	130.6	898.8	274.0	499.5	152.2	995.
Mean	37.08	0.942	531.7	162.1	428.5	130.6	675.0	205.7	143.3	43.7	799.
Tip	46.32	1.177	664.1	202.4	428.5	130.6	540.4	164.7	-123.7	-37.7	689.

	D_2		U_2		V_{a_2}		V_{u_2}		W_{u_2}		
	in.	m	fps	mps	fps	mps	fps	mps	fps	mps	fps
Rotor exit											
Stage 1											
Hub	32.45	0.824	465.3	141.8	510.3	155.5	236.0	71.9	701.2	213.7	562.
Mean	36.60	0.930	524.8	160.0	510.3	155.5	209.2	63.8	734.0	223.7	551.
Tip	40.75	1.035	584.3	178.1	510.3	155.5	187.9	57.3	772.2	235.4	543.
Stage 2											
Hub	32.00	0.813	458.8	139.8	483.8	147.5	235.9	71.9	694.8	211.8	538.
Mean	37.14	0.943	532.5	162.3	483.8	147.5	203.3	62.0	735.8	224.3	524.
Tip	42.28	1.074	606.2	184.8	483.8	147.5	178.6	54.4	784.8	231.2	515.
Stage 3											
Hub	30.93	0.786	443.5	135.2	452.8	138.0	227.5	69.3	671.0	204.5	506.
Mean	37.44	0.951	536.9	163.6	452.8	138.0	187.9	57.3	724.8	220.9	490.
Tip	43.96	1.117	630.3	192.1	452.8	138.0	160.1	48.8	790.3	240.9	480.
Stage 4											
Hub	29.50	0.749	423.0	128.9	442.7	134.9	222.6	67.8	645.6	196.8	495.
Mean	37.53	0.953	538.2	164.0	442.7	134.9	175.0	53.3	713.1	217.4	476.
Tip	45.57	1.157	653.4	199.2	442.7	134.9	144.1	43.9	797.5	243.1	465.
Stage 5											
Hub	25.40	0.645	364.2	111.0	408.2	124.4	141.2	43.0	505.4	154.0	431.
Mean	36.00	0.914	516.2	157.3	408.2	124.4	99.7	30.4	615.8	187.7	420.
Tip	46.60	1.184	668.2	203.7	408.2	124.4	77.0	23.5	745.1	227.1	415.

*The symbols and vectors are defined in Table 3d5-II.

FOLDOUT FRAME

able 3d5-VI.

bine velocity diagram data.

W_{u_1}	V_1		W_1		$\beta_{1_{abs}}$		$\beta_{1_{rel}}$		$M_{1_{abs}}$	$M_{1_{rel}}$
mps	fps	mps	fps	mps	deg	rad	deg	rad		
111.0	972.4	296.4	624.7	190.4	31.46	0.549	54.33	0.948	0.524	0.337
66.6	897.3	273.5	552.5	168.4	34.44	0.601	66.71	1.164	0.482	0.297
27.5	838.9	225.7	515.4	157.1	37.23	0.650	79.93	1.395	0.449	0.276
122.1	998.7	304.4	641.8	195.6	30.14	0.526	51.38	0.897	0.552	0.355
68.6	906.3	276.2	549.7	167.5	33.59	0.586	65.81	1.149	0.500	0.302
22.6	837.3	225.2	506.9	154.5	36.78	0.642	81.59	1.424	0.460	0.279
135.6	1010.1	307.9	643.9	196.3	27.44	0.479	46.31	0.808	0.574	0.366
66.7	887.0	270.4	514.5	156.8	31.66	0.553	64.83	1.131	0.501	0.290
9.5	801.3	244.2	466.7	142.3	35.53	0.620	86.15	1.504	0.451	0.262
154.9	1042.6	317.8	676.3	206.1	25.35	0.442	41.30	0.721	0.611	0.396
66.5	879.7	268.1	496.9	151.5	30.50	0.532	63.93	1.116	0.511	0.288
-3.4	775.4	236.3	446.5	136.1	35.14	0.613	91.44	1.596	0.448	0.258
152.2	995.7	303.5	658.1	200.6	29.49	0.515	40.62	0.709	0.600	0.317
43.7	799.5	243.7	451.8	137.7	32.40	0.565	71.51	1.248	0.477	0.261
-37.7	689.7	210.2	446.0	135.9	38.41	0.670	106.11	1.852	0.409	0.264

W_{u_2}	V_2		W_2		$\beta_{2_{abs}}$		$\beta_{2_{rel}}$		$M_{2_{abs}}$	$M_{2_{rel}}$
mps	fps	mps	fps	mps	deg	rad	deg	rad		
213.7	562.2	171.4	867.3	264.4	65.19	1.138	36.04	0.629	0.306	0.471
223.7	551.6	168.1	894.0	272.5	67.71	1.182	34.81	0.608	0.300	0.486
235.4	543.8	165.8	925.6	282.1	69.79	1.218	33.46	0.584	0.295	0.503
211.8	538.2	164.0	846.6	258.0	64.00	1.117	34.85	0.608	0.300	0.472
224.3	524.7	159.9	880.6	268.4	67.21	1.173	33.32	0.582	0.292	0.490
231.2	515.7	157.2	921.9	281.0	69.74	1.217	31.65	0.552	0.287	0.513
204.5	506.8	154.5	809.5	246.7	63.32	1.105	34.01	0.594	0.290	0.463
220.9	490.3	149.4	854.6	260.5	67.46	1.177	32.00	0.558	0.280	0.489
240.9	480.3	146.4	910.9	277.6	70.53	1.231	29.81	0.520	0.274	0.521
196.8	495.5	151.0	782.8	238.6	63.20	1.103	34.44	0.601	0.290	0.461
217.4	476.0	145.1	839.4	255.8	68.43	1.194	31.83	0.556	0.280	0.494
243.1	465.5	141.9	912.1	278.0	71.97	1.256	29.03	0.507	0.274	0.536
154.0	431.9	131.6	649.7	198.0	70.91	1.238	38.92	0.679	0.260	0.392
187.7	420.2	128.1	738.8	225.2	76.28	1.331	33.54	0.585	0.253	0.445
227.1	415.4	126.6	849.6	259.0	79.32	1.384	28.71	0.501	0.250	0.512

FOLDOUT FRAME 2

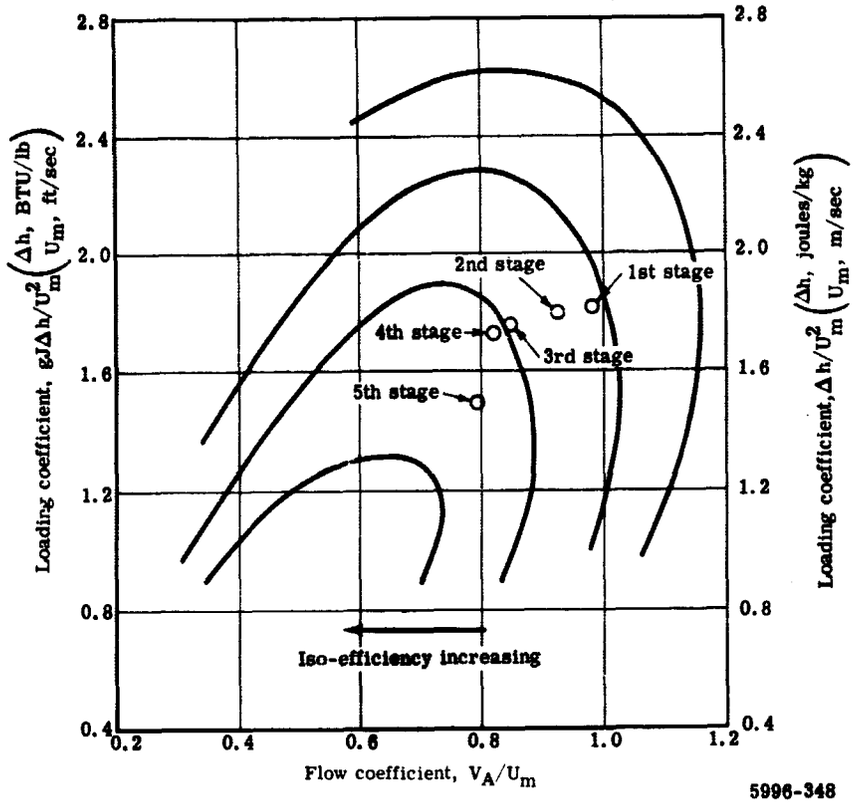

Figure 3d5-5. Individual stage loadings for PD218-Q LP turbine.

The off-design performance of the LP turbine is shown in Figure 3d5-6. This map shows the operating characteristics from a corrected speed of 50 to 120%. The operating range from idle to maximum thrust varies over a wide range from the design point. This performance is characteristic of a fan turbine.

Mechanical Design

HP Turbine

The single-stage HP turbine shown in Figure 3d5-7 drives the eight-stage HP compressor; it is overhung from the HP turbine rotor roller bearing. The inlet vane and the HP turbine blade are air cooled with HP compressor discharge cooling air. See Figure 3d7-2 for internal airflow venting. The inlet vane receives cooling air through the support system on the turbine case OD. The ID support of this vane allows for radial and axial thermal expansion in the attachment to the inner combustion chamber case.

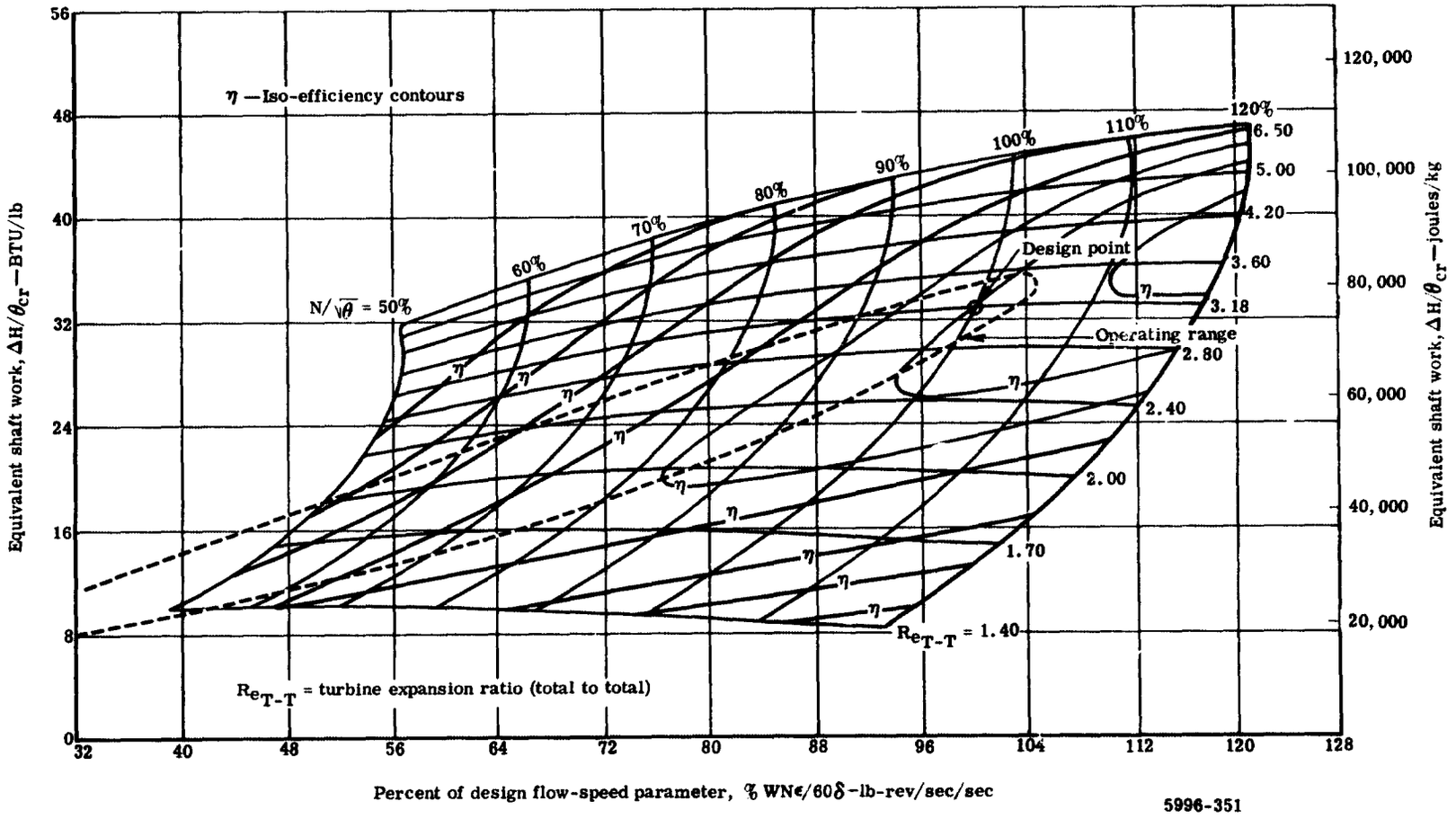

Figure 3d5-6. PD218-Q LP turbine performance map.

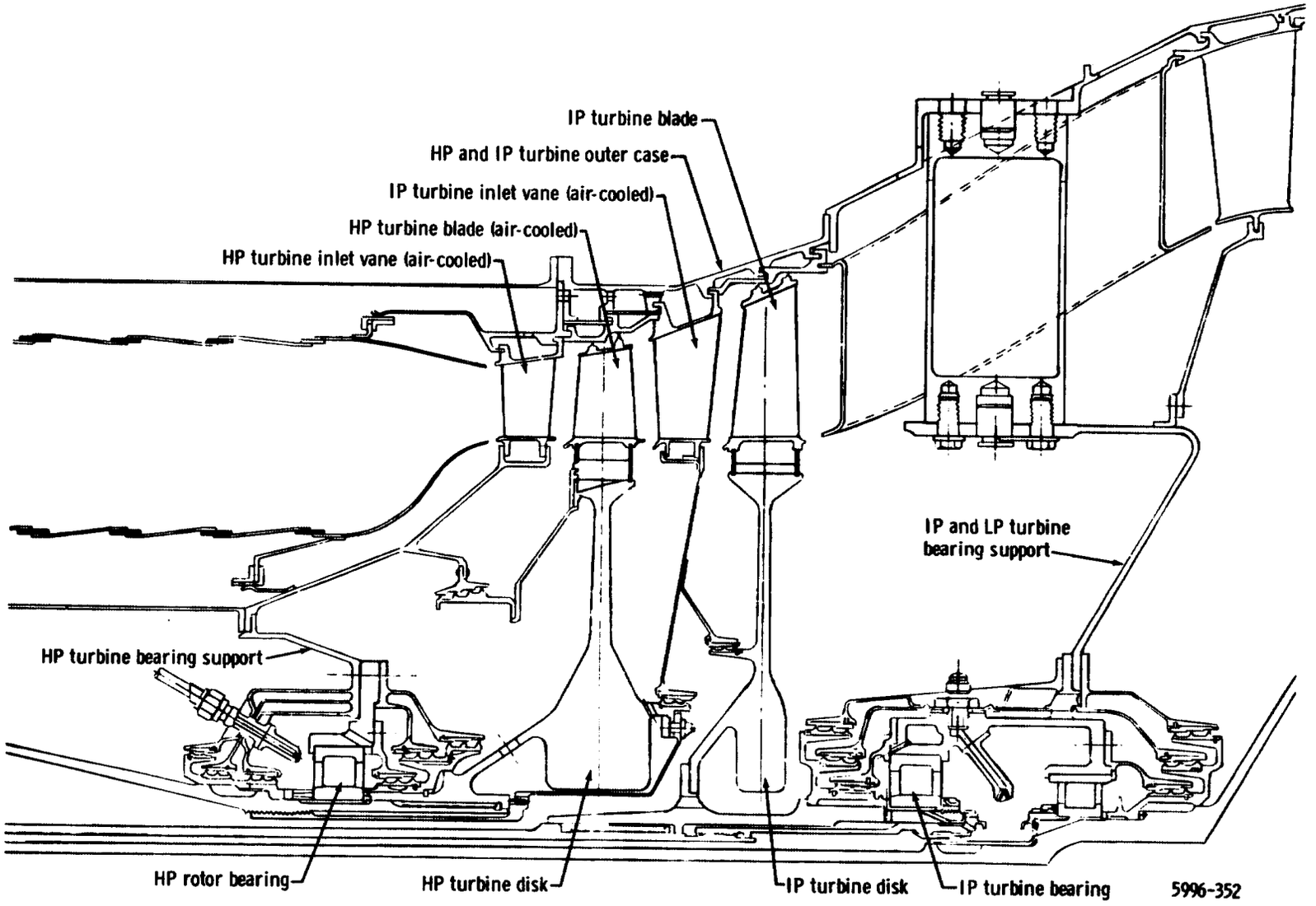

Figure 3d5-7. PD218-Q HP and IP turbines.

The inlet vane is hollow cast of Stellite 31, a cobalt-base alloy with corrosion- and heat-resistant characteristics. It is coated with Alloy S-1 which provides erosion and sulfidation resistance. The leading edge of the vane is impingement cooled. Figure 3d5-8 is a schematic of the impingement-cooled HP turbine inlet vane. The cooling air is delivered to the hollow area inside the vane in a separate Hastelloy X tube; this tube has a series of orifices which distribute the cooling air along the length of the leading edge of the vane. The air is expelled from the orifices in the tube and is impinged on the inside leading edge of the vane. The cooling air then flows around the tube and past several pedestals which support the convex and concave sides of the airfoil to provide convection cooling of the vane walls. The air is then discharged into the main gas flow path through the slotted trailing edge of the vane. The maximum gas temperature at the airfoil mean section is 2120°F (1433°K) for an average vane. This temperature occurs at sea-level takeoff conditions on a hot day where the average turbine inlet temperature is 2014°F (1374°K). The difference between these two temperatures is the radial temperature profile of the combustor. With a circumferential hot spot, an individual vane could have a gas temperature of 2268°F (1515°K) at the mean section. By using 2.0% of the HP compressor discharge air at 932°F (773°K) for cooling and the efficient cooling configuration, the mean airfoil section average metal temperature is 1625°F (1158°K) for the average vane and 1700°F (1200°K) for the individual vane in the hot spot location. These maximum metal temperature conditions, when prorated for the required mission life of 6000 hr, show adequate stress-rupture and sulfidation lives.

The HP turbine blade is hollow cast of Udimet 700, a nickel-base alloy with corrosion- and heat-resistant characteristics. It is coated with Alpak S-1, a slurry coating which provides sulfidation resistance. The blade will be convection cooled with cooling air flowing between the forward cover plate and seal assembly and the disk rim. The cooling air enters the blade at the base of the "fir tree" attachment in the disk and flows radially past a series of pedestals and distribution partitions connecting the concave and convex sides of the airfoil. The cooling air then discharges between the knife edge seals on a tip shroud damper and enters the main gas flow path.

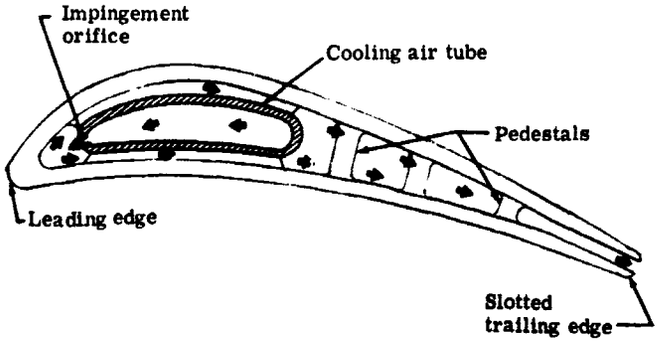

Figure 3d5-8. Schematic of impingement-cooled PD218-Q HP turbine vane inlet.

The maximum gas temperature (caused by the radial temperature profile at the mean section of the airfoil) is 1908°F (1315°K) at sea-level takeoff conditions on a hot day. By using a 1.5% of the HP compressor discharge air at 932°F (773°K) for cooling this blade, the mean airfoil section average metal temperature is 1609°F (1149°K). The centrifugal stress at this section is 19,530 psi (134.6 Mpa). (Although the root section stress of the airfoil is 32,800 psi (226.1 Mpa), the mean section stress becomes the critical area because of the stress-temperature relationship.)

Figure 3d5-9 shows the 0.5% creep and stress rupture properties of the cast Udimet 700 HP turbine blade. This material exhibits life five times that calculated for the prorated mission life of 6000 hr. With 1609°F (1149°K) metal temperature, the HP turbine blade meets these requirements. This metal temperature, when prorated for the required mission life of 6000 hr, shows adequate sulfidation life. The HP turbine blade will have a minimum low cycle fatigue life of 12,000 cycles.

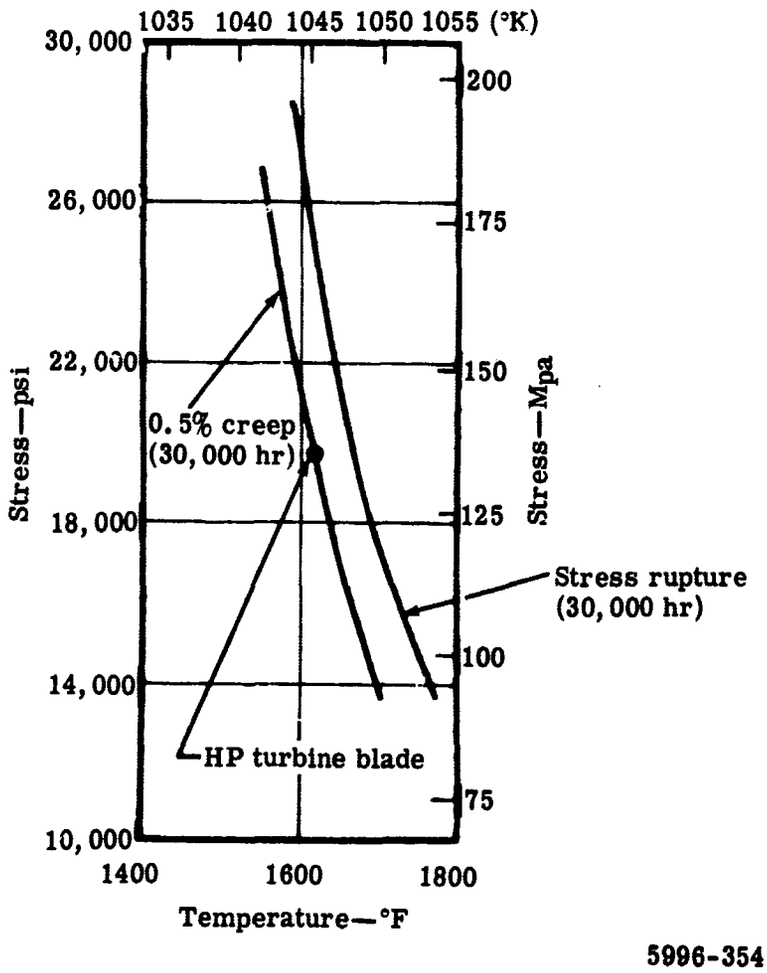

Figure 3d5-9. PD218-Q HP turbine first-stage blade stress versus temperature.

The HP turbine disk of forged Waspaloy material is of conventional wheel geometry. Creep considerations are not critical because of the 1050°F (839°K) rim temperature. The disk minimum low cycle fatigue life is 12,000 cycles. The estimated HP turbine airfoil and disk stresses are given in Tables 3d5-VII and 3d5-VIII, respectively.

Table 3d5-VII.
Airfoil steady-state stresses for PD218-Q HP turbine rotor.

Engine speed	12,555 rpm (209.3 rps)
Mean section metal temperature	1609°F (1149°K)
Airfoil hub centrifugal stress	32,800 psi (226.1 Mpa)
Mean section centrifugal stress	19,530 psi (134.6 Mpa)
0.5% creep mission life	6000 hr

Table 3d5-VIII.
PD218-Q HP turbine disk stresses.

Engine speed	12,555 rpm (209.3 rps)
Metal temperature	
Rim	1050°F (839°K)
Bore	950°F (783°K)
Maximum radial stress	82,150 psi (566.4 Mpa)
Bore tangential stress	86,000 psi (593.0 Mpa)
Average tangential stress	65,090 psi (448.8 Mpa)

The HP and IP turbine outer case is forged of Waspaloy material. It supports the HP and IP turbine stationary blade rub strips, of Hastelloy X alloy steel, and the IP turbine inlet vane.

The HP turbine case requires a minimum containment thickness of 0.059 and 0.063 in. (1.5 and 1.6 mm) at the HP and IP turbine rotor stages, respectively. The thickness obtained by combining the total metal thickness of the stationary blade rub strips and the outer case exceeds this requirement. Bosses located on this case allow borescope inspection of the IP turbine.

IP Turbine

The single-stage IP turbine, shown in Figure 3d5-7, drives the eight-stage IP compressor. It is supported by the IP turbine rotor rear roller bearing. The inlet vane is air cooled with HP compressor discharge cooling air. The vane will receive cooling air through the support

system on the turbine case OD. The inlet vane is hollow cast of Udimet 700 and is coated with Alpak S-1 for sulfidation resistance. The vane will be convection cooled with air entering the tip and flowing radially past a series of pedestals and distribution fences connecting the concave and convex sides of the airfoil. The cooling air discharges through the root of the vane and enters the main gas flow path.

The maximum gas temperature at the mean section of the airfoil is 1683°F (1190°K) for an average vane. This temperature occurs at sea-level takeoff conditions on a hot day. With a circumferential hot spot, an individual vane could have a gas temperature of 1799°F (1255°K) at the mean section. By using 0.5% of HP compressor discharge air at 932°F (773°K) for cooling this vane, the mean airfoil section average metal temperature is 1587°F (1137°K) for the average vane and 1688°F (1193°K) for the individual vane in the hot spot location. These maximum metal temperature conditions, when prorated for a mission life of 6000 hr, show adequate stress-rupture and sulfidation lives.

The IP turbine blade, with a tip shroud damper cast of Udimet 700 nickel base alloy, will also have an Alpak S-1 slurry coating for sulfidation resistance. Table 3d5-IX lists the IP turbine airfoil stresses. Cooling of this airfoil is not required.

Table 3d5-IX.
Airfoil steady-state stresses for PD218-Q IP turbine rotor.

Engine speed	8382 rpm (139.7 rps)
Mean section metal temperature	1352°F (1006°K)
Airfoil hub centrifugal stress	19,500 psi (134.4 Mpa)
Mean section centrifugal stress	12,500 psi (86.2 Mpa)
0.5% creep mission life	6000 hr

The IP turbine rotor disk and integral hub assembly is of Waspaloy material and is attached through a flanged joint and bolt circle to the Inco 718 support shaft from the IP turbine rotor rear roller bearing compartment. Table 3d5-X lists the IP turbine disk stresses. Creep considerations are not critical because of the 1050°F (839°K) rim temperature. The disk is designed with an integral support hub which eliminates the requirement for holes through high stress areas. The disk minimum low cycle fatigue life is 12,000 cycles.

LP Turbine

The five-stage LP turbine, shown in Figure 3d5-10, drives the single-stage fan and is supported between two roller bearings. The transition section forward of the LP turbine contains eight structural struts which support the IP turbine roller bearing and the forward LP turbine roller bearing. These struts also provide access for lubricating oil, scavenge oil, breather air, high pressure air, and vent dump plumbing to the IP and LP turbine bearing compartment.

Table 3d5-X.
PD218-Q IP turbine disk stresses.

Engine speed	8382 rpm (139.7 rps)
Metal temperature	
Rim	1050°F (839°K)
Bore	950°F (783°K)
Maximum radial stress	83,750 psi (577.4 Mpa)
Bore tangential stress	86,050 psi (593.3 Mpa)
Average tangential stress	63,750 psi (439.5 Mpa)

All LP turbine blades are made of Inco 713 heat-resistant alloy steel. They feature tip shroud dampers and have an Alpak S-1 slurry coating for sulfidation resistance. Table 3d5-XI lists the LP turbine airfoil stresses.

All LP turbine disks and integral spacers are made from Inco 901 alloy steel. Table 3d5-XII lists the calculated and allowable disk stresses. All LP turbine disks have a minimum low cycle fatigue life of 12,000 cycles. The fan-to-LP turbine drive shaft is a one-piece forging of D6 alloy steel. This shaft is an integral part of the LP turbine rotor assembly.

All LP turbine vanes are made of Inco 713 heat-resistant alloy steel. They are coated with an Alpak S-1 slurry for sulfidation resistance and are supported from the Inco 901 steel outer case. This case also supports the Hastelloy X stationary blade rub strips. The combined material thickness of the outer case and stationary blade rub strips is greater than the calculated containment requirement of 0.037 to 0.073 in. (0.94 to 1.85 mm). Bosses are located at strategic points on the LP turbine case to allow borescope inspection.

The turbine exhaust case and structural struts are made from AISI 410 steel and coated with heat- and corrosion-resistant aluminum paint. These structural struts provide the support required to transmit the LP turbine rear roller bearing loads to the outer turbine exhaust case. The struts also provide access for oil pressure, oil scavenge, and breather air plumbing to the LP turbine rear bearing compartment.

Materials

The turbine materials list is given in Table 3d5-XIII.

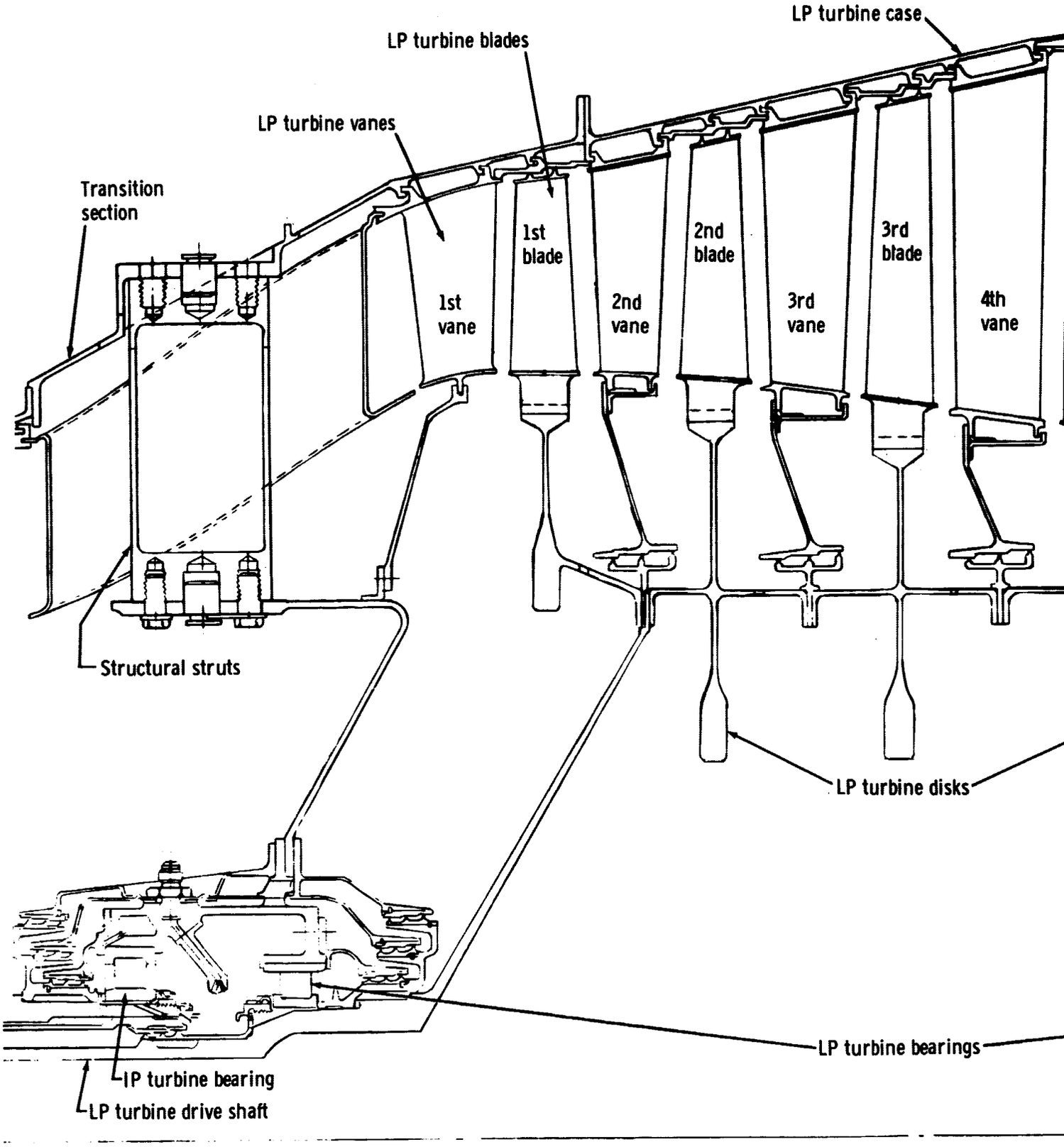

FOLDOUT FRAME 1

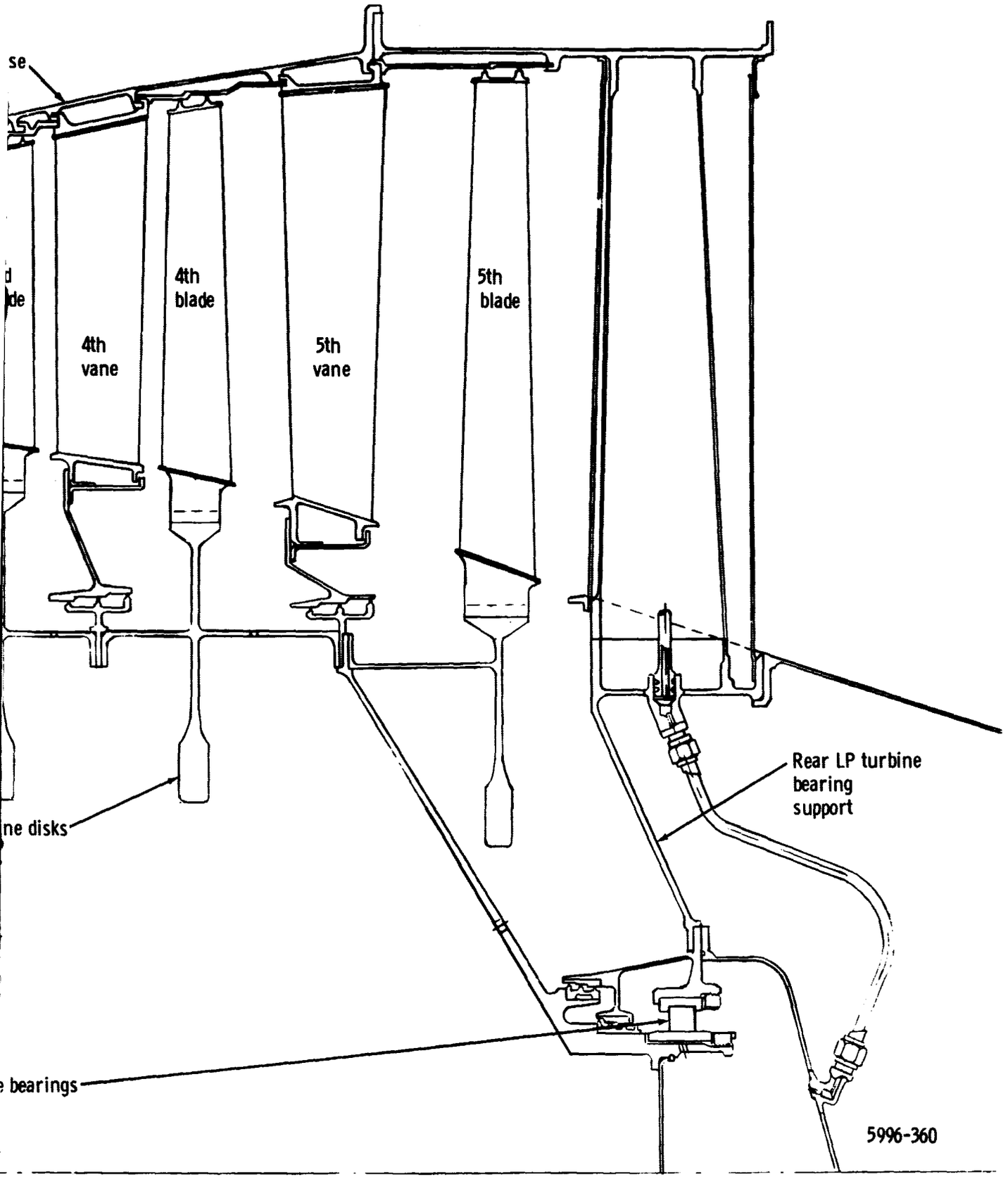

Figure 3d5-10. PD218-Q LP turbine.

FOLDOUT FRAME 2

Table 3d5-XI.

Airfoil steady-state stresses for PD218-Q LP turbine rotor assembly.

Stage	1	2	3	4	5
Engine speed, rpm (rps)	3,286 (54.8)	3,286 (54.8)	3,286 (54.8)	3,286 (54.8)	3,286 (54.8)
Mean section metal temp, °F (°K)	1,327 (992)	1,247 (948)	1,167 (904)	1,088 (860)	1,017 (820)
Airfoil hub centrifugal stress, psi (Mpa)	5,412 (37.3)	6,542 (45.1)	8,889 (61.3)	11,355 (78.3)	13,204 (91.0)
Mean section centrifugal stress, psi (Mpa)	3,482 (24.0)	4,242 (29.2)	5,699 (39.3)	7,225 (49.8)	8,853 (61.0)
0.5% creep mission life	Not limiting	Not limiting	Not limiting	Not limiting	Not limiting

Table 3d5-XII.

PD218-Q LP turbine disk stresses.

Stage	1	2	3	4	5
Engine speed, rpm (rps)	3,286 (54.8)	3,286 (54.8)	3,286 (54.8)	3,286 (54.8)	3,286 (54.8)
Rim metal temp, °F (°K)	936 (775)	880 (744)	824 (713)	770 (683)	720 (655)
Bore metal temp, °F (°K)	660 (622)	400 (477)	400 (477)	400 (477)	400 (477)
Max radial stress, psi (Mpa)	30,212 (208.3)	50,961 (351.4)	55,342 (381.6)	44,135 (304.3)	48,057 (331.3)
Bore tangential stress, psi (Mpa)	80,518 (555.2)	84,405 (582.0)	85,000 (586.1)	85,000 (586.1)	85,000 (586.1)
Average tangential stress, psi (Mpa)	54,000 (372.3)	45,179 (311.5)	50,669 (349.4)	53,557 (369.3)	53,945 (371.9)

Table 3d5-XIII.
PD218-Q turbine materials list.

Item	Material	Specification
HP turbine		
Inlet vane	Cast Stellite 31	AMS-5382
Blade	Cast Udimet 700	—
Disk	Forged Waspaloy	AMS-5708
Front seal support	Forged Waspaloy	AMS-5708
Cover plate and seal	Forged Waspaloy	AMS-5708
Outer case	Forged Waspaloy	AMS-5707
Stationary blade rub strip	Hastelloy X	AMS-5754
IP turbine		
Inlet vane	Cast Udimet 700	—
Blade	Cast Udimet 700	—
Disk	Forged Waspaloy	AMS-5708
Support shaft	Forged Inco 718	AMS-5662
Stationary blade rub strip	Hastelloy X	AMS-5754
LP turbine		
First- through fifth-stage vanes	Inco 713 alloy	AMS-5391
First- through fifth-stage blades	Inco 713 alloy	AMS-5391
First- through fifth-stage disks	Forged Inco 901 alloy	AMS-5661
Fan-to-LP turbine drive shaft	Forged D6 alloy steel	AMS-6431
Stationary blade rub strips	Hastelloy X	AMS-5754
Outer case	Forged Inco 901	AMS-5661
Turbine exhaust		
Outer case	AISI 410 steel	AMS-5613
Structural struts	AISI 410 steel	AMS-5504

3d6. ACCESSORY DRIVE

The accessory drive gearbox assembly is located on the bottom of the engine in front of the HP compressor, as shown in Figures 3d11-1 and 3d11-2. The assembly is a kidney-shaped structure and is supported by a bolted flange from the transition section between the IP and HP compressor cases. Accessory power is extracted from the high pressure rotor system by a bevel gear set located at the front of the HP compressor rotor. Six power takeoff pads are arranged to provide the smallest frontal area and the least disturbance to the fan airflow path consistent with the accessory envelopes. A front and rear plan view of the gear train and accessory drives is shown in Figure 3d6-1. Summary data are given in Table 3d6-I.

Table 3d6-I.
PD218-Q accessory drive summary data.

Item	Function	rpm	rps
1.	Ignition exciter alternator	15,215	253.58
2.	Lube oil pump and tachometer generator	4,190	69.83
3.	Engine fuel pump and fuel control	7,227	120.45
4.	Idler gear	11,383	189.72
5.	Aircraft alternator	18,212	303.53
6.	Starter	6,899	114.98
7.	Aircraft hydraulic pump	5,991	99.85

The alternator, hydraulic pump, and starter drive pads are bolted flanges; however, quick disconnect V-band clamp flanges may be used if desired. The detail drive spline configurations for the alternator, starter, and hydraulic pump incorporate seals that conform to the tentative standards proposed by the Society of Automotive Engineers Technical Committee AE 1 (1 December 1965). All drive splines, except the tachometer and ignition alternator, are mist-lubricated with engine oil. Oil dams are used to ensure tooth immersion in the lubricant. A special jet is used to provide positive lubrication to the fuel pump drive splines.

The housings are AMS-4217 aluminum precision castings with an ultimate tensile strength of 40,000 psi (275.78 Mpa) and are anodized per AMS-2471. Exterior surfaces are painted with gray engine enamel. All spur gears are cut from AMS-6265 vacuum-melted steel forgings. These gears are carburized, hardened, ground, and honed to obtain a superior surface finish. The gear teeth are sized to provide a maximum bending stress at the root of 35,000 psi (241.3 Mpa)—assuming single tooth loading—when subjected to maximum continuous torque. The gear webs are integrally machined or electron-beam welded to their shafts to reduce weight and eliminate splines and fasteners. The shaft ends are machined to form inner races

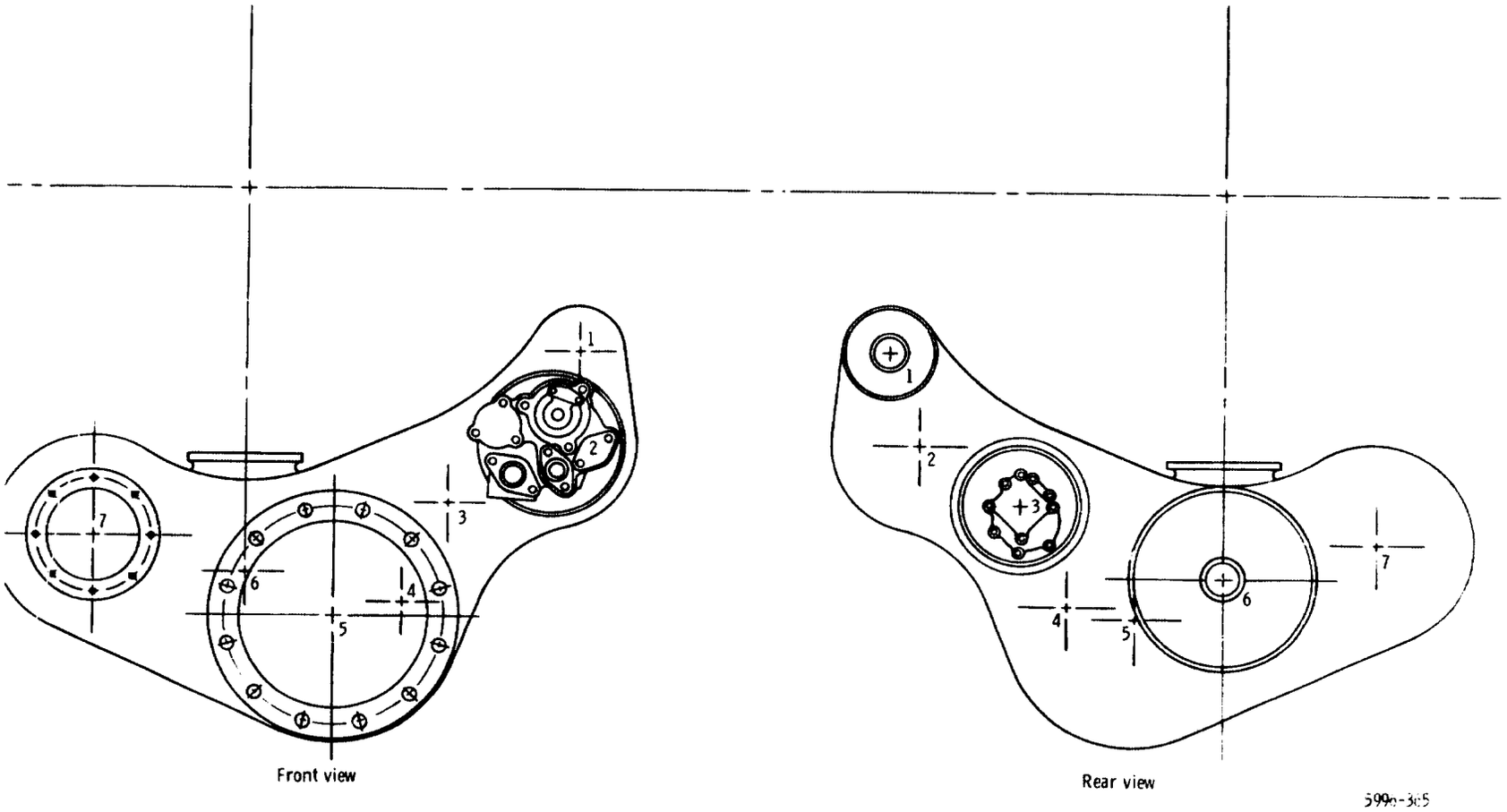

Figure 3d6-1. Front and rear plan view of PD218-Q gear train and accessory drives.

for the supporting roller bearings. This eliminates fasteners and surface interfaces commonly subject to fretting, reduces overall weight, and improves gear and output spline alignments.

The bevel gear train used to drive the accessory gearbox is composed of two meshes capable of transmitting 200 hp (149.4 kw) continuously. The first bevel gear mesh consists of a gear mounted on the hub of the high pressure rotor and a pinion arranged to drive down through a strut to the bottom of the engine. Both gears are shimmed to ensure a proper tooth mesh. The gears use a 20-deg (0.348-rad) pressure angle. At maximum continuous torque, the 10-pitch teeth are subjected to 7400 psi (51 Mpa) in bending stress and 61,200 psi (422 Mpa) in Hertzian stress. The pitch-line velocity for the mesh is 24,400 fpm (124 m/sec)—a value within Allison experience.

The second bevel gear mesh has a diametral pitch of 6.58 and a pressure angle of 25 deg (0.436 rad). At maximum continuous torque, the gear tooth bending stress is 17,100 psi (118 Mpa) and the Hertzian stress is 99,300 psi (684.6 Mpa). Both gears in the second mesh are shimmed for proper engagement.

All bevel gears are cut from AMS-6265 forgings. These gears are carburized, hardened, and ground.

Roller bearings with flanged outer races are used exclusively in the accessory gearbox assembly to provide extended service life. The outer races are locked by studs in the gear case to prevent rotation. The elimination of separate bearing cages provides a lighter design with improved gear alignment.

A high pressure oil jet is provided at each bevel gear mesh to ensure lubricant penetration inside the pitch line of the high-speed gears. Another jet is directed into the main accessory drive gear mesh at the top of the accessory gearbox. The remaining gears and bearings are splash-lubricated by the main drive gear lubricant and by an oil mist. The oil mist is entrained with engine seal leakage air and directed to the gearbox through the drive shaft dust cover.

The accessory drive gearbox assembly is replaceable as a unit at the intermediate maintenance level. All accessory drive shafts and engine component drive shafts are equipped with externally removable oil seals.

Accessory drive materials are listed in Table 3d6-II.

Table 3d6-II.
PD218-Q accessory drive materials list.

Part	Material	Specification
Accessory housing	Aluminum casting—356-T6	AMS-4217
Gears	Vacuum-melted steel forgings	AMS-6265
Bearings	Vacuum-melted 52100 steel	AMS-6444
Shafting	Vacuum-melted steel forgings	AMS-6265

3d7. BEARINGS, SEALS, AND SHAFTING

Bearings

The mechanical arrangement of the engine features nine main shaft bearings to support and locate the three rotor systems. As shown in Figure 3d7-1, the HP rotor system requires two bearings, the IP rotor requires three bearings, and the LP rotor configuration requires four bearings. This three-spool arrangement offers the desirable feature of all main rotor bearings being supported directly from the engine structure. The design point rotor speeds are given in Figure 3d7-1.

The HP turbine is cantilever-mounted by a cylindrical roller bearing forward of the turbine wheel and is coupled directly to the HP compressor by a conical shaft. The thrust load from this rotor system is transferred to the engine frame through a ball bearing located at the front end of the HP compressor.

The IP compressor is straddle-mounted on a front thrust bearing and a rear roller bearing. A rigid shaft extends from the aft of the compressor, is concentrically located through the length of the HP rotor system, and terminates in a roller bearing supported from the transition case between the IP and LP turbines. The IP turbine wheel is located on the shaft extension forward of the bearing through a fixed set of splines. The net thrust from this rotor system is carried through the ball bearing located at the front end of the IP compressor.

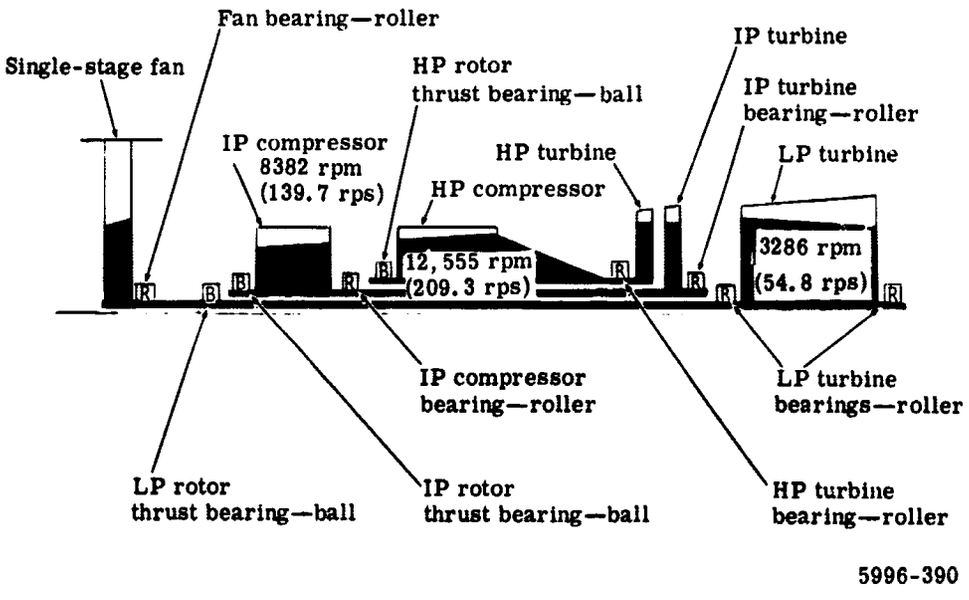

Figure 3d7-1. PD218-Q engine bearing mount system.

The fan is cantilever-mounted on a roller bearing located near the fan disk and the ball bearing some distance to the rear. The LP turbine is straddle-mounted on two roller bearings. A shaft extends from the LP turbine through the center of the IP rotor system and is rigidly coupled to the fan shaft at the thrust bearing location. The thrust bearing removes the net thrust forces from the LP rotor system.

The engine contains nine main shaft bearings as listed in Table 3d7-I. The bore size of each of the bearings is based on the shaft torque and critical speed requirements and experience from similar applications. Externally applied bearing loads are not large and can be carried with very light bearing section sizes. A complete design study, however, will be made of all main shaft bearings with use of computer programs to evaluate the bearings with respect to centrifugal forces, load distribution, possible need for an antiskidding feature, heat rejection, cage design, and the substantiation of adequate life.

Table 3d7-I.
PD218-Q main shaft bearing characteristics.

Position	Size (mm)	Type	Maximum speed rpm	Maximum speed rps	Design point DN* × 10^{-6} 1	Design point DN* × 10^{-6} 2	Material**
1. Fan front	220X300X38	Roller	3,286	54.8	0.726	0.0121	M50
2. Fan rear (thrust)	180X250X33	Ball	3,286	54.8	0.59	0.0098	M50
3. IP compressor, front (thrust)	150X210X28	Ball	8,382	139.7	1.25	0.0208	M50
4. IP compressor, rear	150X210X28	Roller	8,382	139.7	1.25	0.0208	M50
5. HP compressor, front (thrust)	150X225X35	Ball	12,555	209.3	1.88	0.0313	M50
6. HP turbine, front	150X210X28	Roller	12,555	209.3	1.88	0.0313	M50
7. IP turbine , rear	150X210X28	Roller	8,382	139.7	1.25	0.0208	M50
8. LP turbine, front	140X190X24	Roller	3,286	54.8	0.46	0.0077	M50
9. LP turbine, rear	140X190X24	Roller	3,286	54.8	0.46	0.0077	M50

*D is bearing bore in millimeters and N is shaft speed in rpm (column 1) and rps (column 2).
**All ring and rolling element material will be consumable electrode, vacuum-melted steel.

All main rotor bearings have design lives (B10) of 6000 hr, based on the design power rating of the engine. This design life is equal to the anticipated TBO life of the engine and is based on the Antifriction Bearing Manufacturer's Association formula.

Prorated thrust bearing lives were computed using a time-load-speed relationship based on a preliminary aircraft duty mission developed earlier in this study. The prorated thrust bearing lives are listed in Table 3d7-II. The values given are considered adequate until a more detailed duty mission is established.

Table 3d7-II.
PD218-Q prorated thrust bearing life.

	Life (hr)
LP rotor thrust bearing	12,400
IP rotor thrust bearing	9,950
HP rotor thrust bearing	7,780

Seals

The engine vent system controls the engine internal cavity pressures to prevent loss of lubricating oil or cycle air. Figure 3d7-2 shows the cooling air, seal, and venting system.

The engine vent system, in conjunction with the turbine cooling air system, uses the airflow through the rotating seals for the cooling of components and the containment of oil in the sumps at a minimum weight and performance penalty.

Part of the labyrinth seal airflow is returned to the main gas flow path. A quantity of air flows across the air-oil seals, enters the lubrication system, is piped to the accessory housing, passes through an air-oil separator, and is vented overboard through the breather. In the turbine area where the bearings must be protected from the high gas temperature a portion of the seal flow is bled directly overboard and piped into the exhaust stream.

Pressure air from the IP compressor discharge is bled through the IP rotor system into the cavity in the shaft of the LP rotor system. The air is piped in the center of the shaft to both the fan and the LP turbine areas. The air is used in the fan section to deice the spinner and pressurize the front fan bearing air-oil seal. The air to the LP turbine section is used to purge the intrastage cavities—cooling the LP turbine wheels—and to pressurize the LP turbine rear bearing oil seal. This air also provides a positive pressure drop across a set of labyrinth seals in series at the IP compressor rear bearing location.

The pressure rise through the fan is used to provide positive pressurization of the air-oil labyrinth seal at the IP compressor forward bearing. The HP compressor front bearing seal uses two 3-element labyrinth seals in series. The seal is pressurized with air from the HP compressor inlet. A small portion of this air flows through this seal and is discharged through the accessory gearbox breather system.

A three-stage labyrinth seal system is used at the HP turbine front bearing location. The three seal stages are designed with a compartment between each stage which may be pressurized or vented to prevent the hot HP compressor discharge air, used for turbine cooling, from entering the bearing compartment. Figure 3d7-3 shows the plan used in the HP turbine

bearing location. The cavity between the outer and middle seal stages is vented overboard to the exhaust; the cavity between the middle and inner (seal nearest the bearing) seal stages is pressurized with IP compressor discharge air. The cool pressurizing air is piped into the compartment near the bearing and divides, with part of the air flowing past the inner seal into the bearing compartment and out through the breather system. The remaining air flows past the middle seal into the outer compartment. The flow of cool air through the middle seal mixes with an additional flow of hotter air (turbine cooling air) leaking through the outer seal stage and is piped overboard into the exhaust stream. The system is duplicated on the aft side of the bearing to provide an isolated air-cooled bearing compartment.

A similar three-stage seal arrangement is used at the IP turbine rear bearing and LP turbine forward bearing locations. See Figure 3d7-4. In this bearing position, however, the turbine cooling air pressures surrounding the compartment are low enough so that the cavity between the outer and middle seal stages is pressurized with cool IP compressor discharge air and the cavity between the middle and inner (seal nearest the bearing) seal stages is vented overboard to the exhaust. At the forward side of the IP turbine bearing the cool IP compressor discharge air is piped to the outer seal compartment where the flow splits. Part of the air leaks through the outer seal stage into the turbine disk cooling air passage. The remaining air flows through the middle seal stage into the cavity nearest the bearing. This flow splits again with part of the air being piped overboard into the exhaust stream; the remaining air flows past the inner seal stage into the bearing compartment and out through the breather system. This configuration is duplicated on the aft side of the LP turbine bearing to provide an isolated air-cooled bearing compartment.

Sealing between shafting is accomplished with labyrinth seals. The pressure drop in the system was chosen to provide a minimum flow of cool compressor bleed air in these cavities and to prevent back flow of hot turbine gases under all operating conditions.

The preliminary analysis of this flow system resulted in using 5.11% of the gas generator air flow. Included in this 5.11% is 3.43% for turbine cooling. Table 3d7-III shows the breakdown of the turbine cooling air system.

Table 3d7-III.
PD218-Q turbine cooling air (percent of engine airflow).

HP turbine first-stage blade cooling	1.50
Inner flow path cooling	1.40
IP turbine first-stage vane cooling	0.50
Outer flow path cooling	0.03

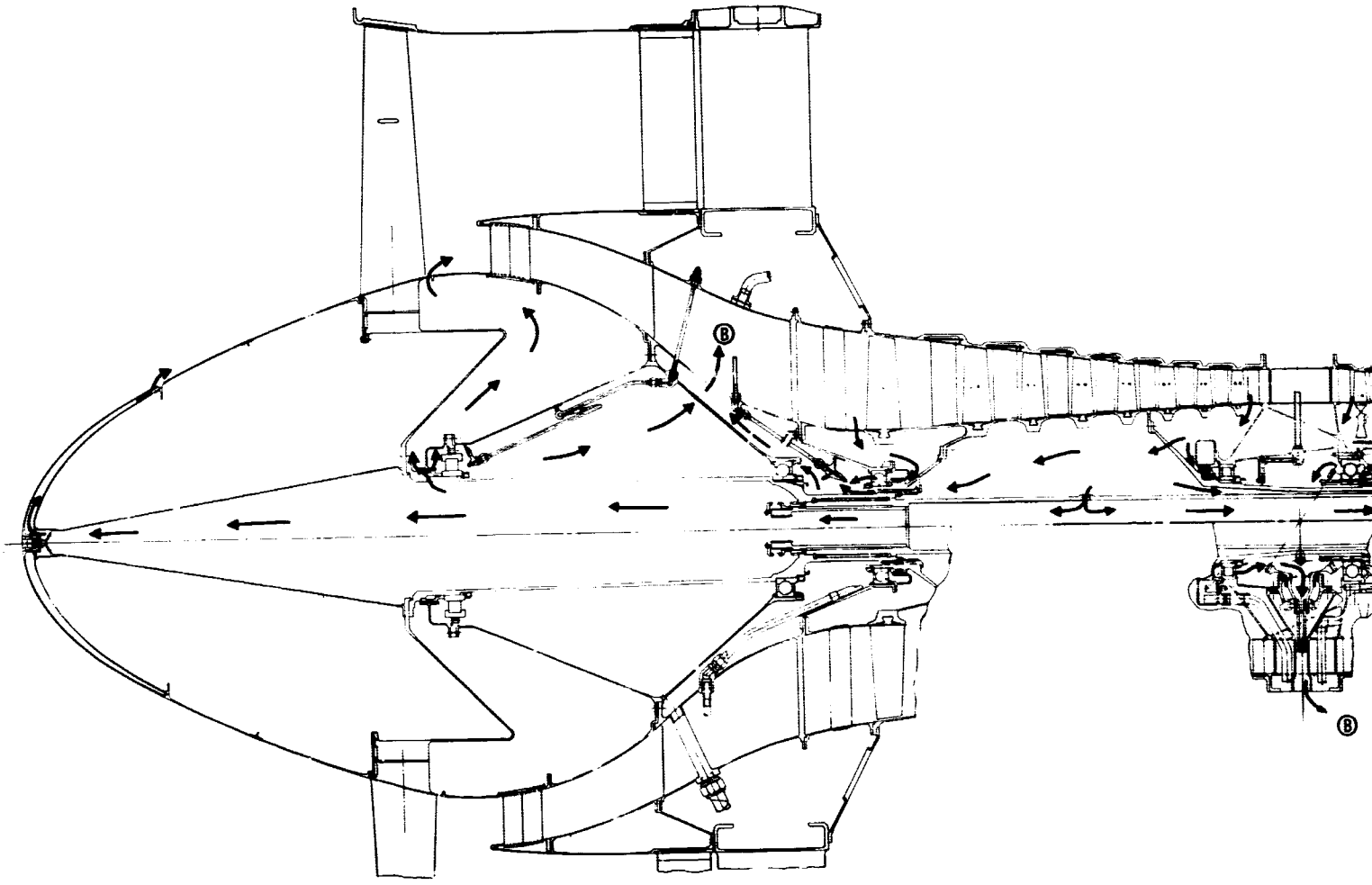

FOLDOUT FRAME 1

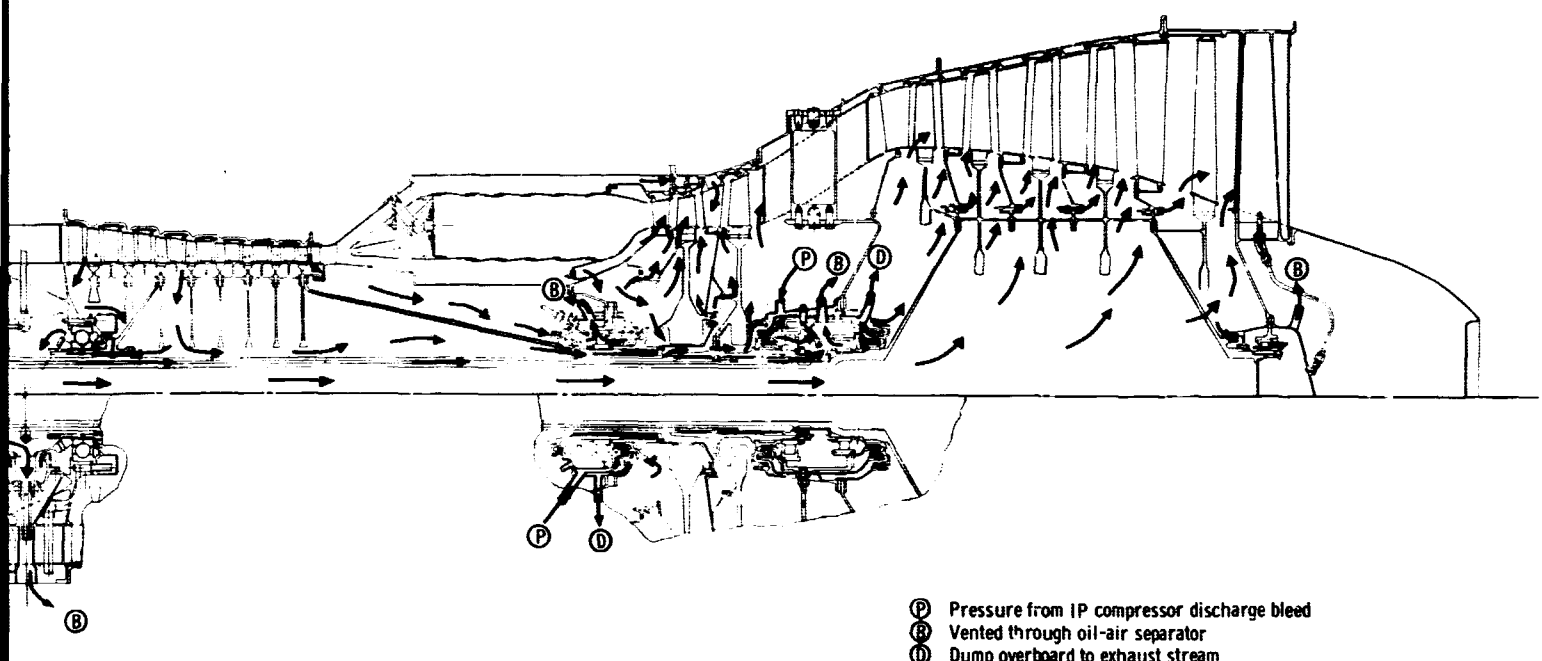

(P) Pressure from IP compressor discharge bleed
(B) Vented through oil-air separator
(D) Dump overboard to exhaust stream

5996-393

Figure 3d7-2. PD218-Q cooling air, seal, and venting system.

FOLDOUT FRAME 2

PRECEDING PAGE BLANK NOT FILMED.

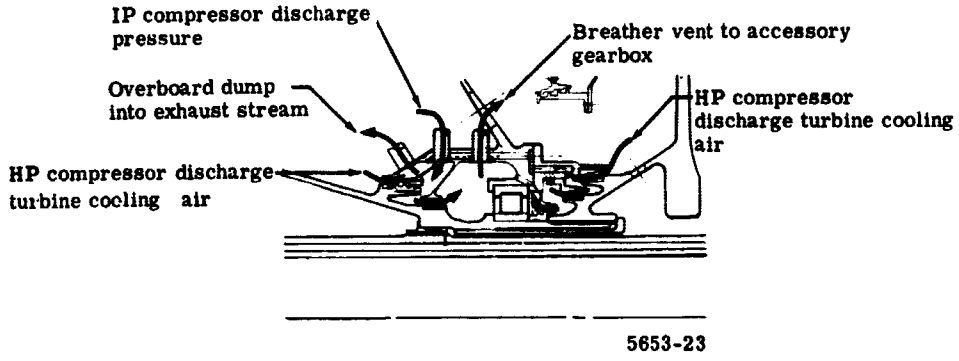

Figure 3d7-3. Front HP turbine seal configuration.

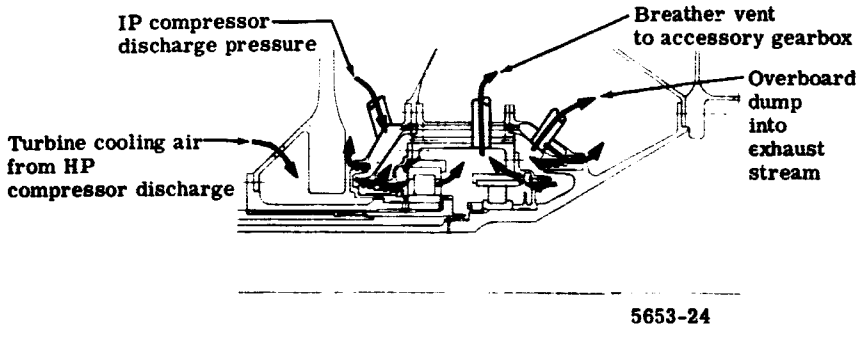

Figure 3d7-4. PD218-Q rear IP turbine and forward LP turbine bearing seal configuration.

An additional 2.0% cooling air is used for the HP turbine first-stage vane and is discharged through the trailing edge and accelerated to gas stream velocity; this air is not chargeable to engine performance.

The balance of 1.68% airflow is used for deicing the spinner and pressurizing the bearing compartments. Table 3d7-IV shows the breakdown of the quantity of air used in the bearing compartments.

Table 3d7-IV.
PD218-Q bearing compartment seal air distribution.

Compartment	Pressurizing air (%)	Piped to breathers (%)	Piped to turbine exhaust (%)	Returned to gas stream (%)
Fan and IP compressor	0.06	0.04	—	0.02
IP and HP compressors	0.16	0.16	—	—
HP turbine	0.19	0.08	1.06	—
IP and LP turbines	0.18	0.08	0.07	0.04
Rear LP turbine	0.03	0.03	—	—

Shafting

The fan-to-LP turbine drive shaft has been designed to carry the maximum torque generated by the fan design which operates at a tip speed of 1011 fps (308.2 m/sec) at sea level takeoff condition. The shaft has a 4 in. (0.1015 m) outside diameter and is forged from D6 alloy steel. The shaft wall thickness is 0.240 in. (6.1 mm) and has been sized to provide a calculated shear stress-to-allowable tensile (0.2% yield strength) stress ratio of 0.57. This thickness provides adequate low cycle fatigue margin. The shaft as designed will carry 390,000 in.-lb (44,000 N-m) of torque which is the required torque at Mach 0.6, sea level.

The stiff bearing critical speed margin is 91% for the LP rotor system, 98% for the IP rotor system, and 128% for the HP rotor system. The requirement is a minimum of 30% critical speed margin with stiff bearing supports.

Materials

Bearing, seal, and shafting materials are listed in Table 3d7-V.

Table 3d7-V.
PD218-Q bearing, seal, and shafting materials list.

Part	Material	Specification
Main shaft bearings		
Two HP rotor bearings	Vacuum-melted consumable electrode M50 steel	AMS-6490
Three IP rotor bearings	Vacuum-melted consumable electrode M50 steel	AMS-6490
Four LP rotor bearings	Vacuum-melted consumable electrode M50 steel	AMS-6490
Seal elements		
Rotating	Inco 901 alloy steel forgings	AMS-5661
Stationary	Inco 718 alloy steel forgings	AMS-5662 with silver facing
Shafting		
HP rotor shaft	Inco 718 alloy steel forgings	AMS-5662
IP rotor shaft	D6 alloy steel forgings	AMS-6431
LP rotor shaft	D6 alloy steel forgings	AMS-6431

3d8. ENGINE STRUCTURAL REQUIREMENTS

A preliminary structural analysis of all critical engine components was made as a part of the preliminary design effort. Analysis considerations and results are detailed in the component description subsections of this report. The criteria were as follows.

- The engine structures will have mechanical design constraints to provide for a minimum structural life of 24,000 hr except on critical hot section parts. For the purpose of life determination, the average flight was considered to be 2 hr. As a result, only 12,000 full stress cycles were required to achieve a 24,000-hr life. Turbine blades and vanes were designed to meet a minimum of 6000-hr service life.
- The engine structures will have an adequate margin to ensure structural integrity when subjected to the loads imposed by operation within the limits of the flight maneuver load diagram shown in Figure 3d8-1.

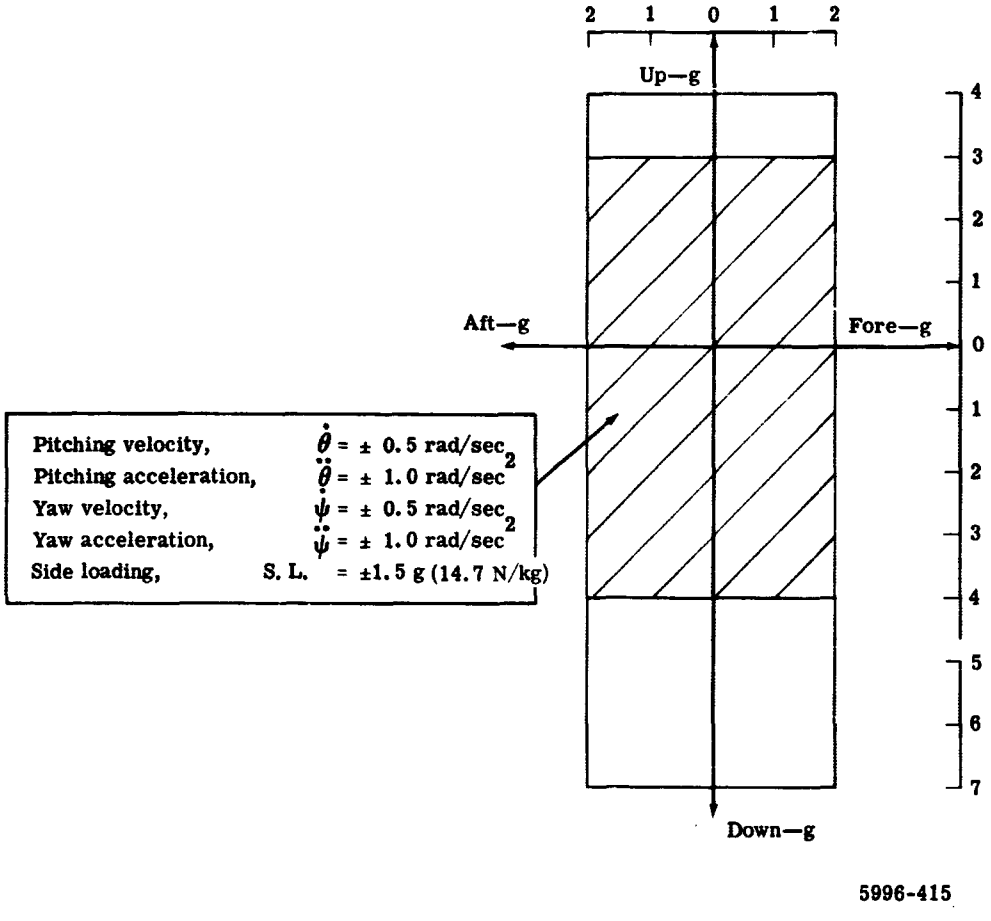

Figure 3d8-1. PD218-Q flight maneuver load diagram.

3d9. LUBRICATION SYSTEM

The lubrication system for the engine is self contained, as shown schematically in Figure 3d9-1. The oil tank, oil cooler, and oil pump are engine mounted. The system is designed to provide adequate lubrication for the engine throughout its operating range as well as to provide a cooling fluid for the bearings.

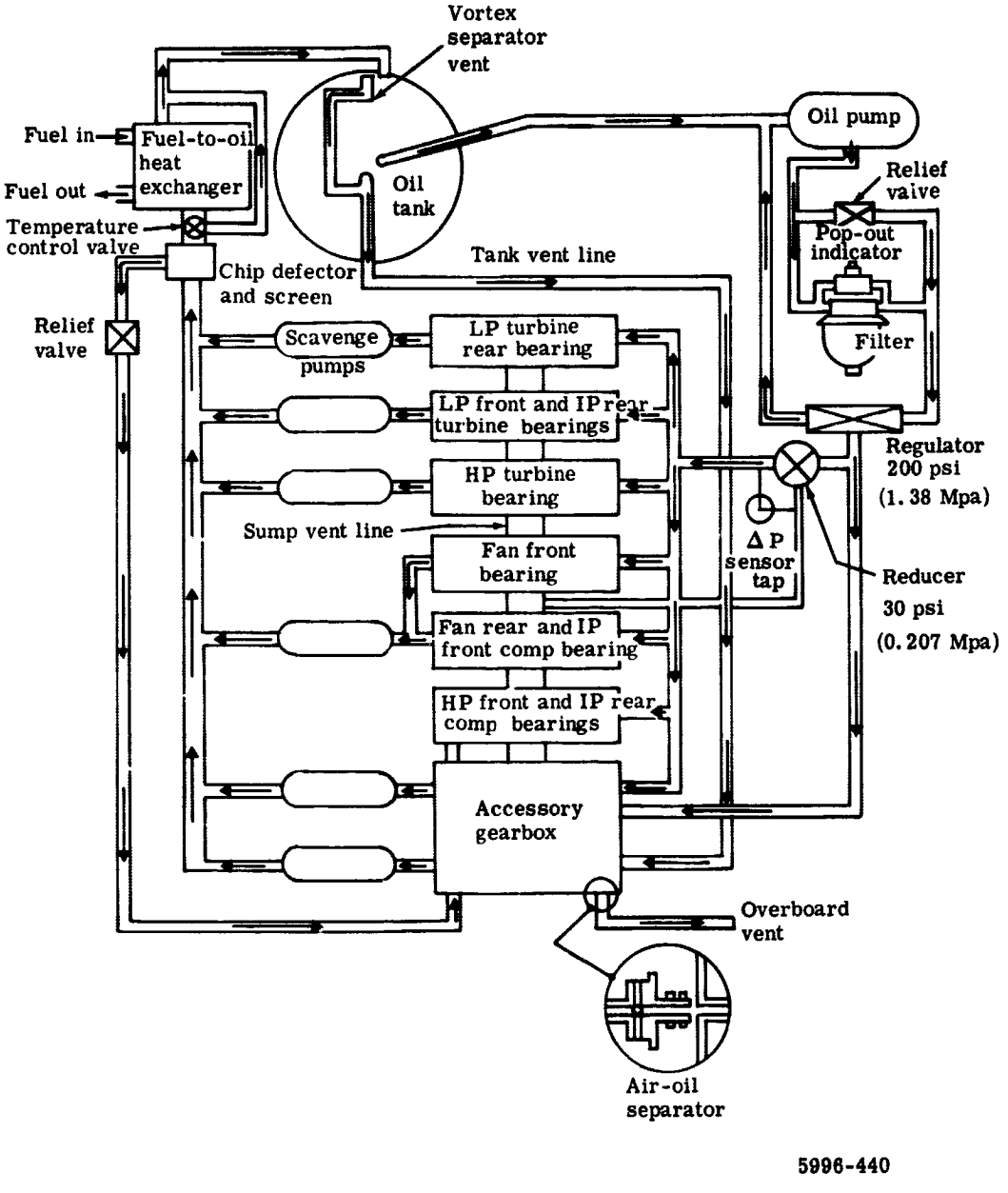

Figure 3d9-1. PD218-Q lubrication system schematic.

The following functions are required of the lubrication system under all engine operating conditions:

- Adequately lubricate and cool all bearings, gears, working splines. and accessories, using MIL-L-7808 or MIL-L-23699 oil
- Adequately seal engine oil cavities to avoid internal oil leakage
- Provide dry sump scavenging capability throughout the engine attitude and altitude range to prevent flooding of labyrinth seals and to limit the residual oil after shutdown
- Cool and deaerate the oil
- Provide adequate drainage of residual oil

Pressure System

The oil flow rate to an area requiring lubrication is established with consideration for heat removal based on experience with similar applications. In the case of low flow requirements, the flow is determined by the practical minimum size jet which will not clog easily. The estimated heat rejection to the engine oil is 3000 BTU/min (52.718 kw). The total engine oil system flow is 40.5 lb/min (306 g/sec) which is held constant throughout the operating speed range of the engine by a regulating valve. This flow results in an estimated oil temperature rise of 150°F (83°K).

The two jets to the main accessory drive gear meshes are supplied by a line pressure of 200 psig (1.38 Mpa) for maximum penetration into the gear teeth at the high pitch-line speed of these gears. The line pressure in the remainder of the system is regulated to 30 psi (0.207 Mpa) above sump cavity pressures by means of a reducing valve which senses pump pressure.

Each power shaft bearing is lubricated by a separate jet. Working splines are fed centrifugally and have oil dams to maintain maximum oil coverage of the spline teeth. Accessory gears and bearings are splash lubricated. A breakdown of the oil flow requirements is presented in Table 3d9-I.

Oil Tank

The oil tank is sized to provide 10 hr of engine operation at the maximum specified hourly oil consumption rate. The 6-gal (0.0264 m^3) oil tank is of welded titanium construction mounted on the IP compressor section. The tank is basically rectangular and follows the cylindrical contour of the IP compressor to avoid protruding into the fan discharge area.

The oil level is indicated by discrete point level sensors. Three sensors indicate by means of panel lights a low, full, or mid-range oil level condition.

Table 3d9-I.

PD218-Q oil flow requirements.

Lubrication point	Line pressure, psi (Mpa)	Jet diameter, in. (mm)	Flow ppm (kg/sec)
Bevel gear mesh (main shaft)	200 (1.38)	0.047 (1.19)	4.2 (0.0317)
Bevel gear mesh (accessory)	200 (1.38)	0.047 (1.19)	4.2 (0.0317)
Forward fan bearing	30 (0.207)	0.052 (1.32)	2.1 (0.0159)
Rear fan bearing	30 (0.207)	0.052 (1.32)	2.1 (0.0159)
IP compressor forward bearing	30 (0.207)	0.052 (1.32)	2.1 (0.0159)
IP compressor rear bearing	30 (0.207)	0.052 (1.32)	2.1 (0.0159)
Accessory drive gearbox assembly	30 (0.207)	0.052 (1.32)	2.1 (0.0159)
Fuel pump spline	30 (0.207)	0.052 (1.32)	2.1 (0.0159)
HP compressor forward bearing	30 (0.207)	0.052 (1.32)	2.1 (0.0159)
HP turbine forward bearing	30 (0.207)	0.081 (2.06)	5.1 (0.0385)
IP turbine rear bearing	30 (0.207)	0.081 (2.06)	5.1 (0.0385)
LP forward bearing	30 (0.207)	0.081 (2.06)	5.1 (0.0385)
LP turbine rear bearing	30 (0.207)	0.052 (1.32)	2.1 (0.0159)
Total flow			40.5 (0.306)

The tank is designed for remote filling and overflow. It has a pressurizing valve to maintain a minimum tank pressure of 4 psig (27.579 kpa) and a baffled vent line connection. The tank is vented overboard through the accessory gearbox.

Pressure Oil Pump

The pressure oil pump is a positive displacement, gear-type pump designed to deliver the required flow of 40 lb/min (302 g/sec) at 60% of maximum rated engine speed. The pump element is based on 80% volumetric efficiency at 240 psig (1.65 Mpa). Above 60% engine speed, the system flow is regulated to 40.5 lb/min (306 g/sec) and the excess pump capacity is bypassed by a regulating valve located in the pump housing. This same valve also serves as a shutoff valve when the engine speed falls below 15% (Figure 3d9-2) to prevent oil from being pumped into the engine when scavenging capability is marginal. This feature is discussed in more detail under the subheading Scavenge Pump.

The complete pump assembly contains the following elements:

- Pressure element
- Spool-type high and low pressure regulating valves

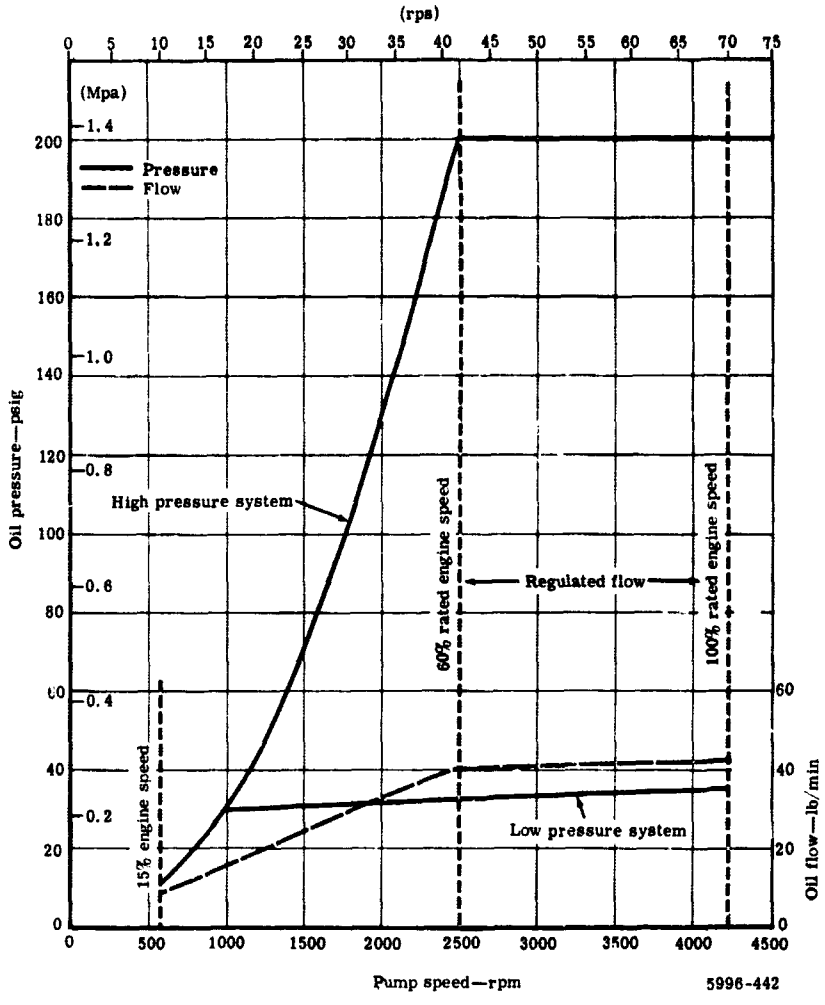

Figure 3d9-2. PD218-Q lubrication system oil flow and pressure.

- Woven-mesh, 40-micron (40-micrometers), full-flow oil filter
- Oil filter bypass valve
- Scavenge pressure
- Scavenge pressure relief valve
- Magnetic chip detector

The two oil pressure regulator valves, the oil filter, and the filter bypass valve are externally accessible for replacement and/or cleaning without disturbing other engine components.

Scavenge System

The scavenging system is designed as a dry sump system. The number and location of scavenge pump pickups are established to effectively remove oil and prevent flooding of labyrinth seals. There are six cavities in the engine where oil is collected for removal by the pumps. These cavities and the number of scavenge pump pickups required for each are as follows:

	Pump pickups
Fan and front IP compressor	2
Midsection (rear IP and front HP compressors)	2
HP turbine	1
IP turbine and front LP turbine	2
Rear LP turbine	1
Accessory gearbox	1
Total scavenge pumps	9

Sufficient volume is provided in each sump so that the maximum oil level is maintained below the level of the labyrinth seals. Slingers are provided on rotating seal members to prevent direct impingement of oil into the seals.

Scavenge Pumps

All of the scavenge pumps are positive-displacement, gear-type elements and are enclosed in the same housing assembly with the pressure oil pump. By placing all the pumping elements in one package, only one drive pad is required.

The scavenge elements are sized to provide a minimum capacity advantage of three times the maximum quantity of oil supplied to each sump. The design point is 60% engine gasifier speed or 925 fpm (4.7 m/sec) pitch-line velocity which provides a 70% volumetric efficiency. For best volumetric efficiency, maximum pitch-line velocity of the pump gears is normally limited to approximately 1000 fpm (5.08 m/sec). Experience has shown, however, that below a pitch-line velocity of 300 fpm (1.5 m/sec), the volumetric efficiency may drop so low that marginal scavenge capacity is available in the starting speed range of the engine. To avoid this situation, the pump speed is selected for the best volumetric efficiency at low engine speed. This approach is shown in Figure 3d9-3. The scavenge pump capacity curve is a typical curve showing volumetric efficiency as a function of pitch-line velocity where the straight line indicates constant volumetric efficiency. The design data for the pump elements are summarized in Table 3d9-II.

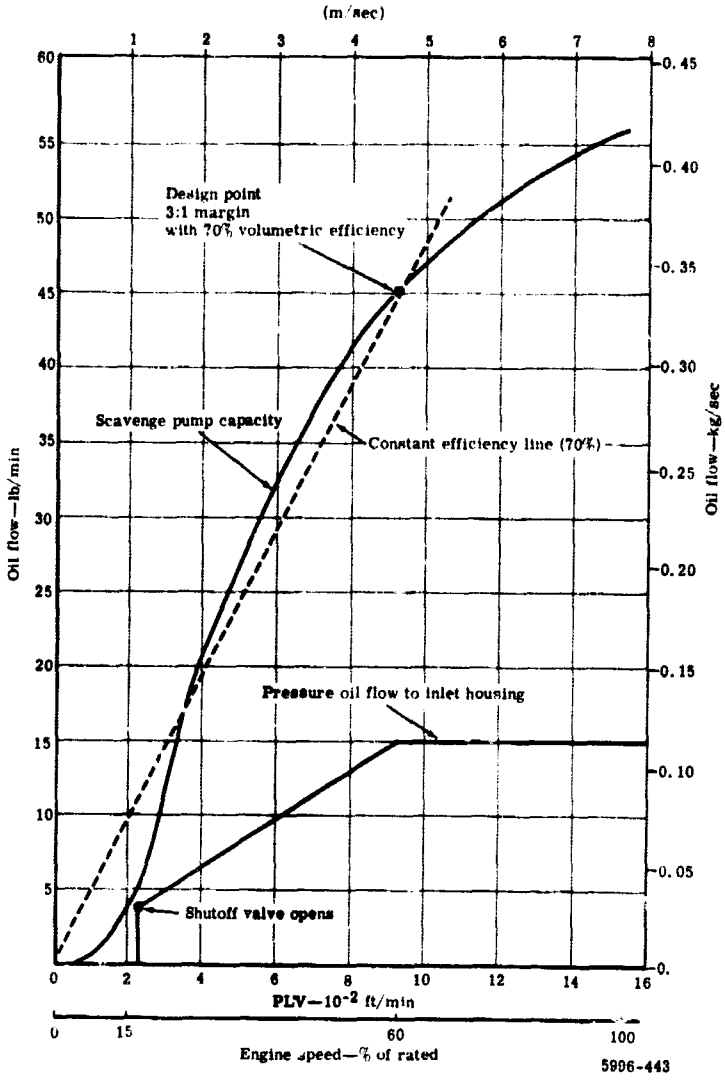

Figure 3d9-3. PD218-Q scavenge oil pump performance.

Pressure Relief Valve

A poppet type pressure relief valve is provided in the scavenge pump discharge manifold of the pump assembly body. If the scavenge oil discharge pressure exceeds 250 psig (1.72 Mpa), which is possible when starting with cold oil, this valve will open to bypass oil to the accessory gearbox.

Magnetic Chip Detector, Drains, and Fittings

An indicating type magnetic chip detector is oriented in the scavenge discharge manifold oil stream to attract any metal debris suspended in the oil.

Table 3d9-II.
PD218-Q gear pump design data.

	Pressure oil pump	Scavenge pump (9 elements)
Diametral pitch	10	10
Number of teeth	14	14
Face width	0.716 in. (18.186 mm)	0.97 in. (24.6 mm)/element
Maximum speed	4200 rpm (70 rps)	4200 rpm (70 rps)
Pitch-line velocity	1540 fpm (7.82 m/sec)	1540 fpm (7.82 m/sec)
Volumetric efficiency	0.8	0.7
Minimum inlet pressure	4 in. Hg abs (13.5 kpa)	4 in. Hg abs (13.5 kpa)
Discharge pressure	220 psig (1.517 Mpa)	40 psig (0.276 Mpa)
Capacity (max)	63 ppm (0.476 kg/sec)	75 ppm (0.566 kg/sec)
Power	4.72 hp (3520 w)	0.68 hp/element (507 w/element)
Total pump power		6.1 hp (4549 w)

The pressure and scavenge system uses rigid titanium tubing with double O-ring type connecting fittings. For connections to hot sections of the engine, the design incorporates standard flared fittings.

3d10. FUEL AND CONTROL SYSTEM

Control Mode

The engine has a variable fuel flow that is regulated to maintain thrust control; LP, IP, and HP rotor speed limiting; transient surge protection; burner blowout protection; and burner pressure limiting.

Steady-state thrust control is effected by a fuel governor which senses and controls the HP rotor speed. Power lever position establishes the governor speed setting, providing thrust modulation from idle to maximum power. The governor function is limited by the acceleration and deceleration schedules. These schedules comprise the basis for transient control.

Start and acceleration control are provided by open-loop scheduling of fuel flow as a function of sensed HP rotor speed and engine pressure. The schedule is also temperature compensated to provide good starting characteristics, responsive and surge-free accelerations, and transient turbine temperature limiting. The deceleration schedule protects against burner blowout by limiting the minimum fuel flow during the transient. The scheduling is pressure compensated to account for variations in burner airflow.

Turbine overtemperature protection is provided by the acceleration fuel schedule during transients and by a closed-loop turbine temperature limiter during steady-state operation. This allows operation up to a peak cycle temperature for maximum performance to ensure that overtemperature operation will not occur. Steady-state temperature limiting is accomplished by using the measured turbine temperature thermocouple signal in an electronic control which alters the fuel scheduling by trimming the hydromechanical control.

LP and IP rotor speeds are allowed to float up to their maximum speed limits during steady-state and transient operation. Automatic overspeed protection on these two rotors is provided using electrical speed sensors and closed-loop limiters to effect a fuel flow reduction. These limiters are integrated into the control system in the same manner as the turbine temperature limiter.

Automatic start sequencing is accomplished by using the sensed HP rotor speed signal to delay the opening of the fuel cutoff valve until the proper conditions are reached. Fuel scheduling during engine acceleration to idle is maintained by the acceleration fuel limit schedule. On-off acceleration bleeds will be used to provide adequate transient surge margin and will be actuated as a function of HP rotor speed.

Control System Description

The fuel control system consists of a pump, control, flow divider, manifold, and 16 nozzles. The system components are designed to operate on MIL-E-5007C contaminated fuel without in-line filtration. The pump and control are mounted together and require only one drive.

The fuel pump is an engine-driven, integrally boosted, positive-displacement type pump and provides fuel under pressure to the control; it can provide fuel for the aircraft (boost) ejector system, if desired. Fuel in excess of metered flow is returned to the pump inlet. The control contains a relief valve to prevent excessive back-pressure on the fuel pump.

The main fuel control is a hydromechanical type with an electronic speed and turbine temperature trim as well as speed-sequencing signals. The main control derives its intelligence through sensing of the HP rotor speed, compressor inlet temperature, compressor discharge pressure, throttle lever position, and an electrical signal from the electronic control. The electronic control, in turn, senses low and intermediate rotor speeds and intermediate turbine outlet temperature. This unit is a miniaturized, solid-state design. Metered fuel is passed from the fuel control through the flow divider and manifold drain valve into the fuel manifold where it is distributed to the 16 dual orifice fuel nozzles.

Turbine temperature is sensed by nine dual-junction thermocouples connected together so as to measure the average temperature and provide separate signals for control purposes and cockpit indication.

The ignition system is self contained and receives its power from an engine-driven permanent magnet generator. The single-package exciter is a dual-circuit, a-c, input-type capacitor discharge unit. Two low-tension, shunted, surface gap igniters are used to ignite the fuel mixture. Flameout protection is also provided. The flameout sensor system consists of a flame sensitive cell, an amplifier, a relay, and a fiber glass flexible conduit.

3d11. ENGINE INSTALLATION

The engine installation layouts are shown in Figures 3d11-1 and 3d11-2 and include three possible mounting arrangements. The mounting loads are shown for each arrangement. The accessory packaging is the same in each arrangement and includes DC-8 type aircraft equipment. Engine loft line dimensions and mounting point dimensions are given on each layout.

The arrangements of the engine installations shown in Figures 3d11-1 and 3d11-2 are typical for pod installation where the engine is mounted to the wing by a pylon. Two mount locations are used to support the engine under the pylon. The main mount transfers thrust and axial loads, proportionally shared vertical and side loads, and the moment produced by side loads. The other mount will transfer proportionally shared vertical and side loads only. This two-mount concept is used in each of the three mounting arrangements.

The thrust mount is located in the top 90-degree quadrant of the engine. This mount consists of a central self-aligning bearing pad and a rod-end link boss on each side. The self-aligning bearing will accept a sliding thrust pin from the pylon. The thrust and side loads are transferred through this central bearing without applied moments. The rod-end links trarsfer the vertical loads to the pylon and take out the moment produced by the side loads.

The steady rest mount is also located within a 90-degree quadrant at the top of the engine. A rod-end boss is located on each side of the vertical center line. Two airframe links are used to carry the vertical loads; these links are placed at a substantial angle to the vertical to resist side loads. The links must have self-aligning features to allow for thermal expansion between the mounts.

Several mount configurations were considered for the PD218-Q engine. Two front thrust mount configurations are shown in Figure 3d11-1 and one rear thrust mount configuration is shown in Figure 3d11-2. The front thrust mount is located on the fan case support strut section or, as an alternate configuration, on the IP compressor case. The rear thrust mount is located on the turbine transition case at the bearing support strut.

The mount reaction diagrams for each of the three arrangements were calculated using the flight maneuver load diagram shown in Figure 3d8-1. The loads shown are those applied to the engine by the mounts. These loads are based on the engine and accessory package weight acting at the corresponding center of gravity (cg). The mount positions are fixed in the axial direction and are defined by a point on the vertical radius. The magnitude and direction of the loads are the maximum experienced when all flight maneuvers are investigated. The weight added by the inlet cowl, thrust reverser, bypass nozzle, and other nacelle equipment on the engine will add to these loads through some resulting cg point.

The arrangement with the thrust mount on the fan case provides the greatest access to the mount during installation. The cutaway in Figure 3d11-1 shows the struts and rings used to support the thrust load and axial inertial loads. The local strut is designed to carry the load and the rings have a high section modulus to reduce deflection.

An alternate front thrust mount is shown in Figure 3d11-1 at a position near the 1P compressor case. Comparison of the mount loads and moments shows this arrangement to have a lower magnitude of forces.

The third mount arrangement is shown in Figure 3d11-2. This drawing depicts a thrust mount attached to the turbine section. The thrust pin bearing pad is reacted on the rear flange and pinned at the front. The airframe side links are attached to the flange rings over the rotor bearing support struts. The steady rest mount is on the fan case for ease of installation.

The engine structure, as shown in Figures 3d11-1 and 3d11-2, will carry thrust reverser loads. The reversed thrust loads are of lower magnitude than the maximum forward thrust loads under maneuver conditions (worst case) and can easily be reacted at the fan case thrust mount.

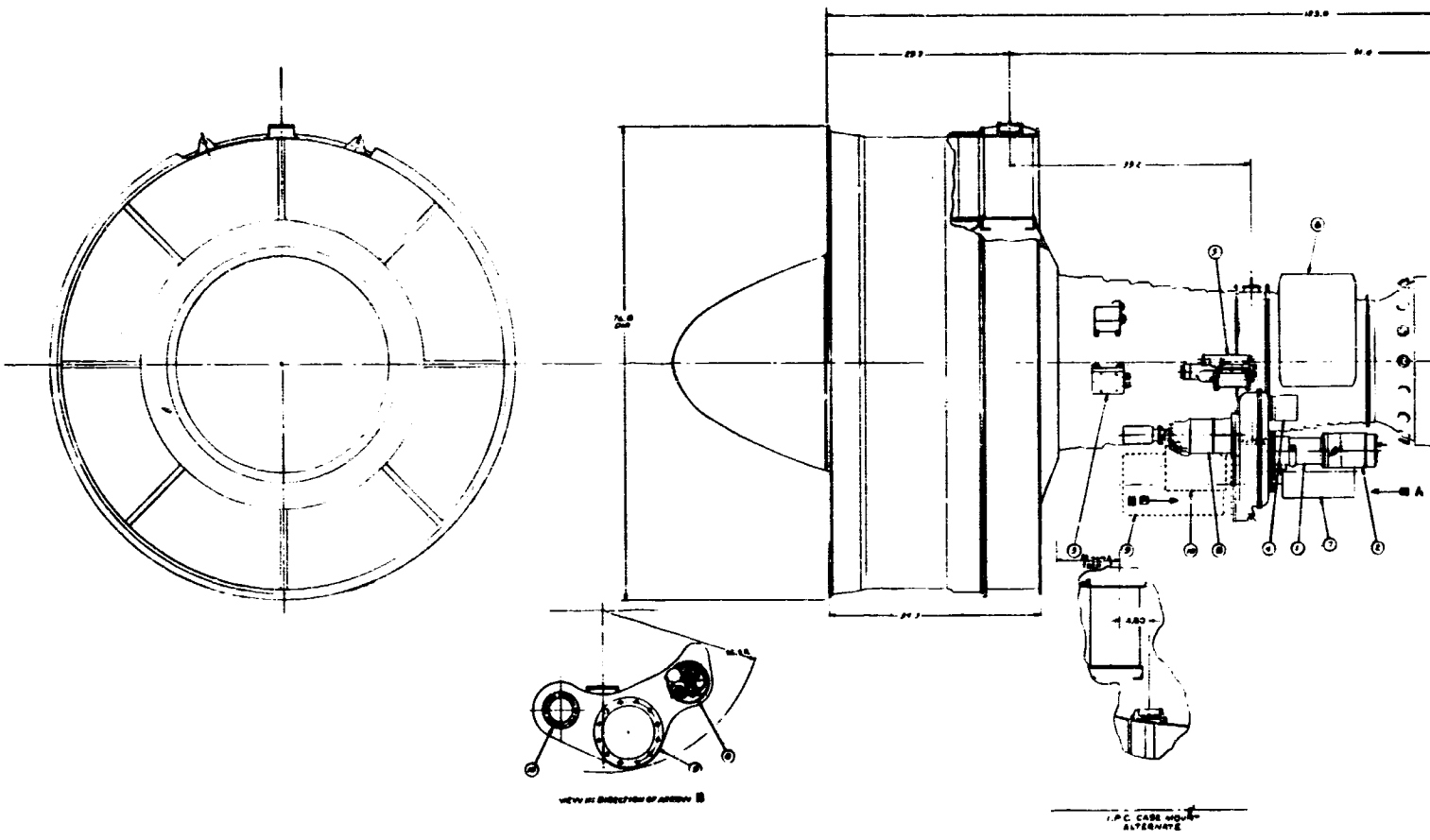

FOLDOUT FRAME 1

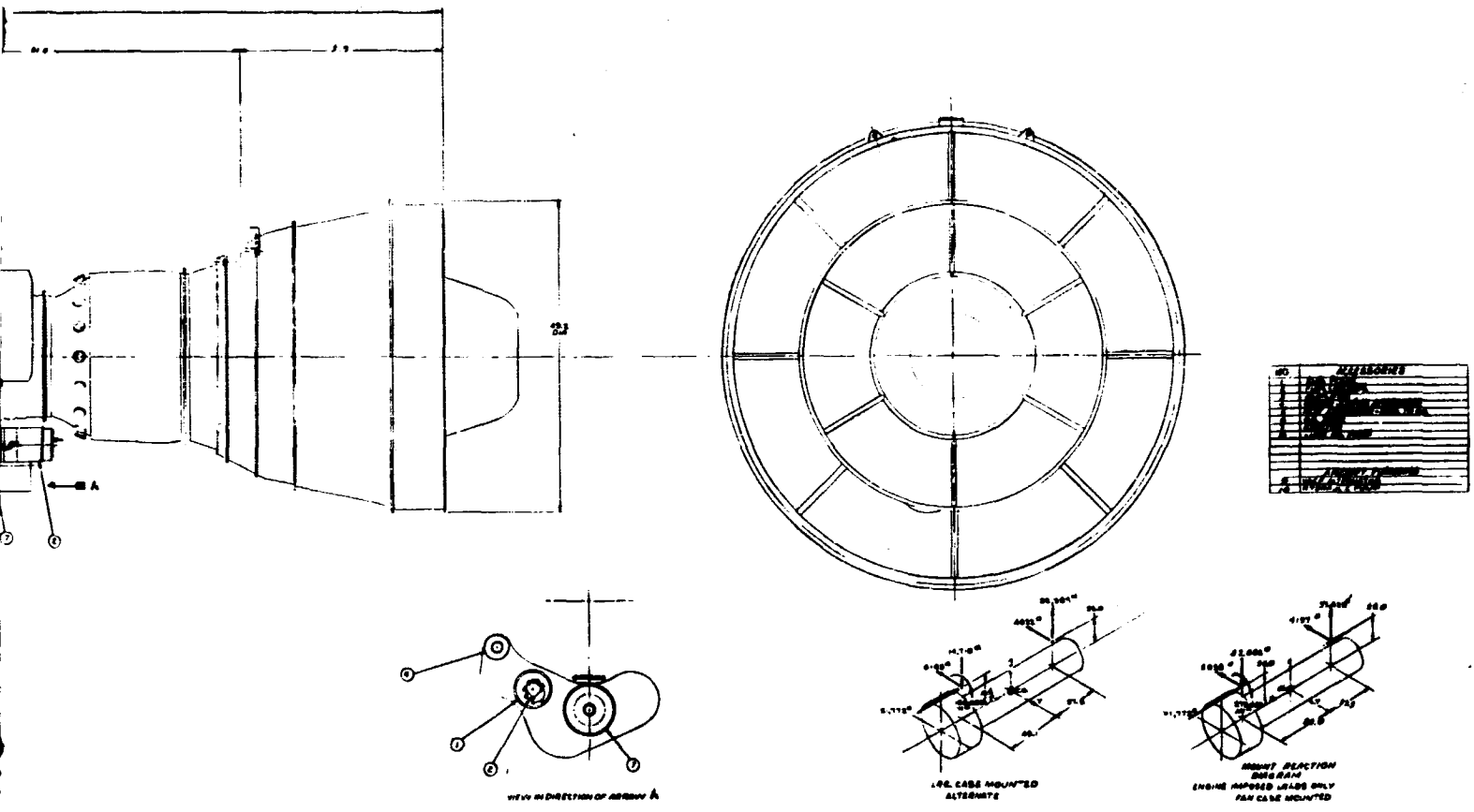

Figure 3d11-1. PD218-Q engine installation, front thrust mounts.

FOLDOUT FRAME 2

PRECEDING PAGE BLANK NOT FILMED.

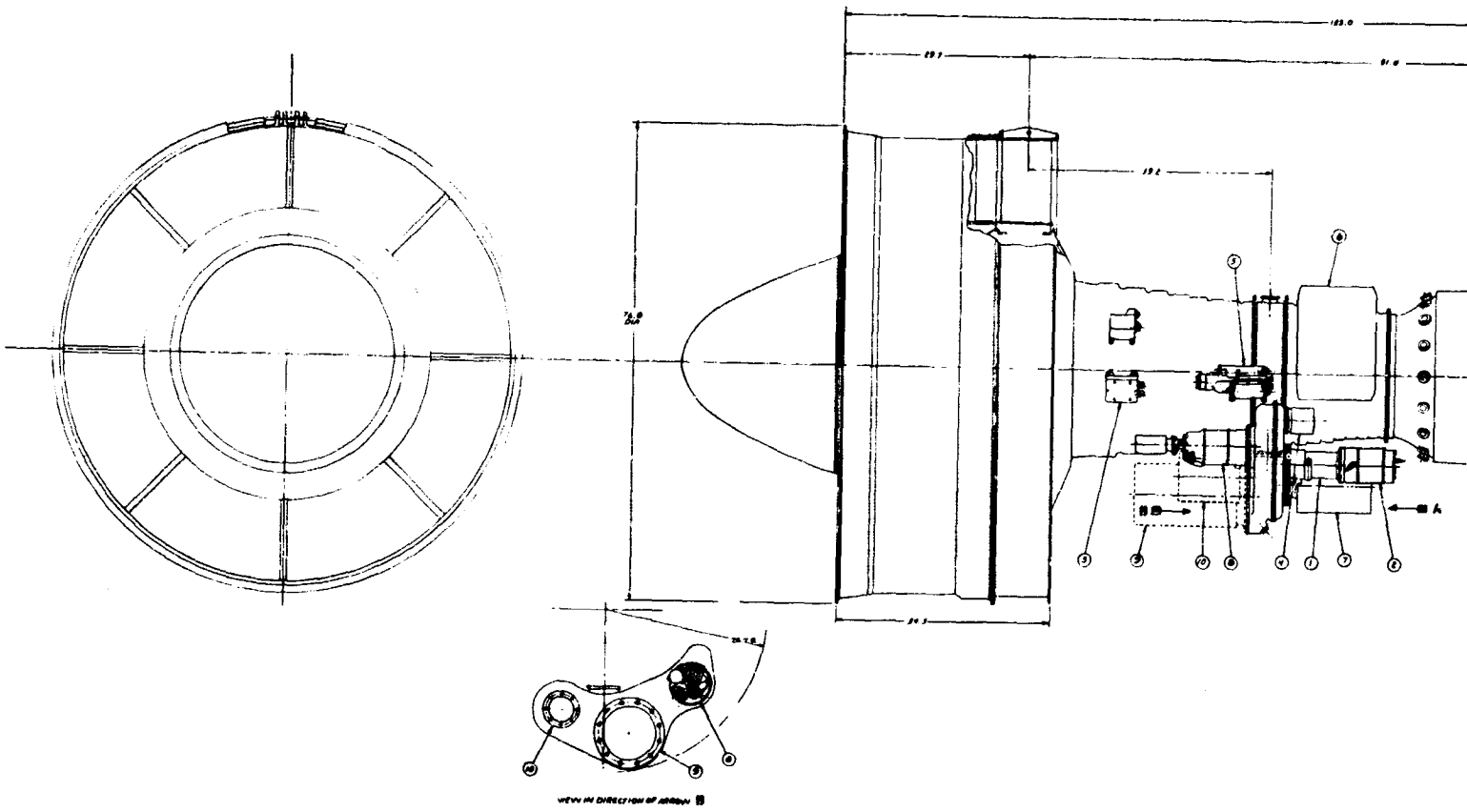

FOLDOUT FRAME 1

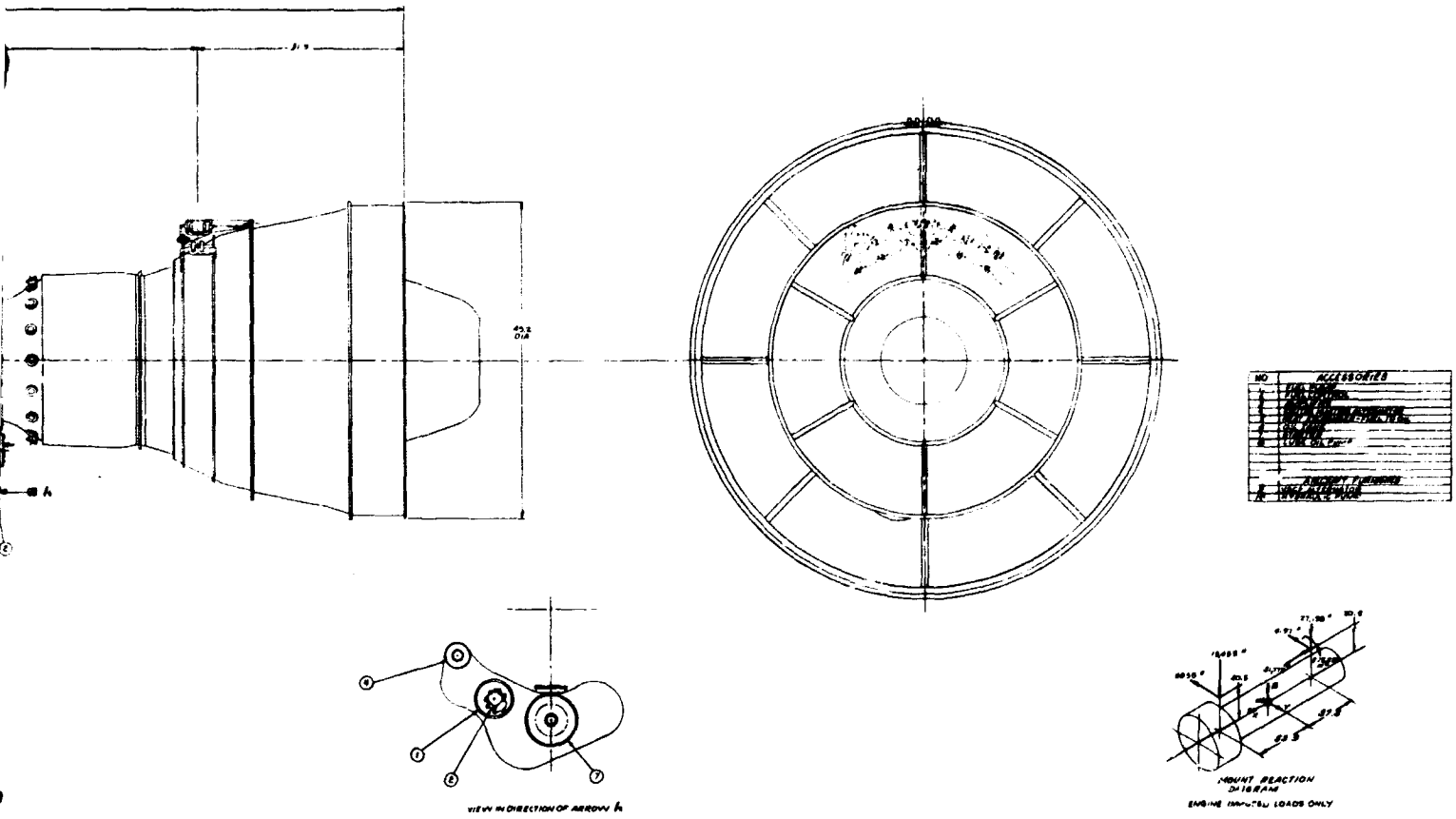

Figure 3d11-2. PD218-Q engine installation, rear thrust mount.

FOLDOUT FRAME 2

IV. SYMBOLS AND UNITS

The abbreviations and symbols used in this report are defined in Table 4-I. The symbols for the international system of units used in this report are defined in Table 4-II.

Table 4-I.
Abbreviations and symbols.

BPR	Bypass ratio
EGV	Exhaust gas velocity
HP	High pressure
H/T	Hub-to-tip radius ratio
IGV	Inlet guide vane
IP	Intermediate pressure
LHV	Lower heating value
LP	Low pressure
L/D	Length-to-diameter ratio
N	Shaft speed
OGV	Outlet guide vane
P_{amb}	Ambient pressure
PLV	Pitch-line velocity
PNdB	Perceived noise decibel
R_c	Pressure ratio
R_{eT-T}	Turbine expansion ratio (total to total)
spl	Sound pressure level
T_{amb}	Ambient temperature
TBO	Time between overhaul
T/C	Thickness-to-chord ratio
TIT	Turbine inlet temperature
tsfc	Thrust specific fuel consumption
U	Wheel speed
U_m	Mean-line wheel speed
V_a	Axial velocity
W	Mass flow
W_a	Airflow
h	Specific work
θ	Temperature correction ratio (T°R/518.7)
θ_{cr}	Turbine inlet temperature to standard temperature further corrected for difference in the ratios of specific heats
ϵ	Correction factor for difference in ratio of specific heats
δ	Pressure correction ratio ($P_{psia}/14.7$)

Table 4-II.
System international symbols.

g	Grams
kg	Kilograms
Mg	Megagrams
mm	Milimeters
m	Meters
km	Kilometers
N	Newtons
kN	Kilonewtons
°K	Degrees Kelvin
pa	Pascals (newtons/meter^2)
kpa	Kilopascals
Mpa	Megapascals
rps	Revolutions per second
mps, m/sec	Meters per second
rad	Radians
w	Watts
kw	Kilowatts

V. REFERENCES

1. Smith, J. T. and House, M. E. Internally Generated Noise from Gas Turbine Engines, Measurement and Predictions. ASME Paper No. 66-GT/N-43. 1966.

2. Investigation of Methods for the Prediction and Alleviation of Lift Fan Noise. USAAML Technical Report 65-4. March 1966.

3. Noise Studies of Inlet Guide Vane-Rotor Interaction of a Single Stage Axial-Flow Compressor. NASA TND-2962. September 1965.

4. Inlet Noise Studies for an Axial-Flow Single Stage Compressor. NASA TND-2615. February 1965.

5. Suppression of Jet Noise with Emphasis on the Near Field. ASD-TDR-62-578. February 1963.

6. Composite Octave Band Spectrum for Boeing Aircraft at 400 Feet Sideline and Flyover. Boeing in-house report D6-17097-TN. May 1967.

7. Bishop, D. E. Descriptions of Flyover Noise Signals Produced by Various Jet Transport Aircraft. FAA DS 67-18. 1 August 1967.

8. Progress of NASA Research Relating to Noise Alleviation of Large Subsonic Jet Aircraft. NASA SP-189. Langley Research Center, Hampton, Virginia. 8-10 October 1968.

9. Procedures for Developing Noise Exposure Forecast Areas for Aircraft Flight Operations. FAA DS 69-10. August 1965.